Transformation of wave spectra across the surf zone

final report

A.S. Vink
June 2001

TU Delft
Delft University ofTechnology

Faculty of Civil Engineering and Geosciences
Subfaculty of Civil Engineering
Section of Fluid Mechanics

Ministry of Transport, Public Works and Water Management
National Institute for Coastal and Marine Management / RIKZ

Transformation of wave spectra across the surf zone

final report
m.sc. thesis

A.S. Vink
June 2001

Under supervision of:

prof.dr.ir. J.A. Battjes
prof.drs.ir. J.K. Vrijling
dr.ir. L.H. Holthuijsen
ir. J.H. Andorka Gal

TU Delft
Delft University ofTechnology

Faculty of Civil Engineering and Geosciences
Subfaculty of Civil Engineering
Section of Fluid Mechanics

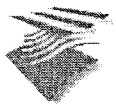

Ministry of Transport, Public Works and Water Management
National Institute for Coastal and Marine Management / RIKZ

Preface

Over the past nine months I have been working on my graduation project. This final report presents the results of my work. The subject of my project is the transformation of wave spectra across the surf zone.
The work has mainly been carried out at Delft University of Technology. However, during my research I have been able to visit different places and meet the world's experts on wave modelling. A lot of these people have significantly contributed to my work.

First of all I would like to express my gratitude to the members of my thesis committee. Their support and advises have been very helpful. Especially I would like to thank dr.ir. L.H. Holthuijsen and ir. J.H. Andorka Gal for their extensive and enthusiastic guidance and the opportunities they have given to me.
I would also like to thank dr.ir. N. Booij and drs. A. Kieftenburg of Delft University of Technology. They have spent a lot of time answering my questions about SWAN. Their help is very much appreciated.

A part of my work has been done at the office of the Dutch National Institute for Coastal and Marine Management in The Hague. The contact with all members of the OSF-G group has been very pleasant. Especially I would like to thank ing. J. Jacobse for his help and suggestions and the nice time I had sharing a room with him.

This spring I have had the opportunity to attend the WISE meeting in Canada and meet the world's top researchers in the field of wave modelling. This has been a very interesting experience. During WISE I have had pleasant conversations with a lot of different people from different countries. Especially the enthusiastic and encouraging reactions on my presentation of Dr. Robert Jensen and Dr. Jane McKee-Smith of the US Army Corps of Engineers have been very stimulating completing my work.

For each person I have mentioned in this preface, I have probably forgotten one as well. Thus, I would like to thank all fellow-students, friends and relatives who have enthusiastically supported me over the past months.

Ard Vink
Delft, June 2001

Abstract

One of the most applied models for wave prediction is the spectral wave model SWAN. SWAN (or any other model) is not always capable of predicting wave conditions in the surf zone with sufficient accuracy.
In this study the transformation of wave spectra across the surf zone and its spectral modelling was investigated. The objective of this thesis work was to improve the prediction of wave spectra and their integral parameters in the surf zone. Focus was on the improvement of the dissipation term for depth-induced wave breaking for the use in SWAN.

At present the source term for wave breaking in SWAN consists of two elements. First, the total, frequency-integrated dissipation is determined. This is done with the model of Battjes and Janssen [1978]. Important elements of this model are the bore analogy for the dissipation in a single breaking wave, the assumed wave height distribution and the breaker parameter (γ), that determines the maximum breaker height. Subsequently the total dissipation is distributed over the frequencies. This distribution is proportional to the energy density level at each frequency.

A literature study was carried out to make an inventory of previous work on wave breaking and its spectral modelling. Various formulations for the breaker parameter, the wave height distribution in the surf zone, the total dissipation by wave breaking and the spectral distribution of the total dissipation were reviewed. This resulted in possible approaches for improvement of the performance of SWAN in the surf zone.

In order to select the most promising alterations wave data was analysed and simulated with SWAN 40.11. Three different data sets were used: field observations of the Petten field site, measurements of bi-modal spectra in a laboratory flume, carried out by Smith and Vincent [1992] and data from the Duck '94 field experiment. Cases form the first two data sets were simulated with SWAN.
It appeared that in both the Petten cases and the laboratory cases SWAN consistently underestimated the significant wave height in the surf zone.

In all cases considered, the high-frequency tail of the measured wave spectrum evolved to a $k^{-2.5}$-equilibrium range in the inner surf zone. This is attributed to a combined effect of wave breaking and triad interactions. In the cases with bi-model spectra all higher-frequency peaks were dissipated. Only the low-frequency peak is maintained. It appeared that dissipation by wave breaking is frequency dependent. In the SWAN simulations the shape of the spectra at the offshore boundary was more or less maintained across the surf zone. This resulted in inaccurate estimations of the mean wave period and wave spectra.

Three different adaptations to the present source term for wave breaking in SWAN were proposed, implemented and tested.
Firstly, the Rayleigh distribution for both breaking and non-breaking waves was implemented. This adaptation did not result in better predictions of the cross-shore variation of the significant wave height on mildly sloping bottoms. However, on a steep bottom the predictions of the significant wave heights and the fraction of breaking waves were significantly improved applying the full Rayleigh distribution.
Secondly, the breaker parameter γ was adapted. An expression depending on the *local* wave steepness was implemented. It was based on the formulation of Battjes and Stive [1985]. This adaptation resulted in a significant improvement of the predicted wave heights across the surf zone on both flat and steep bottoms.
The third adaptation concerned the distribution of energy dissipation over the frequencies. A frequency-dependent expression for the distribution of energy dissipation was tested. The formulation was implemented such that a part was distributed proportional to the energy density and a part proportional to frequency to the power n. Only in a few cases the predicted mean wave period could be slightly improved. In the bi-modal case the high-frequency peak was suppressed. However no optimal formulation of the frequency-dependency could be determined such that both the *qualitative trend* in the cross-shore variation of the mean wave period and the *absolute values* of the mean wave period are predicted with sufficient accuracy.

It was concluded that the prediction of the cross-shore variation of the significant wave height can be considerably improved with the implantation of the breaker parameter depending on the local wave steepness. Applying a full Rayleigh distribution improves the accuracy in the prediction of the fraction of breaking waves and the significant wave heights on a steep slope. Moreover it was concluded that the distribution of energy dissipation is frequency dependent and that distributing energy dissipation proportional to the energy density at each frequency is a wrong assumption. Dissipation of energy is higher at higher frequencies. Adding a frequency-dependency to the source term for wave breaking had an effect on predicted mean wave periods and spectral energy density levels although no unique optimal formulation could be found for this frequency dependency.
Furthermore it was concluded that the effect of triad interactions is not correctly represented in SWAN.

The implementation of both the Rayleigh model and the formulation for the breaker-parameter depending on the local wave steepness as an optional command in SWAN is recommended.
The effect of wave breaking on the spectral distribution of energy is still poorly understood. Investigation of the spectral energy balance of breaking waves in the surf zone might give more insight in the spectral representation of wave breaking.
Besides wave breaking, non-linear triad interactions are very important regarding the transformation of wave spectra across the surf zone. In this study triad-interactions are almost not considered. When triad interactions are better approximated in SWAN the representation of wave breaking in SWAN can be assessed better. Further investigation of the spectral modelling of triad interactions is recommended.

Contents

List of figures

List of symbols

Roman letters

parameter	unity	description
a_n	m	amplitude of wave component n
c	m/s	wave celerity or wave speed
c_g	m/s	group velocity
c_{mn}	m/s	mean wave celerity
d	m	water depth
D	J/m^{2}s	dissipation rate
D_b	J/m^{2}s	dissipation rate in a breaking wave
D_{tot}	J/m^{2}s	total dissipation by wave breaking
E	J/m^2	wave energy
E_{tot}	m^2	total variance
f	1/s	frequency
f_{mn}	1/s	mean frequency
f_n	1/s	frequency of wave component n
$\overline{f}$	1/s	mean frequency
g	m/s^2	gravitational acceleration
h	m	water depth
h_b	m	depth at incipient breaking
H	m	wave height
H_b	m	breaker height
H_m	m	maximum wave height
H_{rms}	m	root mean square wave height
H_s	m	significant wave height
k	rad/m	wave number
k_{mn}	rad/m	mean wave number
K	-	decay coefficient
K_r	-	refraction coefficient
K_s	-	shoaling coefficient
L	m	wave length
L_{mn}	m	mean wave length
$L_{o,p}$	m	wave length at deep water, evaluated at peak frequency
m_0	m^2	0th moment of the spectrum, total variance
P	J/ms	energy flux
Q_b	-	fraction of breaking waves
s_{loc}	-	local wave steepness
s_o	-	incident or deep water wave steepness

parameter	unity	description
t	s	time
T	s	wave period
T_p	s	peak period
T_{mn}	s	mean wave period

Greek letters

parameter	unity	description
α	-	proportionality parameter in dissipation model
α	-	beach slope
α_0	-	proportionality constant in equilibrium range formulation
α_n	-	phase of wave component n
γ	-	breaker parameter
Γ	-	stable wave parameter
η	m	surface elevation
θ	-	angle of wave direction
ξ	-	surf similarity parameter
ρ_w	kg/m^3	mass density of water
σ	rad/s	relative angular frequency
ω	rad/s	angular wave frequency

1 Introduction

1.1 Background of the study

"The surf zone is the nearshore region in which relatively well-ordered irrotational motion of deep water waves is transformed through wave breaking into a range of different fluid motions. These may include turbulent bores, large scale vortices, low-frequency motions and mean cross-shore and long-shore flows" [BATTJES, 1988].
Wave transformations across the surf zone are not only a visually spectacular phenomenon. The mentioned processes are of great influence on sediment transport rates and therefore on the morphological behaviour of beaches. Furthermore, coastal structures are subject to wave loads and nearshore operations are influenced by the wave conditions. Some authors even refer to the importance of an estimation of the 'surfability' of the waves [SMITH AND KRAUS, 1991].
It may be clear that accurate predictions of the wave-climate in the surf zone of (natural) beaches are of great importance for coastal engineers.

In third-generation wave models formulations of processes of wave generation, dissipation and wave-wave interactions are represented explicitly. Although these formulations are state-of-the-art, some are still approximations. Some of the relevant processes in these models are poorly understood. For example, a full understanding of depth-induced wave breaking and triad wave-wave interactions and the formulation of corresponding source terms for spectral models is yet to come.
Triad-interactions and depth-induced wave breaking are the dominant processes in shallow water (e.g. the surf zone). In the literature several alternative formulations to describe these processes can be found. Wave models, in which these formulations are used, are not (always) capable of predicting wave conditions in the surf zone with sufficient accuracy. The prediction of the shape of the spectrum and the resulting mean wave period needs to be improved. Moreover, variations of (significant) wave heights across the surf zone are not always predicted very accurate either.

The third generation, spectral wave model SWAN is (one of) the most applied models for wave prediction in the nearshore zone. Users of SWAN have encountered the problems mentioned above. Specifically in the surf zone a more accurate prediction of wave conditions is needed.

1.2 Objective of the study

The main objective of this study is to improve the prediction of wave energy spectra and their integral parameters in the surf zone. Focus will be on the improvement of the dissipation term for depth-induced wave breaking for the use in SWAN and other spectral models.

1.3 Outline of the report

First, in chapter 2 an overview of the relevant background theory is given. The basics of the spectral representation and the numerical modelling of waves are briefly discussed. The SWAN wave model is shortly presented.
Chapter 3 provides a review of previous work on wave breaking and its spectral modelling. Models for the frequency integrated energy dissipation are presented and compared, as well as formulations for its spectral distribution. The findings from the literature study offer possible approaches for improvement of the performance of SWAN in the surf zone. These are presented at the end of the chapter.
Wave data sets have been analysed and simulated with SWAN. The results are presented in chapter 4. Again a distinction is made between the total (i.e. frequency-integrated) energy dissipation and its spectral distribution. The results of the analysis give an indication of the most promising alterations of the present spectral source term for wave breaking.
Three different adaptations are proposed for further investigation in this study. Two of these concern the adaptation of the total energy dissipation. The results of the implementation of these two adaptations are presented in chapter 5.
The distribution of energy dissipation over the frequencies has been adapted as well. Chapter 6 presents the results of the implementation of a frequency-dependent dissipation term.
Finally, conclusions and recommendations are stated in chapter 7.

2 Water waves - background theory

2.1 Linear wave theory

Monochromatic waves are defined by a wave height, a wavelength and a wave period. These parameters are clarified in figure 2.1. In order to describe the motion of the water (surface), a single wave is reduced to a sinusoidal form. Although waves on the water surface (e.g. the sea) are seldom sinusoidal, linear wave theory gives a good insight into the physical behaviour of waves.

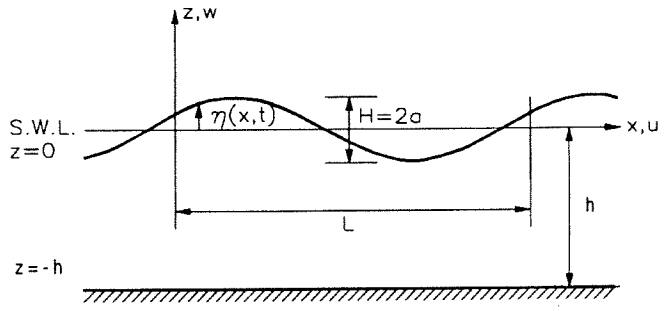

figure 2.1 Definition sketch of a linear sinusoidal wave (source: Young, 1999)

Like any theory, linear wave theory is a model that is based on assumptions. Some important assumptions in linear wave theory are:

- relatively small surface displacements; the wave height is small compared to the wave length and the water depth
- the water is incompressible
- pressure at the water surface is constant and equal to zero
- irrotational movements
- only free surface waves (influenced by gravity) are considered

Without derivation, some important equations that can be used to describe many characteristics of the moving water are given here. The motion of the sea surface is given by:

$$\eta = \frac{H}{2}\cos(kx - \omega t) \tag{2.1}$$

with: H = wave height (m)
k = wave number (rad/m)
ω = angular wave frequency (rad/s)

The dispersion relationship for linear waves states that there is a unique relation between ω, k and the water depth (h) (or T, L and h):

$$\omega^2 = gk \tanh(kh) \tag{2.2}$$

With the dispersion relation expressions for the wavelength (L) and the phase speed or the speed of propagation of a wave (c) can be formulated:

$$L = \frac{gT^2}{2\pi} \tanh\left(\frac{2\pi h}{L}\right) \tag{2.3}$$

$$c = \frac{L}{T} = \frac{\omega}{k} = \sqrt{\frac{g}{k} \tanh(kh)} \tag{2.4}$$

Equation (2.4) indicates that the phase speed varies with water depth. As waves are travelling towards shallower water the wave period remains constant. Hence, according to (2.3) and (2.4) the wavelength and phase speed will both decrease. For given values of ω or k the wave will propagate faster in deep water than in shallow water. The propagation speed also varies with ω and k. Waves with a longer period (or longer wavelength) will propagate faster through water with a given depth than waves with a shorter period (or shorter wavelength).

Waves transfer energy in space. Characteristics of waves, like wave growth and propagation are often described in terms of wave energy and power [BATTJES, 1998]. The energy of a wave per unit area can be shown to be:

$$E = \tfrac{1}{8} \rho_w g H^2 \tag{2.5}$$

The energy that is represented by a group of waves in a wave train does not propagate at the same speed of the individual waves that make up the group (i.e. the phase speed). The energy will propagate at the speed of translation of the group of waves, the group velocity, equal to:

$$c_g = \frac{d\omega}{dk} = \left[\tfrac{1}{2} + \frac{kh}{\sinh(2kh)}\right] c = nc \tag{2.6}$$

The energy flux or wave power, P, is the mean energy transmission in the direction of the propagation per unit time and per unit width. It is given by:

$$P = Ec_g = Enc \tag{2.7}$$

The hyperbolic functions that appear in the relationships of linear wave theory provide a convenient tool for the classification of waves with respect to water depth. The limits of these functions (i.e. $kh \to 0$ and $kh \to \infty$) refer to shallow and deep water (respectively). Table 2.1 gives an overview of the results of the depth classification.

parameter	shallow water $kh < \pi/10$	Transitional water $\pi/10 < kh < \pi$	deep water $kh > \pi$
wave profile	$\eta = a\sin(kx - \omega t)$	ditto	ditto
phase speed	$c = \sqrt{gh}$	$c = g/\omega \tanh(kh)$	$c = g/\omega$
wavelength	$L = T\sqrt{gh}$	$L = gT^2/2\pi \tanh(kh)$	$L = gT^2/2\pi$
angular frequency	$\omega = k\sqrt{gh}$	$\omega = \sqrt{gk \tanh(kh)}$	$\omega = \sqrt{gk}$
group velocity	$c_g = c = \sqrt{gh}$	$c_g = \left[\frac{1}{2} + kh/\sinh(2kh)\right] \cdot c$	$c_g = \frac{1}{2} g/\omega$

table 2.1 Depth classification of linear waves

Assuming that the energy transmission between adjacent lines perpendicular to the wave crest is constant and therefore that no energy is dissipated by wave breaking for example, yields for waves at normal incidence to straight parallel depth contours:

$$E_o n_o c_o = Enc \tag{2.8}$$

in which the zero subscript refers to deep water values. With (2.5) it follows that:

$$\frac{H}{H_o} = K_s = \sqrt{\frac{n_o c_o}{nc}} \tag{2.9}$$

The parameter K_s is called the shoaling coefficient. With decreasing water depth the shoaling coefficient decreases slightly below one before increasing rapidly. As the wavelength decreases with decreasing depth, the wave steepness (H/L) will increase. For a wave that is propagating over a bottom with parallel depth contours at an angle (θ) other than normal, the water depth will vary along the wave crest. Therefore, according to (2.4) the phase speed will also vary along the wave crest. As a result, the crest will tend to bend towards the depth contours. A simple extension of (2.8) yields:

$$Ec_g \cos\theta = \text{constant} \tag{2.10}$$

The wave height variation is then equal to:

$$\frac{H}{H_o} = \sqrt{\frac{n_o c_o}{nc}} \cdot \sqrt{\frac{\cos\theta_o}{\cos\theta}} = K_s K_r \tag{2.11}$$

For parallel depth contours the local direction of wave propagation, θ is given by:

$$\frac{\sin\theta}{c} = \text{constant} \tag{2.12}$$

2.2 Spectral representation of waves

Observations of the sea surface show that real wind waves are far from regular, sinusoidal waves. The water surface elevation appears to be chaotic and complex. This is shown by a time record of the surface elevation.

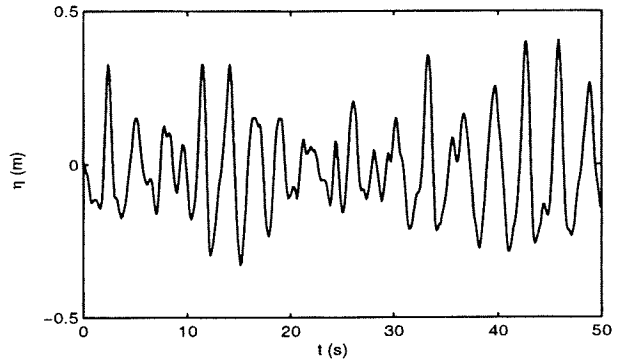

figure 2.2 Typical wave record measured at Lake George, Australia (source: Young, 1999)

In order to describe the chaotic surface elevation, it is considered as a stochastic process. It is common to represent records such as that of figure 2.2 by the use of the random-phase model. The water surface elevation is approximated by the linear superposition of sinusoidal components:

$$\eta(t) = \sum_{n=1}^{N} a_n \sin\left(2\pi f_n t + \alpha_n\right) \tag{2.13}$$

The phases of the components are uniformly distributed between $-\pi$ and π. If the amplitudes a_n are plotted versus frequency, a discrete amplitude spectrum results. The variance of $\eta(t)$ may not change, so for a continuous amplitude spectrum $E(\underline{a}_n) \rightarrow 0$.
The variance of each component (n) is equal to $E(\frac{1}{2}a^2_n)$ and the variance of the total record (which is proportional to the total energy) is:

$$\overline{\eta^2} = E\left(\sum \tfrac{1}{2}\underline{a_n^2}\right) \tag{2.14}$$

The variance in finite frequency bands converges. This can be used to define a continuous function, the variance density spectrum:

$$E(f) = \lim_{\delta f \to 0} \frac{1}{\delta f} E\left(\sum_{\delta f} \tfrac{1}{2}\underline{a_n^2}\right) \tag{2.15}$$

The energy density spectrum can be obtained by multiplying (2.15) by a factor ρg.

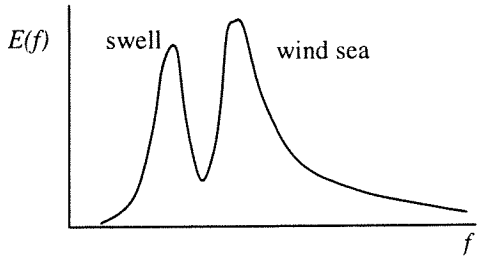

figure 2.3 Example of an energy density spectrum

An extension can be made by including the possibility of wave components propagating in different directions. In a similar manner to $E(f)$ a directional spectrum can be derived, $E(f,\theta)$; it defines the distribution of energy with frequency and direction.

$$E(f)=\int_{-\pi}^{\pi} E(f,\theta)d\theta \tag{2.16}$$

in which $E(f,\theta)$ is often modelled as:

$$E(f,\theta)=E(f)D_f(\theta) \tag{2.17}$$

The phase information represented by α_n has not been taken into account forming the spectrum. The choice of α_n will influence the resulting water surface elevation. However, it will have no influence on the spectrum. The spectrum defines the distribution of energy with frequency but does not describe the actual water surface elevation. Still all statistical characteristics can be derived from the spectrum, as long as the spectral components are independent, i.e. the linear approximation should be applicable. Measures for wave heights and wave periods can easily be obtained with (variance density) wave spectra.
For example, the significant wave height, H_s:

$$H_s=4\sqrt{\iint E(f)dfd\theta}=4\sqrt{E_{tot}} \tag{2.18}$$

the root-mean-square wave height, H_{rms}:

$$H_{rms}=2\sqrt{2}\sqrt{\iint E(f)dfd\theta}=2\sqrt{2}\sqrt{E_{tot}} \tag{2.19}$$

the mean wave period, T_{m01}:

$$T_{m01}=\left(\frac{\iint f\ E(f,\theta)\ dfd\theta}{\iint E(f,\theta)\ dfd\theta}\right)^{-1}=\left(\frac{\iint f\ E(f,\theta)\ dfd\theta}{E_{tot}}\right)^{-1} \tag{2.20}$$

and the mean wave period, T_{m02}:

$$T_{m02}=\left(\frac{\iint f^2\ E(f,\theta)\ dfd\theta}{\iint E(f,\theta)\ dfd\theta}\right)^{-\frac{1}{2}}=\left(\frac{\iint f^2\ E(f,\theta)\ dfd\theta}{E_{tot}}\right)^{-\frac{1}{2}} \tag{2.21}$$

2.3 Development of wind wave spectra

The wave components propagate across the sea from their point of origin. The development of the wave spectrum is influenced by several physical mechanisms: generation by wind, dissipation by bottom friction, white capping, depth-induced breaking and energy transfer by wave-wave interactions.

The evolution of the spectrum is described by:

$$\frac{d}{dt}E(f,\theta)=S(f,\theta) \tag{2.22}$$

The 'source' term $S(f,\theta)$ represents all physical processes which transfer energy to, from or within the spectrum. It can be represented as the summation of a number of independent processes:

$$S=S_{in}+S_{wc}+S_{nl4}+S_{br}+S_{nl3}+S_{bf}+... \tag{2.23}$$

The first three processes on the right-hand side of (2.19) are important for the wave evolution in deep water. They represent input of energy by wind (S_{in}), dissipation by white capping (S_{wc}) and quadruplet wave-wave interactions (S_{nl4}), respectively. The last three represent finite depth effects: depth-induced wave breaking (S_{br}), triad wave-wave interactions (S_{nl3}) and bottom friction (S_{bf}). Young [1999] gives a detailed overview of existing formulations for the processes listed above.

Physical Process	Deep Oceans	Shelf Seas	Shoaling Zone	Harbours
Diffraction	⊙	⊙	○	●
Depth refr./shoaling	⊙	•	●	•
Current refraction	⊙	○	•	⊙
Quad. Interactions	●	●	○	⊙
Triad Interactions	⊙	○	•	○
Atmospheric Input	●	●	○	⊙
White-capping	●	●	○	⊙
Depth Breaking	⊙	○	●	⊙
Bottom Friction	⊙	●	•	⊙

⊙ – negligible; ○ – minor importance; • – significant; ● – dominant.

table 2.2 Relative importance of various physical mechanisms in different domains (source: Battjes, 1994).

In different areas of interest, different mechanisms are important. Table 2.2 gives an overview of the relative importance of the several physical processes. Bottom friction is negligible over the distance of the surf zone. Separate computations with individual processes de-activated have also shown the relatively minor importance of wind generation, white-capping and quadruplet wave-wave interactions in the surf zone [ANDORKA GAL ET AL., 1998]. So, depth-induced wave breaking and triad wave-wave interactions dominate the transformation of the wave spectra across the surf zone and are therefore important in this study. A review of previous work on wave breaking and its spectral modelling is given in the next chapter. The process of non-linear triad interactions is briefly discussed below.

As waves propagate to shallow water the characteristics of the wave field change. From a nearly sinusoidal shape in deep water the waves evolve to a shape with sharp crests and flat troughs in shallow water. This change can be typically attributed to non-linear effects. The influence of non-linear interactions on the frequency spectrum is the energy transfer between spectral components. The influence of these transfers on the shape of the spectrum varies with the shape of the incident (deep-water) spectrum. For narrow-banded incident spectra, the transfer of energy results in secondary peaks at the harmonics of the peak frequency. For

broad-banded spectra, the energy density level increases over a wider range of frequencies above the peak frequency.
Non-linear (triad) interactions only shift energy within the spectrum. The process does not contribute to generation or dissipation of wave energy.

2.4 Numerical modelling of water waves

Numerical wave modelling is aimed at describing and predicting wave evolution from a known (e.g. measured) point (or area) to the area of interest. Generation by wind, white-capping, non-linear interactions, bottom friction, shoaling, refraction and breaking are all involved in practical wave prediction applications. "Accurate prediction of waves requires representation of these physical processes, *as best we understand them*" [YOUNG, 1999].

2.4.1 Classes of models

In general, two classes of numerical wave models can be distinguished: phase-resolving and phase-averaged models. In phase-resolving models the equations are formulated in the time domain or in terms of wave amplitude and phase. These models describe the sea surface elevation in space and time; the instantaneous values of the sea surface elevation are predicted. They are usually based on the mild-slope equations or the Boussinesq equations. Phase-resolving models are computationally demanding compared with the models of the second class and are therefore restricted to smaller domains.
In the second, phase-averaged class of models, the governing equations are formulated in terms of wave energy (or action) density. Phase-averaged models predict integral properties of the wave field. In the simplest form these may be quantities like the significant wave height or peak period. More commonly the evolution of the directional wave spectrum in space and time is predicted. Their computational efficiency makes phase-averaged models feasible for wind wave prediction for the open sea.
With respect to the sophistication of the representation of the source terms in spectral energy models a distinction can be made between first, second and third generation-models.

2.4.2 The SWAN wave model

SWAN is a third-generation spectral wind-wave model, aimed at predicting random waves in coastal regions. It is based on an Eulerian formulation of the discrete spectral balance of wave action density. Action density instead of energy density is considered, because in the presence of currents, action density is conserved, whereas energy density is not. The relation between these quantities is:

$$N(\sigma,\theta)=\frac{E(\sigma,\theta)}{\sigma} \tag{2.24}$$

in which σ is the intrinsic wave frequency.

The evolution of the action density spectrum is described by:

$$\frac{\partial}{\partial t}N+\frac{\partial}{\partial x}c_x N+\frac{\partial}{\partial y}c_y N+\frac{\partial}{\partial \sigma}c_\sigma N+\frac{\partial}{\partial \theta}c_\theta N=\frac{S}{\sigma} \tag{2.25}$$

The first term on the left-hand side of (2.21) represents the local rate of change of action density in time, the second and third term represent propagation of action in geographical space (with propagation velocities c_x and c_y). The fourth term represents shifting of the relative frequency (σ) due to variations in depths and currents. The fifth term represents depth-induced and current-induced refraction. The expressions for the propagation speeds are taken from linear wave theory [BOOIJ ET AL., 1999].

The term S on the right-hand side of (2.24) represents the source term in terms of energy density like in (2.23). The present source term for wave breaking in SWAN is discussed in the next chapter. For an overview of formulations that are adopted in SWAN for the other source terms, the reader is referred to the SWAN user manual [HOLTHUIJSEN ET AL., 2000].

3 Literature review

3.1 Introduction - wave breaking

As waves propagate to shallower water, they increase in height due to the shoaling effect. Theoretically the shoaling coefficient indicates that the wave height will approach infinity in very shallow water. Obviously this is unrealistic. At some depth a wave of given characteristics will become unstable and break.
"The most prominent stage of wave breaking is the initial overturning motion of the wave crest that creates spray and white water, often by the forward projection of a jet of water" [PEREGRINE, 1983]. After breaking the wave either reforms to an unbroken wave with smaller amplitude, or it turns into a bore.

Wave breaking criteria
Much wave-breaking research has been conducted to determine (for given wave characteristics and beach slope) when and where waves will first break and what the maximum breaker height might be. Criteria for incipient wave breaking are usually expressed in terms of a limited wave steepness or a wave height-to-depth ratio. An often-used parameter is the Iribarren or surf-similarity parameter, defined by:

$$\xi = \frac{\tan\alpha}{\sqrt{H / L_o}} \tag{3.1}$$

in which α is the beach slope. The transition between breaking and non-breaking waves on plane slopes is given by a critical value of this ratio, such that breaking occurs for $\xi<\xi_c$ ($\cong$2.3).

The limiting steepness for progressive, periodic waves in any water depth is given by Miche [1944] as:

$$\frac{H_b}{L} = 0.142 \tanh\left(\frac{2\pi h_b}{L}\right) \tag{3.2a}$$

or:

$$H_b \approx \frac{0.88}{k}\tanh(kh) \tag{3.2b}$$

Equation (3.2) indicates that for shallow water the wave height becomes proportional to the water depth (i.e. $H_b \approx 0.88\ h$). In a more general form this can be expressed as the following parameter or 'breaker index':

$$\gamma = \frac{H_b}{h_b} \tag{3.3}$$

When wave decay (of all waves) in the surf zone is estimated with (3.3), it is assumed that the surf zone is saturated. This means that the wave heights in the surf zone are controlled by the local water depth. Any increase in the incident wave energy is dissipated through an increase in wave breaking. Therefore, the wave heights (or energy) in the surf zone are independent of the incident wave heights (or energy). This is generally the case for mildly sloping beaches and with steep incident waves.
However, on steep beaches, or with low steepness incident waves, wave breaking may occur only much closer to or even at the shoreline. As a result, an increase in the offshore incident wave height (or energy) will result in an increase of wave height (or energy). In that case, the surf zone is called unsaturated [BALDOCK ET AL., 1998].

Most existing criteria for wave breaking have been formulated for the breaker height-to-depth ratio γ. It is usually expressed in terms of one or more empirical coefficients or functions, the beach slope ($\tan\alpha$) and wave steepness (H_o/L_o). The Iribarren parameter (3.1) is also used.

Weggel [1972] developed a relationship for γ that is based on small-scale laboratory tests:

$$\gamma = b(\alpha) - a(\alpha)\frac{H_b}{gT^2} \tag{3.4}$$

It appears to yield fairly accurate results for regular waves. The formula is not applicable to irregular waves.

An extensive study of the breaker parameter was carried out by Kaminsky and Kraus [1993]. A large data set containing laboratory test cases from several authors was analysed on depth-limited wave breaking of regular waves, incident to plane sloping beaches. The breaker index was found to be clearly decreasing with increasing (deep-water) wave steepness and increasing with increasing beach slope. An empirical relation for the breaker index as a function of the Iribarren parameter was developed.

$$\gamma = 1.20\xi^{0.27} \tag{3.5}$$

Smith and Kraus [1991] conducted regular and random wave tests to investigate properties of waves breaking over bars and other irregular beach profiles. Significant differences were found in properties such as breaker type and the breaker index, as compared to plane sloping beaches. The breaker type transition values (expressed in terms of the Iribarren parameter) are lower for barred profiles than for plane slopes. Furthermore it was found that for random waves, H_{rms}/h is not constant throughout the surf zone on barred profiles, but exhibits a maximum of nearly unity at the bar crest and a minimum of approximately 0.45 offshore and in the trough.

The data analyses mentioned above were carried out for laboratory data and pertain mostly to regular waves. For random waves, the breakpoint (i.e. the location where incipient breaking takes place) is not well-defined. The largest waves tend to break farthest offshore and the smaller ones closer to the shore. At each location there are broken and unbroken waves (sometimes having the same height) and the percentage of broken waves varies as a function of position.

Nelson [1994, 1997] used field data from the REEF88 experiment, undertaken on the Great Barrier Reef (Australia) to determine the maximum design wave height on a horizontal bed. From the analysis of laboratory data it was already concluded that the characteristics of breaking waves on a gentle slope are not the same as those on horizontal beds. Both for laboratory and field data a maximum value of 0.55 was found for the wave height-to-depth ratio on horizontal beds. For varying bed slopes the maximum wave height-to-depth ratio is given by:

$$\gamma = \left(\frac{H}{h}\right)_{max} = 0.55 + 0.88\exp\left(-0.012\cot\alpha\right) \qquad \text{for } 0<\tan\alpha<0.01 \tag{3.6}$$

However, the data were widely scattered and the formulation describes an upper limit (or envelope curve) for the breaker index fitted through the data. "Such an approach is probably more appropriate for maximum design conditions than for studies on other coastal processes" [SMITH AND KRAUS, 1991]. The expression does not include (deep-water) wave steepness, although the breaker index is often seen to be dependent on this parameter [e.g. BATTJES AND STIVE, 1985; KAMINSKY AND KRAUS, 1993].

Vincent and Smith [2000] have recently formulated an expression that applies to random waves. It is based on their laboratory experiments [Smith and Vincent, 1992] and verified with field measurements at Duck (North Carolina, USA). For both single and double peaked spectra they found:

$$\left(\frac{H_s}{h}\right) = 0.996\exp\left(-50\frac{h}{gT_{mn}^2}\right) \tag{3.7}$$

in which the T_{mn} is defined as the reciprocal of the mean frequency, $f_{mn} = \frac{\int fE(f)df}{\int E(f)df}$.

Breaker types

The Iribarren parameter is also called surf-similarity parameter, as it gives an indication how the waves will break on plane beaches. A continuous gradation of type of initial motion can occur, but generally three breaker types are distinguished:

- Spilling breakers $\xi<0.5$ White water appears at the wave crest and spills down the front face, sometimes preceded by the projection of a small jet. The shape of the wave remains more or less symmetric.
- Plunging breakers $0.5<\xi<3$ Most of the front face of the wave overturns and a prominent jet plunges into the water near the base of the wave.
- Surging breakers $\xi>3$ No significant disturbance of the smooth wave profile occurs except near the moving shoreline.

Sometimes collapsing breakers are distinguished, as a transition between plunging and surging breakers. Collapsing breakers occur at the waterline.

This classification refers to the initial motion. Farther inshore, both spilling and plunging breakers gradually develop into a turbulent bore, of which the properties are mainly controlled by the local depth [BATTJES, 1988].

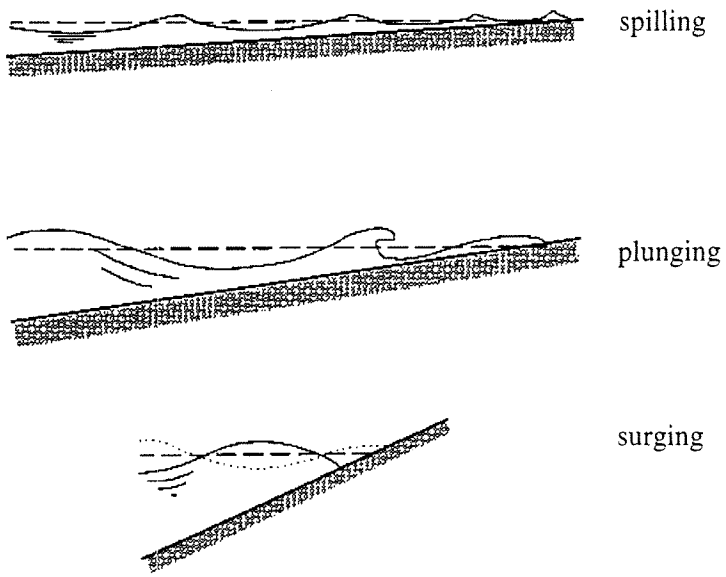

figure 3.1 Types of breaking waves (source: Battjes, 1974)

Incipient wave breaking is an instability, and therefore inherently subject to wide variation for a small change in physical conditions. For example, slight changes in water level or surface conditions like local winds may influence e.g. type of breaking, possible reformation and wave height decay. Altogether, depth-limited wave breaking is an extremely complex process, which is poorly understood.

3.2 Models for the total energy dissipation due to wave breaking

Once waves start to break, turbulent dissipation of the wave energy is the dominant dissipative mechanism. The wave transformation process in the nearshore zone is therefore governed by wave breaking. Models for random wave transformation may generally be divided in two classes; parametric and wave-by-wave models.

In the parametric class of models, a shape of the (breaking) wave height distribution based on locally defined parameters is assumed (a priori). The local, time-averaged dissipation of energy by breaking is used in the energy balance, which is applied across the surf zone to determine the wave transformation.

Models based on the wave-by-wave approach divide the incident distribution of wave heights into a number of discrete classes. "It is assumed that each class behaves like a periodic subgroup, that propagates shorewards independently of the others" [ROELVINK, 1993]. At required locations new probability density functions (pdf) can be constructed.

3.2.1 Parametric models

Parametric models consist of two important elements: the probability of breaking and the dissipation of energy in a single (representative) breaking wave, which are applied to the wave energy balance. Battjes and Janssen [1978] were the first to set up a model for breaking waves like this, and most parametric models are based on their model. Considering only waves normally incident to a coastline with straight and parallel contours and assuming a stationary wave field the wave energy balance reduces to:

$$\frac{\partial\left(Ec_g\right)}{\partial x}+D=0 \tag{3.8}$$

Inside the surf zone dissipation due to wave breaking is dominant. Other energy sinks and sources like bottom friction and wind input are negligible across the surf zone. By integrating (3.8), the variation of the wave energy across the surf zone is obtained.

The total energy dissipation rate is given by the product of the dissipation in a breaking wave (D_b) and the probability of the occurrence of a breaking wave (Q_b). The energy dissipation in a breaking wave is modelled after analogy with a bore of corresponding height.

$$D_b \sim \tfrac{1}{4} f \rho_w g \frac{H_b^3}{h} \tag{3.9}$$

In application to random waves, the mean frequency ($\overline{f}$) of the wave energy spectrum is used as a representative value of the frequency (f). The expression for the maximum breaker height in the model of Battjes and Janssen is based on the Miche criterion (3.2b) and adapted to allow for effects of the bottom slope and the incident wave steepness.

$$H_m = \frac{0.88}{k}\tanh\left(\frac{\gamma kh}{0.88}\right) \tag{3.10}$$

The distribution of all wave heights is assumed to be a Rayleigh distribution, truncated at a maximum (depth-limited) height, such that all breaking waves have a height equal to $H_m=H_b$. The probability of occurrence of a breaking wave or the local fraction of breaking waves is then found from the implicit equation:

$$\frac{1-Q_b}{\ln Q_b} = -\left(\frac{H_{rms}}{H_m}\right)^2 \tag{3.11}$$

The final result for the mean energy dissipation rate per unit area is given by

$$D = \frac{\alpha}{4} Q_b \overline{f} \rho_w g H_b^2 \tag{3.12}$$

The model contains two internal parameters; the coefficient of proportionality α and the breaker parameter γ, which indicates a breaker height-to-depth ratio. These coefficients control the level of energy dissipation in a breaker and the fraction of breaking waves, respectively. Both laboratory and field data have been used by Battjes and Stive [1985] to calibrate the model for α and γ. Effectively, there is only one degree of freedom in tuning the

model. The calibration was carried out by estimating optimal values for γ under the constraint α=1 [BATTJES AND STIVE, 1985]. It was found that there was a relation between γ and the incident wave steepness (s_o) evaluated at the peak frequency of the spectrum (s_o=$H_{rms,o}/L_{o,p}$).

$$\gamma = 0.5 + 0.4\tanh(33 s_o) \tag{3.13}$$

Optimal values of γ fall in a realistic range of 0.60 to 0.83, even though the variation of γ with the wave steepness is opposite to that found from measurements (of periodic waves). Although these values are realistic, they cannot be compared to measured breaker height-to-depth ratios, as the value of α is more or less arbitrarily set equal to 1. However, the wave height variations on both barred and planar beach profiles are predicted reasonably well by the calibrated model.

Several refinements of the model of Battjes and Janssen have been proposed in the literature. These are mostly focussing on the a priori assumed wave height distribution of both non-breaking and breaking waves. According to an analysis of field data by Thornton and Guza [1983], wave heights are reasonably well described by the Rayleigh distribution, even within the surf zone. According to Battjes and Groenendijk [2000] the Rayleigh distribution shows the best performance in a range of intermediate wave heights, but underestimates the lower wave heights and overestimates the higher wave heights. It makes only a relatively small error in the significant wave height, though.
Thornton and Guza [1983] modelled the proportion of breaking waves using an empirical function based on field data. The distribution of breaking waves is expressed using a weighting function of the Rayleigh distribution for all waves:

$$p_b(H) = W(H)\,p(H) \tag{3.14a}$$

in which $W(H)$ is a function that is skewed to the larger waves:

$$W(H) = \left(\frac{H_{rms}}{\gamma h}\right)^n \left[1 - \exp\left(-\left(\frac{H}{\gamma h}\right)^2\right)\right] \le 1 \tag{3.14b}$$

Roelvink [1993] added a depth-limited Weibull distribution to the parametric class of models and compared it to the approaches used by Battjes and Janssen [1978] and Thornton and Guza [1983]. It was found that all three approaches could be used to predict with reasonable accuracy the spatial distribution of the mean wave energy across the surf zone. Like the model of Battjes and Janssen, the models of Thornton and Guza and Roelvink assume saturation in the inner surf zone.

As stated in paragraph 3.1 on steep beaches with low steepness incident waves surf zones may be unsaturated. Saturated and unsaturated surf zones induce different hydrodynamic conditions, which have for example significant implications for sediment transport rates. Recently a parametric model has been developed that addresses this problem [BALDOCK ET AL., 1998]. It incorporates the observation by Thornton and Guza [1983] that the wave heights in the surf zone are best described by a Rayleigh distribution. The proportion of

breaking waves is obtained directly from the Rayleigh distribution, by integrating over all waves for which $H/H_{rms} \geq H_b/H_{rms}$:

$$Q_b = \int_{H^*}^{\infty} 2\frac{H}{H_{rms}} \exp\left[-\left(\frac{H}{H_{rms}}\right)^2\right] d\left(\frac{H}{H_{rms}}\right) \tag{3.15}$$

where $H^* = H_b/H_{rms}$, resulting in a explicit expression for Q_b:

$$Q_b = \exp\left[-\left(\frac{H_b}{H_{rms}}\right)^2\right] \tag{3.16}$$

Equation (3.16) implies for the fraction of breaking waves:

$Q_b = 0$ if $H_b \gg H_{rms}$

$Q_b \to 1$ if $H_b / H_{rms} \to 0$

$Q_b \approx 0.4$ if $H_b / H_{rms} = 1$

The latter result is in contrast to the model of Battjes and Janssen [1978] where all waves are broken if $H_b/H_{rms}=1$, i.e. $Q_b=1$. The breaker height may be evaluated by any of the conventional expressions. The total energy dissipation is calculated by:

$$D_{tot} = \tfrac{1}{4}\rho g \bar{f} \int_{H^*}^{\infty} H^2 p\left(\frac{H}{H_{rms}}\right) d\left(\frac{H}{H_{rms}}\right) \tag{3.17}$$

The results of the Rayleigh model were compared to laboratory measurements on a steep slope. The model provides a better estimation of the nearshore wave heights and the fraction breakers.

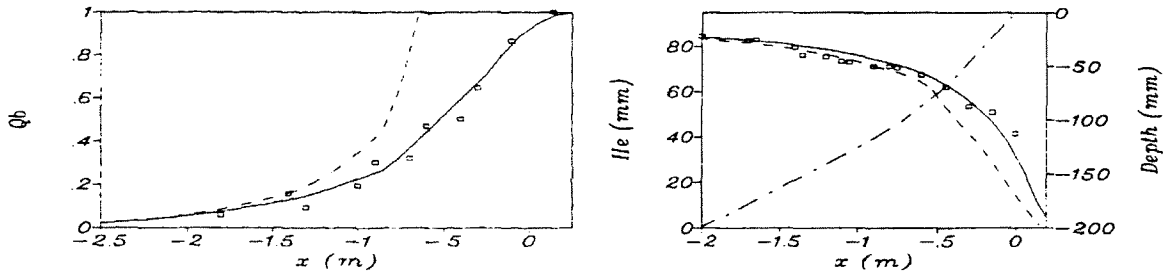

figure 3.2 Measured and predicted cross-shore variation in the fraction of breaking waves (Q_b) and wave height ($H_s=\sqrt{8}m_0$); — Rayleigh model, -- Battjes and Janssen model and —·— beach profile. Incident waves: JONSWAP-spectrum f_p=0.67 Hz. (source: Baldock et al., 1998)

The model is also capable of predicting the wave height transformation across mildly sloping beaches, where the surf zone is saturated. The prediction of the wave height variation is similar to the results of the model of Battjes and Janssen, but the variation of the fraction of broken waves is different. The reason for this is that although the fraction of broken waves is smaller using the Rayleigh model, the model includes a greater rate of energy dissipation from the largest waves in the pdf. The energy dissipation is therefore more realistic than that in the Battjes Janssen model, since large broken waves will clearly dissipate more energy than small broken waves [BALDOCK ET AL., 1998].

More authors have addressed the prediction of the fraction of breaking waves by the model of Battjes and Janssen. According to Kuriyama [1996], Rivero et al. [1994] and Southgate and Wallace [1994] the fraction of breaking waves is not predicted accurately by Q_b. The largest deviations from measurements occur for bar-trough profiles, as wave reforming is not considered. The persistence of breaking is not reproduced. The model determines Q_b entirely in terms of local parameters and has no knowledge of wave behaviour at previous points along the profile. This behaviour tends to be masked on monotonically sloping beaches because breaking is continuously re-triggered. Southgate and Wallace [1994] describe a method that introduces a persistence length of breaking waves. The variations in Q_b are smoother than in the model of Battjes and Janssen, but are not as accurate as in the Rayleigh model of Baldock et al [1998].
It should be noticed however, that the parameter Q_b in the Battjes and Janssen model was never meant to predict the fraction of breaking waves and that the model only implicitly uses this parameter.

3.2.2 Probabilistic wave-by-wave models

Mase and Iwagaki [1982] adopted the wave-by-wave method of modelling random wave transformation in the nearshore. However, their model is limited to use on planar beach profiles.
Dally [1990] developed a wave-by-wave model for the pdf of wave heights in the surf zone for planar beaches and verified it later for use on shore profiles of arbitrary shape as well. Individual waves are shoaled until the condition for incipient breaking according to Weggel [1972] (3.4) is satisfied. The formulation for wave height decay that is used relates the dissipation rate to the excess energy contained in the wave above a stable limit:

$$\frac{\partial Ec_g}{\partial x} = -\frac{K}{h}(Ec_g - Ec_{g,s}) \tag{3.18}$$

in which K is a decay coefficient. The stable limit ($Ec_{g,s}$) is defined in terms of a stable wave condition ($H_s = \Gamma h$). It allows broken waves to reform if they cross a trough feature.
Histograms of wave heights are predicted quite well, although observed histograms evolve never as peaked and narrow as predicted by the model.
The model is only verified for conditions of unidirectional swell. In the presence of both swell and sea the model is not accurate.

Roelvink [1993] derived a model using the wave energy balance (3.8). The dissipation in a breaking wave is calculated by using the bore analogy and the probability of breaking is assumed to be only depending on local and instantaneous wave parameters:

$$P_b(E,h) = 1 - \exp\left[-\left(\frac{E}{\gamma^2 E_{ref}}\right)^{n/2}\right] \quad \text{with } E_{ref} = \frac{1}{8}\rho g h^2 \tag{3.19}$$

An exponential distribution for the wave energy, which is equal to a Rayleigh distribution for the wave height, is given as a number of energy levels, with decreasing probability of exceedance. For each deep-water energy level the energy balance is solved. As a result a

number of (wave energy decay) lines, starting at deep water at a certain energy level with corresponding probability of exceedance, will represent this probability throughout the surf zone.
The model was compared to laboratory measurements for single peaked wave conditions on both barred and planar profiles. Qualitatively, the results obtained by the model show good agreement with measurements, quantitatively it underestimates the wave height. This is probably due to the presence of long waves (slowly varying water levels). In the model the higher waves are limited by the mean local depth, in reality they are limited by the slowly varying depth.

Measurements obtained from the DUCK '85 experiment show that, although starting as a Rayleigh distribution, the pdf shape undergoes considerable transformation across the surf zone. According to Dally [1990] the vast majority of laboratory and field data indicate that inside the surf zone the Rayleigh pdf is not a valid assumption. It is also well established that due to non-linearity in waveform, the free surface displacement is non-Gaussian.

The major assumption in the wave-by-wave approach is that shoaling and breaking are not affected by wave-wave interaction. The classes of waves are propagated independently of the others towards the shore, using a monochromatic wave model. Secondly, slowly varying water level fluctuations must be minimal [BALDOCK ET AL., 1998]. This makes the applicability of these models limited.

3.3 Spectral distribution of energy dissipation due to wave breaking

Both classes of models mentioned in the previous paragraph do not provide any information about the spectral distribution of the dissipated energy due to the breaking of waves. Formulations for the spectral distribution of the total energy dissipation are mostly based on observations. Three different approaches can be distinguished: the spectral shape approach, frequency-dependent formulations and relaxation of the spectrum to an empirical equilibrium.

3.3.1 Spectral shape approach

Experiments were carried out by Battjes and Beji [1992] to investigate breaking waves propagating over a submerged bar. By normalisation of measured spectra (such that the area under the spectra is equal to unity) the development of the wave spectrum for breaking and non-breaking cases was compared. Figure 3.3 shows some of the comparisons.

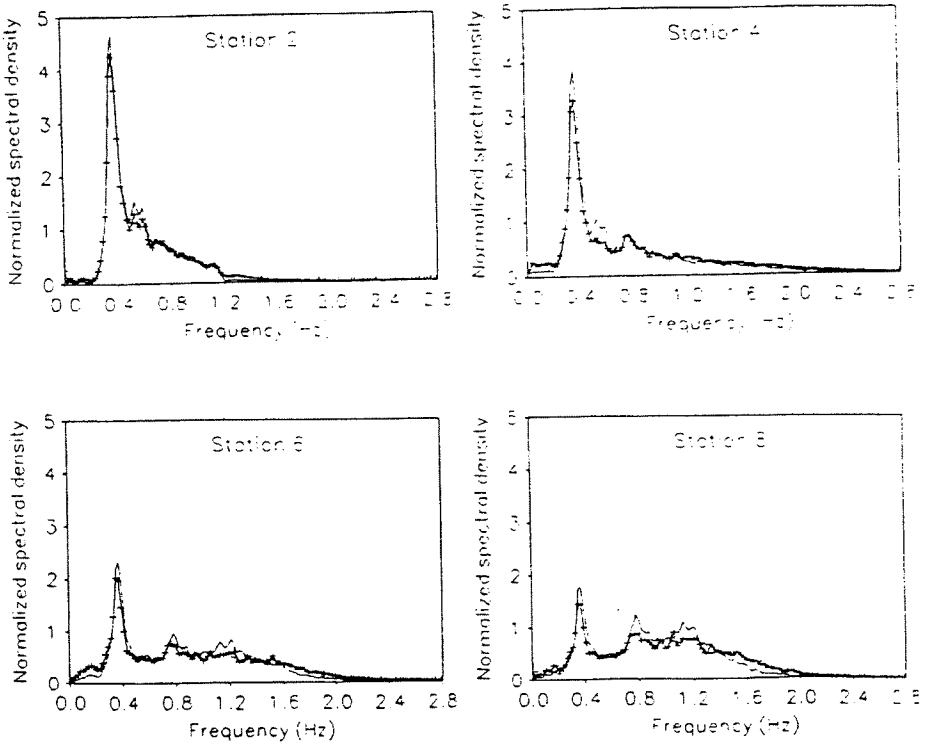

figure 3.3 Normalised spectra at different stations in the surf zone; ++ plunging breakers, — non-breaking waves. Incident waves; JONSWAP-spectrum with f_p=0.4 Hz. (source: Battjes and Beji, 1992).

The normalised spectra for the breaking and non-breaking cases are roughly the same. This was also observed for other wave conditions. From these results it is concluded that the spectral shape is not significantly affected by wave breaking, but that wave breaking contributes in proportion to the local spectral energy density level [BATTJES AND BEJI, 1992]. More laboratory measurements have been examined, all with single-peaked spectra [VINCENT AND SMITH, 1994 and ARCILLA ET AL., 1994]. The same results were found; the shape of initially unimodal spectra propagating across beach profiles is fairly insensitive to depth-induced breaking. This conclusion is not entirely correct, though. If that would be so, then non-linear triad interactions would relatively have had the same effect in the breaking and non-breaking cases. This is certainly not the case for such a highly non-linear process. The comparison of the normalised spectra shows that the *combined effect* of the non-linear interactions and breaking does not influence the shape of the spectrum.

However, it has been found that modelling the spectral distribution of energy dissipation due to wave breaking, such that it does not affect spectral shape, has given accurate results [see e.g. BATTJES ET AL., 1993 and ELDEBERKY AND BATTJES, 1996]. The spectral breaking term is based on the total (frequency-integrated) rate of energy dissipation by breaking and can be formulated as:

$$S_b(f) = -\frac{D_{tot}}{\int_0^\infty E(f)df} E(f) \tag{3.20}$$

It is stressed that only single-peaked spectra are considered. It may be expected that for combinations of sea and swell the low-frequency waves are less affected by breaking than the higher frequency components [ELDEBERKY AND BATTJES, 1996].

3.3.2 Frequency-dependent formulations

Based on a comparison of calculated and measured spectral energy densities Mase and Kirby [1992] deduced a form for a damping coefficient (α), applied to the component amplitudes (a_n) in the Boussinesq equations. Restricting attention to wave breaking effects, the evolution equation was written as:

$$a_{n,x} = -\alpha_n a_n + \ldots \tag{3.21}$$

The coefficient was found to be partly proportional to the frequency squared. This resulted in the following equation:

$$\alpha_n = \beta_0 + \left(\frac{f_n}{\overline{f}}\right)^2 \beta_1 \tag{3.22}$$

with:

$$\beta_0 = FD_{tot} \tag{3.23}$$

and:

$$\beta_1 = (1-F)D_{tot}\frac{\overline{f}^2 \sum a_n^2}{\sum f_n^2 a_n^2} \tag{3.24}$$

D_{tot} is determined from a bulk dissipation model as in (3.12). The free parameter F controls the relative importance of the two terms. For F=1 the dissipation is distributed proportional to the energy density at each frequency (as suggested by Battjes and Eldeberky [1996]).

Chen et al. [1997] examined the optimal values for F for model simulations of different data sets with a wide range of wave conditions (single and double peaked spectra) and beach profiles (barred and plane sloping). The optimal values of F for the cases considered span the entire range from 0.0 to 1.0. Roughly it can be stated that for bimodal spectra the optimal value for F is lower than for unimodal spectra. So for dual peaked spectra, relatively more energy is dissipated by wave breaking at the higher frequencies.
Chen et al. [1997] found that the predicted spectra are fairly insensitive to the frequency dependence of the dissipation. This has also been concluded from the validation tests that were done with SWAN by Booij et al. [1999]. It appears that in the models there is a preferred spectral shape that is obtained in shallow water, for which the reasons are still unclear. The effect of redistributing the loss differently across the spectrum serves mainly to enhance or suppress the non-linear transfer of energy needed to maintain the target spectral shape [KIRBY AND KAIHATU, 1996]. However, errors in the predicted skewness and asymmetry (i.e. statistical measures of the wave shapes) appear to increase with increasing F. So in contrast to the insensitivity of predicted spectral levels, model predictions of skewness and asymmetry are sensitive to the frequency dependence of the dissipation [CHEN ET AL., 1997; KIRBY AND KAIHATU, 1996; BOOIJ ET AL., 1999].

Breaking-induced dissipation and non-linear triad interactions dominate the spectral evolution of wave fields in the surf zone (see section 2.4). So if directional spreading of waves and reflection from the shore is neglected, there is a balance in the surf zone between the cross-shore gradient of the energy flux spectrum $F_x(f)$ on the one hand and a non-linear source term, $S_{nl3}(f)$ and a dissipation term, $S_{br}(f)$ that accounts for depth-induced breaking on the other.

$$F_x(f)=\frac{\partial}{\partial x}\left(c_g(f)E(f)\right)=S_{nl3}(f)+S_{br}(f) \tag{3.25}$$

The energy flux spectrum can be evaluated from measurements at adjacent instruments in the cross-shore array. With an accurate approximation of the triad wave-wave interaction term, the cross-shore development of the spectral 'source' term for depth induced breaking can be inferred. Elgar et al. [1997] approximated the non-linear energy transfer between two points with a (non-dissipative) Boussinesq model. For field cases with varying wave conditions it was shown that inferred dissipation rates in the surf zone increase with increasing frequency. Such an approach has also been applied by Herbers et al. [2000]. Using field observations from a dense cross-shore array of pressure sensors on a barred beach, an accurate estimation of the (development of) the non-linear source term across the surf zone is made. The results of one case are shown in figure 3.4.

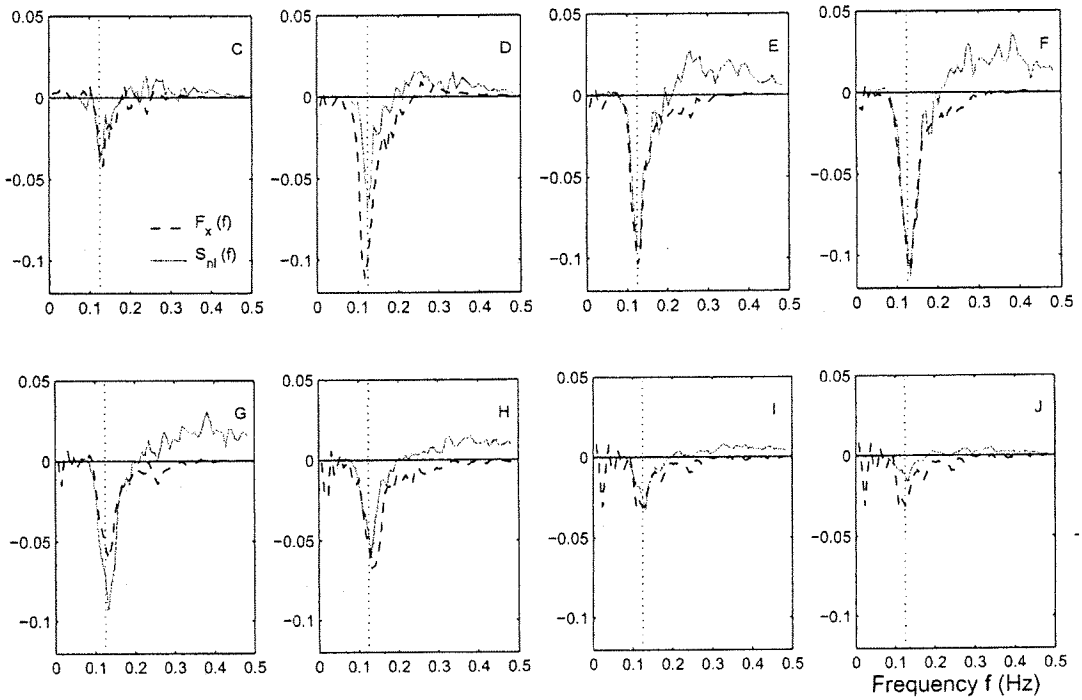

figure 3.4 Comparison of the energy flux gradient $F_x(f)$ with the non-linear source term $S_{nl}(f)$ in Duck '94 case II, location C farthest offshore, location J closest near shore (source: Herbers et al., 2000)

The observations include narrow spectra of remotely generated swell, broad spectra of locally generated seas and bimodal spectra of mixed swell-sea conditions. Analysis of the results indicates that the observed decay of wave spectra in the surf zone is primarily the result of non-linear energy transfers to higher frequencies and that dissipation occurs in the high-frequency tail of the spectrum where energy levels are relatively low [HERBERS ET AL, 2000]. As stated before, it is possible to infer the spectral 'source' term for depth-induced breaking in every case. This has not been done, though.

Smith and Vincent [1992] conducted laboratory tests to investigate the development of double-peaked spectra. It was found that when wave breaking occurred the energy level was lowered from the low-frequency peak through all the higher frequencies. The energy level at the low-frequency peak is only weakly reduced. This peak became the dominant peak of the spectrum as the waves shoaled and broke. By simulating each peak in the bimodal spectra as a separate wave train, the developments of single-peaked and double-peaked spectra were compared. The higher frequencies have significantly lower energy levels in the dual peak case than in the equivalent single-peak case. The higher frequencies appear to be strongly affected by the presence of a low-frequency peak. However, the results were obtained from simplified laboratory results. The effect of having the wave trains approach the beach at different angles or having different directional spreads is not considered.

3.3.3 Empirical spectral equilibrium

To some extent, the shape of growing wind wave spectra in deep water is subject to similarity laws. The similarity form in deep water is thought to arise due to a balance between atmospheric input, transfers within the spectrum due to non-linear interactions and dissipation. Using a dimensional analysis argument, with the gravitational acceleration (g) as the only relevant parameter, Phillips [1958] showed that:

$$E(f) \sim g^2 f^{-5} \tag{3.26}$$

However, it was not specified in what depth this hypothesis would be valid. Kitaigorodskii et al. [1975] applied the similarity principles of Phillips [1958] to spectra in finite depth, where the water depth (h) also becomes a relevant parameter. With g and h as governing parameters in the saturation range, they showed that the frequency wave spectrum is given by:

$$E(f) \sim f^{-3} \tag{3.27}$$

Thornton [1977] derived the saturation range for frequency spectra with the wave celerity (c) as the relevant parameter at breaking. Although the derivation of Thornton [1977] is different, it agrees both with the –5 slope in deep water and the –3 slope suggested by Kitaigorodskii et al. [1975] for shallow water.

Bouws et al. [1985] have presented a parameterised spectral shape to describe waves in water of finite depth. The hypothesis that the evolution of wave spectra in shallow water may also be approached through similarity principles is investigated with three data sets; Texel, MARSEN and ARSLOE. This resulted in a parameterised spectral shape, the TMA-spectrum. The proposed spectral form is written as:

$$E(k) \sim k^{-3} \psi(k, f_m, H) \tag{3.28}$$

where ψ is a spectral shape function [BOUWS ET AL., 1985].

It should be noted, however, that the research was mainly confined to the area outside the surf zone.

Recently an algorithm for breaking, based on a parameterised shape of the high frequency tail of the spectrum in the surf zone has been developed [VINCENT AND SMITH, 2000]. By re-analysing laboratory data [SMITH AND VINCENT, 1992] they found that the transformation process across the surf zone pushes multi-peak spectra towards a single peak located at the initial low-frequency peak. A joint action of non-linear interactions and dissipation is assumed to establish the following equilibrium range:

$$E_{eq}(k) = \alpha_0 \beta g^{-0.5} k^{-2.5} \tag{3.29}$$

with $\beta = 5.0\, c_{mn}(H_s/d)$ and c_{mn} the phase speed at the mean frequency $f_{mn} = E_{tot}^{-1} \int fE(f)df$.

Dissipation as a function of frequency is determined by the spectral deviation from (3.29) and scaled by the intensity of breaking as measured by H_s/d (according to 3.7).

$$D(f) = \left[E_{eq}(f) - E(f)\right] \Phi\left(\frac{H_s}{d}\right) \tag{3.30}$$

Non-linear interactions are parameterised as a function of the wave height-to-depth ratio. Details of the harmonics are not accurately represented.
The method is computationally efficient. It is applied to both single-peaked and double-peaked spectra and yields satisfactory results (figure 3.5). It should be noticed, however, that relaxation to an empirical equilibrium spectral shape is a second-generation approach.

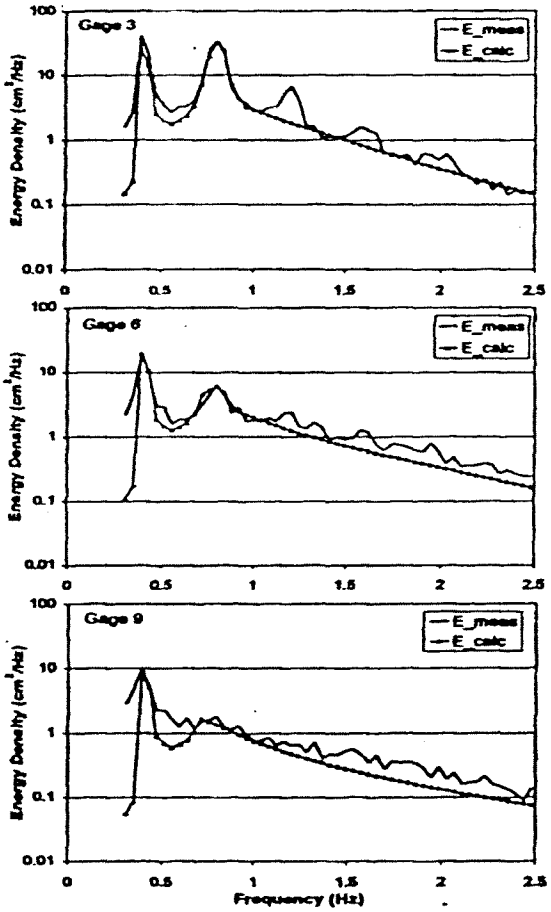

figure 3.5 Comparison of measured and calculated spectra for case 1 of the Smith and Vincent data set [1992] (source: Vincent and Smith, 2000).

3.4 Present source term for depth-induced wave breaking in SWAN

The present formulation for the source term for dissipation by depth-induced breaking is based on the observations of Battjes and Beji [1992], Vincent et al. [1994] and Arcilla et al. [1994] that the shape of initially unimodal spectra propagating across beach profiles is not affected by depth-induced breaking. Eldeberky and Battjes [1996] showed that such an approach applied to Boussinesq equations yielded reasonably accurate results. Including directions the expression in SWAN is:

$$S_{br}(\sigma,\theta) = -\frac{D_{tot}}{\int_{-\pi}^{\pi}\int_{0}^{\infty} E(\sigma,\theta)\,d\sigma\,d\theta} E(\sigma,\theta) \tag{3.31}$$

D_{tot} is calculated with the model of Battjes and Janssen [1978]. From validation tests, the results from SWAN runs appeared to be fairly insensitive to frequency-(in)dependency [BOOIJ ET AL., 1999].

The maximum wave height (H_m) in the dissipation model is governed by the breaker parameter γ. The default value of the breaker parameter in SWAN is equal to 0.73, which is the average of the calibration of Battjes and Stive [1985].
SWAN is locally defined and therefore the expression for the breaker parameter derived by Battjes and Stive [1985] (3.13) cannot be included, as it is dependent on the deep-water wave steepness. In general, the deep-water wave steepness is not a suitable parameter, as this value is not (always) well-defined.
However, Baaijens [1998] has shown that using (3.13) to adapt the γ-values improves the prediction of the significant wave heights, but worsens the predicted mean wave period.

3.5 Possible approaches for improvement of S_{br}

The findings from the literature review offer various possible approaches for improvement of the spectral modelling of wave breaking. The present formulation in SWAN for depth-induced wave breaking consists of two important elements: the frequency-integrated (total) dissipation rate according to the parametric model of Battjes and Janssen [1978] and an assumed spectral distribution of the total dissipation (i.e. the dissipation is proportional to the energy density level at each frequency). The possible approaches for improvement of the performance of SWAN in the surf zone are divided according to this distinction.

Frequency-integrated dissipation rate

- At present, the breaker height-to-depth ratio γ is held constant across the surf zone in SWAN, with a default value of 0.73. Several authors have formulated empirical expressions for γ as a function of the beach slope and the wave steepness. Battjes and Stive [1985] estimated optimal values for γ (as a calibration of the model of Battjes and Janssen [1978]). Their expression is a function of deep-water wave steepness. This is not

a convenient parameter in (spectral) models. The accuracy in the prediction of variation of the wave heights across the surf zone could possibly be improved by implementation of an expression for γ that incorporates the local wave steepness.

- At present the maximum wave height is frequency-independent. It might be possible to express the breaker height as a function of frequency ($H_m=H_m(f)$) and combine it with a joint probability of wave height and frequency (or wave period), $p(H,f)$ [BATTJES AND JANSSEN, 1978].

- The probability of occurrence of breaking in the model of Battjes and Janssen [1978] is estimated with Rayleigh distribution of the wave heights that is truncated at a maximum breaker height H_m. Application of the full Rayleigh distribution for the wave heights as proposed by Baldock et al. [1998] might improve the predictive capabilities of SWAN for the wave height (especially on steep beaches or with low steepness incident waves). Moreover the fraction of breaking waves appears to be better predicted by the Rayleigh model.

- The present dissipation model does not reproduce the persistence of breaking waves. The fraction of breaking waves, Q_b is determined in terms of local parameters. Although Q_b in the model of Battjes and Janssen was never meant to give a(n) (accurate) prediction of the fraction of breaking waves, incorporation of the persistence of wave breaking may be an improvement.

Spectral distribution of energy dissipation

- Introduction of a (quadratic) frequency dependency (similar to (3.22)). Although according to some authors [e.g. CHEN ET AL., 1997; KIRBY AND KAIHATU, 1996; BOOIJ ET AL., 1999] calculated energy spectra are insensitive to such a dependency, Herbers et al. [2000] showed that dissipation by wave breaking is indeed dependent of frequency.

- If (more) observations show that the high-frequency tail of the spectra in the inner surf zone evolves to a saturation range such as (3.29), this might be used to formulate a distribution of the energy dissipation as a function of (the deviation of the spectral energy density level at each frequency from) this saturation range.

- Recently a formulation has been developed for dissipation by white capping [HOLTHUIJSEN ET AL., 2000]. It enhances dissipation at the higher frequencies when low frequency waves (swell) is present. Depth-induced wave breaking is affected by low frequency waves in a similar way (see section 3.3.2). The formulation can be used to increase dissipation by depth-induced breaking at the higher frequencies as well.

The possible approaches for improvement mentioned above might not all be effective. In order to determine what the most promising alterations to the present source term for wave breaking are, the performance of SWAN with default settings should be examined first. This is done in the next chapter.

4 Analysis and simulation of wave data

4.1 Introduction

In this chapter three wave data sets are considered. The first data set contains observations of waves off the Dutch coast near the town of Petten. The second data set contains data of waves observed in a laboratory experiment, carried out by Smith and Vincent [1992]. The third data set includes four field cases from the Duck '94 field experiment. All three data sets are analysed with regards to the development of the wave spectrum across the surf zone.
The Petten data and the data of Smith and Vincent (SV) have also been simulated with SWAN. The results of the calculations of both integral spectral parameters and spectra are compared to measurements. Because only a 1D-profile of the bathymetry at Duck was available, these cases have not been simulated with SWAN.

It has already been stated that the present formulation for depth-induced wave breaking in SWAN consists of two elements: first the frequency-integrated energy dissipation due to depth-induced wave breaking is calculated, which is then distributed over the frequencies (see chapter 3). This distinction is also made in this chapter. After a description of the wave data that were used and the applied model settings, the results of the SWAN runs with respect to the significant wave height (~ total energy) are discussed first. Then the results with respect to mean wave periods, i.e. T_{m01} or T_{m02}, (~ relative energy distribution) will follow. Next, the calculated wave spectra are discussed. From the analysis of the SWAN results, compared to the measurements, the most promising alterations are inferred. These are discussed in the last paragraph.

4.2 Description of wave data

4.2.1 Field observations near Petten

Since the fall of 1994 the Dutch National Institute for Coastal and Marine Management/RIKZ has been running a measurement campaign near Petten at the Dutch North Sea coast. The campaign was set up to provide hydraulic input parameters for safety analysis along the Dutch coast.
The Petten field site consists of a cross-shore array of instruments, measuring wind, (mean) water level and wave data (i.e. surface elevations and wave run-up). In table 4.1 an overview is given of the instruments relevant for this study.

location code	distance to dike crest	sensor	measured parameters
MP 1	8300/8050* m	directional waverider	surface elevation wave direction
MP 2	3500 m	waverider	surface elevation
MP 3	620 m	stepgauge digital level meter	surface elevation (mean) water level
MP 5	290 m	directional waverider	surface elevation wave direction
MP 6	135 m	capacity wire anemometer wind vane	surface elevation wind speed wind direction

* distance in 1995 and 1999 respectively

table 4.1 Overview of relevant instruments at the Petten field site

Only wave data that have been obtained during storms in 1995 and 1999 were available and appropriate for this study. In 1995, a northwestern storm occurred on January 1st and 2nd, and another one on January 10th. For 1999 storm data were only available for February 23rd.

The sea bed near Petten is characterised by a bar-trough profile with nearly parallel depth contours. However, depending on the wave conditions, the exact depth profile can change significantly during storms. Obviously, the bathymetry is an important parameter when investigating depth-induced wave breaking. For both 1995 and 1999 only one bottom profile is available though[1]. Figure 4.1 shows the bathymetry at the Petten field site for January 1st.

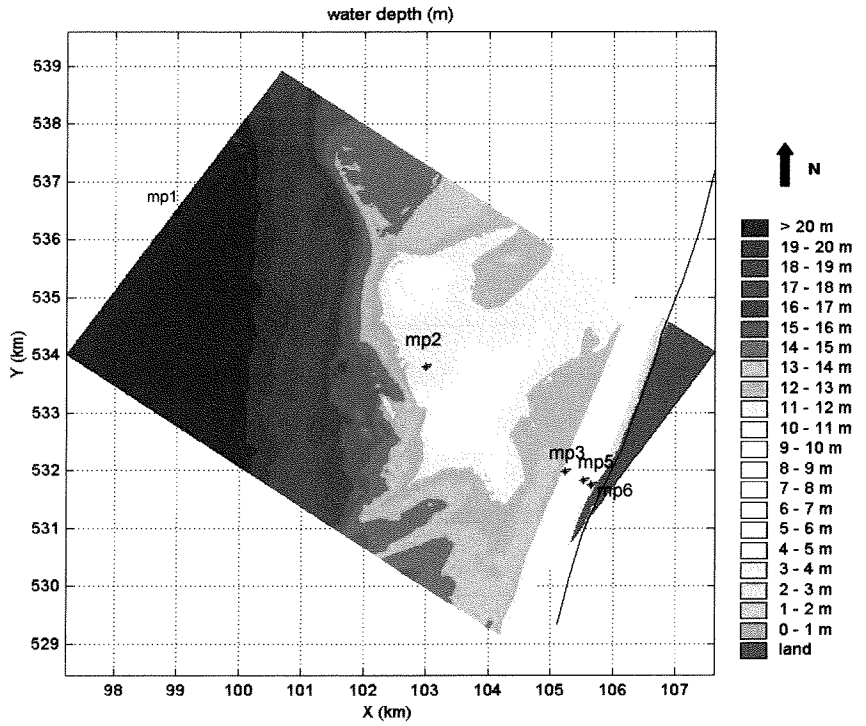

figure 4.1 Water depth at the Petten field site, January 1st 1995, 05:00h (Parisian co-ordinates)

[1] Fortunately, the depth surveys took place close to the storm dates, in November '94 and in March '99

Figure 4.3 shows the 1D-bottom profile and the locations of the instruments. The depth profiles of 1995 and 1999 only differ within the surf zone.

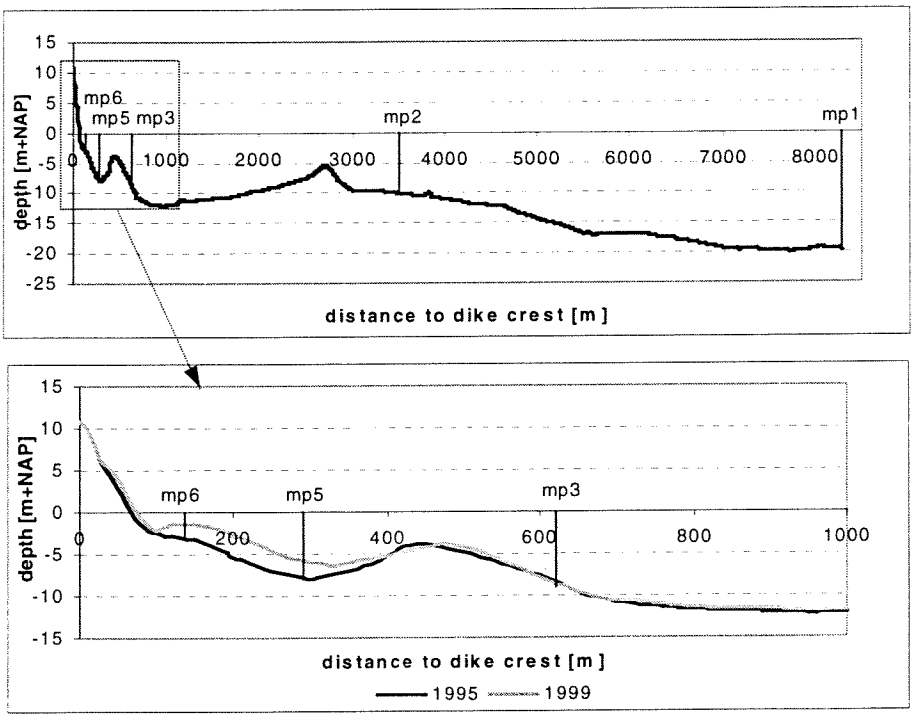

figure 4.2 Cross-shore bottom profile and measurement locations at Petten

Seven cases have been selected for simulation with SWAN in this study. In 1995 the suitable data were limited due to the malfunctioning of the capacity wire at MP 6. This instrument was only working at higher water levels. Instruments at MP 1, MP 2, MP 3 and MP 5 were working well in 1995. Available data in 1999 were also limited. On February 23rd only MP 1, MP 3 and MP 6 produced reliable data.
Spectra have been constructed from time series of surface elevation with a duration of 20 minutes. Generally, wave conditions are considered stationary in such an interval. Therefore the cases have been selected at times when the (mean) water level was more or less constant (i.e. high tide or low tide), see appendix 4A. In table 4.2 the selected cases have been outlined.

date	time	water level [m+NAP[2]]	$H_{s,mp1}$ [m]	θ waves (cartesian)	wind speed [m/s]	θ wind (cartesian)
01-01-95	05:00	1.47	3.60	330	16.0	302
01-01-95	18:20	1.92	5.06	315	19.5	281
02-01-95	06:00	1.58	5.39	335	19.0	309
02-01-95	17:00	1.66	3.77	330	12.0	350
10-01-95	11:40	2.04	4.12	335	13.5	274
23-02-99	00:40	1.05	4.53	310	19.0	305
23-02-99	04:40	0.10	4.23	305	13.0	335

table 4.2 Parameters of the wave climate in the selected cases

[2] NAP is the Dutch reference level.

4.2.2 Laboratory data of Smith and Vincent

Smith and Vincent [1992] carried out laboratory experiments to examine the development of double-peaked spectra across the surf zone. The tests were performed at the US Army Engineer Waterways Experiment Station, Vicksburg, USA. The configuration of the wave flume is shown in figure 4.3.

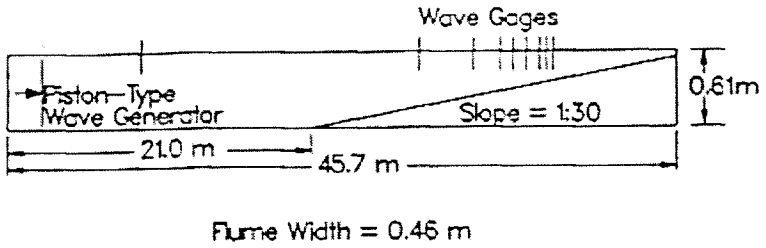

figure 4.3 Flume configuration in experiments of Smith and Vincent

The flume is 45.7 m long, 0.45 m wide and was used with a water depth of 61 cm. The bottom of the flume is smooth concrete and rises at a slope of 1:30 from the middle of the flume. In this configuration, the reflection coefficients are in the range of 5-10%. Nine electrical-resistance gauges were in still water depths of 61.0 cm, 36.6 cm, 24.4 cm, 18.3 cm, 15.2 cm, 12.2 cm, 9.1 cm, 7.6 cm and 6.1 cm [SMITH AND VINCENT, 1992].
Twelve cases have been investigated, differing in the position and the energy density level of the two peaks. The four most energetic cases (i.e. cases 1, 3, 7 and 9) of the Smith and Vincent dataset (hereafter referred to as SV) have been selected for simulation with SWAN in this study. These cases are outlined in table 4.3.

case	$T_{p,low}$ [s]	$T_{p,high}$ [s]	$E_{p,\,low}/E_{p,high}$	incident H_s [cm]
1	2.5	1.25	1:2	13.54
3	2.5	1.25	2:1	14.50
7	2.5	1.75	1:2	13.98
9	2.5	1.75	2:1	14.51

table 4.3 Selected cases with relevant parameters

4.2.3 Field data of Duck '94

During September and October 1994 data were collected on a barred ocean beach near Duck, NC, USA. A dense cross-shore array of 13 pressure sensors was deployed between the shoreline and about 350 m offshore. Four cases that span a wide range of wave conditions have been used by Herbers et al. [2000] to investigate the spectral energy balance across the surf zone (see section 3.3.2). For each case the 1D-bottom profile is available (figure 4.4). The depth profiles for cases I and II are almost equal. In case III and IV the bar is located farther offshore.

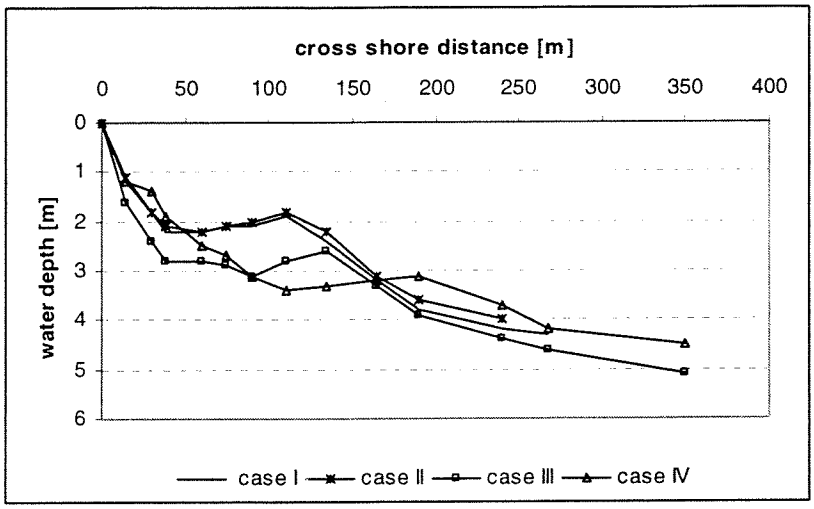

figure 4.4 Depth profiles for each case at Duck

Case I is characterised by small non-breaking waves. Cases II-IV are far more energetic. In cases II and III, taken from storms, an irregular surf zone with spilling breakers extended across the entire array of instruments. In case IV, during the waning of a storm, directionally narrow, moderately energetic swell was observed. This case is characterised by a narrow surf zone [HERBERS ET AL., 2000].

The spectra and 1D-bottom profiles have been digitised from Herbers et al. [2000]. In this study, the spectra have been used to examine the spectral shape, in particular the high-frequency tail of the spectrum in the surf zone.

4.3 Model settings for the SWAN computations

In this paragraph the model settings for the SWAN computations is discussed. SWAN cycle III, version 40.11 is used. The SWAN-input files for one Petten case and for one SV case are shown in appendix 4B.

Grids and resolutions

The simulation of the Petten cases is executed in the stationary two-dimensional mode. The offshore boundary is located approximately 8300 m from the shoreline. The length of the computational grid is 8500 m in cross-shore direction and 6000 m in longshore direction. The resolution used in the computational grid is chosen equal to the resolution of the available bottom profile: $\Delta x = 20$ m and $\Delta y = 20$ m. The spectral directions cover the full circle in 36 directional bins ($\Delta\theta = 10^{\circ}$). The observed energy density is almost zero for $f > 0.5$ Hz, therefore f_{high} is chosen equal to this value. The minimum frequency (f_{low}) is chosen equal to 0.03 Hz.

The SV cases have been computed in the stationary one-dimensional mode. The applied resolution of the computational grid is $\Delta x = 0.05$ m. The spectral directions cover a sector of 30° (15° on either side of the mean wave direction) in 60 directional bins ($\Delta\theta = 0.5^{\circ}$). The frequency range ($f_{low}$-$f_{high}$) is chosen equal to 0.25 –3.00 Hz.

Physics
Both the computations of the Petten cases and of the SV cases are executed in the third-generation mode. Besides the physical processes that are activated in the default option (wind growth, quadruplet interactions and white capping), non-linear triad interactions, bottom friction, depth-induced wave breaking and wave-induced set-up are activated. All relevant parameters are set at default values.

Boundary conditions
In the Petten cases the two-dimensional spectra at deep water are taken from the observations at MP 1 (directional waverider). The obtained (directional) spectra are also applied as boundary conditions at the lateral boundaries, to reduce the error caused by the lack of wave information there[3].

In the SV cases, the spectra observed at the wave gauge that is located in a depth of 61.0 cm are used as offshore boundary condition. However, no information of the directional spread is available from the measurements. As waves in a flume are long-crested a small directional spread is chosen: $\sigma_\theta = 5^\circ$. This seems reasonable for flume conditions. The sensitivity of the results of the computations to different directional spreads is examined. The results are shown and discussed in appendix 4C. The results of the computations appear to be fairly insensitive to the different directional spreads that have been tested.

4.4 Transformation of the significant wave height across the surf zone

Petten cases
An example of a comparison of the measured and calculated cross-shore transformation of the significant wave height is given in figure 4.5. The results of the simulation of all cases are presented in appendix 4D.
The measurements show a consistent trend for all seven cases. From the offshore boundary (MP1) the significant wave height (H_s) slightly decreases towards MP 2. No measurements are available on or right after the first bar (approximately 2700 from the dike crest), which would probably show a distinct decrease in H_s. Between MP 2 and MP 3 H_s can increase due to wind growth. MP 3 is located on the seaward edge of the second bar (approximately 500 m from the dike crest). Increased wave breaking occurs here and H_s is reduced at this location. Wave breaking on the second bar causes a sharp decrease in the significant wave height between MP 3 and MP 5. Between MP 5 and MP 6 the water depth steadily decreases, resulting in a decreasing H_s, due to wave breaking.
A comparison of the cases in 1995 with the cases in 1999 shows that wave breaking is more intense for the 1999 cases. In figure 4.2 it can be seen that in 1999 the bottom at MP 5 and MP 6 is significantly higher in 1999 than it was in 1995.

[3] The locations of the lateral boundaries have been varied (+500 m and +1000 m on either side to investigate the effect of this boundary error. The results of the calculations appeared to be hardly affected by these variations.

The results of the calculations of H_s are also very similar in all seven cases. The SWAN calculations indeed show a decrease in H_s at the first bar. Then, in the trough H_s increases again, due to wind input and shoaling. Wave breaking at the second bar and near the shoreline causes a reduction in H_s.

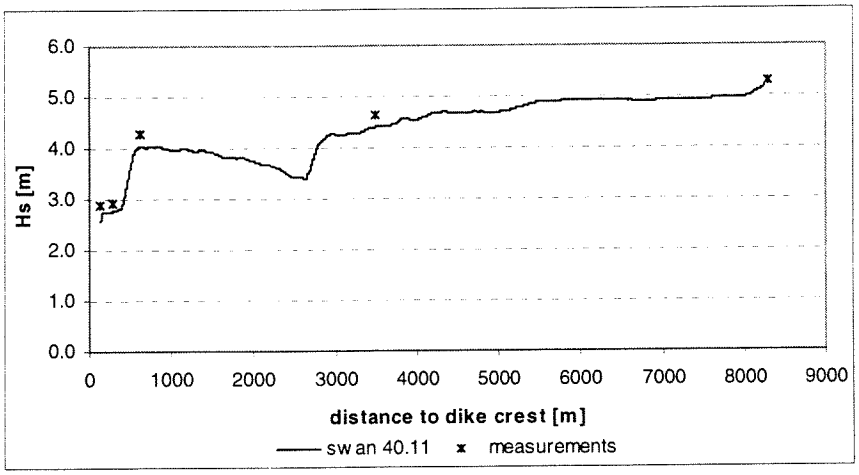

figure 4.5 Cross-shore variation of significant wave height in Petten case 02-01-95, 06:00h

The results of the SWAN simulations show a cross-shore variation of the significant wave height that is similar to the measurements. However, at all measurement locations SWAN underestimates the significant wave height. The largest deviations occur at MP 6; the wave heights calculated by SWAN differ about 6-18% from the measurements. Apparently, SWAN is overestimating the dissipation by wave breaking[4].

SV cases

The measurements of the laboratory experiment show results as expected. In figure 4.6 a comparison is made between the measured and the calculated variation in significant wave height in case 1. The results for the all cases are presented in appendix 4E.

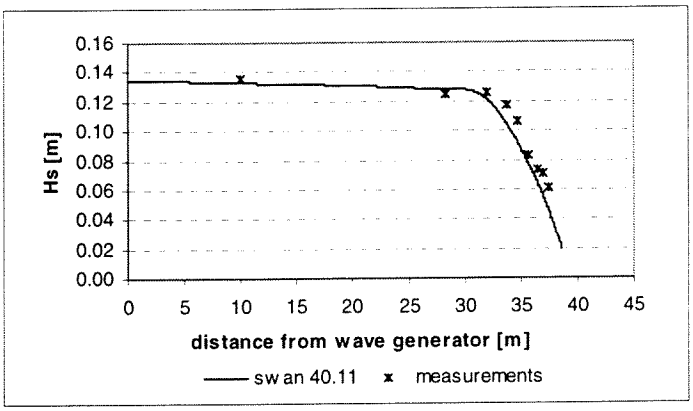

figure 4.6 Variation of significant wave height in SV case 1

In the first part of the flume the significant wave height remains roughly constant over the change in water depth from 61 to 24 cm. For depths less than 20 cm, the wave height decays

[4] Bottom friction is negligible over the distance of the surf zone.

monotonically. The SWAN results show a similar trend, but in all cases SWAN underestimates the significant wave height.
The difference between the measurements and the SWAN calculations increases with decreasing water depth. At the first measurement location where wave breaking (i.e. d = 18.3 cm) occurs, the calculated significant wave height differs 8-12% from the measurements. At the shallowest location the error has increased up to 19-27%. Again, it appears that SWAN is overestimating energy dissipation due to wave breaking.

4.5 Transformation of mean wave periods across the surf zone

Petten cases
The measurements show that the mean wave period decreases slightly towards MP 6. Triad interactions shift energy from the lower to the higher frequencies. So in the surf zone, the wave spectra have relatively more energy at higher frequencies than spectra farther offshore. Figure 4.7 presents a comparison of measured and calculated mean wave periods (T_{m01}) for case 02-01-95, 06:00h. The results of all cases are presented in appendix 4F.

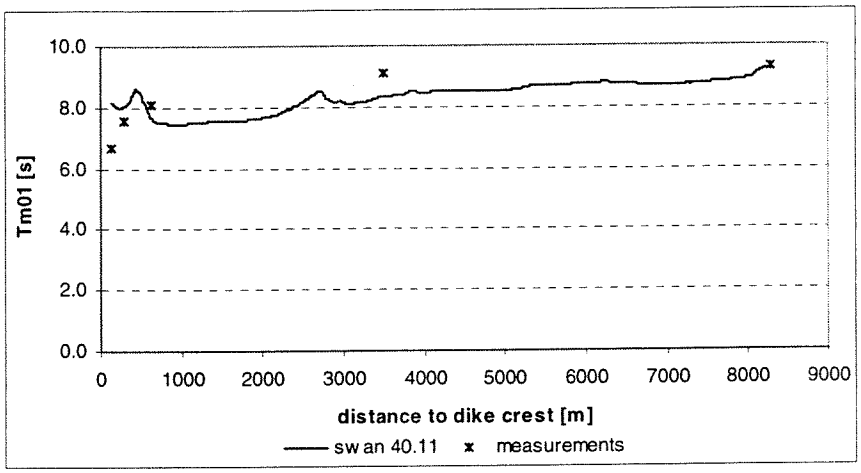

figure 4.7 Cross-shore variation of the mean wave period in Petten case 02-01-95, 06:00h

The decrease in the mean wave period towards MP6 (caused by the triad interactions) is not represented in the calculations. However, except for the shallowest station (MP 6) in 1995, the predictions of the mean wave period by SWAN are quite accurate (deviations from measurements are smaller than 10%). Specifically for the 1999 cases the predictions are remarkably good. For the 1995 cases SWAN overestimates the mean wave period at MP6 by about 15-25%. Apparently, the calculated spectra contain too much energy at lower frequencies.

A possible explanation of the difference in accuracy in the prediction of the mean wave period at MP 6 between the 1995 cases and the 1999 cases can possibly be found in the effect of the non-linear triad interactions. The effect of these interactions increases with decreasing water depth. In 1999 water depths in the surf zone are much lower than in 1995. So for the 1999 cases, relatively more energy is shifted towards higher frequencies, resulting in a lower mean wave period. Appendix 4G presents a comparison of the scaled source term for triad

interactions at MP 6 (S_{nl3}/E_{tot}) for a 1995 case and a 1999 case. The effect is indeed smaller for the 1995 case.

SV cases

In the measurements the mean wave period decreases in first part of the surf zone (in water depths from 61 to 15 cm). This is caused by triad interactions that shift energy to higher frequencies within the spectrum (see paragraph 4.6). Approaching the water line, in the inner surf zone, where intense wave breaking occurs, the mean wave period increases again. Dissipation by wave breaking appears to be higher at higher frequencies.
The SWAN results show a different variation of the mean wave period. In figure 4.8 the results for T_{m01} for case 1 are presented. The results of all cases are presented in appendix 4H. Throughout the entire surf zone the calculated mean wave period decreases steadily.

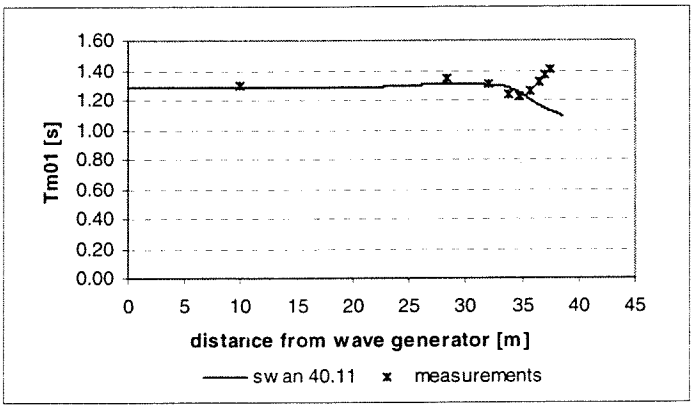

figure 4.8 Variation of the mean wave period in SV case 1

The present source term for wave breaking in SWAN does not influence the shape of the spectrum. The effect of the non-linear triad interactions on the relative distribution of energy (i.e. shifting energy to higher frequencies) is therefore not annulled by wave breaking in the calculations, resulting in decreasing mean wave periods across the surf zone.

Although the trend in the calculated mean wave period is consistent for the four simulated cases, there is a striking difference between cases 1 and 7 on the one hand and cases 3 and 9 on the other. In cases 1 and 7, SWAN *under*estimates the mean wave period in the inner surf zone by about 10-20 %.

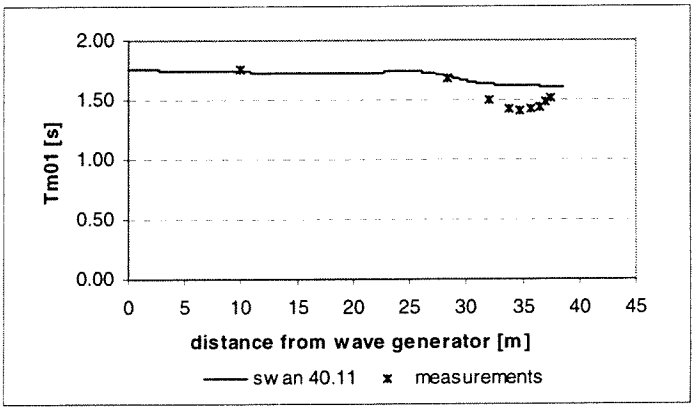

figure 4.9 Variation of the mean wave period in SV case 3

In the inner part of the surf zone SWAN *over*estimates the mean wave period by 5-15% for cases 3 and 9 (see figure 4.9). The differences between the calculations and the measurements are also smaller for these cases.

In case 1 and 7 the *high*-frequency peak contains more energy than the *low*-frequency peak (see table 4.3). The measurements show that in the (inner) surf zone the high-frequency peak decays faster than the low-frequency peak and the mean wave period increases accordingly. As wave breaking in SWAN does not affect the spectral shape, this is not the case in the calculations.
In case 3 and 9 the *low*-frequency peak contains more energy than the *high*-frequency peak. The bimodal character of the spectra in these cases is less distinct than in case 1 and 7 (see paragraph 4.6). In SWAN calculations relatively more energy is contained at lower frequencies, resulting in a higher mean wave period.

4.6 Evolution of the spectral shape in the surf zone

4.6.1 Development of the wave spectrum across the surf zone

Petten cases
In figure 4.10 the spectra for Petten case 02-01-95, 06:00h are shown. The spectra of all cases are presented in appendix 4I.

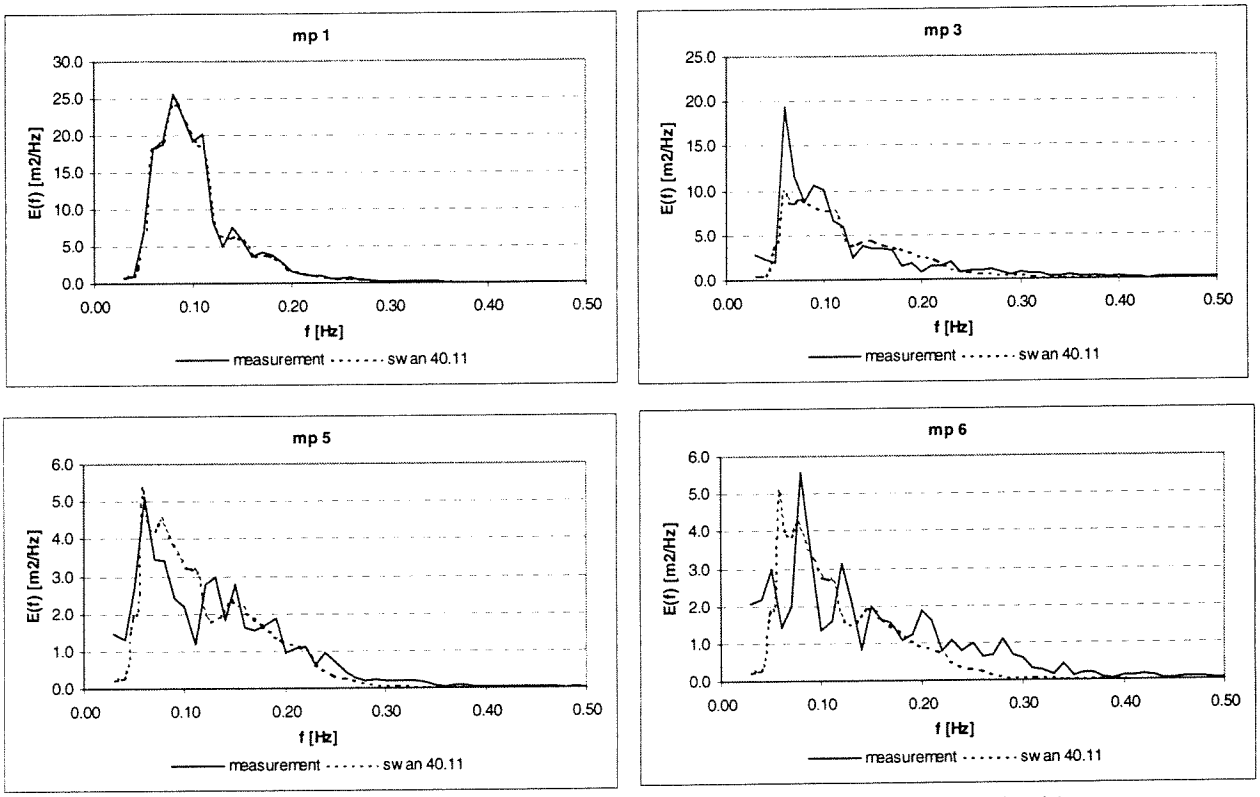

figure 4.10 Evolution of the wave spectrum in Petten case 02-01-95, 06:00h (scaled energy density levels)

The differences in both total energy and the distribution of energy over the frequencies between the measured and the calculated spectra increase shorewards. The measured spectra contain more energy than the calculated spectra, leading to a higher significant wave height in the measurements (see paragraph 4.4).
The measurements show a relative increase in the energy density levels at higher frequencies towards the shore. This is caused by the triad interactions that shift energy from the lower frequencies to the higher frequencies.
The SWAN calculations show less energy at the higher frequencies. In the computations the initial shape of the spectra is more or less maintained, resulting in a steeper high-frequency tail at the shallowest station. A comparison of the source terms for wave breaking and for non-linear triad interactions shows that relative to wave breaking the triad interactions have little effect in the calculations (see appendix 4G). The source term for breaking does not affect the shape of the spectrum. This explains why in the calculations the shape of the spectrum is not changed much across the surf zone.
The energy level at the peak of the spectrum is predicted fairly accurately by SWAN. The accuracy in the location of the peak varies from case to case.

SV cases

Figure 4.11 shows the measured and calculated spectra for case 1 (spectra for all cases are shown in appendix 4J).

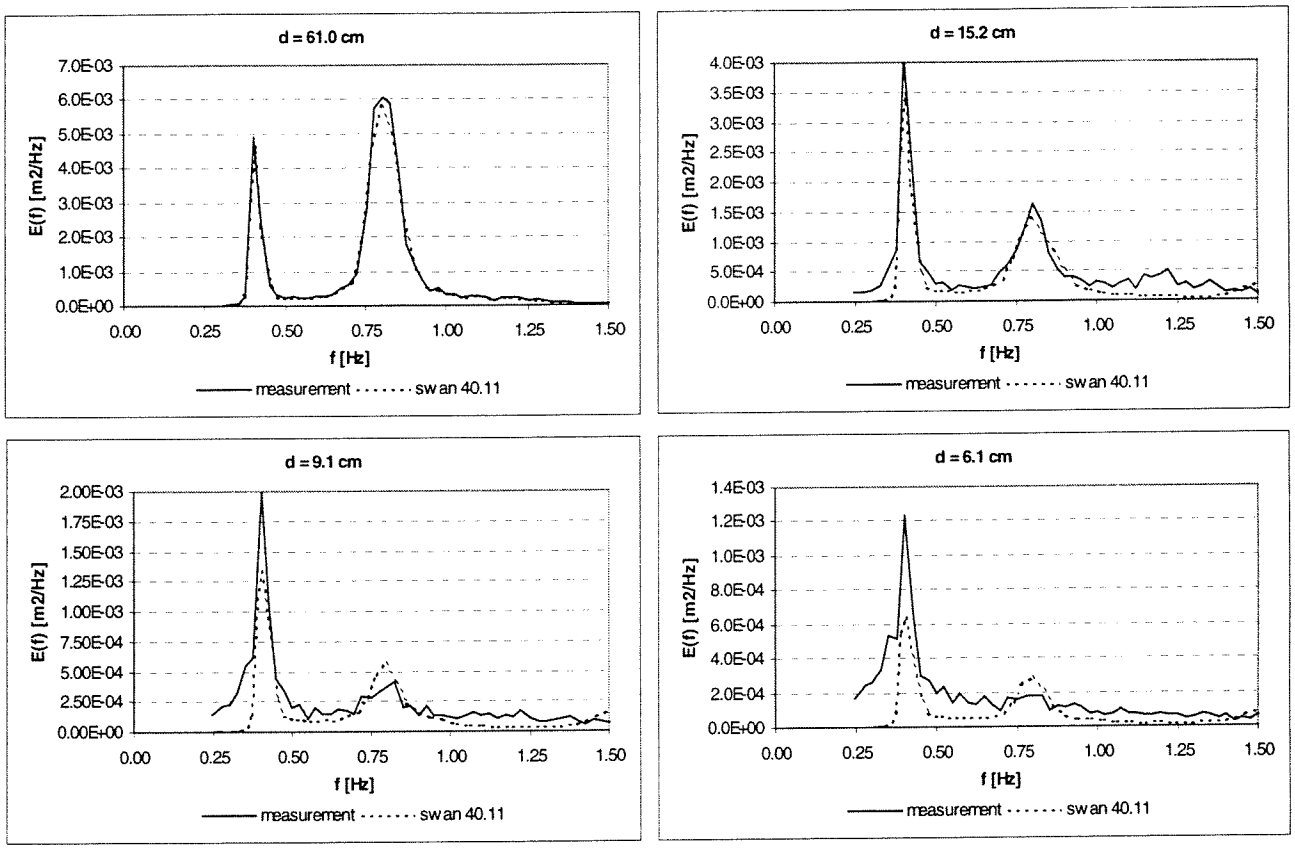

figure 4.11 Evolution of the wave spectrum in SV case 1 (scaled energy density levels)

The trend in the evolution of the measured spectra is very similar for each case. Across the surf zone the low-frequency peak becomes the dominant peak. The dissipation of energy at

the low-frequency peak is initially low. Wave breaking lowers the energy level from the low-frequency peak through all higher frequencies. At the shallowest wave gauge, all energy peaks above the low-frequency peak have been eliminated by wave breaking.

Again some differences between the calculations and the measurements can be explained by the fact that the source term for wave breaking is frequency-independent and conserves the spectral shape. Firstly, in the SWAN calculations the high-frequency peak is maintained throughout the surf zone.
Secondly, the amount of energy at the peak frequency is *under*estimated for cases 1 and 7. In these cases there was initially little energy at the low-frequency peak. The measurements show that the low-energy peak is relatively weakly reduced. As the shape of the spectrum is more or less conserved by SWAN, the computed spectra show too little energy at the lower frequencies, leading to an underestimation of the mean wave period in the surf zone.(see paragraph 4.5).
The energy density level at the peak frequency is *over*estimated for cases 3 and 9, i.e. the cases with initially more energy at the low-frequency peak (see figure 4.12). In the measurements more energy is shifted to higher frequencies, that smoothes the tail of the spectrum (see section 4.6.2). Due to the conservation of the spectral shape (by wave breaking), the computed spectra have too much energy at the lower frequencies, resulting in a overestimation of the mean wave period in the surf zone (see paragraph 4.5).

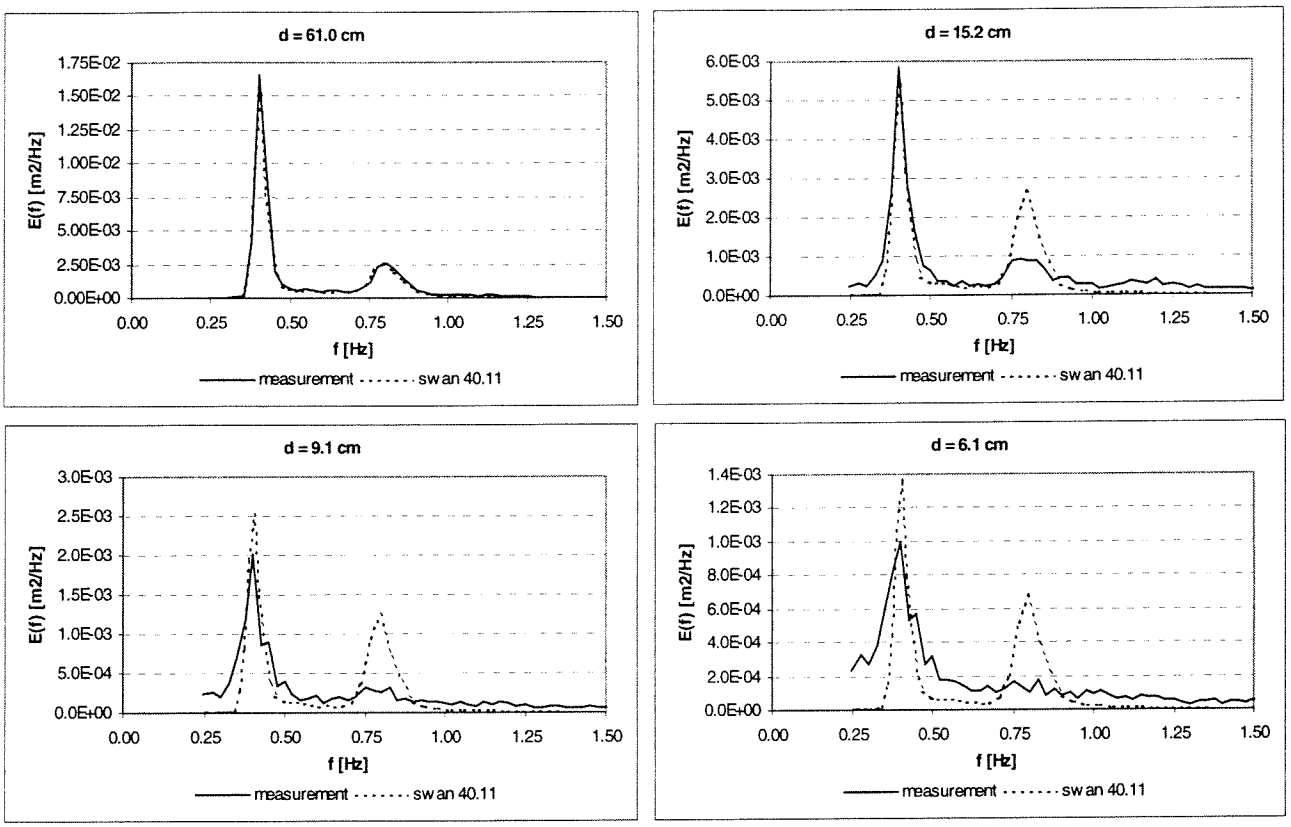

figure 4.12 Evolution of the wave spectrum in SV case 3 (scaled energy density levels)

Thirdly, in the range of 0.50 Hz – 0.75 Hz and for high frequencies (f>0.90 Hz) the calculations show too little energy at the shallowest station(s). The high-frequency tail of the measured spectra is much smoother than the tail of the calculated spectra.

4.6.2 Shape of the high-frequency tail in the surf zone

Vincent and Smith [2000] show that in the breaker zone the high-frequency tail of initially double-peaked spectra in their laboratory experiments evolves to a $k^{-2.5}$-equilibrium range (see paragraph 3.3). This is attributed to a combined effect of the triad interactions and wave breaking. However, the effect of wave breaking on the spectral distribution of energy is not clear [VINCENT AND SMITH, 2000].
The equilibrium range form is given as:

$$E_{eq}(k) = \alpha_0 \beta g^{-0.5} k^{-2.5} \tag{4.1}$$

in which α_0 is a constant and $\beta = 5.0\ c_{mn}(H_s/d)$.

From figure 4.11, figure 4.12 and appendix 4J it is obvious that the shape of the spectra calculated by SWAN in the SV cases does not comply with this equilibrium range.

The high-frequency tail of the spectra at the offshore boundary and at the shallowest station of the Petten cases and the Duck '94 cases have been examined. In order to investigate whether the evolution of the spectra of field data is similar to those in laboratory experiments, the measured spectra in the surf zone are compared to the equilibrium range given by (4.1).

Petten cases
In all Petten cases the high-frequency tail of the spectrum at the offshore boundary (MP1) is proportional to $k^{-3.0}$ (see figure 4.13 and appendix 4K).

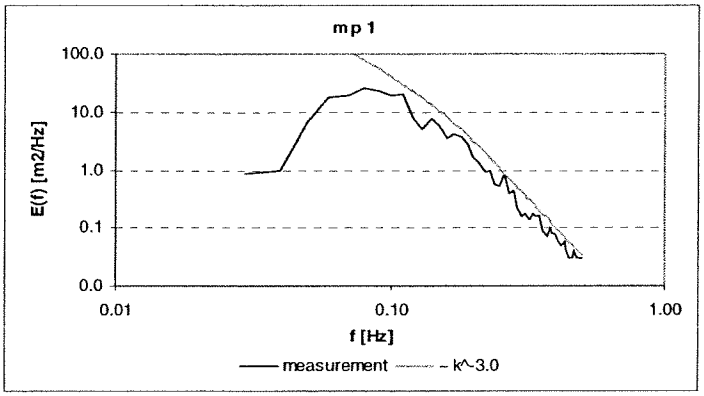

figure 4.13 Spectra and approximation of high-frequency tail at MP1 in Petten case 02-01-95, 06:00h

In figure 4.14 the spectra at MP 6 for Petten case 02-01-95, 06:00h are plotted on linear, semi-logarithmic and double-logarithmic scale. Equilibrium ranges proportional to $k^{-2.5}$ and proportional to $k^{-3.0}$ are plotted as well (see appendix 4K for all cases).
The $k^{-2.5}$-equilibrium range proves to be a good approximation of the high-frequency tail of the measured spectra in shallow water. It should be noted that the value of the parameter α_0 had to be adjusted to fit equation (4.1) through the data. With $\alpha_0 = 0.0085$-0.0090 for the 1995 cases and $\alpha_0 = 0.0045$-0.0050 for the 1999 cases the $k^{-2.5}$-equilibrium range describes the high-frequency tail of almost all measured spectra remarkably well. The parameter α_0 probably depends on the bottom profile. This would explain the difference in the optimal

values of α_0 for the 1995 cases and the 1999 cases. As stated before, the bottom at MP 6 is considerably lower in 1995 than it was in 1999.

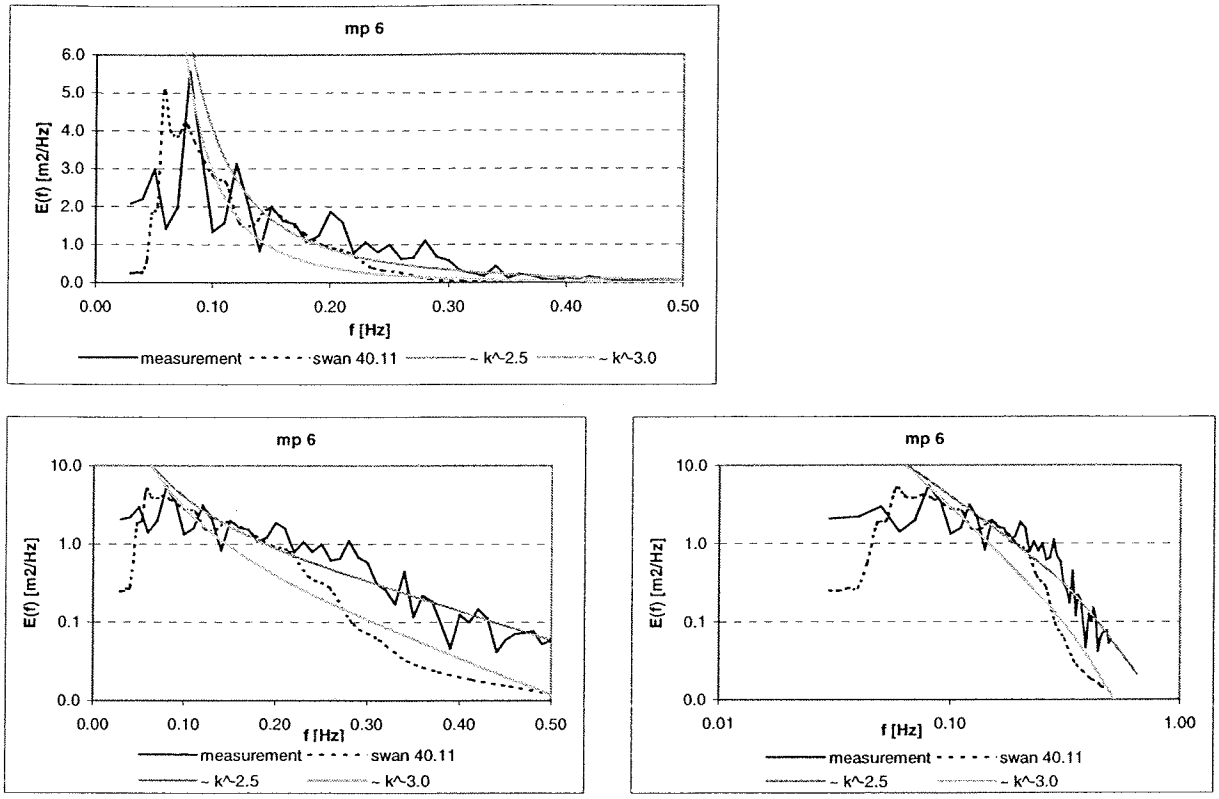

figure 4.14 Spectra and equilibrium range at MP 6 in Petten case 02-01-95, 06:00h

It appears that the high-frequency tail of the spectra calculated by SWAN is steeper than in the measurements. The tail of the computed spectra appears to be approximately proportional to $k^{-3.0}$. So the steepness of the tail of the spectrum is not altered (much) by SWAN. This corresponds with section 4.6.1.

Duck '94 cases

The tails of the spectra measured at the offshore boundary in the DUCK '94 cases are steeper than in the Petten cases. In all cases the tail of the spectrum is proportional to $k^{-3.5}$ (see figure 4.15 and appendix 4L).

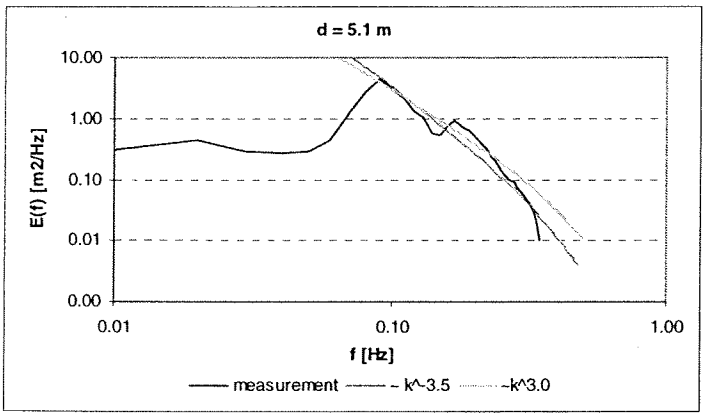

figure 4.15 Spectrum and approximation of high-frequency tail at the offshore boundary in DUCK '94 case III

Figure 4.16 presents the spectra and the equilibrium ranges ($\sim k^{-2.5}$ and $\sim k^{-3.5}$) on linear, logarithmic and double-logarithmic scale.

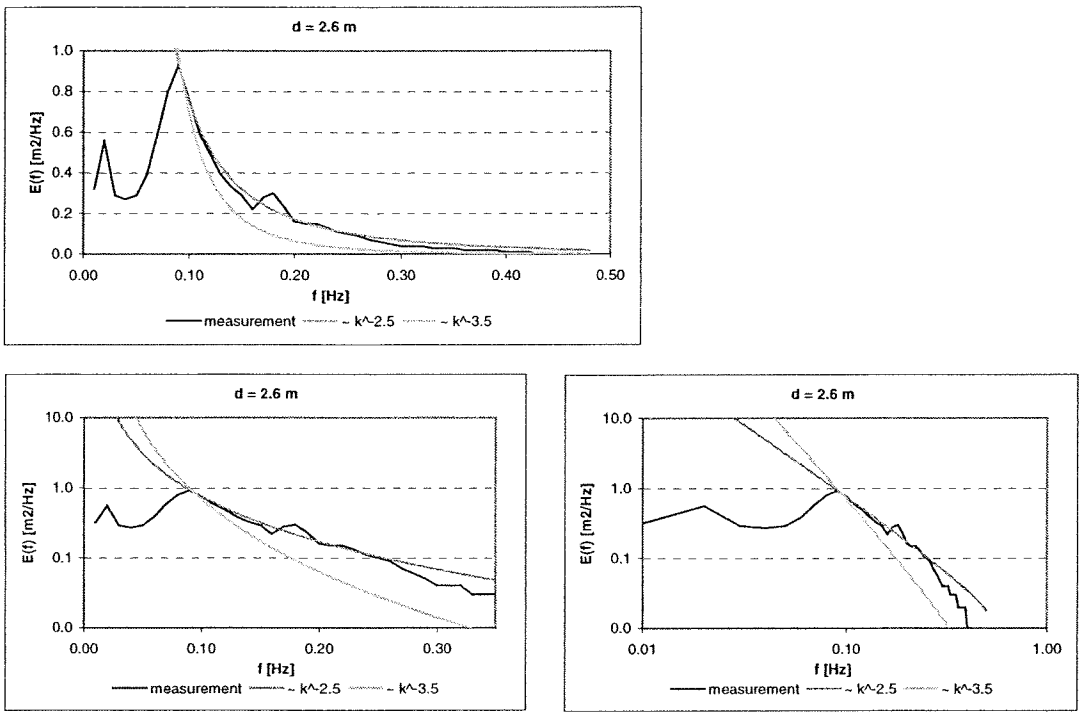

figure 4.16 Spectrum and equilibrium range in the inner surf zone in DUCK '94 case III

Except for case I, the $k^{-2.5}$-equilibrium range gives an accurate prediction of the measured spectra in the breaker zone. In case I, however, wave breaking only occurred at the water line. The other three cases (i.e. II, III and IV) are more energetic and wave breaking occurred along the entire array of instruments. In these cases the tail of the spectra in the surf zone is well described by the $k^{-2.5}$-equilibrium range. So wave breaking seems to influence the evolution of the spectra to saturation in very shallow water.

Like for the Petten cases, the constant α_0 had to be adjusted to fit (4.1) to the measurements. For case II (and I) the optimal value of α_0 was $\pm$ 0.0060. For case III and IV the optimal value of α_0 was $\pm$ 0.0035. Once more it seems that this parameter depends on the bottom profile. Figure 4.4 shows that the bottom profile for case II (and I) differs considerably from the bottom profiles for case III and IV. In case III and IV the bar is less distinct and farther offshore than in case II (and I).

4.7 Discussion and proposed improvements

Total energy dissipation by wave breaking

It appeared that for both the Petten cases and the SV cases, SWAN consistently underestimated the significant wave height in the surf zone. As dissipation due to bottom friction is almost negligible, SWAN overestimates the energy dissipation by depth-induced wave breaking.

Presently, SWAN incorporates the model of Battjes and Janssen for the calculation of the total energy dissipation due to wave breaking (see paragraph 3.2). An important element of this model is the assumed wave height distribution. Battjes and Janssen [1978] assumed that the wave height distribution could be modelled with a Rayleigh distribution truncated at a maximum (depth-limited) breaker height. According to chapter 3, a full Rayleigh distribution throughout the entire surf zone is a good approximation [e.g. THORNTON & GUZA, 1983 and BALDOCK ET AL., 1998].

Figure 4.17 shows the measured wave height distribution, a truncated Rayleigh distribution and the full Rayleigh distribution at MP 6 for Petten case 02-01-1995, 06:00h. The wave height distributions for all the cases are presented in appendix 4M.

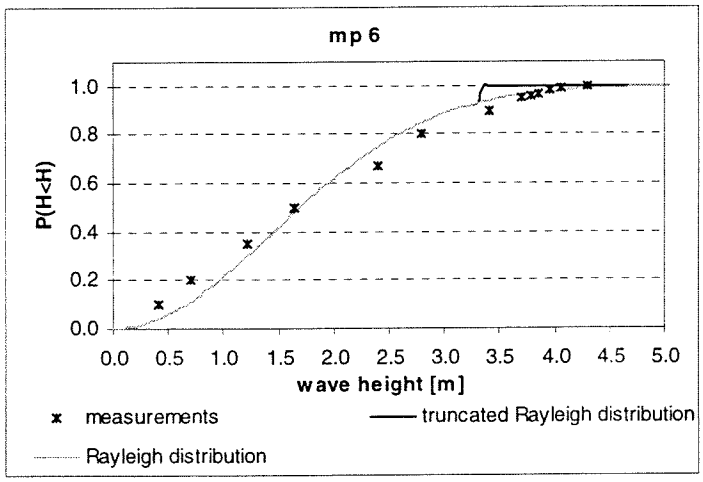

figure 4.17 Wave height distribution in the surf zone in Petten case 02-01-95, 06:00h

The Rayleigh distribution is given by:

$$P(\underline{H} < H) = 1 - \exp\left[-\left(\frac{H}{H_{rms}}\right)^2\right] \tag{4.2}$$

in which $H_{rms} \approx H_s/1.42$ (H_s is obtained from the measurements).
The truncated Rayleigh distribution is obtained by cutting off (4.2) at 0.73×water depth.

It can be seen that the full Rayleigh distribution is a better approximation of the measured wave height distribution than the truncated Rayleigh distribution. Baldock et al. [1998] have developed a dissipation model, based on the model of Battjes and Janssen, but adopting a full Rayleigh distribution (see section 3.2.1). According to Baldock et al. [1998] the model provides a better estimation of the wave heights in the nearshore zone.

Another important parameter in the model of Battjes and Janssen is the breaker parameter γ. It controls the fraction of breaking waves and therefore the total dissipation (see section 3.2.1). At present γ is held constant in SWAN at a default value of 0.73. Battjes and Stive [1985] calibrated the model of Battjes and Janssen. They found that optimal values for γ appeared to vary slightly with the incident wave steepness.

$$\gamma = 0.5 + 0.4 \tanh(33 s_o) \tag{4.3}$$

As stated before the deep-water wave steepness is not well-defined. However, in order to get an indication whether 0.73 is a representative value for the cases that are considered in this study, the wave steepness at the offshore boundary is assumed to be the deep-water wave steepness and applied to (4.3). The resulting γ-values are presented in table 4.4.

case	s [-] at offshore boundary	γ [-]
Petten		
01-01-95, 05:00	0.040	0.85
01-01-95, 18:20	0.049	0.87
02-01-95, 06:00	0.041	0.85
02-01-95, 17:00	0.032	0.81
10-01-95, 11:40	0.039	0.84
23-02-99, 00:40	0.045	0.86
23-02-99, 04:40	0.045	0.86
SV		
case 1	0.045	0.86
case 3	0.032	0.81
case 7	0.032	0.81
case 9	0.026	0.78

table 4.4 γ-values according to Battjes-Stive formulation for all cases with wave steepness at off shore boundary as deep-water wave steepness

For all cases γ according to (4.3) are higher than 0.73. A higher γ-value allows for higher maximum wave heights in the model and thus less dissipation.

Distribution of energy dissipation by wave breaking

The fact that the present source term for wave breaking is frequency independent and therefore does not affect the shape of the spectrum may give a possible explanation for differences between measurements and SWAN computations of mean wave periods and spectra.

It appeared that SWAN overestimated the mean wave period at MP 6 in the Petten cases. The calculated spectra show that the shape is not much altered by SWAN across the surf zone. Whereas in the measurements the spectra evolve to a $k^{-2.5}$-equilibrium range, SWAN maintains the proportionality to $k^{-3.0}$ for the high-frequency tail of the spectrum, that is imposed on the offshore boundary.

Measurements of the evolution of initially double-peaked spectra in a laboratory flume exhibit an increase in the mean wave period. In the SWAN calculations the mean wave period steadily decreases across the surf zone. In the measurements wave breaking lowers the energy level through the higher frequencies. At the shallowest station all harmonic peaks have been dissipated. Because the shape of the spectrum is not affected by wave breaking, SWAN maintains the higher frequency peak.

Evidently, dissipation by wave breaking affects the spectral shape. It can be concluded that dissipation by wave breaking is frequency dependent, as was already shown by Herbers et al. [2000] (see section 3.3.2).

Proposed improvements
In order to improve the accuracy of SWAN calculations of the (development of) wave spectra and their integral parameters across surf zones, the following improvements are proposed to be further investigated in this study:

- Application of the parametric model for the frequency-integrated dissipation (rate) of Baldock et al. [1998]. The wave height distribution is described with a full Rayleigh distribution across the entire surf zone. In this model a greater dissipation rate from the highest waves is included. This approach is more realistic; higher waves will dissipate more energy.

- Implementation of a formulation for the breaker parameter γ that depends on the *local* wave steepness. An expression similar to the formulation of Battjes and Stive [1985] (4.3) can be applied with the incident wave steepness replaced by the local wave steepness and adjustable coefficients.

- Presently the total dissipation of energy is distributed over the frequencies proportional to the local energy density level. This has appeared to be a wrong assumption. In the literature a quadratic dependency on the frequency has been proposed. According to e.g. Chen et al. [1997] the predicted spectral levels are fairly insensitive to quadratic dependency. Still, the effect of a frequency-dependent distribution of energy dissipation on the simulations of the wave data used in this study can be examined.

At the end of this chapter a final important note should be made. Both wave breaking and triad interactions are important processes in the surf zone. For example the evolution of the spectrum towards the $k^{-2.5}$-equilibrium range is probably the result of the combined effect of wave breaking and triad interactions. The source term for wave breaking has been discussed in detail. However, the effect of non-linear triad interactions and its approximation in SWAN are (almost) not considered in this study; in any case, not with respect to (possible) improvement of the performance of SWAN in the surf zone. The validity of some statements and proposed improvements may therefore be limited.

5 Adaptation of frequency-integrated energy dissipation by wave breaking

5.1 Introduction

In paragraph 4.7 three adaptations to the present source term for wave breaking in SWAN have been proposed. Two of those concern the frequency-integrated dissipation by wave breaking, i.e. the implementation of the dissipation model of Baldock et al. [1998] (from now referred to as the Rayleigh model) and the implementation of a formulation for the breaker parameter γ as a function of the local wave steepness. Both have been implemented in an experimental version of SWAN.
In this chapter the results of these two adaptations are presented. In paragraph 5.2 the application of the Rayleigh model is discussed. According to Baldock et al. [1998] the Rayleigh model offers better predictive capabilities with regard to the fraction of breaking waves and the wave height on steep slopes. No data on the fraction of breaking waves were available for the Petten cases or the SV cases. Therefore, the variation of the fraction of breaking waves and the significant wave height on a 1:10 sloping bottom of one case from Baldock et al. [1998] has been digitised and simulated with SWAN as well.
In paragraph 5.3 the results of the implementation of expression for the breaker parameter dependent on the local wave steepness is presented.

5.2 Application of the dissipation model of Baldock et al.

5.2.1 Model formulation

Basically, the Rayleigh model is a reformulation of the model of Battjes and Janssen [1978]. The total dissipation rate is calculated by the product of the dissipation in a breaking wave (D_b) and the probability of occurrence of a breaking wave (Q_b). For the dissipation in a single breaking wave a bore analogy is used (3.9). The fraction of breaking waves is determined by assuming a full Rayleigh distribution and integrating this over all waves for which $H \geq H_b$:

$$Q_b = \int_{H_b}^{\infty} p(H)dH = \int_{H_b}^{\infty} \frac{H}{4m_0} \exp\left[-\frac{H^2}{8m_0}\right] dH \tag{5.1}$$

in which m_0 is the 0^{th} moment of the spectrum, the total variance (E_{tot}).

This results in:

$$Q_b = \exp\left[-\left(\frac{H_b}{H_{rms}}\right)^2\right] \tag{5.2}$$

with $H_{rms}^2 = 8m_0$.

The Rayleigh model includes a greater rate of energy dissipation from the largest waves in the pdf. The total energy dissipation is given by:

$$D_{tot} = \frac{\alpha}{4}\rho g \bar{f} \int_{H_b}^{\infty} H^2 p(H) dH \tag{5.3}$$

Integrating (5.3) results in a simple, explicit expression for D_{tot}:

$$D_{tot} = \frac{\alpha}{4}\rho g \bar{f} \exp\left[-\left(\frac{H_b}{H_{rms}}\right)^2\right]\left(H_b^2 + H_{rms}^2\right) \tag{5.4}$$

Like in the model of Battjes and Janssen [1978], the breaker height H_b is evaluated by the breaker parameter ($\gamma = H_b/h$). So the Rayleigh model has the same adjustable parameters, i.e. the proportionality parameter α and the breaker height-to-depth ratio γ.

As the governing equations of the Rayleigh model, i.e. (5.2) and (5.4) are explicit and rather simple, the model could easily be implemented in SWAN.
In the following sections the results of the experimental version of SWAN are compared with measurements and the results of SWAN 40.11 (see chapter 4). The calculations with SWAN 40.11 (which incorporates the dissipation model of Battjes and Janssen [1978]) have been carried out with proportionality parameter $\alpha = 1.0$ and breaker parameter $\gamma = 0.73$. So, for a fair comparison α and γ have also been set to 1.0 and 0.73 respectively. The results of the experimental version of SWAN are denoted by 'SWAN Baldock'.

5.2.2 Effect on predicted wave heights and fraction of breaking waves

Petten cases
A comparison between the measured variation of the significant wave height and that calculated by SWAN 40.11 and SWAN Baldock for case 02-01-95, 06:00h is presented in figure 5.1. Comparisons for all cases are presented in appendix 5A. The trend is similar in all cases.

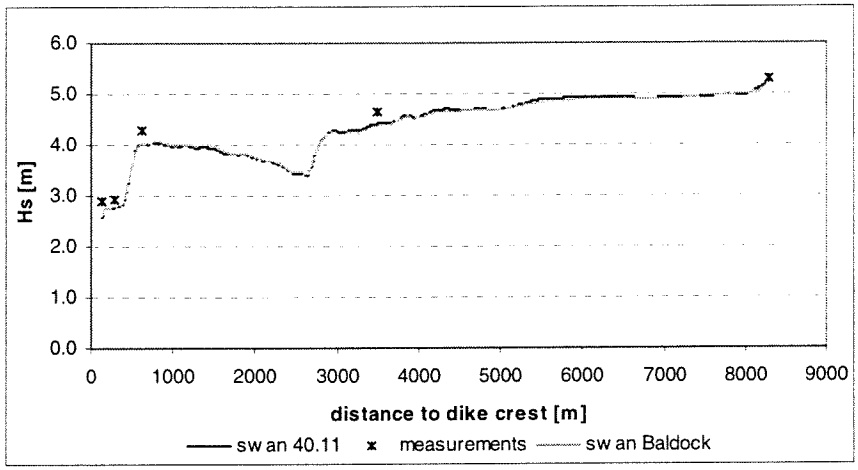

figure 5.1 Comparison of the predicted significant wave heights with SWAN 40.11 and SWAN Baldock in Petten case 02-01-95, 06:00h

Obviously, the prediction of the significant wave height in the Petten cases is not improved with the implementation of the Rayleigh model. The predicted variations with SWAN 40.11 and with SWAN Baldock are almost identical. This should be reflected in the predictions of the source term for wave breaking as well. As an example, the computed source terms for wave breaking at the shallowest station (MP 6) have been compared. Figure 5.2 shows that these are nearly the same indeed.

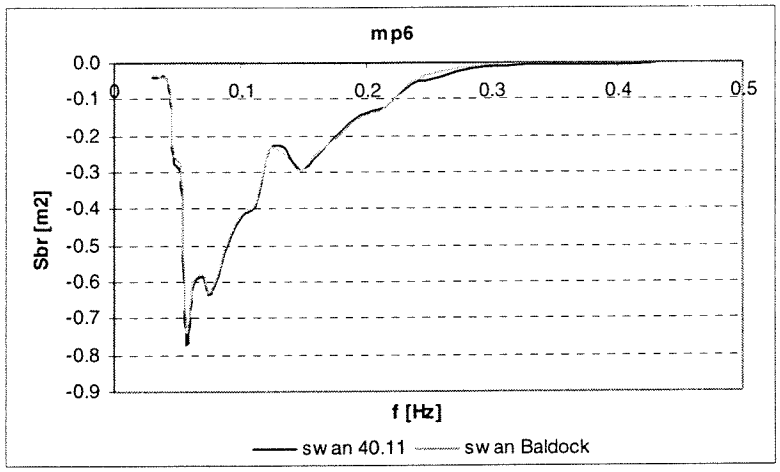

figure 5.2 Comparison of the source term for wave breaking with swan 40.11 and SWAN Baldock in Petten case 02-01-95, 06:00h

The almost identical results can be explained by the fact that the bottom slope near Petten is mildly sloping, i.e. approximately 1:80. On mild bottom slopes the wave heights are mainly controlled by the local water depth. In the model of Battjes and Janssen [1978], all breaking waves have a height equal to $H_b (= \gamma h)$, so the dissipation rate is assumed to be equal in each breaking wave.

In the Rayleigh model a greater dissipation rate is attributed to the larger waves, but the fraction of breaking waves is less than in the model of Battjes and Janssen [1978]. On mildly sloping bottoms, this results in the same mean dissipation rate.

Although no measurements of the fraction of breaking waves are available in the Petten cases, a comparison is made between the prediction by SWAN 40.11 and SWAN Baldock (see figure 5.3). In appendix 5B, the predictions of the variation of the fraction of breaking waves in all cases are presented.

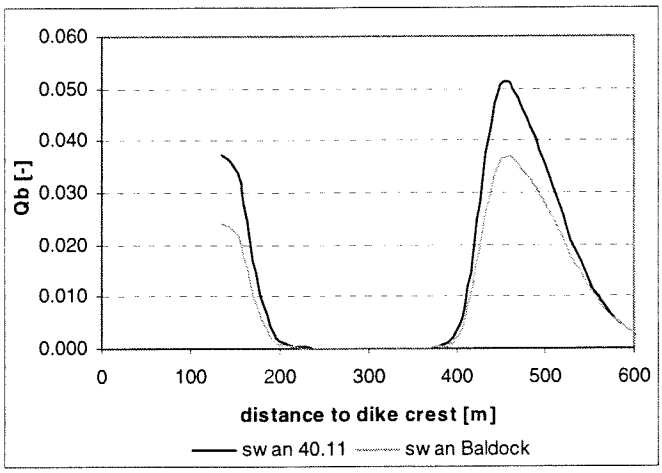

figure 5.3 Comparison of the predicted fraction of breaking waves with SWAN 40.11 and SWAN Baldock in Petten case 02-01-95, 06:00h

As expected (see section 3.2.1), the predicted fraction of breaking waves is smaller using the Rayleigh model. However, it could not be verified whether the Rayleigh model provides a more more accurate estimation of the fraction of breaking waves than the model of Battjes and Janssen [1978].

SV cases

Figure 5.4 shows a comparison of the measurements and the predictions of the significant wave height in SV case 1. As in the Petten cases, the trend is similar in all cases (see appendix 5C): the two models (i.e. SWAN 40.11 and SWAN Baldock) give nearly identical results.

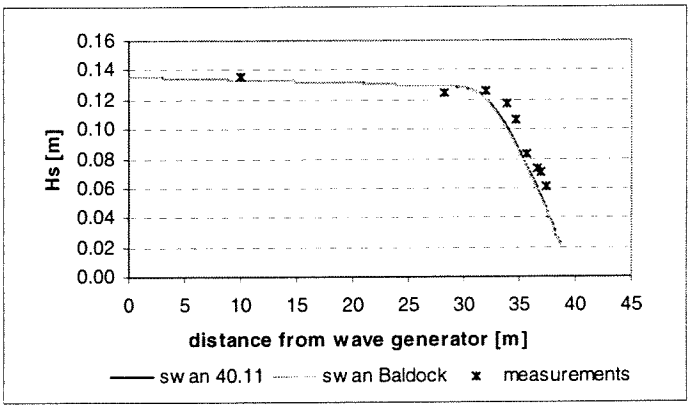

figure 5.4 Comparison of the predicted significant wave heights with SWAN 40.11 and SWAN Baldock in SV case 1

The bottom slope of the laboratory flume, in which the measurements were done, was equal to 1:30. This is also considered as mildly sloping. On mild slopes, the two models predict the

same mean energy dissipation rate and thus the same significant wave heights across the surf zone.
In figure 5.5 a comparison of the calculated mean dissipation rate is presented. The results of the two models are nearly identical indeed (see appendix 5D for all cases).

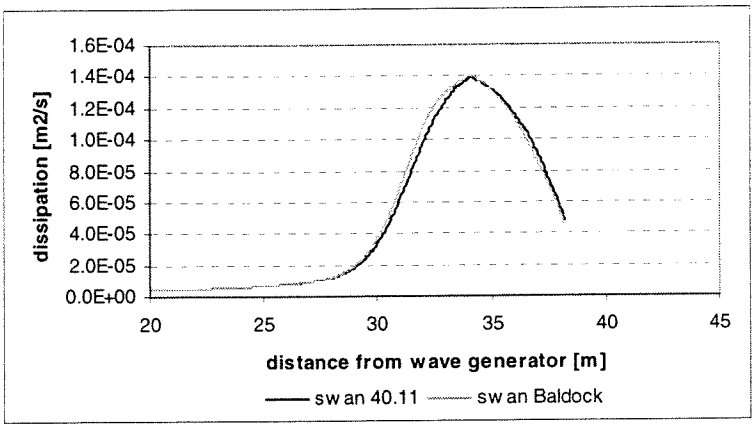

figure 5.5 Comparison of the predicted dissipation rate with SWAN 40.11 and SWAN Baldock in SV case 1

In the first part of the surf zone SWAN Baldock predicts a slightly higher dissipation rate than SWAN 40.11. From figure 5.6 it can be seen that the two models predict nearly the same fraction of breaking waves in the outer surf zone. Because the Rayleigh model includes a greater dissipation rate from the higher waves, the total dissipation rate predicted by SWAN Baldock is higher there.
In the inner surf zone SWAN Baldock predicts a slightly lower dissipation rate. The fraction of breaking waves, predicted by SWAN Baldock, is significantly lower there.

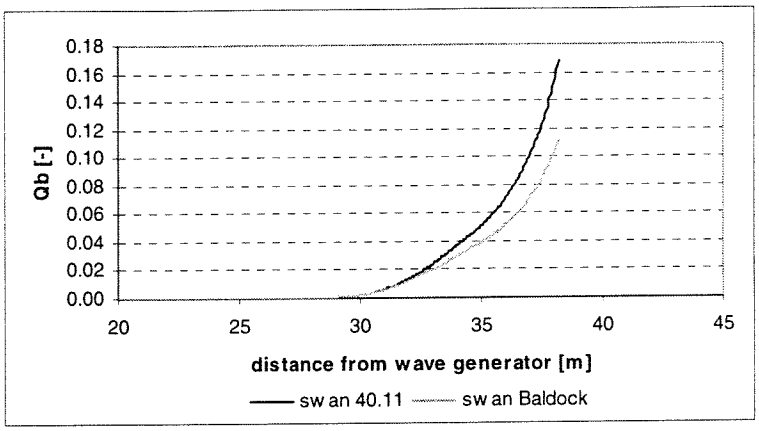

figure 5.6 Comparison of the predicted fraction of breaking waves with SWAN 40.11 and SWAN Baldock in SV case 1

The predictions of the fraction of breaking waves in all cases are also presented in appendix 5D. Because no data of the fraction of breaking waves were available, the accuracy of the two models in the prediction of the fraction of breaking waves could not be verified in the SV cases either.

Performance on a steep slope

Calculations with SWAN 40.11 and SWAN Baldock on flat slopes (i.e. 1:80 and 1:30) show nearly identical results. In order to examine whether the prediction of significant wave heights on steep slopes is improved by the implementation of the Rayleigh model in SWAN, data have been digitised from Baldock et al. [1998].

The experiments were carried out in a 50 m long wave flume, with a bottom slope of 1:10 in the surf zone. It was used with a (maximum) still water depth of 0.9 m. In the surf zone, electrical-resistance wave gauges were placed at a distance of 150 mm from each other. Video analysis was used to obtain the fraction of breaking waves. So the data can also be used to investigate whether SWAN Baldock better predicts the fraction of breaking waves indeed. Random wave simulations were based on JONSWAP spectra with varying H_s and T_p. In the case that has been digitised H_s was equal to 0.105 m and T_p was 1.5 s (case J2, see Baldock et al. [1998]).

The SWAN calculations were carried out with the same model settings that were used in the SV cases. Due to convergence problems, triad interactions had to be deactivated[1]. The boundary conditions, the computational grid and the bottom were different, of course.

In figure 5.7 the results of the computations with the two models are presented and compared to the measurements. The largest differences between the two calculations occur in the inner surf zone. At the last four wave gauges the wave heights calculated by SWAN 40.11 differ about 8-22% from the measurements. At these measurement positions the waves heights calculated by SWAN Baldock differ only 5-13% from the observations. SWAN Baldock appears to offer a better estimation of the nearshore wave heights indeed.

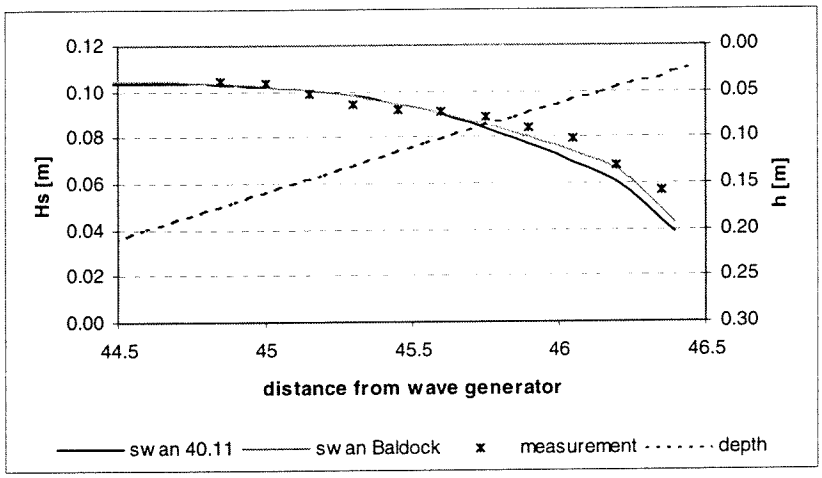

figure 5.7 Comparison of the predicted significant wave heights on a steep slope with SWAN 40.11 and SWAN Baldock in case J2 of Baldock et al. [1998]

[1] The present approximation of the triads in SWAN cannot handle rapid bottom changes (e.g. steep slopes) properly.

The results of the computations of the fraction of breaking waves are compared with the measurements in figure 5.8. SWAN 40.11, using the model of Battjes and Janssen [1978] significantly overestimates the fraction of breaking waves. At some locations the deviation from the observations is more than 150%. SWAN Baldock gives a much better fit to the data. The model results differ 35% at most from the measurements.

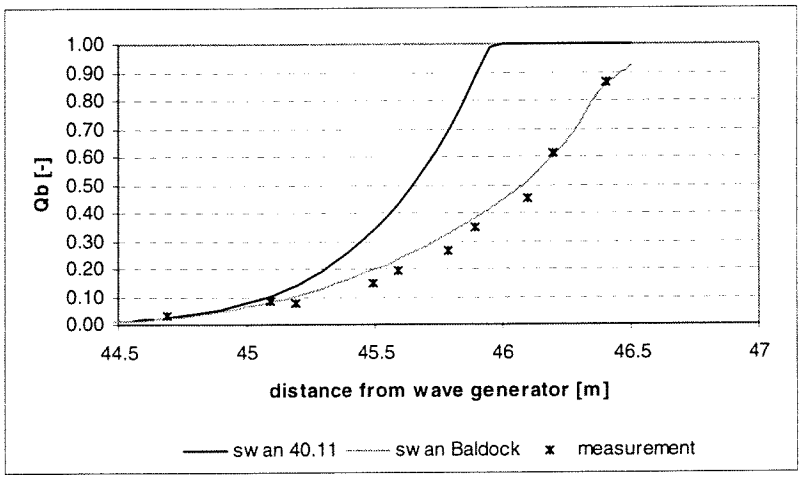

figure 5.8 Measured and predicted variation of the fraction of breaking waves with SWAN 40.11 and SWAN Baldock in case J2 of Baldock et al. [1998]

5.2.3 Effect on predicted mean wave periods and wave spectra

In the previous section it has been shown that the predicted variation of the significant wave height is nearly the same by SWAN 40.11 and SWAN Baldock in the both the Petten and the SV cases. The distribution of the energy dissipation has not been changed. So in the calculations with SWAN Baldock the energy dissipation by wave breaking is still distributed proportional to the energy density level.
With the same significant wave heights (i.e. same total energy) and the same distribution of the energy dissipation, the predicted mean wave periods and spectra should also be identical. In figure 5.9 this is shown for Petten case 02-01-95, 06:00h, as example. In fact, this is true for all Petten cases as well as for all SV cases.

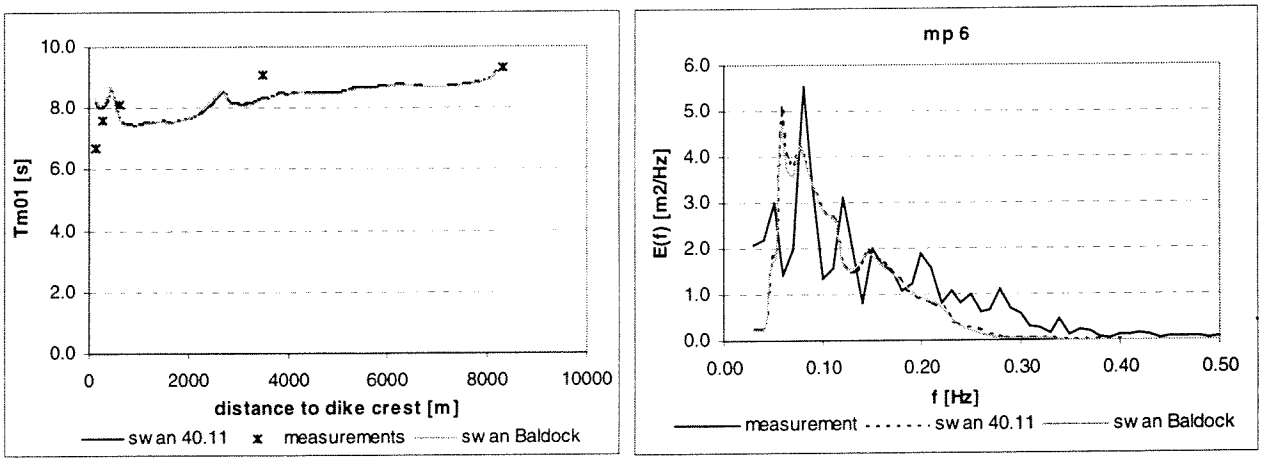

figure 5.9 Comparison of the mean wave period and the spectrum at MP 6 with SWAN 40.11 and SWAN Baldock in Petten case 02-01-95, 06:00 h

5.3 Adaptation of the breaker parameter

5.3.1 Implemented formulation

The formulation for the breaker parameter γ depending on the local wave steepness that has been implemented in SWAN is based on the expression Battjes and Stive [1985] derived in their calibration of the model of Battjes and Janssen [1978] (see section 3.2.1).
In the expression, the incident wave steepness (s_o) is replaced by the local wave steepness (s_{loc}). The formulation has been implemented such that all coefficients could be easily adjusted in each model run:

$$\gamma = A + B\tanh(Cs_{loc}) \tag{5.5}$$

with A, B and C the adjustable coefficients.

The definition of the local wave steepness is chosen almost equal to the definition Battjes and Stive [1985] used for the deep-water wave steepness (i.e. $s_o = H_{rms,o}/L_{o,p}$):

$$s_{loc} = \frac{H_{rms}}{L_{mn}} = \frac{H_{rms}k_{mn}}{2\pi} \tag{5.6}$$

The (local) mean wavelength (L_{mn}) or mean wave number (k_{mn}) is used because this is a more convenient measure than the wavelength at the peak frequency (L_p) in the case of dual peaked spectra. The mean wave number that is used is given by:

$$k_{mn} = \left(\frac{\iint k^{-\frac{1}{2}} E(\sigma,\theta) d\sigma d\theta}{\iint E(\sigma,\theta) d\sigma d\theta} \right)^{-2} = \left(\frac{\iint k^{-\frac{1}{2}} E(\sigma,\theta) d\sigma d\theta}{E_{tot}} \right)^{-2} \tag{5.7}$$

This formulation puts more emphasis on the lower wave numbers of the spectrum and is therefore a robust measure for the mean wave number.

The implementation of the formulation (5.5) in SWAN was rather straightforward.
As mentioned before, in the calculations with SWAN 40.11 the two adjustable parameters with regard to wave breaking, α and γ, were set to1.0 and 0.73 respectively. As an adjustable parameter γ is replaced by A, B and C in the experimental version of SWAN[2]. As a first guess, the coefficients A, B and C are chosen equal to the coefficients in the original formulation of Battjes and Stive [1985], i.e. A = 0.5, B = 0.4 and C =33. For a fair comparison α is set to 1.0.

In the following sections the results of the experimental version of SWAN are compared with measurements and the results of computations with SWAN 40.11 (see chapter 4). The results of the experimental version of SWAN are denoted by 'SWAN gamma'.

[2] For the sake of clarity; in order to separate the effect of the two adaptations the adapted γ is applied to the model of Battjes and Janssen [1978] in SWAN 40.11, not to the Rayleigh model in SWAN Baldock

5.3.2 Effect on predicted wave heights

Petten cases

In figure 5.10 the variation of the local wave steepness and the corresponding value of the breaker parameter γ according to (5.5) are presented for Petten case 02-01-95, 06:00h. Appendix 5E presents the same figures for all cases, showing similar results.

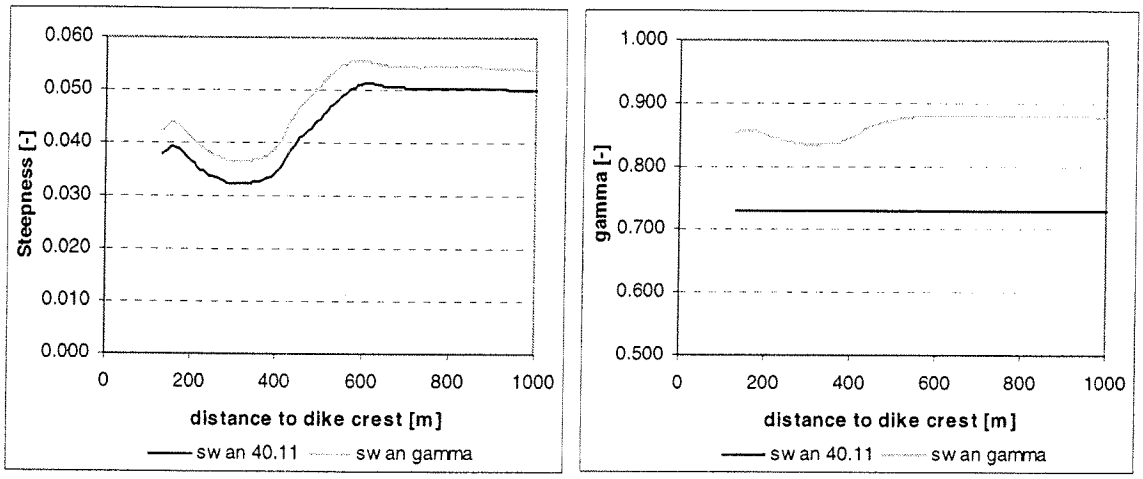

figure 5.10 Computed variation of the wave steepness and breaker parameter γ in Petten case 02-01-95, 06:00h

In the left panel of figure 5.10 it can be seen how the wave steepness is lowered by wave breaking at the bar, that is located approximately 500 m offshore. Then towards the shore the wave steepness increases again.

The right panel in figure 5.10 shows the variation of the breaker parameter across the surf zone. The breaker parameter exhibits a maximum at the bar crest and foreshore and a minimum in the trough.

The value of the breaker parameter according to (5.5) is higher than 0.73 (i.e. 0.83-0.88). A higher γ-value implies that the maximum wave height H_m in the model is also higher and therefore the dissipation due to wave breaking in the model will be less. Figure 5.11 shows that the source term for wave breaking at MP 6 was indeed lower in the calculations with SWAN gamma.

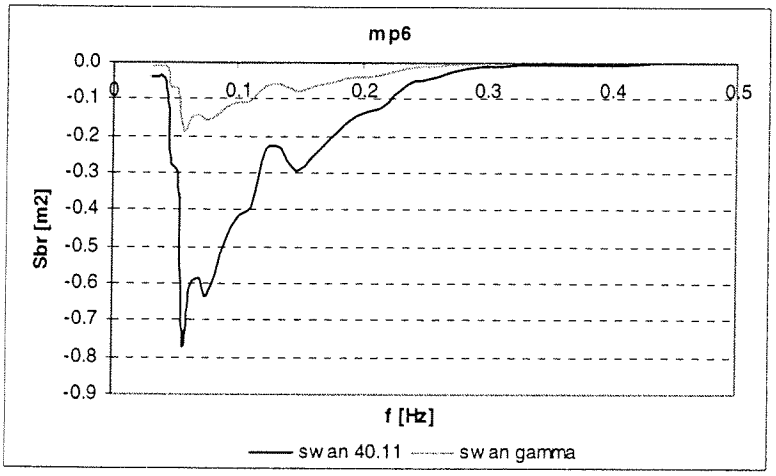

figure 5.11 Comparison of the source term for wave breaking with SWAN 40.11 and SWAN gamma in Petten case 02-01-95, 06:00h

Obviously, lower dissipation results in higher predicted wave heights across the surf zone (see figure 5.12). In appendix 5F a comparison of the variation of the significant wave heights is presented for all cases.
It can be seen that the higher γ-value in the simulation with SWAN gamma allows for higher waves. Whereas in the SWAN 40.11 computations the wave heights are first decreased at approximately 4500 m from the dike crest, SWAN gamma predicts a more or less constant wave height down to 3000 m from the dike crest.

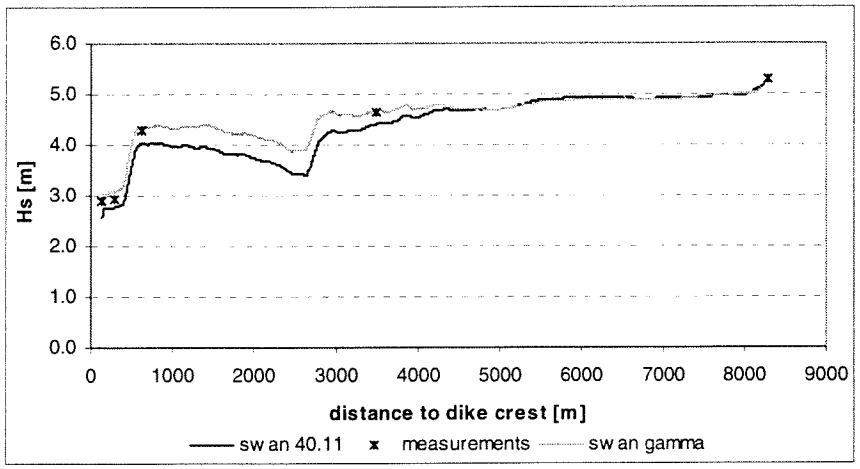

figure 5.12 Comparison of the predicted significant wave heights with SWAN 40.11 and SWAN gamma in Petten case 02-01-95, 06:00h

The prediction of the wave heights across the surf zone is significantly improved by SWAN gamma. The wave height predictions by SWAN gamma only deviate a few percent from the measurements, whereas SWAN 40.11 underestimated the wave heights by about 6-18%.

SV cases

The simulations of the SV cases with SWAN gamma show similar results as the simulations of the Petten cases. In the SV cases the expression depending on the local wave steepness also gives γ-values higher than 0.73 (see figure 5.13 and appendix 5G).

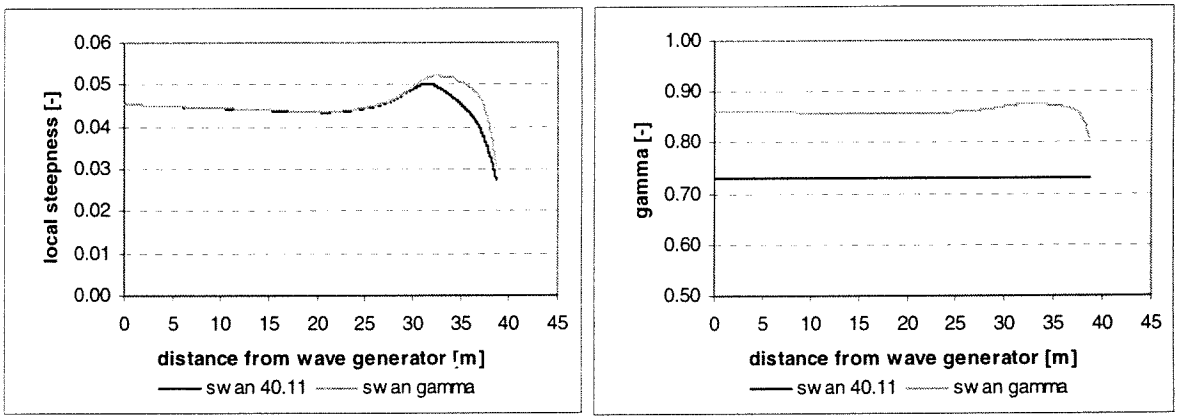

figure 5.13 Computed variation of the wave steepness and breaker parameter γ in SV case 1

The left panel of figure 5.13 shows that the local wave steepness is higher in the calculations with SWAN gamma. In SWAN gamma the decrease in the local wave steepness near the waterline is more rapid.

A comparison of the dissipation rate computed with the two models is made in figure 5.14. It shows results that are consistent with figure 5.13. Due to the higher γ-values, SWAN gamma predicts a smaller dissipation rate in the first part of the surf zone than SWAN 40.11. Near the waterline the dissipation by SWAN gamma is higher; it predicts more shore breaks. In appendix 5H the computed dissipation rates of all cases are presented.

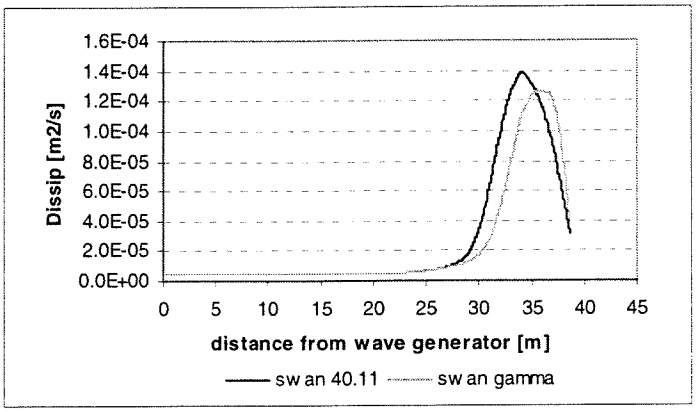

figure 5.14 Comparison of the predicted dissipation rate with SWAN 40.11 and SWAN gamma in SV case 1

In all cases the variation of the significant wave height across the surf zone is much better with SWAN gamma. In figure 5.15 the results of SV case 1 are presented (see appendix 5I for all cases). SWAN 40.11 underestimated the wave heights in the surf zone by about 19-27%. The predictions of the wave heights by SWAN gamma deviate only a few percent from the measurements. The maximum error occurs at the shallowest station (5-10%).

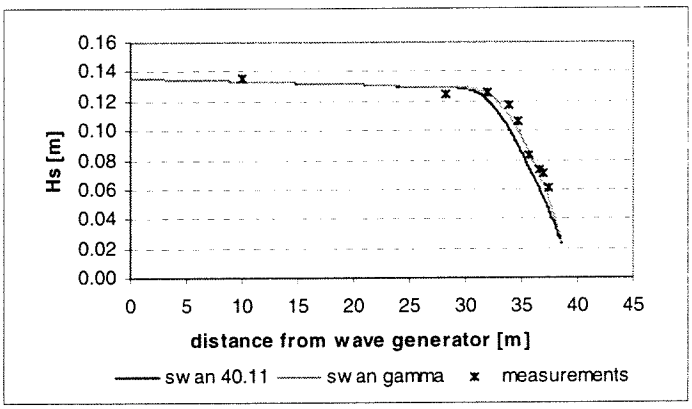

figure 5.15 Comparison of the predicted significant wave heights with SWAN 40.11 and SWAN gamma in SV case 1

Performance on a steep slope

The breaker parameter governs the fraction of breaking waves in the model of Battjes and Janssen [1978]. So when an adapted expression for the breaker parameter is implemented, the prediction of the fraction of breaking waves changes as well. To compare the accuracy in the prediction of the fraction of breaking waves of SWAN gamma with SWAN 40.11, case J2, digitised from Baldock et al. [1998] (see section 5.2.2) has been run with SWAN gamma as well.

Figure 5.16 presents a comparison of the predicted variation of the significant wave height, calculated with SWAN 40.11, SWAN Baldock and SWAN gamma, respectively.
As in the Petten cases and the SV cases, SWAN gamma provides a much better estimation of the significant wave heights across the surf zone. The deviations of the calculated wave heights from the measurements are less than 5%. The performance of SWAN gamma is (even) slightly better than SWAN Baldock.

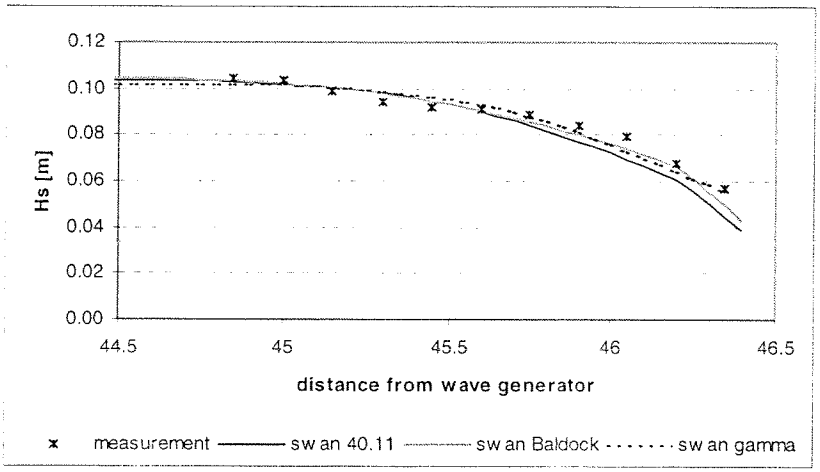

figure 5.16 Comparison of the predicted significant wave heights on a steep slope with SWAN 40.11, SWAN Baldock and SWAN gamma in case J2 of Baldock et al. [1998]

A comparison of computations of the fraction of breaking waves with the three models is presented in figure 5.17. The simulation with SWAN gamma provides slightly better estimations than SWAN 40.11. However the error in the predicted variation of the fraction of breaking waves is still very large (40-100%). By far, the prediction of the fraction of breaking waves by SWAN gamma is not as accurate as the prediction of SWAN Baldock.

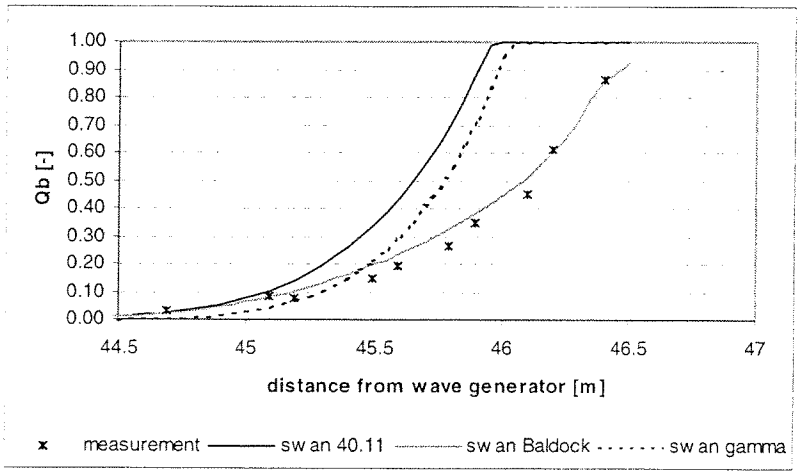

figure 5.17 Comparison of predicted fractions of breaking waves with SWAN 40.11, SWAN Baldock and SWAN gamma in case J2 of Baldock et al. [1998]

5.3.3 Effect on predicted mean wave periods and wave spectra

Petten cases

Figure 5.18 shows that the computations of the mean wave period by SWAN 40.11 and SWAN gamma are nearly the same in the Petten case 02-01-95, 06:00h. In fact, this is true for all cases.

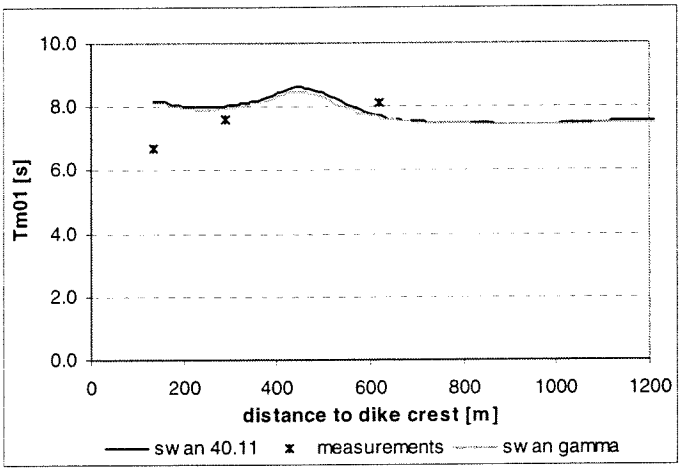

figure 5.18 Comparison of the predicted mean wave period with SWAN 40.11 and SWAN gamma in Petten case 02-01-95, 06:00 h

So the distribution of the total energy over the frequencies is the same. This implies that, although spectral energy density levels are higher, the triad interactions have had the same effect (relatively) in the computations with SWAN gamma as in the computations with SWAN 40.11. The left panel of figure 5.19 shows a comparison of the computed source terms for triad interactions (S_{nl3}) at MP 6, scaled by the total energy in Petten case 02-01-95, 06:00h. The two lines nearly overlie each other indeed.
The right panel of figure 5.19 presents the computed spectra at MP 6 with SWAN 40.11 and SWAN gamma for Petten case 02-01-95, 06:00h. The energy density levels in the two model runs differ (of course). The computed spectral shapes are nearly identical. The computed spectra at all measurement locations in all the cases are presented in appendix 5J.

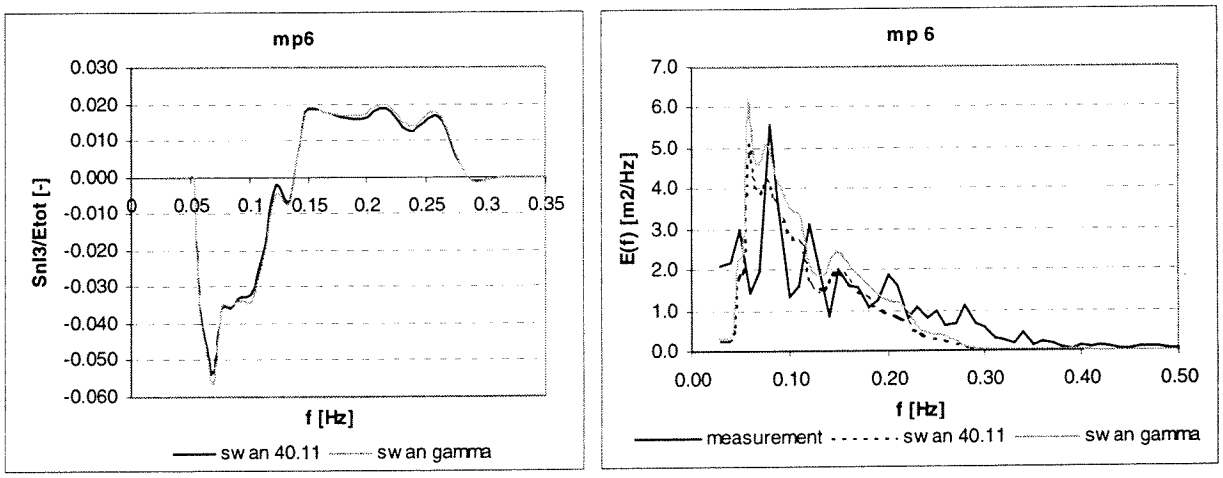

figure 5.19 Relative magnitude of S_{nl3} and predicted spectra at MP 6 with SWAN 40.11 and SWAN gamma in Petten case 02-01-95, 06:00h

SV cases

The trend in the predicted variation of the mean wave period and the spectra in the simulations of the SV cases with SWAN gamma are more or less the same as in the Petten cases. The predictions of the mean wave period with SWAN 40.11 and SWAN gamma are almost identical. So in the dual peak cases the triad interactions have had the same effect in the computations with SWAN 40.11 and SWAN gamma as well, despite the different energy density levels. As an example the predictions of the mean wave period in SV case 1 are compared in figure 5.20.

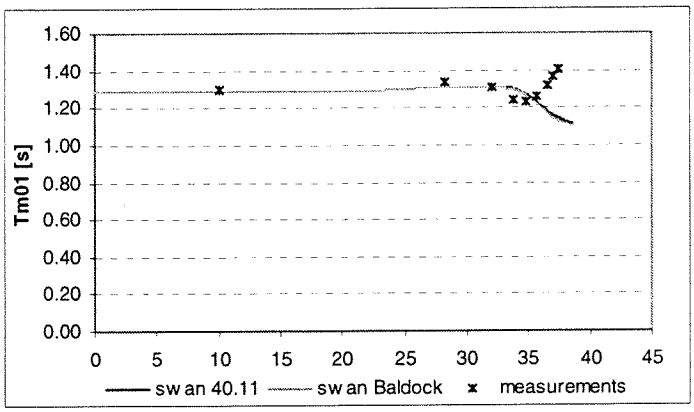

figure 5.20 Comparison of the predicted mean wave period with SWAN 40.11 and SWAN gamma in SV case 1

So the only difference in the computations with SWAN 40.11 and SWAN gamma with regards to the wave spectra is the energy density level at each frequency. The predicted mean wave periods and wave spectra have not been improved. The distribution of the total energy, i.e. the spectral shape is the same. Figure 5.21 shows the computed wave spectra at the shallowest station in SV case 1 (see appendix 5K for all cases).

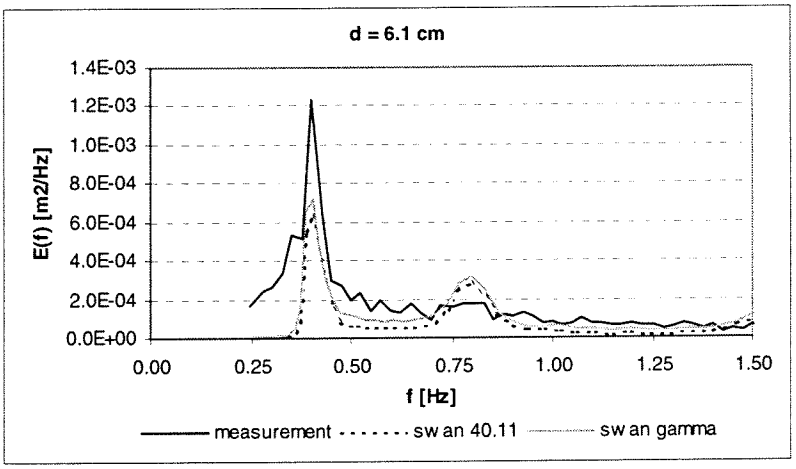

figure 5.21 Predicted spectra at the shallowest station with SWAN 40.11 and SWAN gamma in SV case 1

6 Adaptation of the distribution of energy dissipation by wave breaking

6.1 Introduction

The analysis of wave data and the simulations with SWAN 40.11 (see chapter 4) led to three different proposals for adaptation of the present source term for wave breaking. In the previous chapter the results of two adaptations to the computation of the frequency-integrated energy dissipation have been presented. In this chapter the results of the third adaptation, concerning the distribution of energy dissipation by wave breaking are presented.
An effort has been made to improve the results of the SWAN simulations regarding mean wave periods and wave spectra by implementing a frequency-dependent distribution of the total energy dissipation by wave breaking.

6.2 Model formulation

In the literature a dissipation term for wave breaking depending on the frequency squared have been proposed [MASE AND KIRBY, 1992]. According to some authors [e.g. CHEN ET AL., 1997; KIRBY AND KAIHATU, 1996; BOOIJ ET AL., 1999] spectral energy density levels are insensitive to such a quadratic dependency.
However, after the analysis of the wave data sets in chapter 4, it was found interesting to investigate the effect of a frequency-dependent dissipation term on the simulations of the data sets used in this study.

The formulation that has been implemented is based on the expression Mase and Kirby [1992] proposed (see section 3.3.2). This consists of a term that distributes (a part of) the energy dissipation proportional to the energy density level at each frequency and a term that distributes the energy dissipation proportional to the frequency squared (f^2).
The formulation has been implemented such that the fraction (F) of the total energy dissipation that is distributed dependent on the frequency could be varied. Furthermore the dependency on frequency has not been restricted to a quadratic dependency. The frequency dependent term has been expressed proportional to f^n and n could be varied in each model run as well. The resulting source term for wave breaking is:

$$S_{br}(\sigma,\theta) = (1-F)\frac{D_{tot}}{\iint E(\sigma,\theta)d\sigma d\theta}E(\sigma,\theta) + F\left(\frac{f}{f_{mn}}\right)^n \frac{D_{tot}}{\iint E(\sigma,\theta)d\sigma d\theta}E(\sigma,\theta) \qquad (6.1a)$$

Or simplified:

$$S_{br}(\sigma,\theta) = \left[(1-F) + F\left(\frac{f}{f_{mn}}\right)^n \right] \frac{D_{tot}}{E_{tot}} E(\sigma,\theta) \qquad (6.1a)$$

with F and n adjustable parameters and f_{mn} the mean wave frequency: $f_{mn} = E_{tot}^{-1} \int fE(f)df$

With different combinations of F and n, the total energy dissipation D_{tot} is differently distributed over the frequencies. When $F = 0$ and n any value, or with F any value and $n = 0$ the original source term for wave breaking (in SWAN 40.11) is obtained and all energy dissipation is distributed proportional to the energy density level at each frequency. With $1.0 \geq F > 0$ the energy dissipation is (partly) distributed proportional to the frequency to the power n.

Equation (6.1) has been implemented in an experimental version of SWAN. In the following paragraphs the results of the simulations with the experimental version of SWAN are presented.
The computations have been carried out with the experimental version of SWAN that incorporates the expression for the breaker parameter γ dependent on the local wave steepness (see paragraph 5.3). In paragraph 5.3 it was shown that the predicted mean wave periods in the simulations with SWAN 40.11 and SWAN gamma are almost identical. So the results of the computations with different combinations of F and n can be compared with the results presented in chapter 4 as well. In SWAN gamma the energy distribution was proportional to the energy density at each frequency. In this chapter, the results of the simulations with SWAN gamma (see paragraph 5.3) are denoted by '$F = 0$, $n = 0$'.

The variation of the significant wave height across the surf zone was the same for different combinations of F and n. Therefore, the results of the variation of the significant wave heights are not considered here.

6.3 Effect on predicted mean wave periods

Petten cases
In paragraph 4.5 it was shown that with a distribution of the energy dissipation proportional to the energy density level, the mean wave period was overestimated by SWAN in the Petten cases. So the computed spectra contained too much energy at the lower frequencies. In section 4.6.1 it was shown that this could be explained by the fact that the shape of the spectrum was maintained by SWAN throughout the surf zone. The measurements show a relative increase in the energy density levels at higher frequencies towards the shore, probably caused by non-linear interactions.

When the mean wave period is initially overestimated, it is obvious that by enhancing dissipation at the higher frequencies, the accuracy of the predicted mean wave period is worsened. To show this a computation has been carried out of Petten case 02-01-95, 06:00h

with $F = 0.75$ and $n = 2$. The predicted variation of the mean wave period is presented in figure 6.1 and compared to the calculation with $F = 0$ and $n = 0$. Obviously, the mean wave period is overestimated more with a frequency-dependent dissipation.

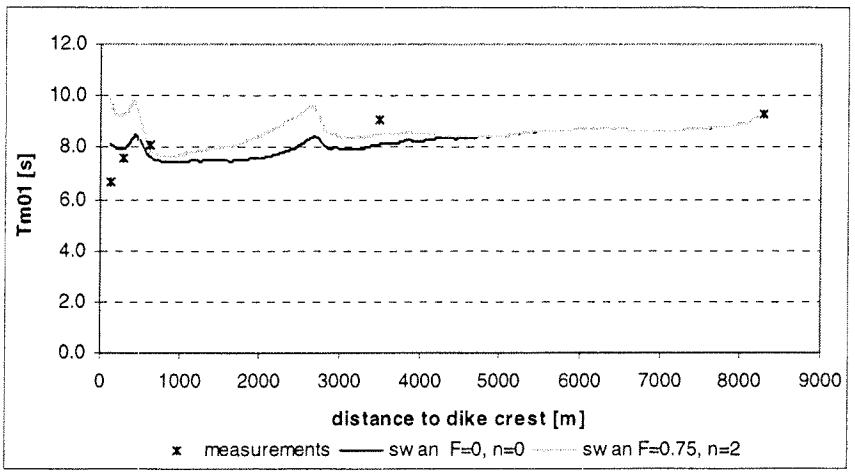

figure 6.1 Comparison of the mean wave period with SWAN F=0, n=0 and SWAN F=0.75, n=2 in Petten case 02-01-95, 06:00h

SV cases

In the measurements the mean wave period initially decreases in the surf zone, due to a transfer of energy to the higher frequencies by triad interactions. Approaching the water line, in the inner surf zone, the mean wave period increases again. So dissipation by wave breaking appears to be more intense at higher frequencies (see also paragraph 4.5).

Figure 6.2 presents cross-shore variations of the mean wave period resulting from simulations of SV case 1 with different combinations of F and n.

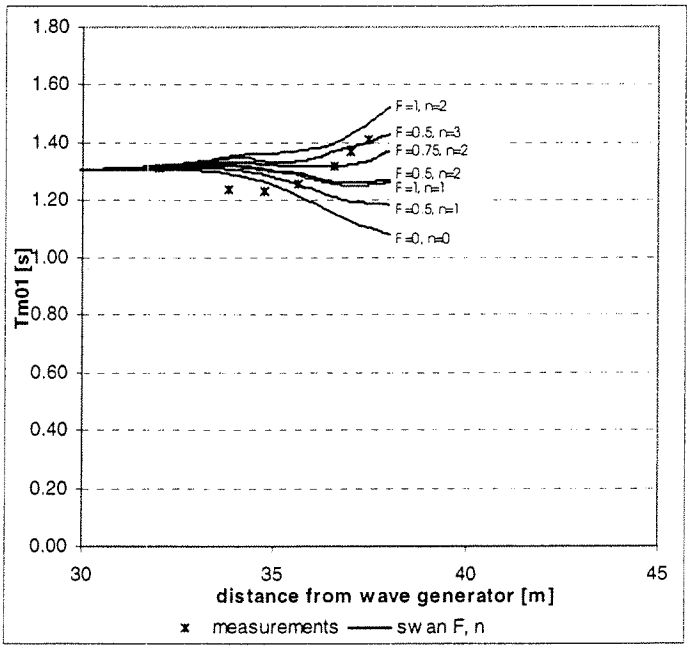

figure 6.2 Comparison of the mean wave period with different combinations of F and n in SV case 1

In the calculations with a distribution of energy proportional to the energy density level (F=0, n=0), the mean wave period decreases steadily across the surf zone. Because wave breaking does not influence the shape of the spectrum in the computation, the transfer of energy to the higher frequencies is not cancelled out. In the inner surf zone the mean wave period is significantly underestimated.
For F>0 and n>0, wave breaking is enhanced at the higher frequencies. Obviously, for constant values of n (>0), the mean frequency increases with increasing F. And, vice versa, for constant values of F (>0), the mean frequency increases with increasing n.
The *qualitative trend* in the cross-shore variation of the mean wave period seems to be approximated best in the simulation with F=1, n=2. However, the *overall error* in the mean wave period across the surf zone seem to be the smallest in the simulation with F=0.75, n=2.

Similar results are found for case 7 (see figure 6.3). In this case the mean wave period was also underestimated in the simulation with F=0, n=0. The best approximation of the trend in the variation of the mean wave period is in the simulation with F=1, n=2. On average the mean wave period is estimated best in the simulation with F=0.5, n=2.

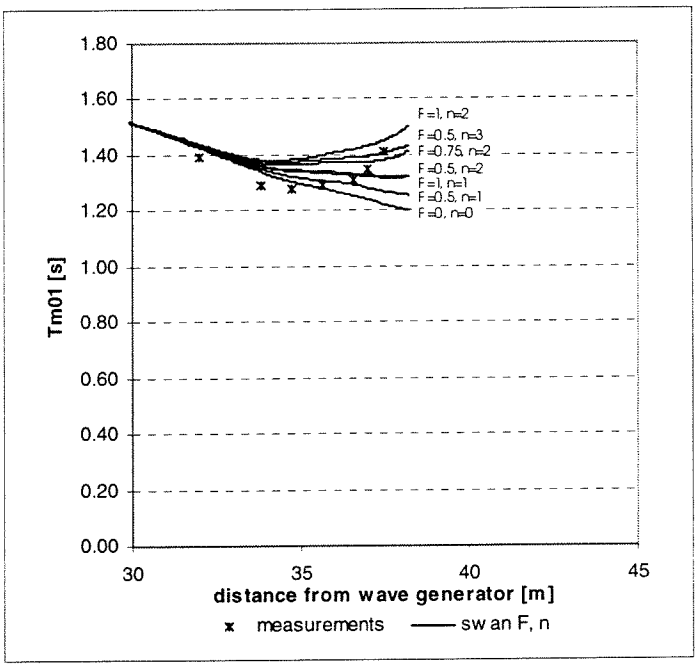

figure 6.3 Comparison of the mean wave period with different combinations of F and n in SV case 7

In case 1 and 7 the low-frequency peak of the spectra at the offshore boundary contained less energy than the high-frequency peak. Initially (with F=0, n=0), the mean wave period was underestimated. By implementing a frequency-dependent dissipation, the prediction of the mean wave period can be slightly improved. However, there is no optimal combination of F and n, such that both the *qualitative trend* in the variation of the mean wave period and the *absolute values* of the mean wave period are estimated with sufficient accuracy.

In SV case 3 and 9 the mean wave period was overestimated in the simulations with F=0, n=0 (see paragraph 4.5). In these cases the shape of the spectra at the offshore boundary was more or less the same. The low-frequency peak contained more energy than the high-frequency peak. Obviously, a frequency-dependent dissipation term, enhancing dissipation at the higher frequencies does not improve the predicted mean wave period in these cases. As an example, this is show in figure 6.4 for SV case 3.

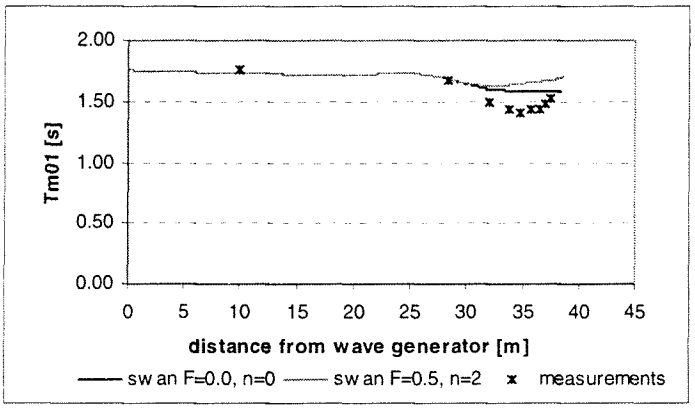

figure 6.4 Comparison of the mean wave period with SWAN F=0, n=0 and SWAN F=0.5, n=2 in SV case 3

6.4 Effect on predicted wave spectra

Petten cases

The prediction of the mean wave period is getting worse when a frequency-dependent dissipation term for wave breaking is applied. More energy is dissipated at the higher frequencies and the mean wave period is overestimated more.

In a simulation with F>0 and n>0, the computed spectrum at MP 6 contains relatively too much energy at the lower frequencies and too little at the higher frequencies. This is shown in the right panel of figure 6.5 for Petten case 02-01-95, 06:00h. The left panel of figure 6.5 shows a comparison of the source term for wave breaking with a frequency-independent and a frequency-dependent dissipation term for this case. The difference is clear.

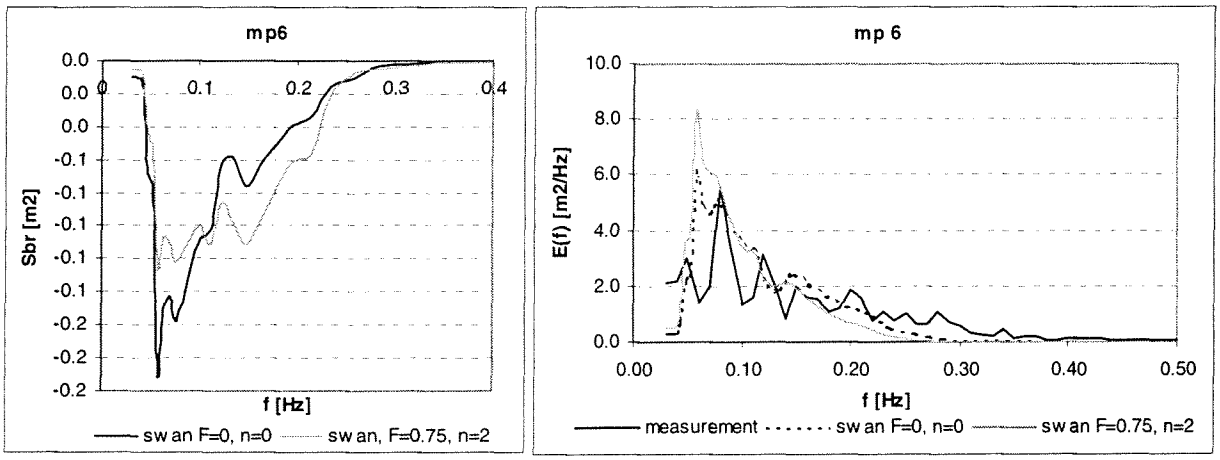

figure 6.5 Comparison of S_{br} and predicted spectra at MP 6 with SWAN F=0, n=0 and SWAN F=0.75, n=2 in Petten case 02-01-95, 06:00h

SV cases

Figure 6.6 presents computed spectra at the shallowest gauge in SV case 1 with different combinations of F and n. In the measurements, all energy peaks above the low-frequency peak have been eliminated by wave breaking. It has been shown that the tail of the spectra evolves to a $k^{-2.5}$-equilibrium range (see paragraph 3.3).

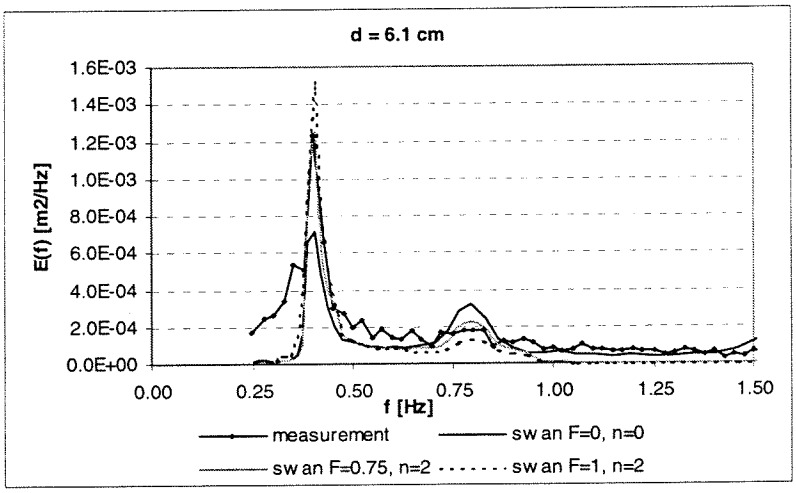

figure 6.6 Comparison of predicted spectra at the shallowest station with SWAN F=0, n=0, SWAN F=0.75, n=2 and SWAN F=1, n=2

In the simulation with the distribution of energy dissipation proportional to the energy density level a distinct high-frequency peak is maintained. Figure 6.6 shows that with increasing F this high-frequency peak becomes less distinct and that the low-frequency peak becomes higher. The high frequency tail of the spectrum becomes smoother.
However, the equilibrium range is not established in any of the simulations with the different combinations of F and n. Triad interactions in SWAN seem to transfer too little energy to the frequencies in the range of 0.50 Hz – 0.75 Hz and f>0.90 Hz.

6.5 Additional remarks

From the results presented in this chapter, no unambiguous statements can be done regarding the frequency-dependency of dissipation by wave breaking for operational use of SWAN. It is clear that no unique combination of F and n can be determined, such that both the *qualitative trend* in the cross-shore variation and the *absolute values* of the mean wave period and wave spectra are predicted accurately.
However, the remark that has been made at the end of chapter 4 should be kept in mind. It was stated that the present approximation of triad interactions in SWAN is not considered in this study and that the validity of some statements regarding the effectiveness of some improvements may be limited. This is certainly the case for the results of the various simulations with the frequency-dependent dissipation. It might be that there is an optimal combination of F (>0) and n (>0), when the triad interactions are accurately approximated.

Furthermore, it should be noted that although according to e.g. Chen et al. [1997] and Booij et al. [1999] energy density levels and spectral shapes are insensitive to a quadratic dependency, this is not the case in the cases that are considered here. The shape of the computed spectra and thus the predicted mean wave period appeared to change with varying frequency-dependency of the distribution of energy dissipation by wave breaking.

7 Conclusions and recommendations

7.1 Introduction

In this research the transformation of wave spectra and their integral parameters across the surf zone has been studied. Focus has been on improvement of the dissipation term for depth-induced wave breaking in SWAN. A literature study has been carried out in order to make an inventory of various formulations regarding dissipation by wave breaking. Data with a wide range of wave conditions have been analysed and used to assess the performance of SWAN. This has given an indication of which formulations might improve the accuracy of SWAN predictions of wave spectra in the surf zone. Finally, three adaptations to the source term for wave breaking have been proposed and implemented in SWAN.
In this chapter the conclusions of this research are presented. Furthermore some recommendations are made regarding future research of the transformation of wave spectra across the surf zone and further improvement of SWAN.

7.2 Conclusions with regard to measured wave data

Measurements of the evolution of initially bi-modal spectra across the surf zone show that the low-frequency peak becomes the dominant peak. At the shallowest station all higher frequency peaks have been eliminated by wave breaking. Dissipation of energy at the low-frequency peak is relatively low. Apparently dissipation of energy by wave breaking is more intense at higher frequencies.

In laboratory measurements of double-peaked spectra, field measurements of single- peaked spectra at Petten and field measurements at Duck, the high-frequency tail of all spectra evolves to a $k^{-2.5}$-equilibrium range in the inner surf zone. This is attributed to the effect of non-linear interactions and depth-induced wave breaking.
Regardless of the shape of the spectrum at the offshore boundary, the tail of the spectra can be parameterised by a formulation that is among other things dependent on the (significant) wave height-to-depth ratio, the gravitational acceleration and a constant. The optimal value of this constant appeared to vary with the bottom profile.

In the Petten cases, a full Rayleigh distribution is a better approximation of the measured wave height distribution in the surf zone than a truncated Rayleigh distribution. Applying a full Rayleigh distribution of all waves (breaking and non-breaking) to dissipation models implies that more dissipation is attributed to the higher waves.

7.3 Conclusions with regard to SWAN results

Prediction of wave heights across the surf zone

SWAN 40.11 incorporates the model of Battjes and Janssen [1978] with a constant value of the breaker parameter γ (0.73). In all simulations that have been done with SWAN 40.11, the total energy dissipation was not accurately predicted. The significant wave height was significantly underestimated in all cases. Deviations of model results from the measurements varied up to 25% in the inner surf zone.

The implementation of the Raleigh model of Baldock et al. [1998] did not improve the predicted significant wave height on flat bottom slopes. The predictions of SWAN 40.11 and SWAN with the Rayleigh model nearly overlay each other.
On steep slopes the Rayleigh model proved to be a significant improvement. Implementation of the Rayleigh model reduced the error in the predicted significant wave height from 8-22% by SWAN 40.11 to 5-13% (by SWAN the Rayleigh model).

In SWAN the total dissipation rate in the surf zone and therefore the predicted variation of the significant wave height is dominated by the breaker parameter γ.
An expression for the breaker parameter γ depending on the local wave steepness was implemented. It is based on the formulation of Battjes and Stive [1985]. In the cases that were simulated in this study, the resulting variable γ was higher than 0.73 (the default value in SWAN 40.11). A higher γ-value allows for higher waves and thus for less dissipation. The prediction of the significant wave heights in the surf zone was significantly improved by SWAN with the adapted γ-value. The wave height predictions by SWAN with the adapted γ-value only deviated a few percent from the measurements.
The prediction of the significant wave heights on a steep slope is slightly more accurate with SWAN with the adapted γ-value than with SWAN with the Rayleigh model.
The breaker parameter depending on the local wave steepness exhibits a maximum at the bar crest and foreshore and a minimum in the trough.
It should be noted that this expression for the breaker parameter cannot be used as a rule-of-thumb for a quick estimation of maximum wave heights in the surf zone. It is an expression for an internal parameter of the dissipation model in SWAN and although resulting γ-values are in a realistic range, they have no direct physical meaning.

Prediction of fraction of breaking waves

The error in the prediction of the fraction of breaking waves by SWAN 40.11 was very large (more than 100%). The prediction of the fraction of breaking waves with SWAN with the adapted γ-value is slightly better, but still very inaccurate.
Implementation of the full Rayleigh distribution for both breaking and non-breaking waves according to Baldock et al. [1998] improved the results enormously. The error in the predicted fraction of breaking waves is 35% at most with SWAN with the Rayleigh model.

Prediction of wave period and wave spectra across the surf zone

In the simulations of the field data obtained at Petten SWAN overestimated the mean wave period at the shallowest station. In SWAN the shape of the spectra at the offshore boundary is more or less maintained across the surf zone. In the Petten cases too little energy is transferred to the higher frequencies by triad interactions, resulting in an overestimation of the mean wave period in the surf zone.

SWAN did not represent the trend in the measured variation of the mean wave period in the cases with bi-modal spectra. In the measurements the mean wave period decreases it the first part of the surf zone, caused by the shift of energy to the higher frequencies by triad interactions. In the last part of the surf zone, the mean wave period increases again due to dissipation of energy by wave breaking at the higher frequencies. In contrast to this, the SWAN results showed a steadily decreasing mean wave period across the surf zone.

In the simulations of the double-peaked spectra the mean wave period was overestimated in two cases and underestimated in two cases. Whether SWAN underestimates or overestimates the mean wave period is depending on the shape of the spectrum at the offshore boundary. In the two cases in which the mean wave period was underestimated the high-frequency peak contained more energy than the low-frequency peak. Because wave breaking does not influence the shape of the spectrum, the low-frequency peak was lowered too much in SWAN, resulting in an underestimation of the mean wave period. In the two cases in which the mean wave period was overestimated, the low-frequency peak contained more energy than the high-frequency peak. In the SWAN calculations relatively more energy is contained at the lower frequencies, resulting in an overestimation of the mean wave period.

In all the cases with the double-peaked spectra a distinct a high-frequency peak is maintained in the SWAN calculations, whereas in the measurements this is eliminated by wave breaking.

It can be concluded that distributing the energy dissipation by wave breaking proportional to the energy density level at each frequency is a wrong assumption. However, according to previous publications some good results have been obtained with it [e.g. ELDEBERKY AND BATTJES, 1996].

In contrast to e.g. Chen et al. [1997], Kirby and Kaihatu [1996] and Booij et al. [1999], adding a frequency-dependency of dissipation by wave breaking that enhances dissipation at the higher frequencies had an effect on predicted spectral shapes. It improved the *trend* in predicted variation of the mean wave period in the double-peaked cases. The *values* of the mean wave period were only improved in two cases. No unique formulation for the frequency dependency could be found such that the cross-shore variation of the mean wave period is qualitatively *and* quantitatively predicted with sufficient accuracy. No operational conclusions can be stated regarding the frequency-dependent formulation for wave breaking.

Furthermore it can be concluded that at present the effect of triad interactions is not correctly represented in SWAN. In none of the cases the $k^{-2.5}$-equilibrium range is established. Although in two cases the mean wave period was underestimated, too little energy is transferred to the frequency range between the two peaks and to frequencies higher than the high-frequency peak in all cases with bi-modal spectra. In all Petten cases too little energy is transferred to higher frequencies as well.

Moreover, on steep bottom slopes the present formulation of triads caused convergence problems. Apparently the present formulation cannot handle rapid bottom changes.

The predicted variation of the mean wave period by SWAN 40.11, SWAN with the Rayleigh model and SWAN with the adapted γ-value were almost identical.

7.4 Recommendations

- Implementation of the Rayleigh model of Baldock et al. [1998] in an operational version of SWAN as an optional command. However, a further testing of SWAN with the Rayleigh model is needed. The performance on a steep slope, regarding the predicted wave heights and the fraction of breaking waves, is only tested in one case. Moreover, attention should be paid to the exact programming, regarding the numerical solving of the equations.

- Implementation of the formulation for the breaker parameter γ depending on the local wave steepness as an optional command. A further calibration of the expression for the breaker parameter is recommended. In the present formulation it is positively depending on the local wave steepness. This implies that the steeper the waves the higher the value of γ, the higher the maximum wave height. This is against physical intuition.

- Investigation of the formulation for the breaker parameter depending on the local wave steepness applied to the Rayleigh model in SWAN. It might be that applying the Rayleigh model in SWAN with the adapted γ-value improves the prediction of both the significant wave height and the fraction of breaking waves across the surf zone.

- In this study the expression for the breaker parameter γ is only depending on the local wave steepness. In the literature a lot of formulations for γ are proposed, many in terms of the wave steepness and/or the bottom slope. After all it is the bottom that causes wave breaking and beach shapes vary widely. It is interesting to investigate whether the results of the computations can be improved further with an expression for γ that is dependent of the local wave steepness *and* the bottom slope.

- When studying spectral wave evolution across the surf zone, depth-induced wave breaking should not be the only process considered. Both wave breaking and triad interactions are very important processes in the surf zone. The evolution of the spectra to a $k^{-2.5}$-equilibrium range is a combined effect of these two processes. An important limitation of this study is the fact that only wave breaking is considered. As long as triad interactions are not accurately represented in SWAN it is difficult to isolate the inaccuracies caused by the formulation for depth-induced wave breaking regarding the spectral distribution of energy.

- A further examination and implementation of more accurate approximations of the triad interactions in SWAN is therefore also recommended. Referring to the previous statement in this paragraph, this should have priority in the process of improving the performance of SWAN calculations in the surf zone. When triad interactions are better approximated, the process of depth-induced wave breaking can be assessed better.

- An exact understanding of the effect of wave breaking on the spectral distribution of energy is still to come. Implementation of a frequency-dependent dissipation did not improve the performance of SWAN. According to Battjes and Eldeberky [1996] it may be expected that the low-frequency waves are less affected by breaking than the higher-frequency components, but there is no theoretical foundation at present to formulate this in a quantitative sense.
  Investigation of the spectral energy balance of breaking waves in the surf zone with both field and laboratory observations of a wide range of wave conditions might give more insight in the spectral source term for wave breaking.

- The placement of instruments at more positions in the cross-shore array of instruments at the Petten field site is recommended. More measurement positions would give more insight in the transformation of wave spectra across the surf zone. For an investigation of the spectral energy balance a denser array of instruments is needed.

- It is the bottom that causes wave breaking. It is therefore very important to have accurate measurements of the bottom profile when investigating wave breaking. Depending on the wave conditions the exact bottom profile can change significantly. At present surveys of the bathymetry at the Petten field site are not available on storm days. It is recommended to put effort in a way to measure the bathymetry during storms.

- In the present version of SWAN the results of predictions of the wave spectra in the surf zone might be improved by making the distribution of the frequency-integrated dissipation proportional to the deviation of the energy density level from the $k^{-2.5}$-equilibrium range given by (4.1) at each frequency. The resulting source term for wave breaking would be:

$$S_{br}(\sigma,\theta) = -D_{tot}\frac{\Delta E(\sigma,\theta)}{\iint[\Delta E(\sigma,\theta)]d\sigma d\theta} \tag{7.1}$$

  with:

$$\Delta E(\sigma,\theta) = E(\sigma,\theta) - E_{sat}(\sigma,\theta) \tag{7.2}$$

  However, the optimal value of the constant α_0 in the expression for the equilibrium range appeared to vary with changing bottom profile. This value should be estimated for a wide range of bottom profiles.

References

Andorka Gal, J.H., Holthuijsen, L.H., Jong, J.C.M. de, and Kieftenburg, A.T.M.M., 1998: *"Wave transformation near a quasi-1D coast"*, Proc. of 26th Int. Conf. on Coastal Eng., p.151-159.

Andorka Gal, J.H., 1996: *"Verification set Petten"*, National Institute for Coastal and Marine Management/RIKZ

Arcilla, A.S., Roelvink, J.A., O'Connor, B.A. and Jimenez, J.A., 1994: *"The delta flume '93 experiment"*, Proc. Coastal Dynamics Conf. '94, p. 488-502.

Baaijens, A.E., 1998: *"Verification of SWAN with DELILAH data"*, M.sc. thesis, Delft University of Technology.

Baldock, T.E., Holmes, P., Bunker and S., Weert, P. van, 1998: *"Cross-shore hydrodynamics within an unsaturated surf zone"*, Coastal Engineering, 34, p.173-196.

Battjes, J.A., 1974: *"Surf similarity"*, Proc. of 14th Int. Conf. on Coastal Eng., p. 467-479.

Battjes, J.A. and Janssen, J.P.F.M., 1978: *"Energy loss and set-up due to breaking of random waves"*, Proc. of 16th Int. Conf. on Coastal Eng., p. 596-588.

Battjes, J.A. and Stive, M.J.F., 1985: *"Calibration and verification of a dissipation model for random breaking waves"*, Journ. of Geophys. Res., 90 (C5), p. 9159-9167.

Battjes, J.A., 1988: "Surf-zone dynamics", Ann. Rev. Fluid Mechanics, p. 257-293.

Battjes, J.A. and Beji, S., 1992: *"Breaking waves over a shoal"*, Proc. of 23rd Int. Conf. on Coastal Eng., p. 42-50.

Battjes, J.A., Eldeberky, Y. and Won, Y., 1993: *"Spectral Boussinesq modeling of breaking waves"*, Ocean Wave Measurement and Analysis, Proc. of 2nd int. symp., p. 813-820.

Battjes, J.A., 1994: *"Shallow water wave modelling"*, Proc. of international symposium: waves – physical and numerical modelling, p. 1-22.

Battjes, J.A., 1998: *"Korte golven"*, lecture notes (in Dutch), Delft University of Technology.

Battjes, J.A. and Groenendijk, H.W., 2000: *"Wave height distributions on shallow foreshores"*, Coastal Engineering, 40, p. 161-182.

Beji, S. and Battjes, J.A., 1992: *"Experimental investigation of wave propagation over a bar"*, Coastal Engineering, 19, p.151-161.

Beji, S. and Battjes, J.A., 1994: *"Numerical simulation of nonlinear wave propagation over a bar"*, Coastal Engineering, 23, p. 1-16.

Booij, N., Ris, R.C. and Holthuijsen, L.H., 1999: *"A third-generation wave model for coastal regions"*, Journ. of Geophys. Res., 104 (C4), p. 7649-7666.

Bouws E., Günther, H., Rosenthal W., Vincent, C.L., 1985: *"Similarity of the wind wave spectrum in finite depth water, 1. Spectral form"*, Journ. of Geophys. Res., 90 (C1), p. 974-986.

Cai, M., Basco, D.R. and Baumer, J., 1992: *"Bar/trough effects on wave height probability distributions and energy losses in surf zones"*, Proc. of 23rd Int. Conf. on Coastal Eng., p. 103-115.

Chen, Y., Guza, R.T. and Elgar, S., 1997: *"Modelling spectra of breaking surface waves in shallow water"*, Journ. of Geophys. Res., 102 (C11), p. 25035-24046.

Dally, W.R., 1990: *"Random breaking waves: a closed-form solution for planar beaches"*, Coastal Engineering, 14, p. 233-263.

Dally, W.R., 1992: *"Random breaking waves: field verification of a wave-by-wave algorithm for engineering application"*, Coastal Engineering, 16, p. 369-397.

Eldeberky, Y., 1996: *"Nonlinear transformation of wave spectra in the nearshore zone"*, Ph.D. thesis, Delft University of Technology.

Eldeberky, Y. and Battjes, J.A., 1996: *"Spectral modeling of wave breaking: application to Boussinesq equations"*, Journ. of Geophys. Res., 101 (C1), p. 1253-1263.

Elgar, S., Guza, R.T., Herbers, T.H.C. and Gallagher, E.L., 1997: *"Spectral evolution of shoaling and breaking waves on a barred beach"*, Journ. of Geophys. Res., 102 (C7), p. 15797-15805.

Herbers, T.H.C., Russnogle, N.R. and Elgar, S., 2000: *"Spectral energy balance of breaking waves within the surf zone"*, submitted to Journ. of Phys. Oceanography.

Holthuijsen, L.H., Booij, N., Ris, R.C., Haagsma, IJ.G., Kieftenburg, A.T.M.M., and Kriezi, E.E., 2000: *"User manual – SWAN cycle III version 40.11"* , Delft University of Technology.

Holthuijsen, L.H., Ris, R.C., Booij, N., Cecchi, E., 2000: *"The effect of low-frequency waves on white capping"*, draft.

Kaminsky, G.M. and Kraus, N.C., 1993: *"Evaluation of depth-limited wave breaking criteria"*, Ocean Wave Measurement and Analysis, Proc. of 2nd int. symp., p. 180-193.

Kirby, J.T. and Kaihatu, J.M., 1996: *"Structure of frequency domain models for random wave breaking"*, Proc.of 25th Int. Conf. on Coastal Eng., p. 1144-1155.

Kitaigorodskii, S.A., Krasitskii, V.P., and Zaslvskii, M.M., 1975: *"On Phillips' theory of equilibrium range in the spectra of wind-generated gravity waves"*, Journ. of Phys. Oceanography, vol. 5, p. 410-420.

Kruif, A.C. de, 2000: *"Storm data of the Petten field site: 1995-2000"*, National Institute for Coastal and Marine Management/RIKZ

Kuriyama, Y., 1996: *"Models of wave height and fraction of breaking waves on a barred beach"*, Proc.of 25th Int. Conf. on Coastal Eng., p 247-260.

Mase, H. and Iwagaki, M., 1982: *"Wave height distributions and wave grouping in the surf zone"*, Proc. of 18th Conf. on Coastal Eng., p. 58-76.

Mase, H. and Kirby, J.T., 1992: *"Hybrid frequency-domain Kdv equation for random wave transformation"*, Proc. of 23rd Int. Conf. on Coastal Eng., p.474-487.

Miche, R., 1944: *"Mouvements ondulatoires des mers en profondeur constante ou décroissante"*, Annales des Ponts et Chaussées.

Nelson, R.C., 1994: *"Depth limited wave heights in very flat regions"*, Coastal Engineering, 23, p. 43-59.

Nelson, R.C., 1997: *"Height limits in top down and bottom up wave environments"*, Coastal Engineering 32, p. 247-254.

Phillips, O.M., 1958: *"The equilibrium range in the spectrum of wind-generated waves"*, Journ. of Fluid Mech., vol. 4, p426-434.

Ris, R.C., Dingemans, M.W., Cecchi, E., Wallast, I., Holthuijsen, L.H. and Booij, N., 2000: *"SWAN: Physical formulations and data for validation"*, WL/Delft Hydraulics.

Rivero, F.J., Arcilla, A.S. and Beyer, D., 1994: *"Comparison of a wave transformation model with LIP-11D data"*, Proc. Coastal Dynamics Conf. '94, p. 518-532.

Roelvink, J.A., 1993: *"Dissipation in random wave groups incident on a beach"*, Coastal Engineering, 19, p. 127-150.

Smith, E.R. and Kraus, N.C., 1991: *"Laboratory study of wave-breaking over bars and artificial reefs"*, Journ. of Waterway, Port, Ocean and Coastal Eng., vol. 117, p. 307-324.

Smith, J. and Vincent, C.L., 1992: *"Shoaling and decay of two wave trains on a beach"*, Journ. of Waterway, Port, Ocean and Coastal Eng., vol. 118, p. 517-533.

Southgate, H.N. and Wallace, H.M, 1994: *"Breaking wave persistence in parametric surf zone models"*, Proc. Coastal Dynamics Conf. '94, p. 543-555.

Thornton, E.B., 1977: *"Rederivation of the saturation range in the frequency spectrum of wind-generated gravity waves"*, Journ. of Phys. Oceanography, vol. 7, p. 137-140.

Thornton, E.B. and Guza, R.T., 1983: *"Transformation of wave height distribution"*, Journ. of Geophys. Res., 88 (C10), p. 5925-5938.

Tuba Özkan, H. and Kirby, J.T., 1993: *"Evolution of breaking directional spectral waves in the nearshore zone"*, Ocean Wave Measurement and Analysis, Proc of 2nd int. symp., p. 753-761.

Vincent, C.L., Smith, J. and Davis. J., 1994: *"Parameterization of wave breaking in models"*, Waves – physical and numerical modelling, Proc of int. symp., p. 753-761.

Vincent, C.L. and Smith, J., 2000: "Spectral model for depth-limited wave breaking", personal copy.

Young, I.R., 1999: *"Wind generated ocean waves"*, Amsterdam Elsevier Science.

Appendices

4A Water levels at Petten

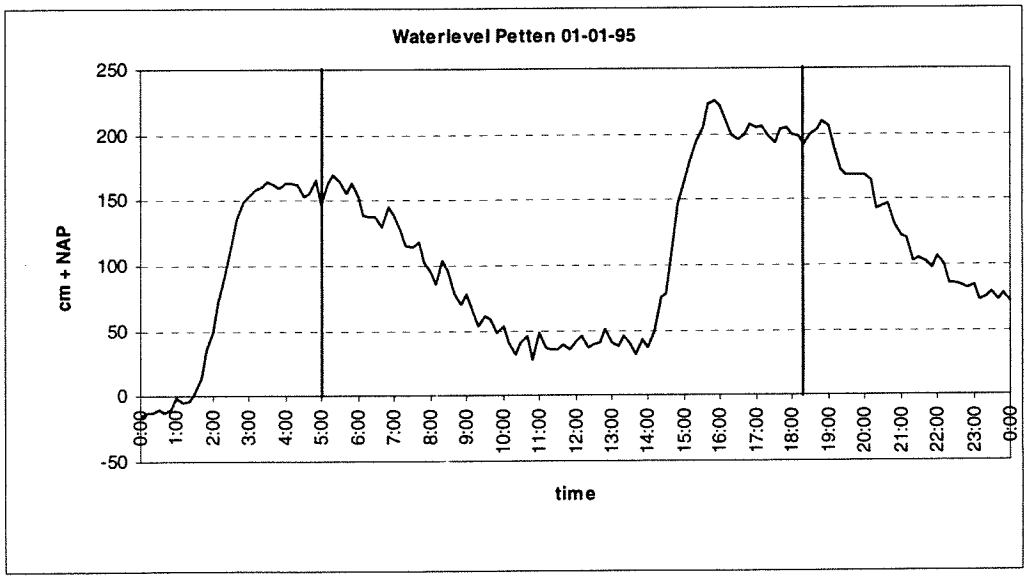

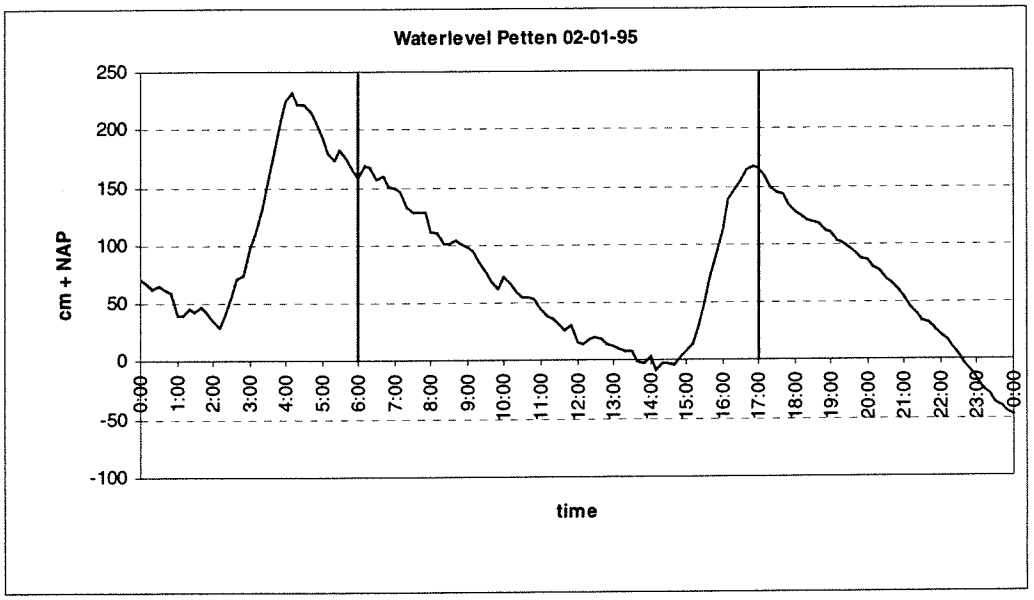

(Vertical lines show selected times for simulation with SWAN)

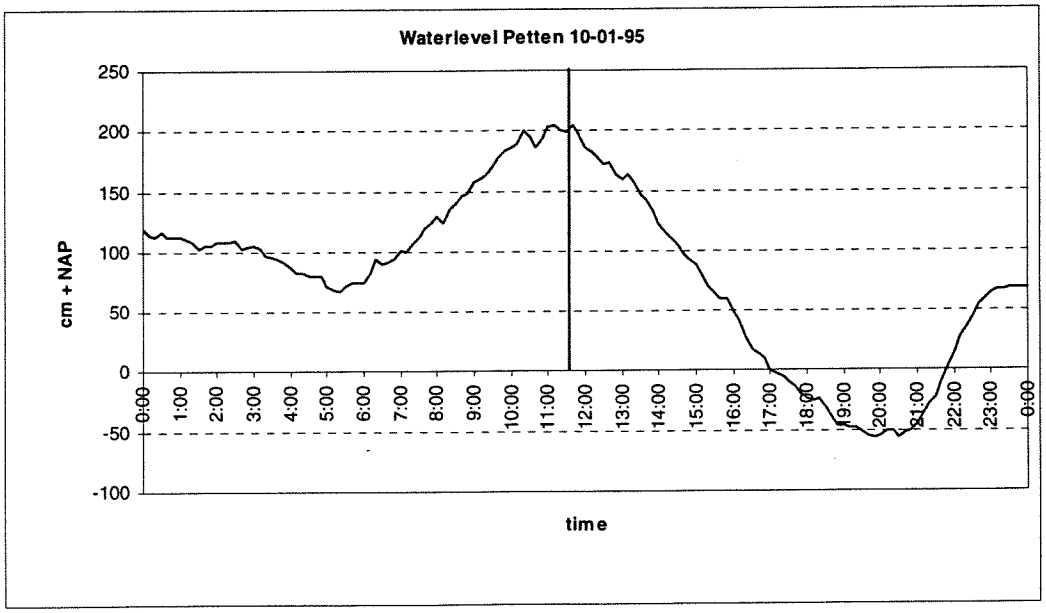
Waterlevel Petten 10-01-95
250
200
150
100
50
0
-50
-100
cm + NAP
0:00
1:00
2:00
3:00
4:00
5:00
6:00
7:00
8:00
9:00
10:00
11:00
12:00
13:00
14:00
15:00
16:00
17:00
18:00
19:00
20:00
21:00
22:00
23:00
0:00
time

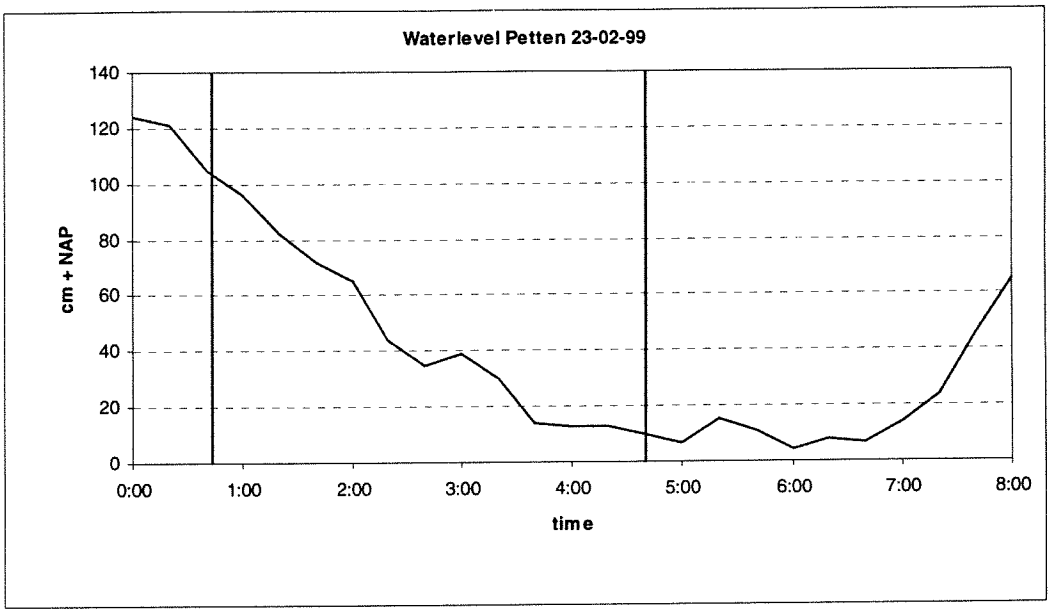
Waterlevel Petten 23-02-99
140
120
100
80
60
40
20
0
cm + NAP
0:00
1:00
2:00
3:00
4:00
5:00
6:00
7:00
8:00
time

4B SWAN input files

```
PROJect  'Petten 1995'  '1'
           '01-01-1995'
           '05:00'
$
$  ******************************************************************************
$  LET OP: per tijdstip aanpassen: WLEVEL, WIND, NAMEN IN- EN OUTPUT-FILES
$  ******************************************************************************
$  PROBLEEMDEFINITIE - INSTELLINGEN
$
$  set  wlevel nor depmin maxmes maxerr grav rho inrhog hserr cartesian pwtail
   SET   1.47  90   0.05   100     3    9.81 1025 0      0.1  CARTesian   5
$
   MODE    STATionary     TWODimensional
$
   COORDinates CARTesian
$
$  cgrid rectang  xpc  ypc    alpc xlenc ylenc mxc myc circle mdc flow fhigh msc
   CGRID REGular 97227 534010 325  8500  6000  425 300 CIRcle 36  0.03 0.5   30
$
$
$  inpgrid bottom rectang xpinp ypinp  alpinp mxinp myinp dxinp dyinp
   INPgrid BOTtom REGular 92000 526000   0     824   849   20    20
$
$
$  readinp bottom fac   fname1          idla nhedf format
   READ   BOTtom  -0.01 'petten95.asc'  1    6     FREe
$
$  wind  vel  dir
   WIND  16   302
$
$
$  bnd cond  side  dir     constant file fname
   BOUNdspec SIDE  NW  CCW CONSTANT FILE '01010500mp1.bnd'
   BOUNdspec SIDE  NO  CCW CONSTANT FILE '01010500mp1n.bnd'
   BOUNdspec SIDE  SW  CCW CONSTANT FILE '01010500mp1z.bnd'
$
$
$******************************************************************************
$  FYSICA
$
   GEN3   KOMen
$
$  breaking  constant alpha gamma
   BREaking  CONstant 1.0   0.73
$
$  friction
   FRICtion JONswap
$
$  triad
   TRIad
$
   SETUP
```

```
$*************************************************************************
$  NUMERIEK
$
$  numerics        drel dhoval dtoval npnts stationary  mxitst limiter
   NUMeric   ACCUR 0.02 0.02   0.02    98.  STATionary  15      0.1
$
$
$*************************************************************************
$  OUTPUT
$
$  curve 'sname'    xp1     yp1  int xp2    yp2    int xp3    yp3
$                                 int xp5    yp5    int xp6    yp6
   CURve 'meetraai' 98981 536444 481 103000 533800 287 105230 531990 &
                                 33  105520 531830 15  105650 531746
$
$  points  'sname' xp     yp
   POINts  'MP1'   98981  536444
   POINts  'MP2'   103000 533800
   POINts  'MP3'   105230 531990
   POINts  'MP5'   105520 531830
   POINts  'MP6'   105650 531746
$
$
$  block  compgrid  header   'fname'            layout idla parameter
   BLOck 'COMPGRID' NOHEADer '01010500dep.blk' LAYout  1   DEPth
   BLOck 'COMPGRID' NOHEADer '01010500Hs.blk'  LAYout  1   HSing
   BLOck 'COMPGRID' NOHEADer '01010500Tm1.blk' LAYout  1   TM01
   BLOck 'COMPGRID' NOHEADer '01010500Tm2.blk' LAYout  1   TM02
   BLOck 'COMPGRID' NOHEADer '01010500Qb.blk'  LAYout  1   QB
$
$
$  tabel 'sname'    header 'fname'
   TABle 'meetraai' HEADer '01010500.tbl' XP YP DEPth HS TM01 TM02 RTP STEEPNESS

   &   DIR DSPR DISSIP QB
$
$
$  specout 'sname' spec1D/2D abs/rel 'fname'
   SPECout  'MP1'  SPEC1D     ABs    '01010500MP1.sp1'
   SPECout  'MP2'  SPEC1D     ABs    '01010500MP2.sp1'
   SPECout  'MP3'  SPEC1D     ABs    '01010500MP3.sp1'
   SPECout  'MP5'  SPEC1D     ABs    '01010500MP5.sp1'
   SPECout  'MP6'  SPEC1D     ABs    '01010500MP6.sp1'
$
$*************************************************************************
$  COMMANDO'S UITVOEREN
$
   TEST 30 0 POINTS XY  98981 536444 103000 533800 105230 531990 105520 531830
   &    105650 531746 S1D '01010500.src'
$
   COMPUTE
$
   POOL
$
   STOP
```

```
PROJect  'SV data'  '1'
           'case01'
$
$*****************************************************************************
$  mode
   MODE    STATionary   ONEDimensional
$
$  coordinates
   COORDinates  CARTesian
$
$  set level nor  depmin maxmes maxerr grav rho  inrhog hserr cartesian pwtail
   SET  0    90.0  0.02   200     3     9.81 1000  0     0.1  CARTesian 5
$
$*****************************************************************************
$  PROBLEEMDEFINITIE
$
$  compgrid rectang xpc ypc alpc xlenc ylenc mxc myc
   CGRID    REGular  0   0   0.0  45.7  0    914  0
$
$  sector dir1 dir2 mdc flow fhigh msc
   SECTOR -15  15   60  0.25 3.00  62
$
$
$  inputgrid bottom rectang xpinp ypinp alpinp mxinp myinp dxinp dyinp
   INPgrid   BOTtom REGular  0     0     0       914    0     0.05  0
$
$
$  readinp   bottom fac 'fname1'       idla nhedf format
   READinp   BOTtom -1  'SVbottom.txt'  2    0    FREe
$
$  randvwd    side west constant file 'fname' seq
   BOUNdspec  SIDE  W   CONSTANT FILE 'bnd01.bnd'  1
$
$  initial
   INITial   ZERO
$
$*****************************************************************************
$  FYSICA
$
   GEN3  KOMen
$
$  breaking            alpha  gamma
   BREaking  CONstant   1.0    0.73
$
$
$  friction           cfjon
   FRICtion  JONswap  0.067
$
$  triads   trfac   cutfr
   TRIad     0.1    2.2
$
   OFF QUADrupl
$
   SETUP
$
```

```
$*************************************************************************
$  NUMERIEK
$
$  numerics        drel dhoval dtoval npnts stationary  mxitst limiter
   NUMeric   ACCUR 0.02 0.02   0.02    98.  STATionary  15      0.1
$*************************************************************************
$  OUTPUT
$
$  curve           xp1 yp1 int  xp   yp
   CURve   'goot'  0   0   913  45.7 0
$
$
$  punten   naam    xp    yp
   POINts  'd=61.0' 10.00 0
   POINts  'd=36.6' 28.30 0
   POINts  'd=24.4' 32.00 0
   POINts  'd=18.3' 33.80 0
   POINts  'd=15.2' 34.75 0
   POINts  'd=12.2' 35.65 0
   POINts  'd=9.1'  36.55 0
   POINts  'd=7.6'  37.00 0
   POINts  'd=6.1'  37.45 0
$
$
$  tabel    naam   header fname
   TABle   'goot'  HEADer 'output01.tbl' XP YP DEPth HSign TM01 TM02 DISSip
   &   STEEPNESS DIR DSPR WIND QB
$
$
$  spectrum  punt
   SPECout  'd=61.0' SPEC1D ABs   'd610.sp1'
   SPECout  'd=36.6' SPEC1D ABs   'd366.sp1'
   SPECout  'd=24.4' SPEC1D ABs   'd244.sp1'
   SPECout  'd=18.3' SPEC1D ABs   'd183.sp1'
   SPECout  'd=15.2' SPEC1D ABs   'd152.sp1'
   SPECout  'd=12.2' SPEC1D ABs   'd122.sp1'
   SPECout  'd=9.1'  SPEC1D ABs   'd91.sp1'
   SPECout  'd=7.6'  SPEC1D ABs   'd76.sp1'
   SPECout  'd=6.1'  SPEC1D ABs   'd61.sp1'
$
$                      fname  titel
$   PLOtspec 'd=61.0'  FIle  'pld610.plt' 'SVcase01' d=61.0 SPECtrum NONORM
    &   FReq
$
$*************************************************************************
$  COMMANDO'S UITVOEREN
   TEST 30 0 POINTS IJ 200 0 566 0 640 0 676 0 695 0 713 0 731 0 740 0 749 0 S1D
   &   'srcterm.src'
$
   COMPUTE
$
$
   POOL
$
   STOP
```

4C Sensitivity analysis of directional spreading in the laboratory flume

			measurement	swan			
Xp	Xp	Depth	Hsig	Hsig dir10	Hsig dir5	Hsig 3.5	Hsig 2.0
[m]	[m]	[m]	[m]	[m]	[m]	[m]	[m]
0.00	0.00	0.610	0.135	0.136	0.135	0.134	0.133
28.80	28.30	0.366	0.125	0.129	0.128	0.129	0.128
32.45	31.95	0.244	0.126	0.123	0.121	0.119	0.115
34.25	33.75	0.184	0.118	0.106	0.104	0.099	0.096
35.20	34.70	0.152	0.106	0.093	0.091	0.087	0.083
36.10	35.60	0.122	0.084	0.080	0.079	0.076	0.070
37.00	36.50	0.092	0.073	0.064	0.064	0.062	0.057
37.60	37.10	0.072	0.072	0.052	0.052	0.052	0.051
37.95	37.45	0.060	0.062	0.045	0.045	0.045	0.044

			measurement	swan			
Xp	Xp	Depth	Tm01	Tm01 dir10	Tm01 dir 5	Tm01 dir 3.5	Tm01 dir 2.0
[m]	[m]	[m]	[sec]	[sec]	[sec]	[sec]	[sec]
0.00	0.00	0.610	1.30	1.288	1.288	1.288	1.288
28.80	28.30	0.366	1.34	1.312	1.310	1.307	1.310
32.45	31.95	0.244	1.31	1.300	1.302	1.296	1.308
34.25	33.75	0.183	1.24	1.268	1.284	1.277	1.300
35.20	34.70	0.152	1.23	1.233	1.251	1.253	1.213
36.10	35.60	0.122	1.26	1.192	1.206	1.206	1.216
37.00	36.50	0.091	1.32	1.156	1.163	1.159	1.161
37.60	37.10	0.071	1.37	1.136	1.139	1.135	1.141
37.95	37.45	0.061	1.41	1.126	1.128	1.123	1.124

It appears that the results of the computations are fairly insensitive to different directional spreads, in particular for the significant wave height.

The mean wave period seems fairly insensitive for the directional spread.

In the calculation with a directional spread at the boundary of 10 degrees, the directional spread was reduced to approximately 5 degrees at the measurement locations in the surf zone.
In the calculation with a directional spread at the boundary of 2.0, 3.5 and 5.0 degrees, the directional spread remained more or less constant; approximately 2.0, 3.5 and 5.0 respectively.

A smaller directional spread requires a higher directional resolution. This increases the computational time, although this can partly be compensated with a smaller sector that is covered in the computations As a directional spread of 10 degrees seems fairly high for flume conditions, a directional spread of 5 degrees is applied in the calculations.

4D Variation of the significant wave heights in the Petten cases

Petten 1/1/1995 5:00

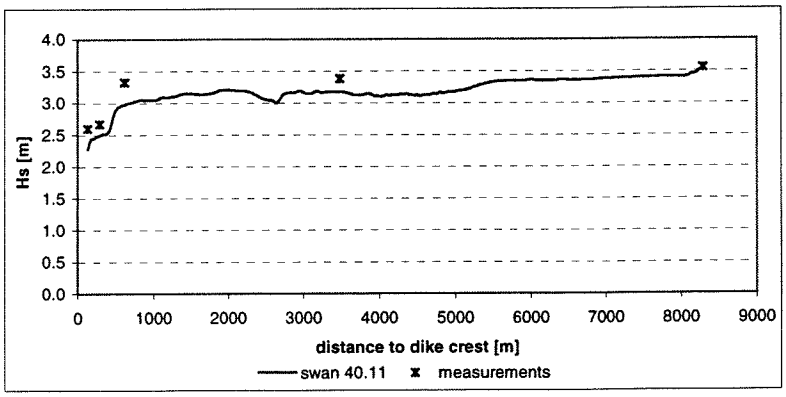

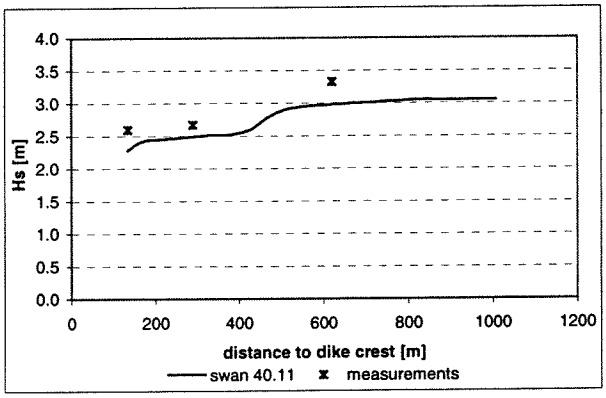

Petten 1/1/1995 18:20

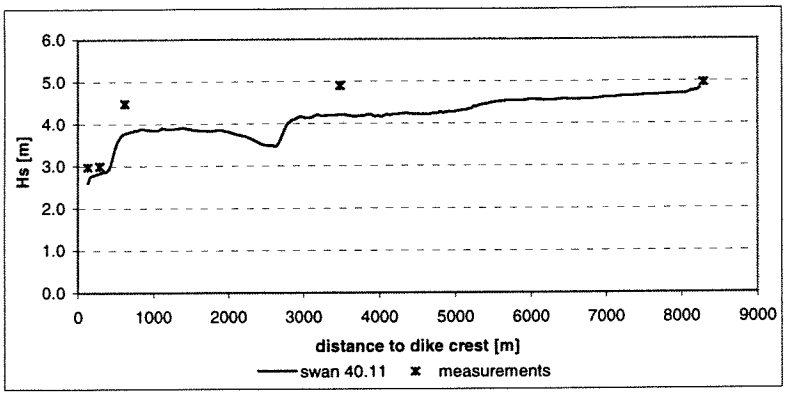

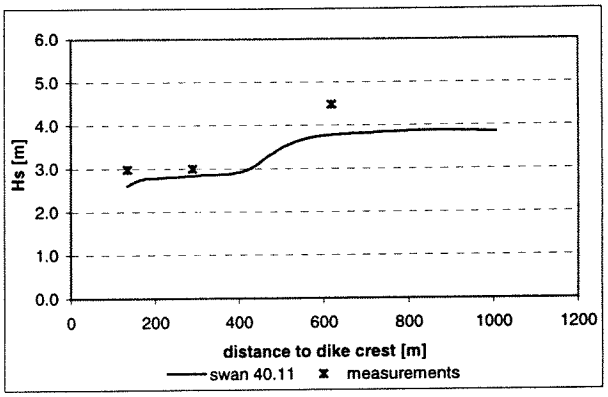

Petten 2/1/1995 6:00

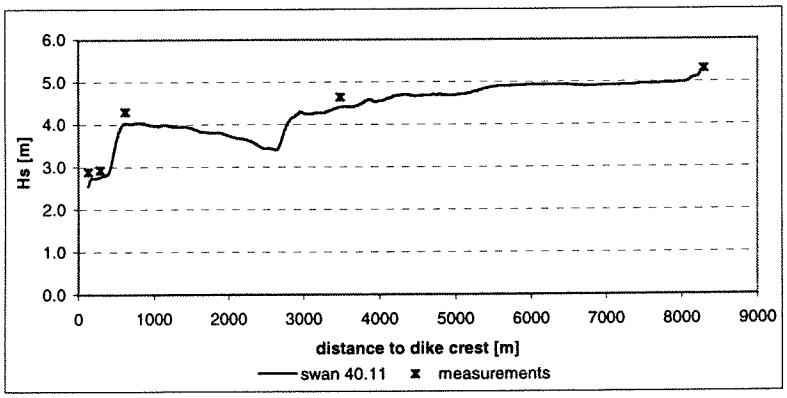

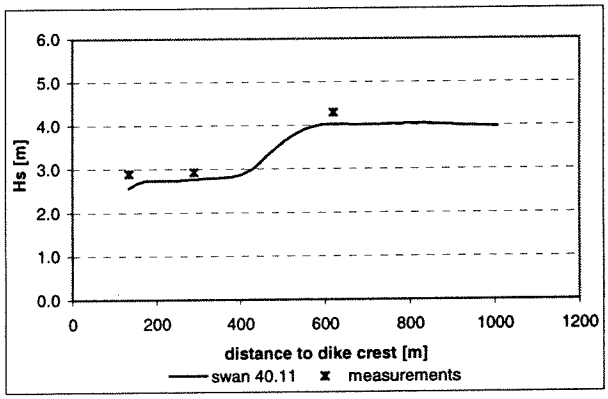

Petten 2/1/1995 17:00

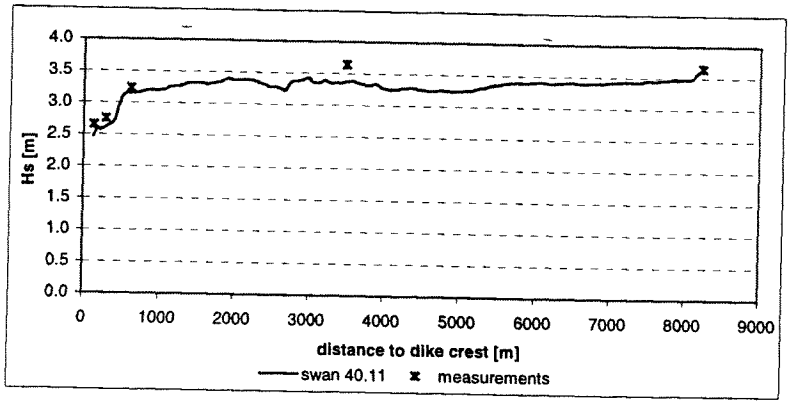

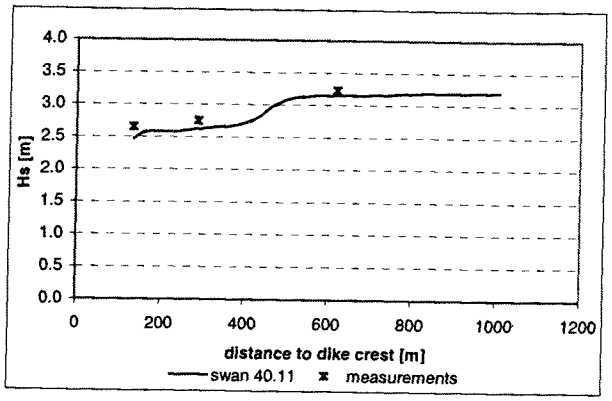

Petten 10/1/1995 11:40

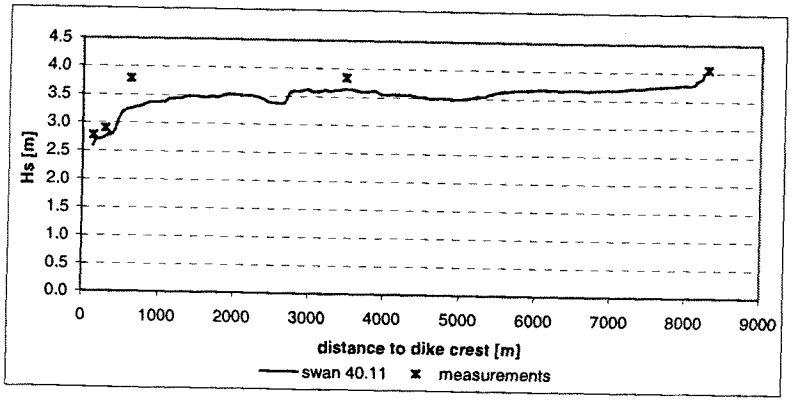

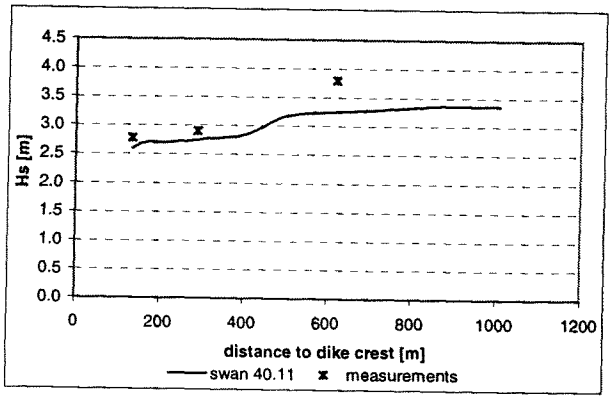

Petten 23-02-99 0:40

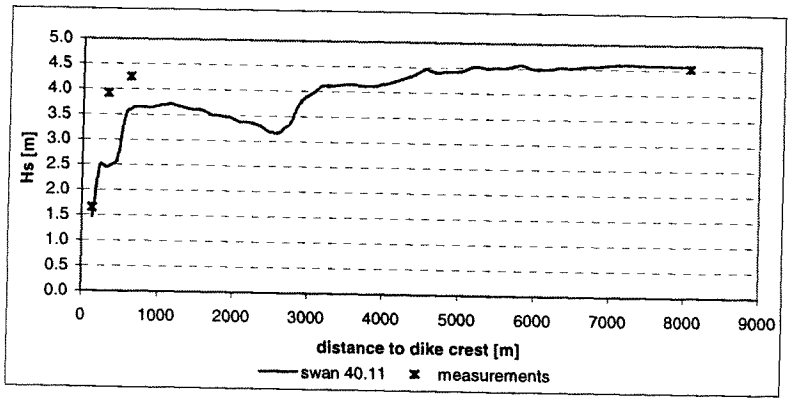

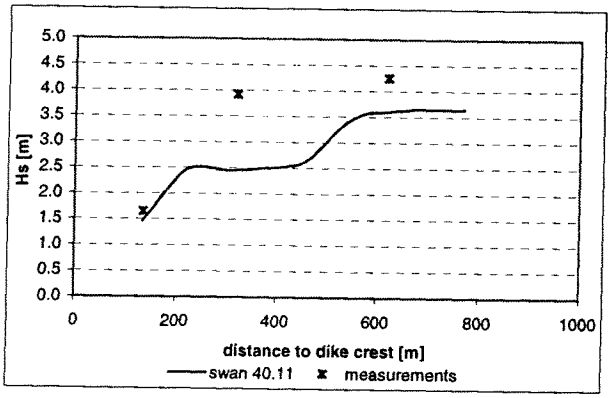

Petten 23-02-99 4:40

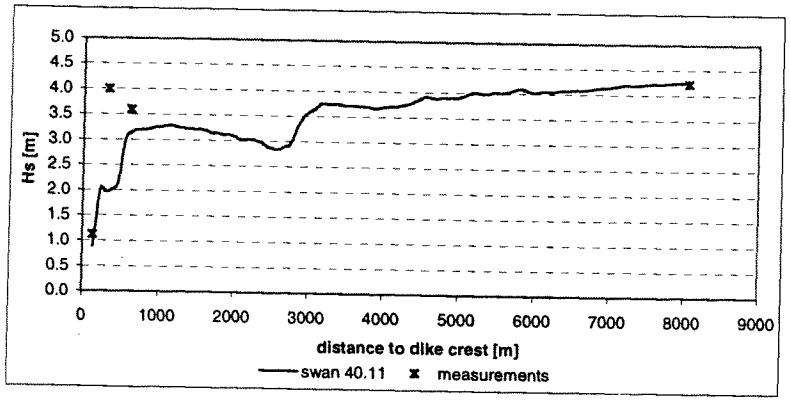

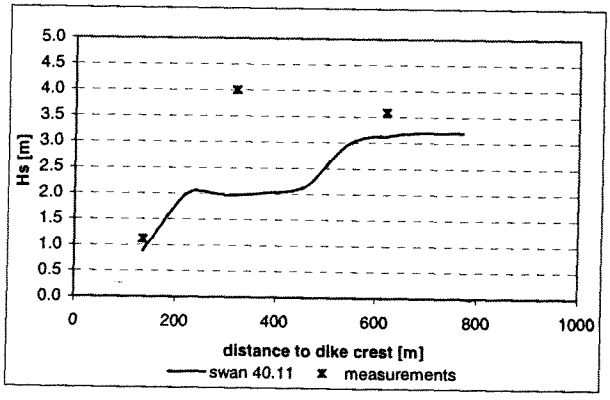

1995

01-01-0500

	measured	swan 40.11	
	Hs [m]	Hs [m]	difference
mp 1	3.60	3.60	0%
mp 2	3.38	3.18	-6%
mp 3	3.33	2.98	-11%
mp 5	2.67	2.49	-7%
mp 6	2.60	2.28	-12%

01-01-1820

	measured	swan 40.11	
	Hs [m]	Hs [m]	difference
mp 1	4.98	4.96	0%
mp 2	4.90	4.21	-14%
mp 3	4.48	3.77	-16%
mp 5	3.00	2.83	-6%
mp 6	2.98	2.60	-13%

02-01-0600

	measured	swan 40.11	
	Hs [m]	Hs [m]	difference
mp 1	5.39	5.28	-2%
mp 2	4.64	4.41	-5%
mp 3	4.30	4.02	-7%
mp 5	2.93	2.75	-6%
mp 6	2.89	2.56	-11%

02-01-1700

	measured	swan 40.11	
	Hs [m]	Hs [m]	difference
mp 1	3.77	3.77	0%
mp 2	3.64	3.37	-7%
mp 3	3.23	3.15	-2%
mp 5	2.75	2.62	-5%
mp 6	2.65	2.46	-7%

10-01-1140

	measured	swan 40.11	
	Hs [m]	Hs [m]	difference
mp 1	4.12	4.10	0%
mp 2	3.84	3.64	-5%
mp 3	3.79	3.25	-14%
mp 5	2.90	2.74	-6%
mp 6	2.78	2.60	-6%

1999

23-02-0040

	measured	swan 40.11	
	Hs [m]	Hs [m]	difference
mp 1	4.53	4.54	0%
mp 3	4.25	3.6	-15%
*mp 5**	*3.92*	*2.45*	*-38%*
mp 6	1.65	1.46	-12%

23-02-0440

	measured	swan 40.11	
	Hs [m]	Hs [m]	difference
mp 1	4.23	4.24	0%
mp 3	3.59	3.13	-13%
*mp 5**	*4.00*	*1.97*	*-51%*
mp 6	1.12	0.92	-18%

* instrument probably not working

4E Variation of the significant wave heights in the SV cases

SV case 01

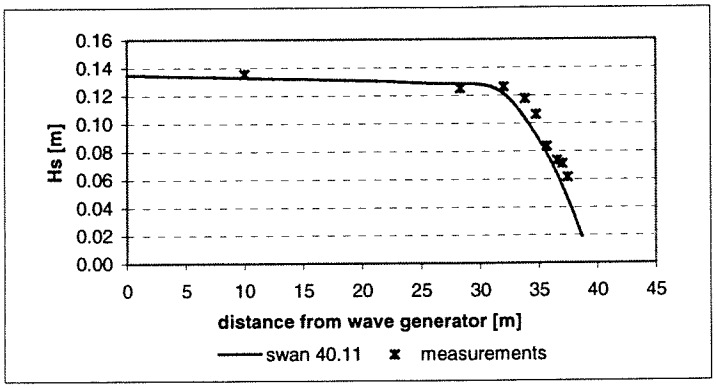

SV case 03

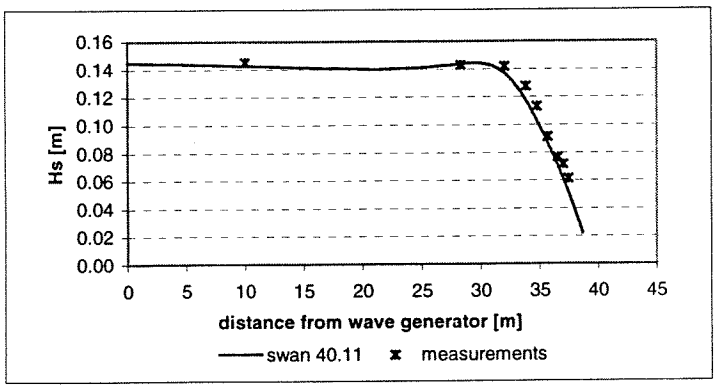

SV case 07

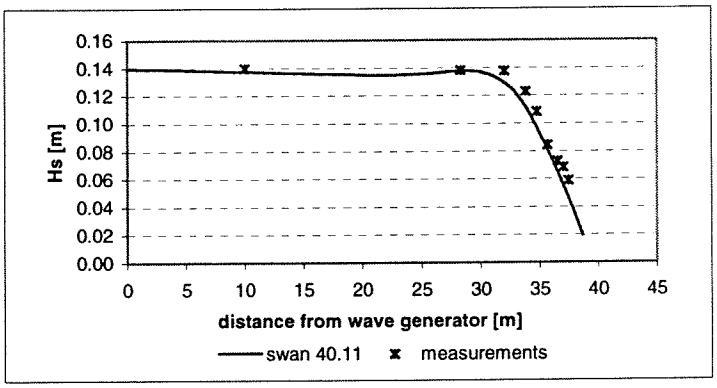

SV case 09

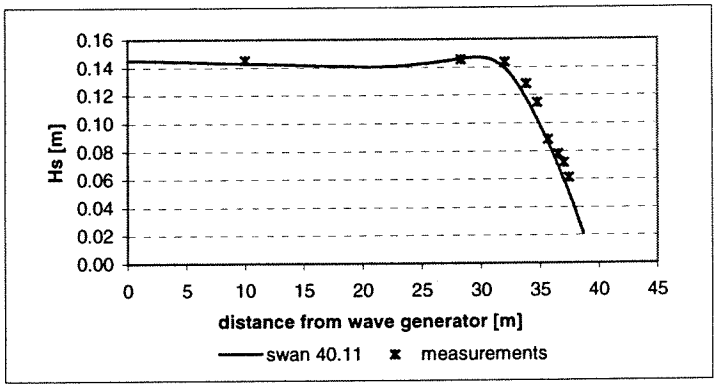

case 1

	measurement	swan 40.11	
depth [cm]	Hs [m]	Hs [m]	difference
61	13.5	13.4	-1%
36.6	12.5	12.9	3%
24.4	12.6	12.0	-5%
18.3	11.8	10.2	-13%
15.2	10.6	8.9	-16%
12.2	8.5	7.5	-11%
9.7	7.5	6.1	-19%
7.6	7.2	5.6	-23%
6.1	6.2	4.5	-26%

case 3

	measurement	swan 40.11	
depth [cm]	Hs [m]	Hs [m]	difference
61	14.5	14.4	-1%
36.6	14.3	14.4	1%
24.4	14.2	13.6	-4%
18.3	12.8	11.7	-9%
15.2	11.3	10.2	-10%
12.2	9.1	8.6	-6%
9.7	7.7	7.0	-9%
7.6	7.2	6.1	-15%
6.1	6.1	5.3	-14%

case 7

	measurement	swan 40.11	
depth [cm]	Hs [m]	Hs [m]	difference
61	13.98	13.81	-1%
36.6	13.81	13.80	0%
24.4	13.77	12.64	-8%
18.3	12.28	10.91	-11%
15.2	10.82	9.54	-12%
12.2	8.43	8.00	-5%
9.7	7.25	6.39	-12%
7.6	6.84	5.58	-18%
6.1	5.89	4.76	-19%

case 9

	measurement	swan 40.11	
depth [cm]	Hs [m]	Hs [m]	difference
61	14.51	14.46	0%
36.6	14.57	14.61	0%
24.4	14.38	13.74	-4%
18.3	12.8	11.69	-9%
15.2	11.47	10.14	-12%
12.2	8.83	8.50	-4%
9.7	7.79	6.83	-12%
7.6	7.17	6.00	-16%
6.1	6.1	5.07	-17%

4F Variation of the wave period in the Petten cases

Petten 1/1/1995 5:00

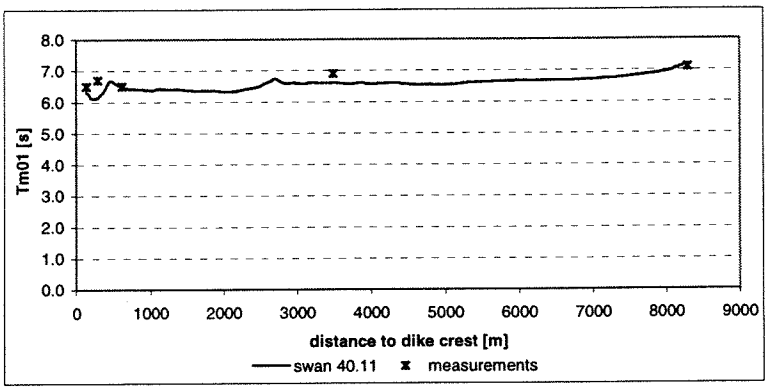

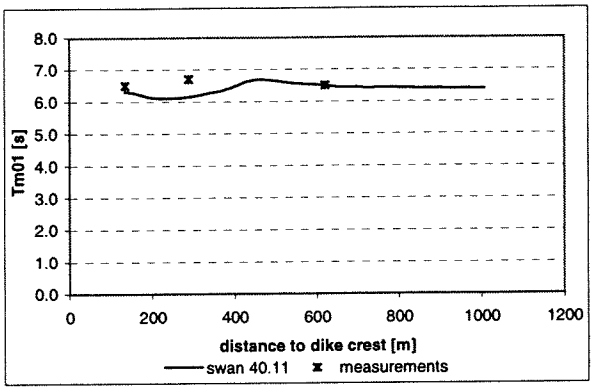

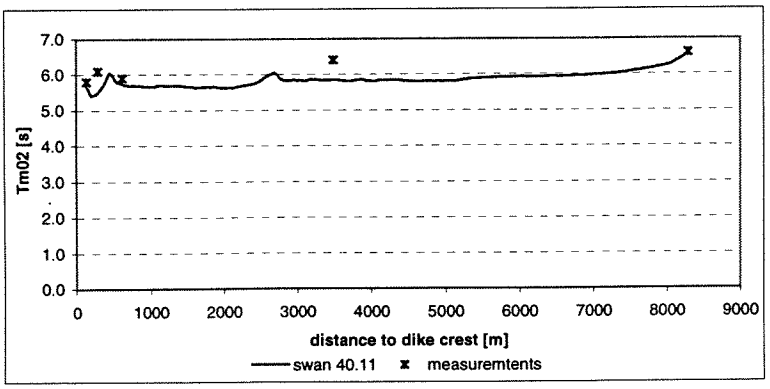

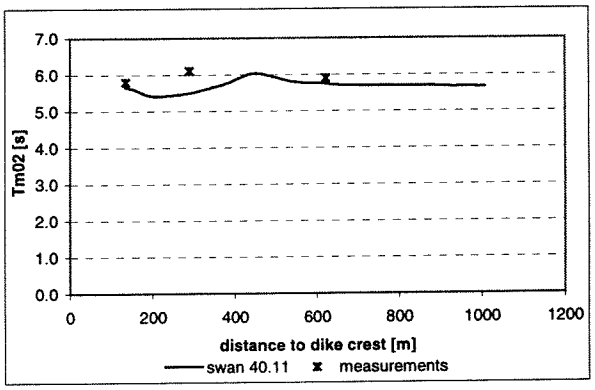

Petten 1/1/1995 18:20

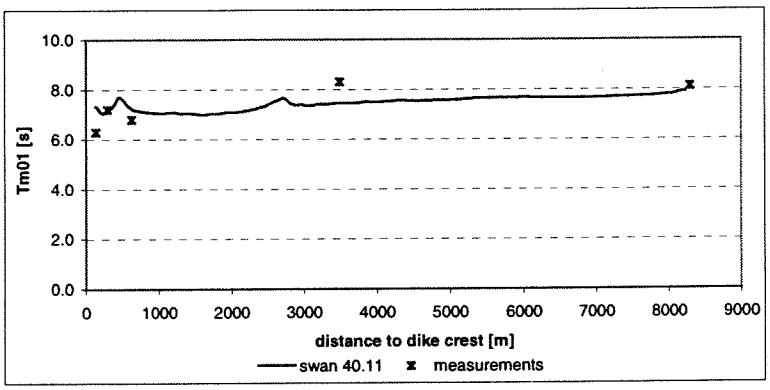

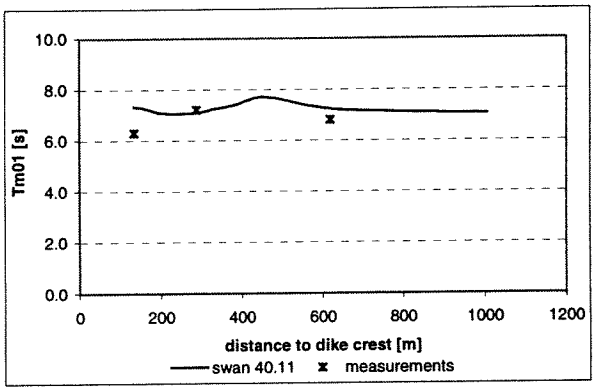

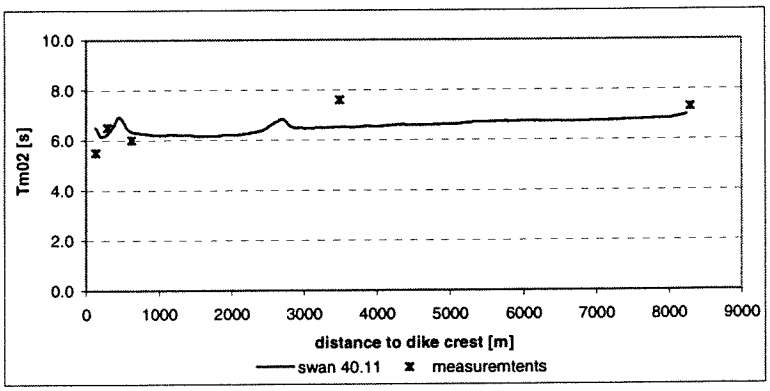

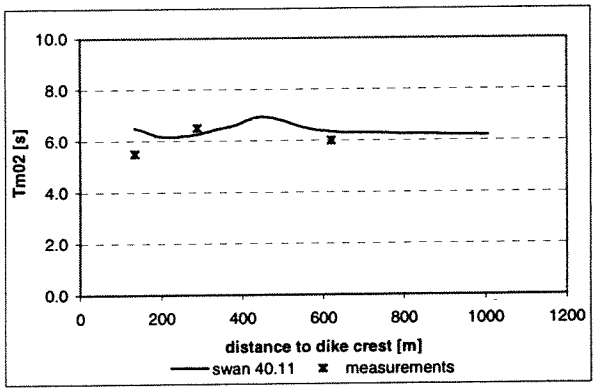

Petten 2/1/1995 6:00

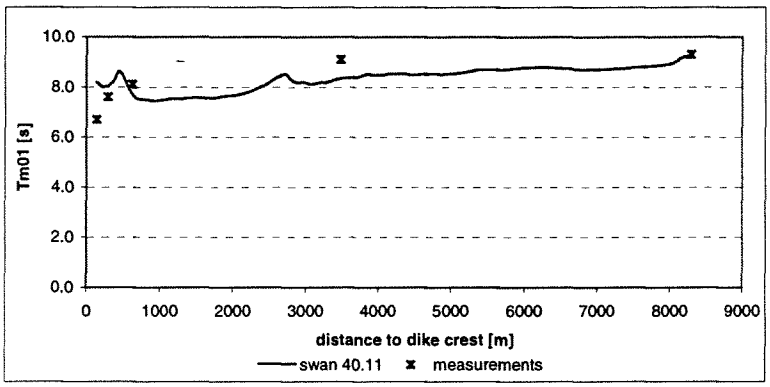

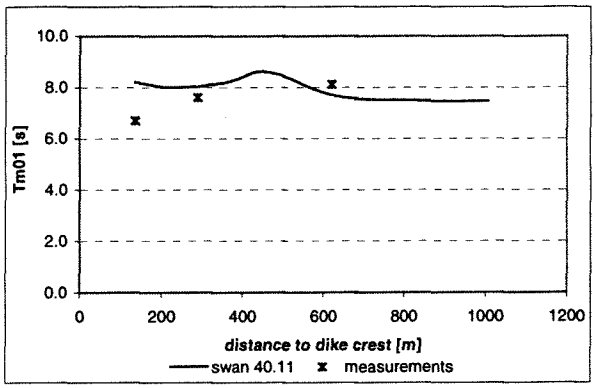

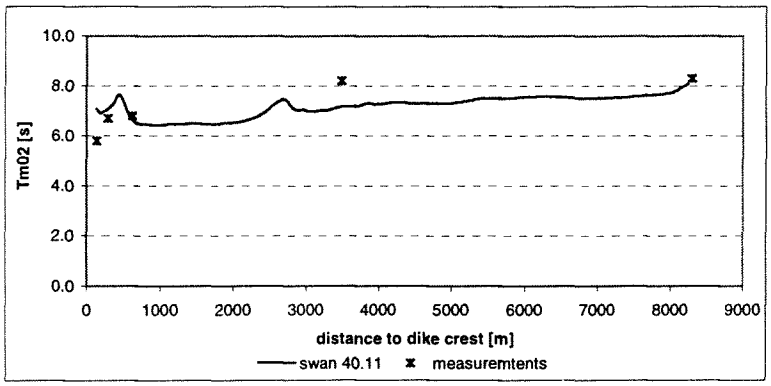

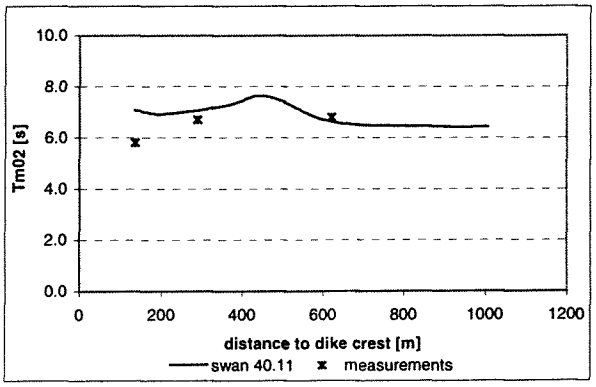

Petten 2/1/1995 17:00

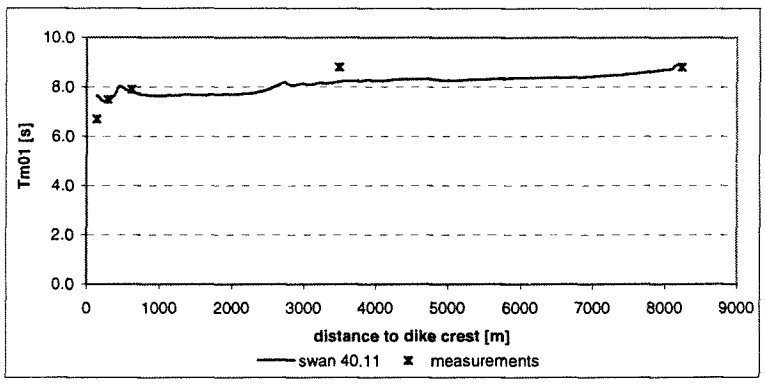

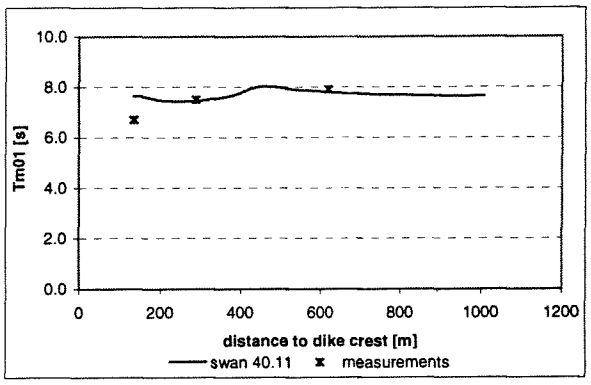

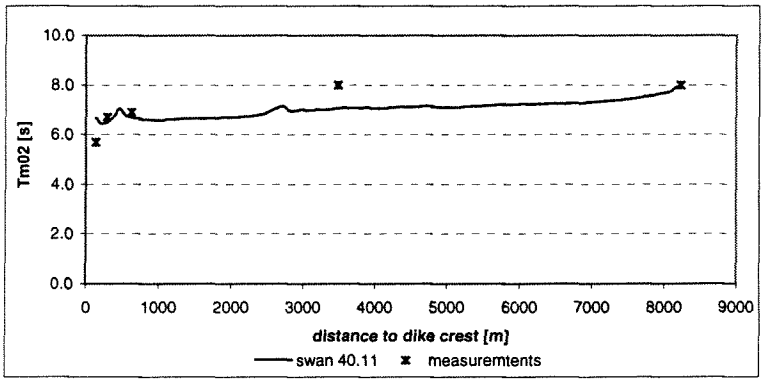

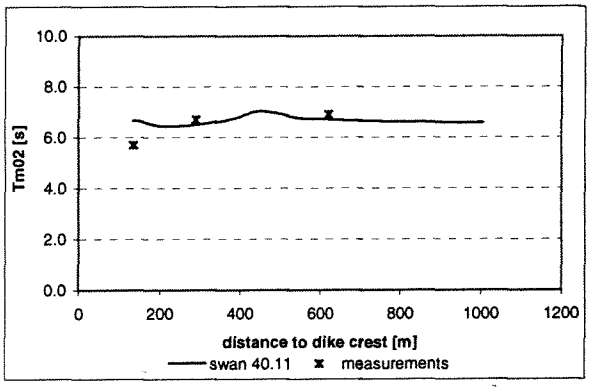

Petten 10/1/1995 11:40

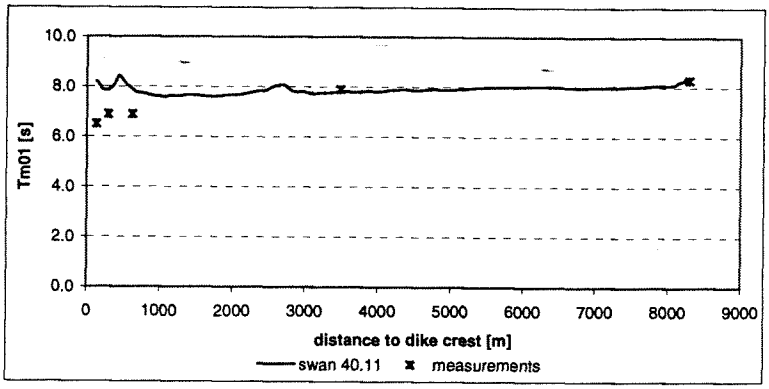

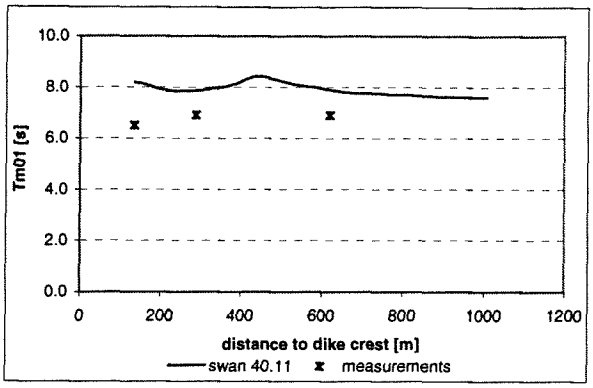

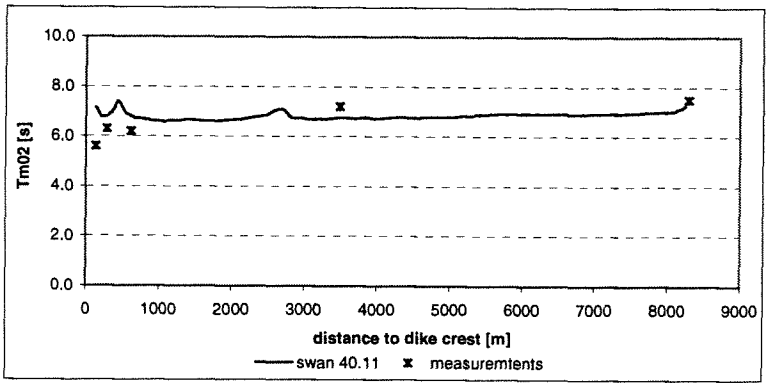

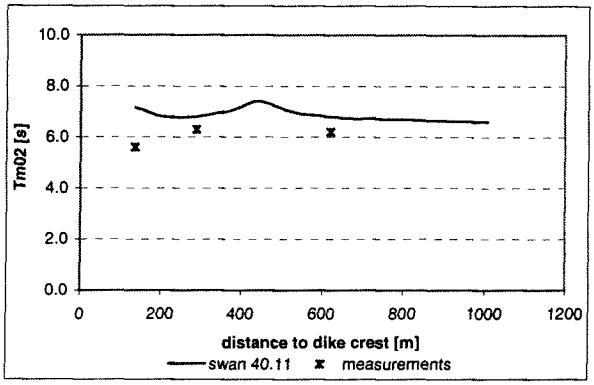

Petten 23-02-99 0:40

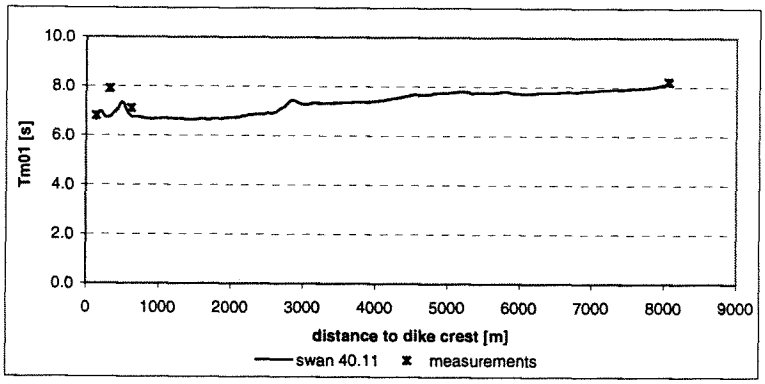

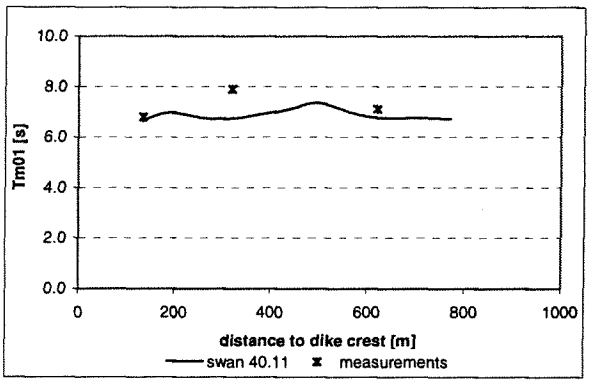

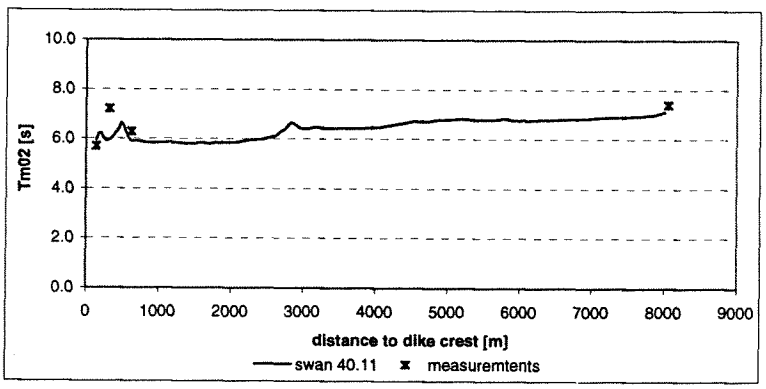

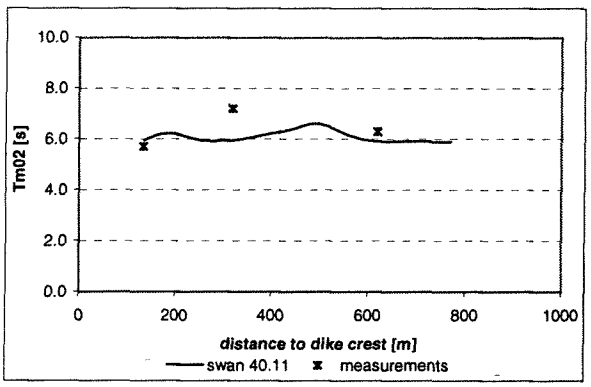

Petten 23-02-99 4:40

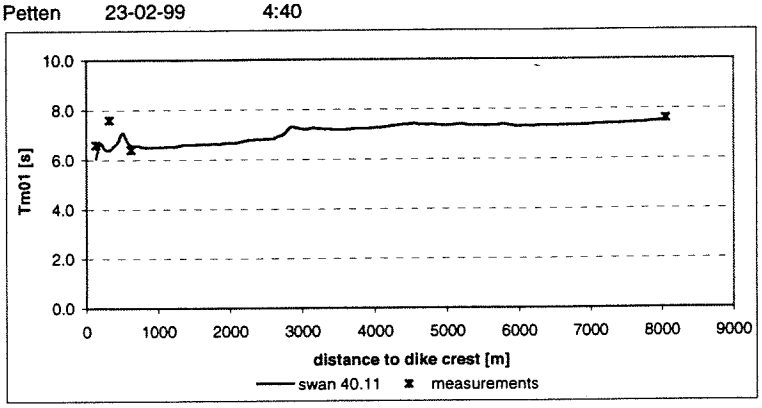

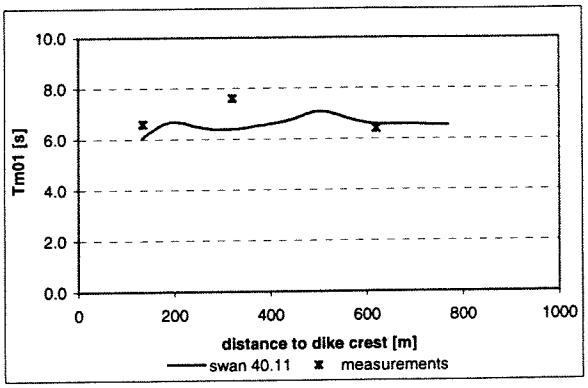

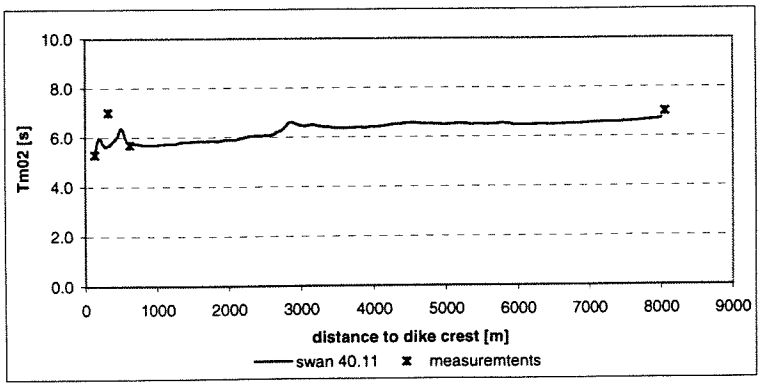

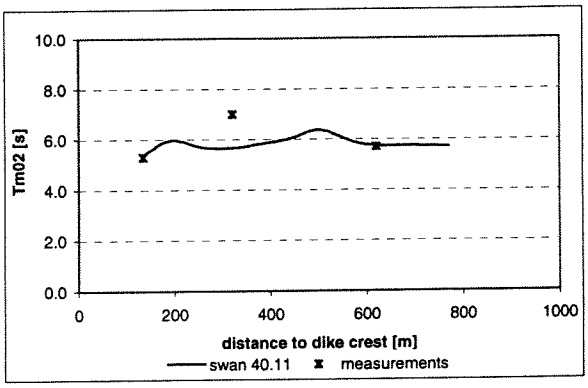

1995

01-01-0500

	measured	swan 40.11	
	Tm01 [s]	Tm01 [s]	difference
mp 1	7.10	7.20	1%
mp 2	6.90	6.62	-4%
mp 3	6.50	6.50	0%
mp 5	6.70	6.15	-8%
mp 6	6.50	6.31	-3%

01-01-1820

	measured	swan 40.11	
	Tm01 [s]	Tm01 [s]	difference
mp 1	8.10	7.95	-2%
mp 2	8.30	7.45	-10%
mp 3	6.80	7.24	6%
mp 5	7.20	7.09	-2%
mp 6	6.30	7.33	16%

02-01-0600

	measured	swan 40.11	
	Tm01 [s]	Tm01 [s]	difference
mp 1	9.30	9.30	0%
mp 2	9.10	8.35	-8%
mp 3	8.10	7.71	-5%
mp 5	7.60	8.03	6%
mp 6	6.70	8.18	22%

02-01-1700

	measured	swan 40.11	
	Tm01 [s]	Tm01 [s]	difference
mp 1	8.80	8.90	1%
mp 2	8.80	8.22	-7%
mp 3	7.90	7.80	-1%
mp 5	7.50	7.45	-1%
mp 6	6.70	7.63	14%

10-01-1140

	measured	swan 40.11	
	Tm01 [s]	Tm01 [s]	difference
mp 1	8.30	8.35	1%
mp 2	7.90	7.82	-1%
mp 3	6.90	7.9	14%
mp 5	6.90	7.86	14%
mp 6	6.50	8.19	26%

1999

23-02-0040

	measured	swan 40.11	
	Tm01 [s]	Tm01 [s]	difference
mp 1	8.20	8.14	-1%
mp 3	7.10	6.76	-5%
*mp 5**	*7.90*	*6.74*	*-15%*
mp 6	6.80	6.64	-2%

23-02-0440

	measured	swan 40.11	
	Tm01 [s]	Tm01 [s]	difference
mp 1	7.60	7.55	-1%
mp 3	6.40	6.58	3%
*mp 5**	*7.60*	*6.39*	*-16%*
mp 6	6.60	6.06	-8%

* instrument probably not working

1995

01-01-0500

	measured	swan 40.11	
	Tm02 [s]	Tm02 [s]	difference
mp 1	6.60	6.60	0%
mp 2	6.40	5.85	-9%
mp 3	5.90	5.74	-3%
mp 5	6.10	5.49	-10%
mp 6	5.80	5.66	-2%

01-01-1820

	measured	swan 40.11	
	Tm02 [s]	Tm02 [s]	difference
mp 1	7.30	7.05	-3%
mp 2	7.60	6.53	-14%
mp 3	6.00	6.35	6%
mp 5	6.50	6.25	-4%
mp 6	5.50	6.49	18%

02-01-0600

	measured	swan 40.11	
	Tm02 [s]	Tm02 [s]	difference
mp 1	8.30	8.23	-1%
mp 2	8.20	7.17	-13%
mp 3	6.80	6.62	-3%
mp 5	6.70	7.06	5%
mp 6	5.80	7.07	22%

02-01-1700

	measured	swan 40.11	
	Tm02 [s]	Tm02 [s]	difference
mp 1	8.00	8.00	0%
mp 2	8.00	7.06	-12%
mp 3	6.90	6.70	-3%
mp 5	6.70	6.50	-3%
mp 6	5.70	6.67	17%

10-01-1140

	measured	swan 40.11	
	Tm02 [s]	Tm02 [s]	difference
mp 1	7.50	7.30	-3%
mp 2	7.20	6.75	-6%
mp 3	6.20	6.79	10%
mp 5	6.30	6.80	8%
mp 6	5.60	7.14	28%

1999

23-02-0040

	measured	swan 40.11	
	Tm02 [s]	Tm02 [s]	difference
mp 1	7.40	7.2	-3%
mp 3	6.30	5.91	-6%
*mp 5**	*7.20*	*5.95*	*-17%*
mp 6	5.70	5.94	4%

23-02-0440

	measured	swan 40.11	
	Tm02 [s]	Tm02 [s]	difference
mp 1	7.00	6.79	-3%
mp 3	5.70	5.75	1%
*mp 5**	*7.00*	*5.66*	*-19%*
mp 6	5.30	5.37	1%

* instrument probably not working

4G - Comparison of relative magnitude of S_{nl3} and S_{br} at MP6

comparison of the relative magnitude of Snl3 in 1995 and 1999

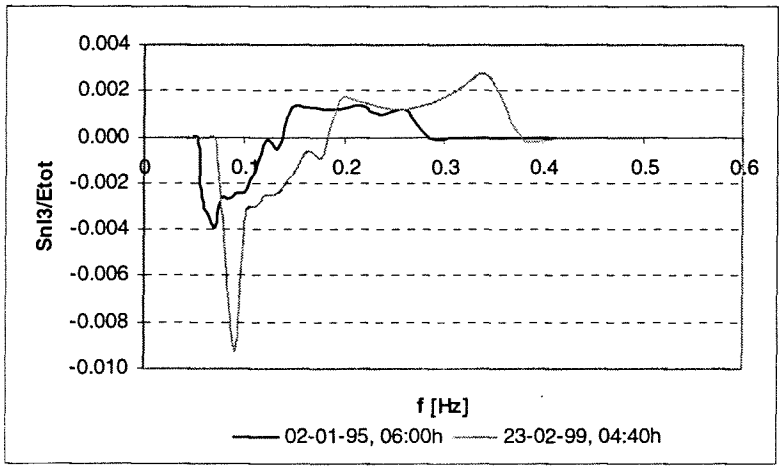

comparison of Sbr and Snl3 in Petten case 02/01/95, 06:00h

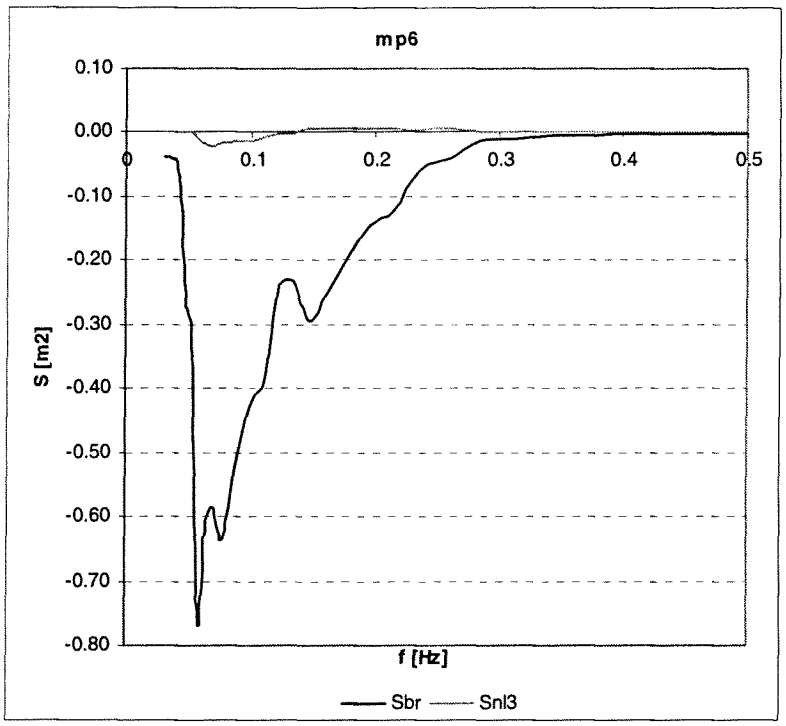

4H Variation of the wave period in the SV cases

SV case 01

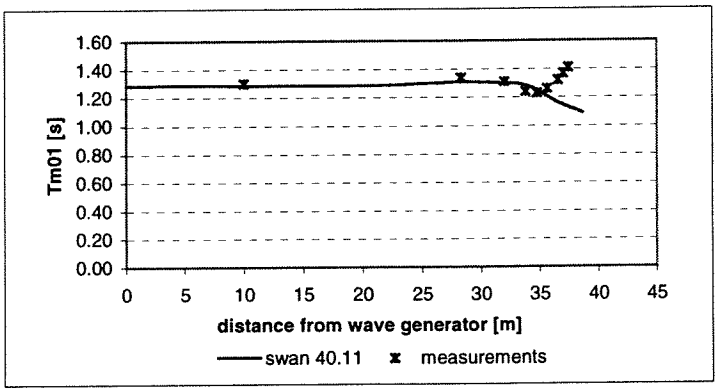

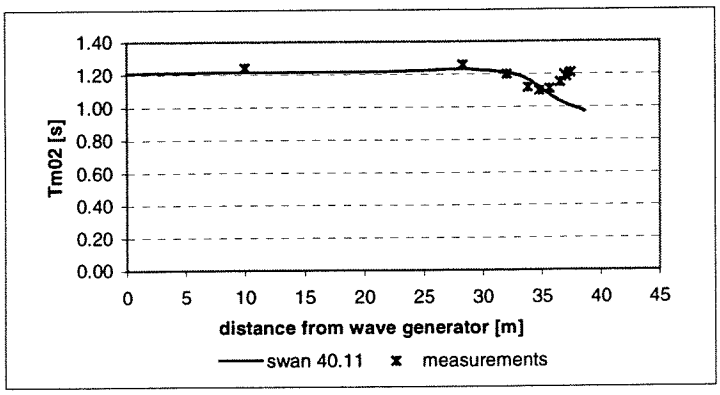

SV case 03

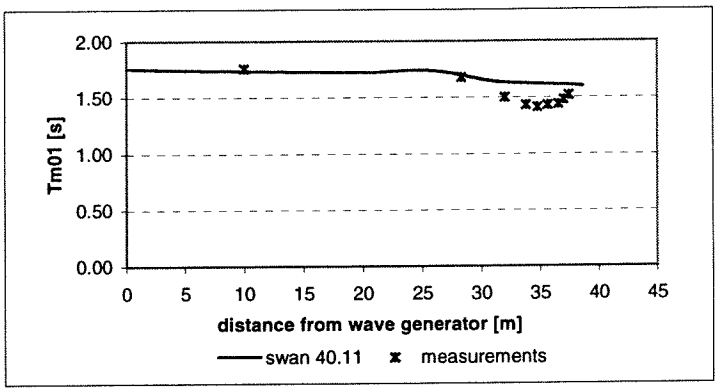

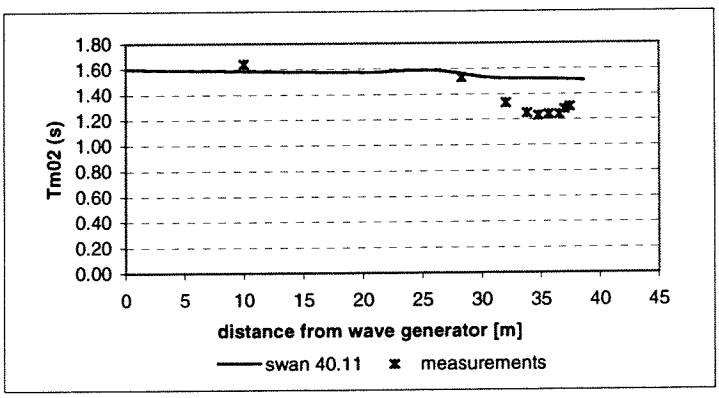

SV case 07

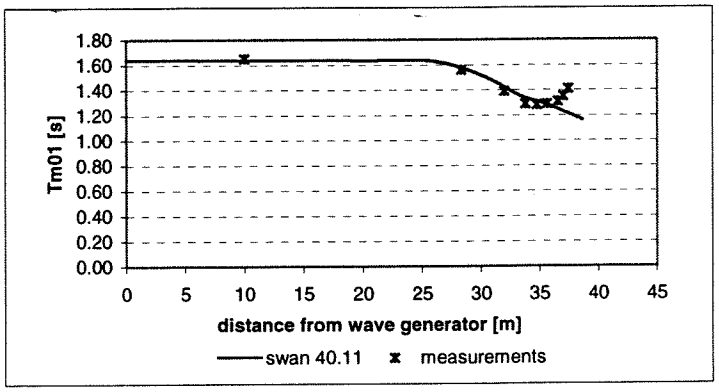

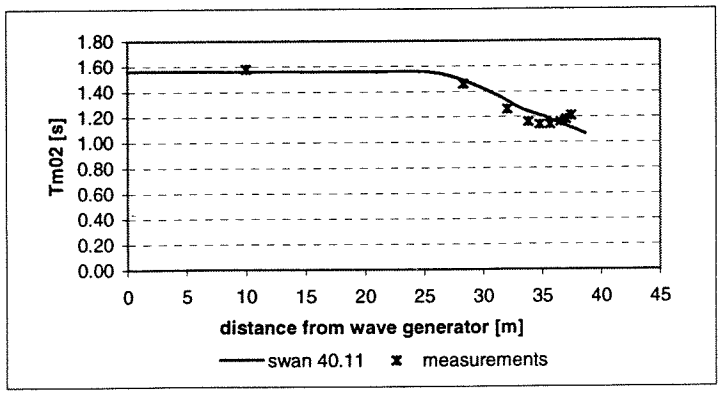

SV case 09

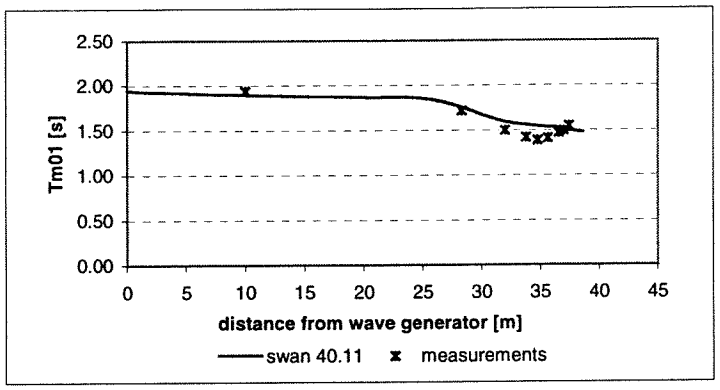

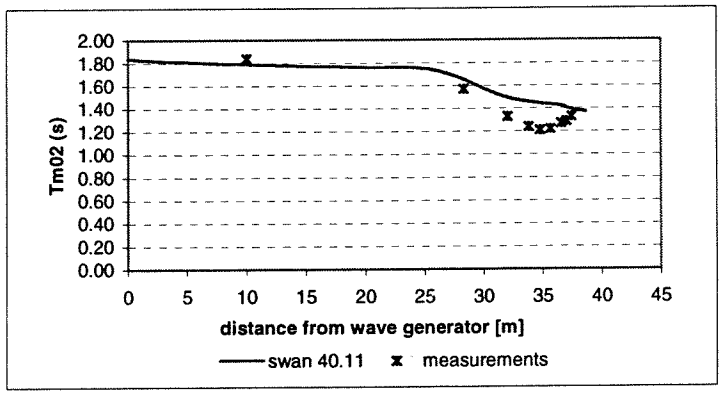

case 1

	measurement	swan 40.11	
depth [cm]	Tm01 [s]	Tm01 [s]	difference
61	1.30	1.29	-1%
36.6	1.34	1.31	-2%
24.4	1.31	1.31	0%
18.3	1.24	1.30	5%
15.2	1.23	1.27	3%
12.2	1.26	1.23	-2%
9.7	1.32	1.18	-11%
7.6	1.37	1.16	-15%
6.1	1.41	1.14	-19%

case 3

	measurement	swan 40.11	
depth [cm]	Tm01 [s]	Tm01 [s]	difference
61	1.76	1.73	-2%
36.6	1.68	1.69	0%
24.4	1.50	1.62	8%
18.3	1.43	1.61	13%
15.2	1.41	1.61	14%
12.2	1.43	1.61	13%
9.7	1.44	1.61	12%
7.6	1.48	1.60	8%
6.1	1.52	1.60	5%

case 7

	measurement	swan 40.11	
depth [cm]	Tm01 [s]	Tm01 [s]	difference
61	1.65	1.64	-1%
36.6	1.56	1.57	1%
24.4	1.39	1.43	3%
18.3	1.29	1.34	4%
15.2	1.28	1.32	3%
12.2	1.29	1.30	1%
9.7	1.31	1.27	-3%
7.6	1.35	1.25	-7%
6.1	1.41	1.24	-12%

case 9

	measurement	swan 40.11	
depth [cm]	Tm01 [s]	Tm01 [s]	difference
61	1.94	1.89	-3%
36.6	1.72	1.73	1%
24.4	1.5	1.58	5%
18.3	1.42	1.54	8%
15.2	1.39	1.53	10%
12.2	1.41	1.53	9%
9.7	1.47	1.52	4%
7.6	1.5	1.52	1%
6.1	1.55	1.50	-3%

case 1

	measurement	swan 40.11	
depth [cm]	Tm02 [s]	Tm02 [s]	difference
61	1.24	1.22	-2%
36.6	1.26	1.23	-2%
24.4	1.2	1.22	1%
18.3	1.12	1.19	6%
15.2	1.1	1.15	5%
12.2	1.11	1.11	0%
9.7	1.15	1.06	-8%
7.6	1.19	1.04	-13%
6.1	1.21	1.02	-16%

case 3

	measurement	swan 40.11	
depth [cm]	Tm02 [s]	Tm02 [s]	difference
61	1.64	1.58	-4%
36.6	1.53	1.55	1%
24.4	1.33	1.51	13%
18.3	1.25	1.51	21%
15.2	1.23	1.51	23%
12.2	1.24	1.51	22%
9.7	1.24	1.51	22%
7.6	1.28	1.50	17%
6.1	1.30	1.50	15%

case 7

	measurement	swan 40.11	
depth [cm]	Tm02 [s]	Tm02 [s]	difference
61	1.58	1.56	-1%
36.6	1.46	1.48	2%
24.4	1.26	1.33	6%
18.3	1.16	1.25	8%
15.2	1.14	1.22	7%
12.2	1.14	1.20	5%
9.7	1.16	1.17	1%
7.6	1.18	1.16	-2%
6.1	1.21	1.14	-6%

case 9

	measurement	swan 40.11	
depth [cm]	Tm02 [s]	Tm02 [s]	difference
61	1.84	1.78	-3%
36.6	1.57	1.63	4%
24.4	1.33	1.48	11%
18.3	1.24	1.44	16%
15.2	1.21	1.43	18%
12.2	1.22	1.43	17%
9.7	1.27	1.42	12%
7.6	1.29	1.42	10%
6.1	1.33	1.39	4%

4I Transformation of the wave spectra in the Petten cases

Petten 1/1/1995 5:00

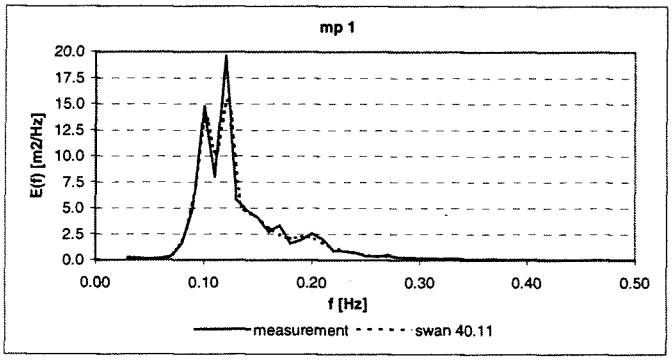

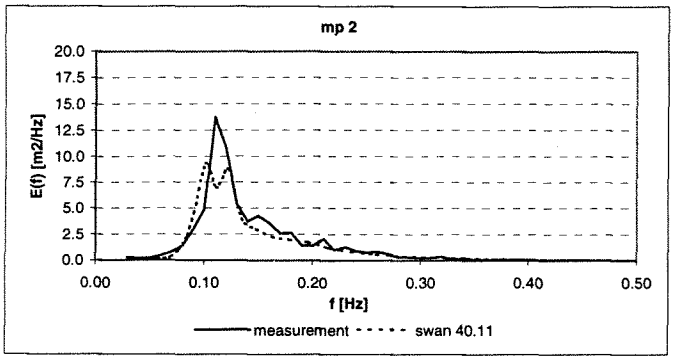

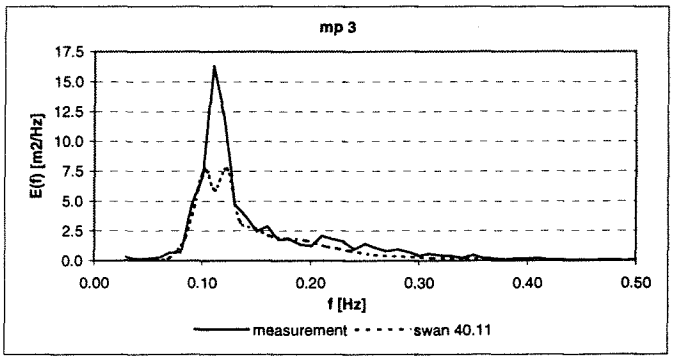

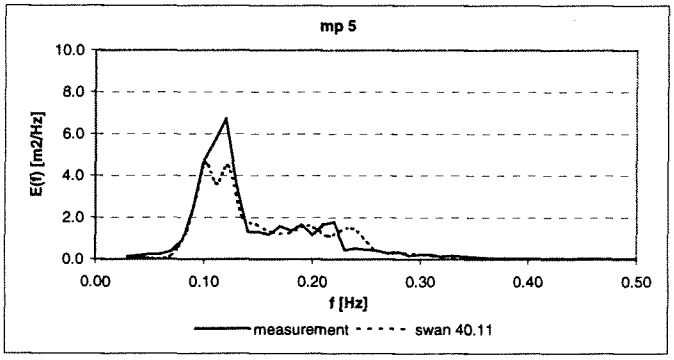

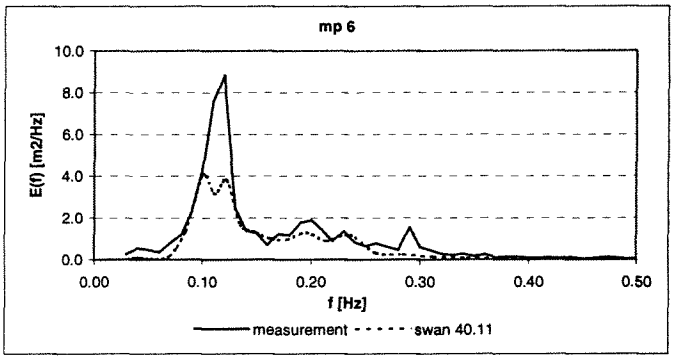

Petten 1/1/1995 18:20

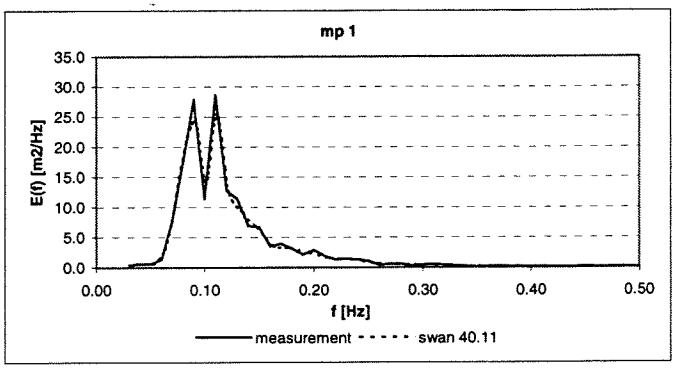

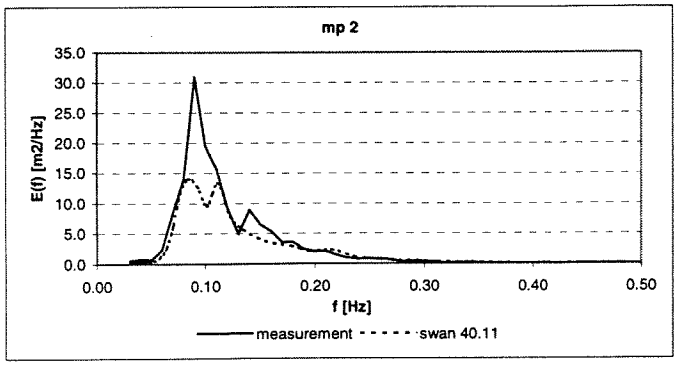

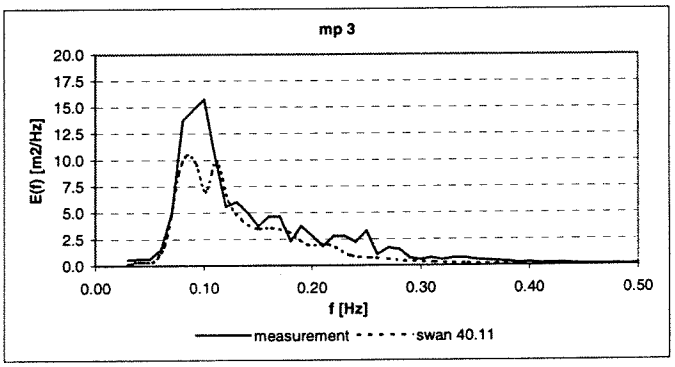

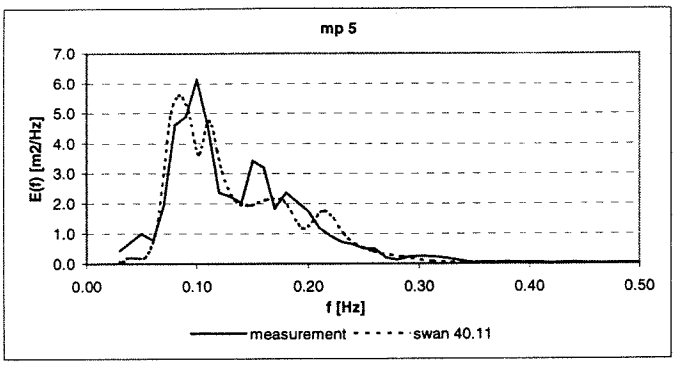

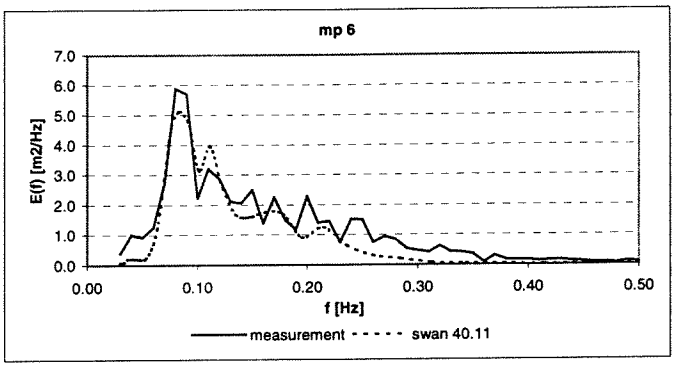

Petten 2/1/1995 6:00

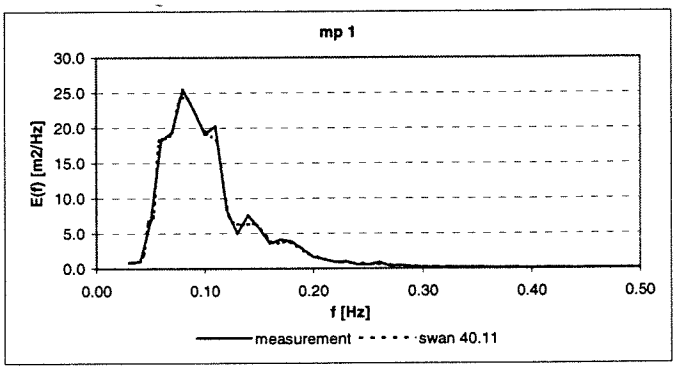

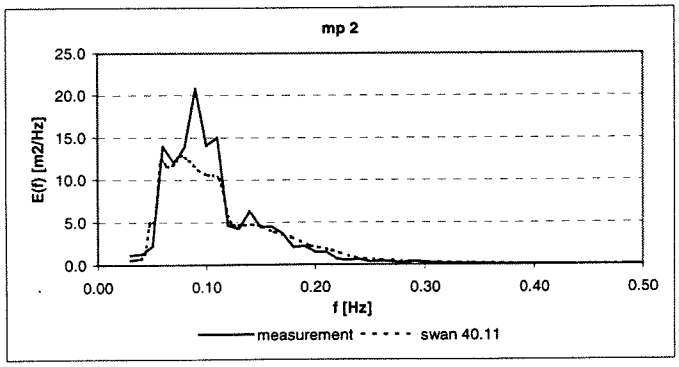

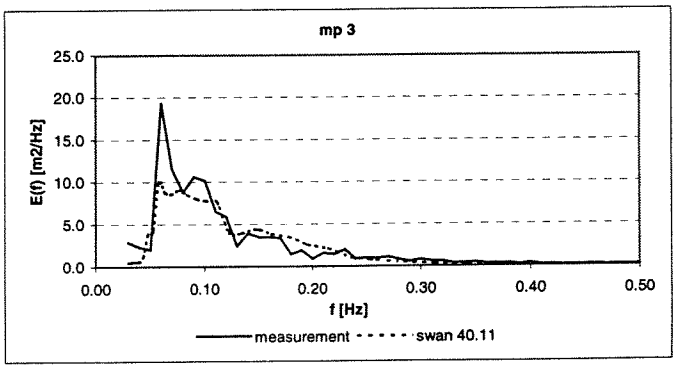

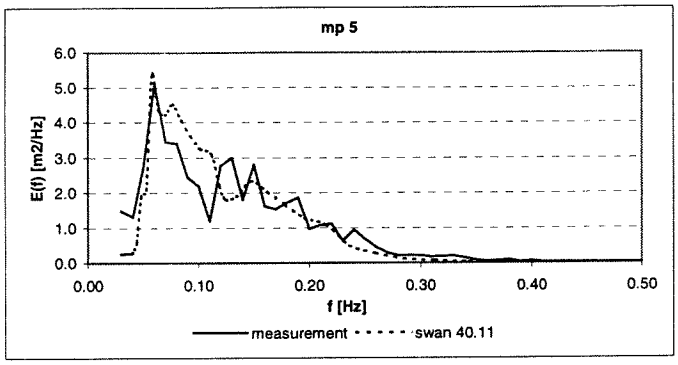

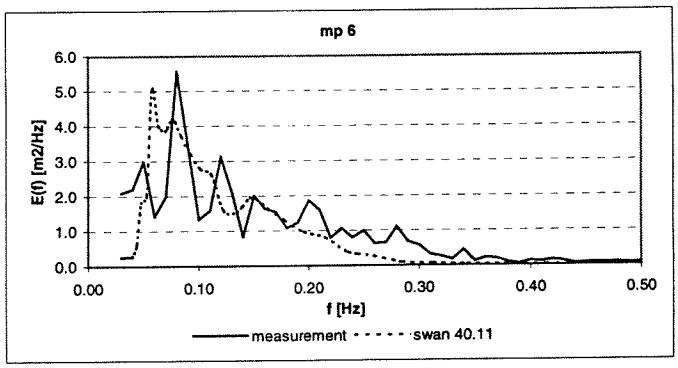

Petten 2/1/1995 17:00

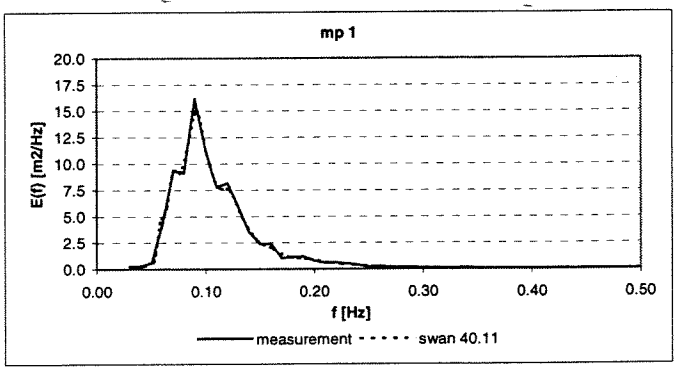

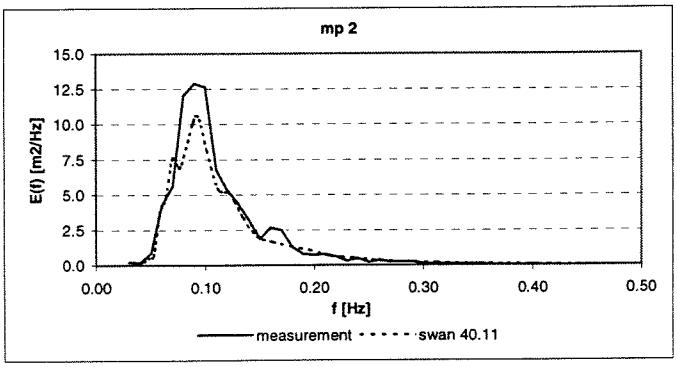

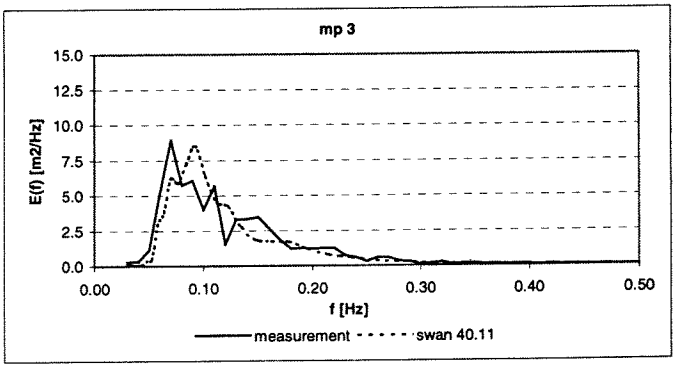

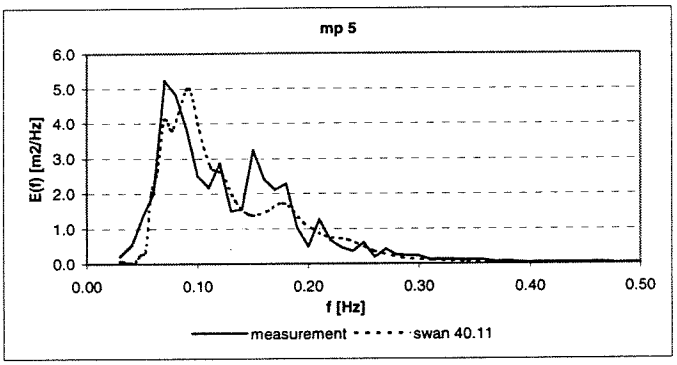

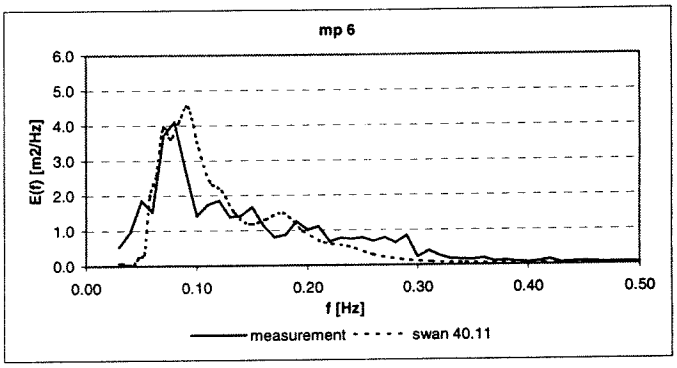

Petten 10/1/1995 11:40

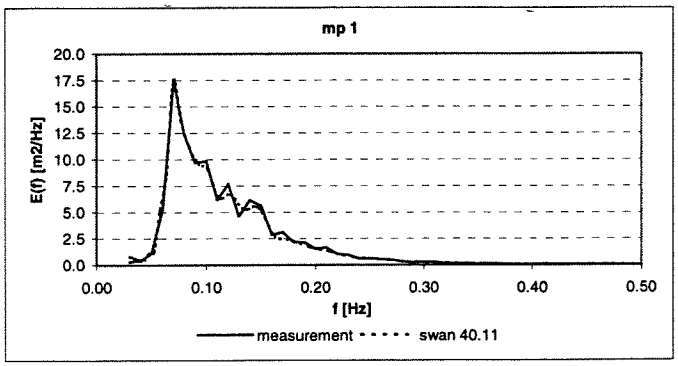

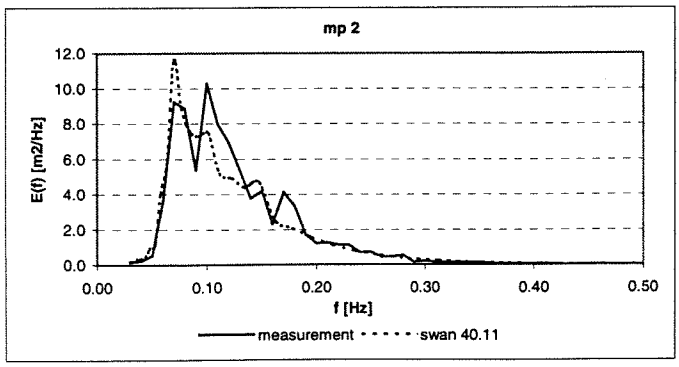

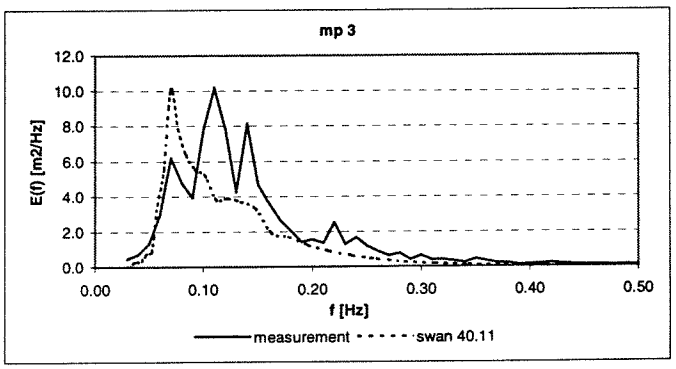

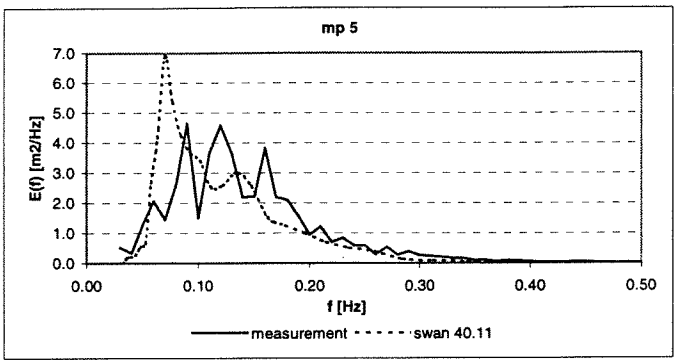

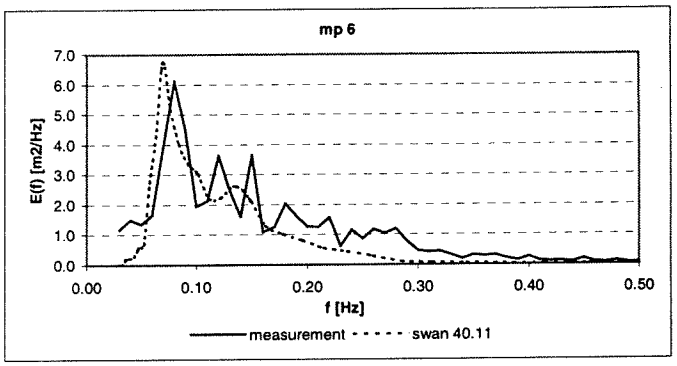

Petten 23-02-99 0:40

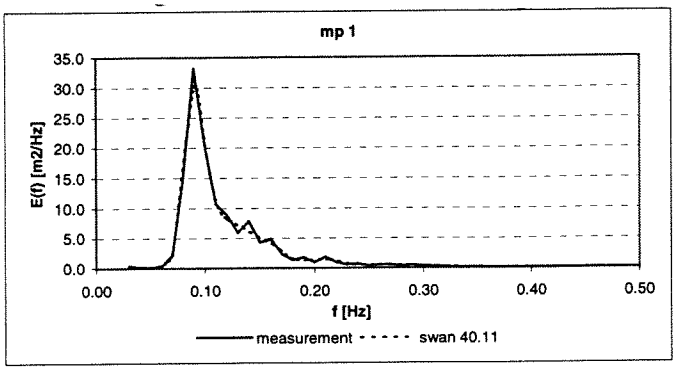

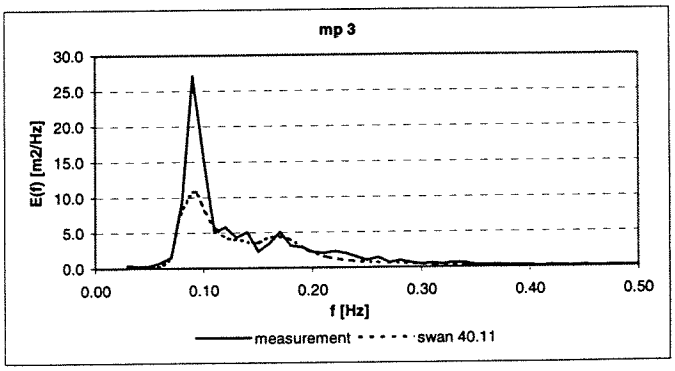

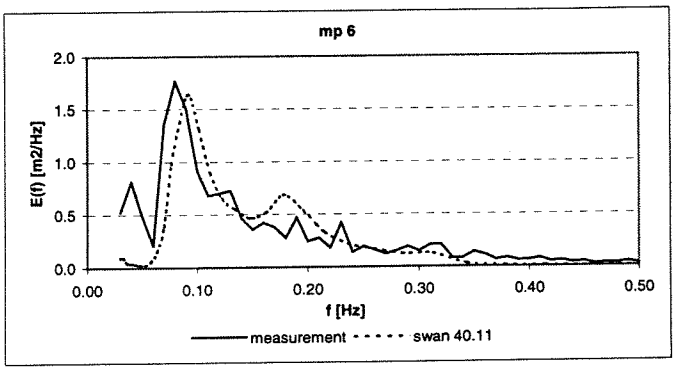

Petten 23-2-99 4:40

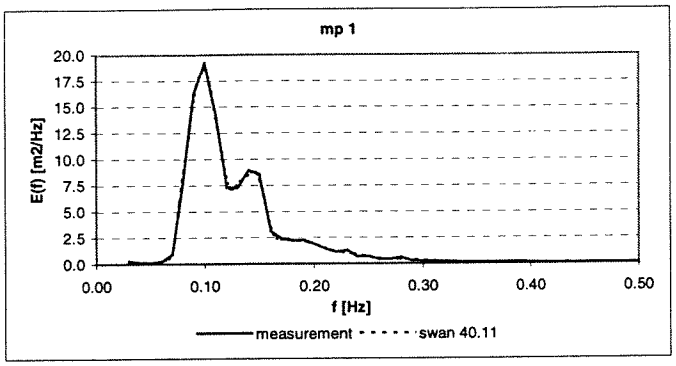

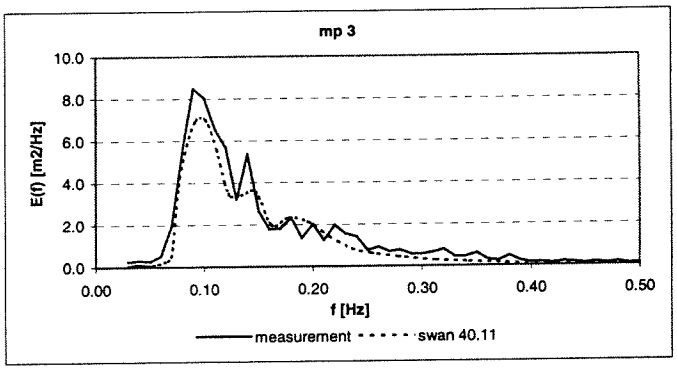

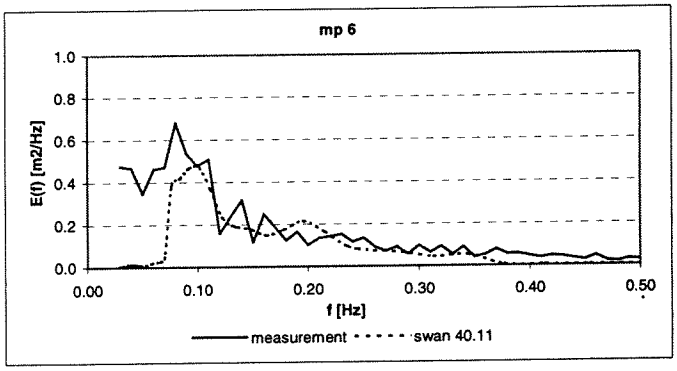

4J - Transformation of the wave spectra in the SV cases

SV case 01

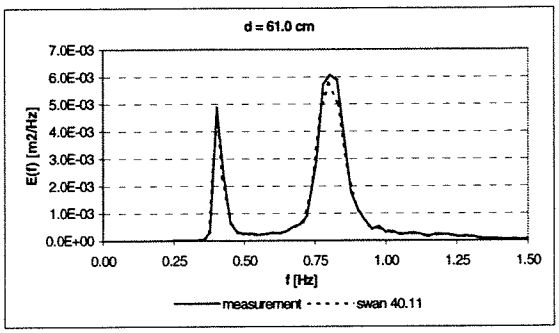

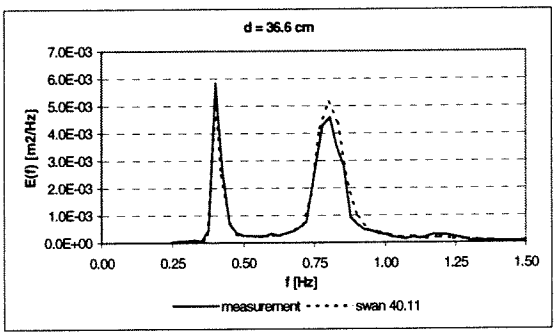

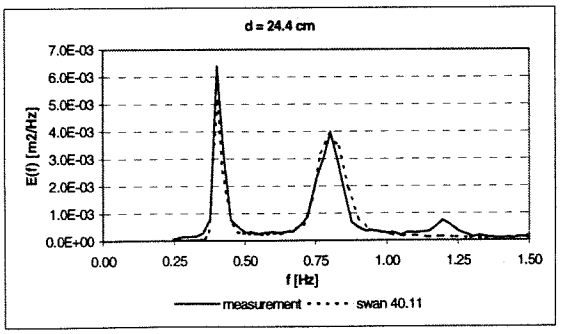

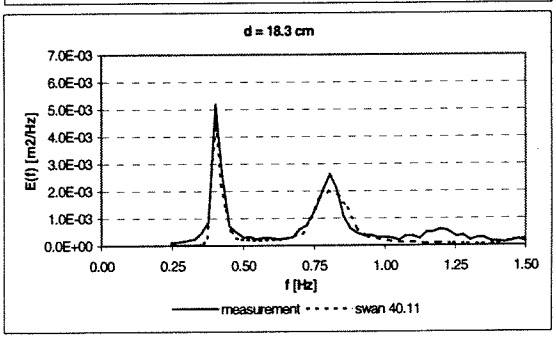

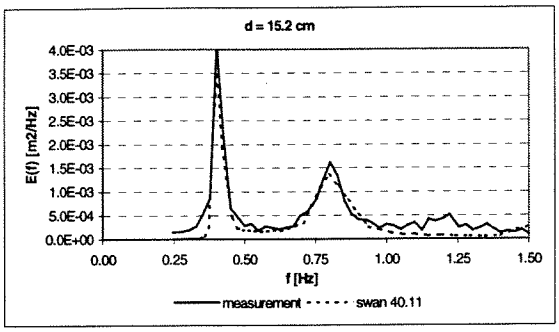

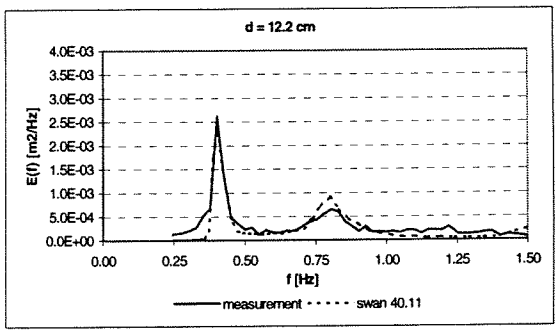

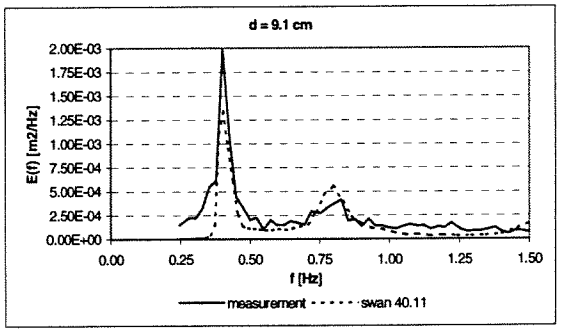

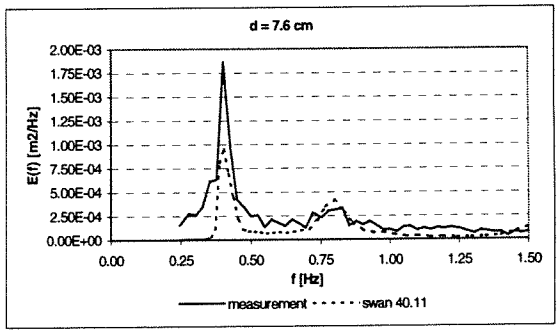

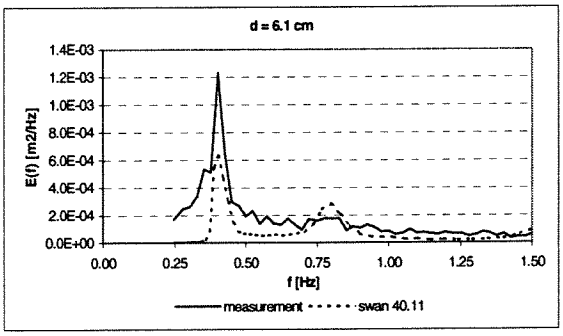

SV case 03

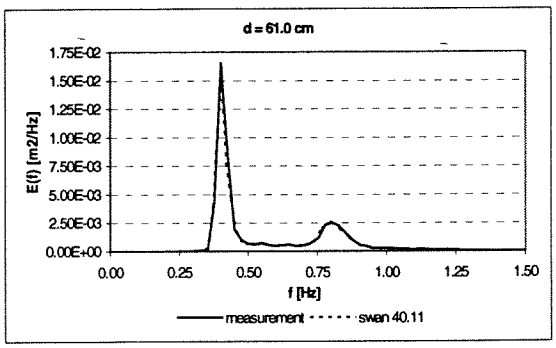
d = 61.0 cm
E(f) [m2/Hz]
1.75E-02
1.50E-02
1.25E-02
1.00E-02
7.50E-03
5.00E-03
2.50E-03
0.00E+00
0.00 0.25 0.50 0.75 1.00 1.25 1.50
f [Hz]
measurement
swan 40.11

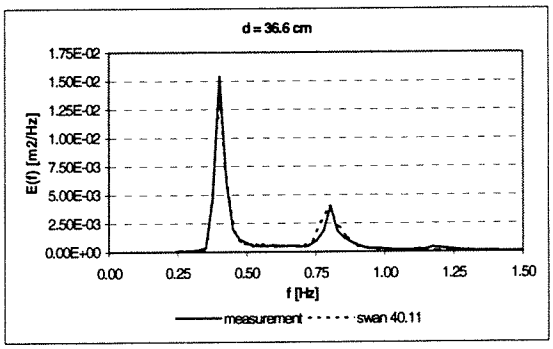
d = 36.6 cm
E(f) [m2/Hz]
1.75E-02
1.50E-02
1.25E-02
1.00E-02
7.50E-03
5.00E-03
2.50E-03
0.00E+00
0.00 0.25 0.50 0.75 1.00 1.25 1.50
f [Hz]
measurement
swan 40.11

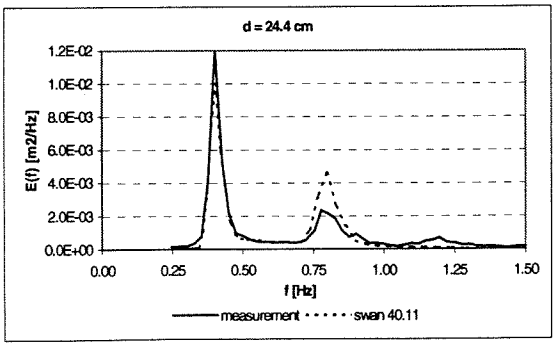
d = 24.4 cm
E(f) [m2/Hz]
1.2E-02
1.0E-02
8.0E-03
6.0E-03
4.0E-03
2.0E-03
0.0E+00
0.00 0.25 0.50 0.75 1.00 1.25 1.50
f [Hz]
measurement
swan 40.11

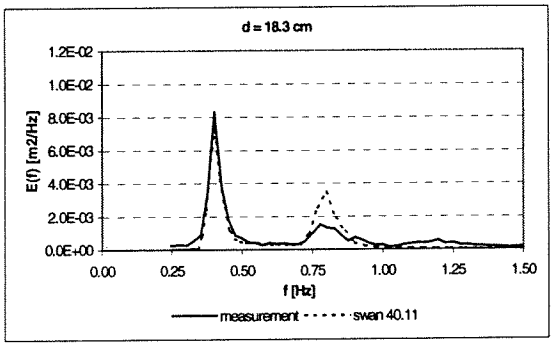
d = 18.3 cm
E(f) [m2/Hz]
1.2E-02
1.0E-02
8.0E-03
6.0E-03
4.0E-03
2.0E-03
0.0E+00
0.00 0.25 0.50 0.75 1.00 1.25 1.50
f [Hz]
measurement
swan 40.11

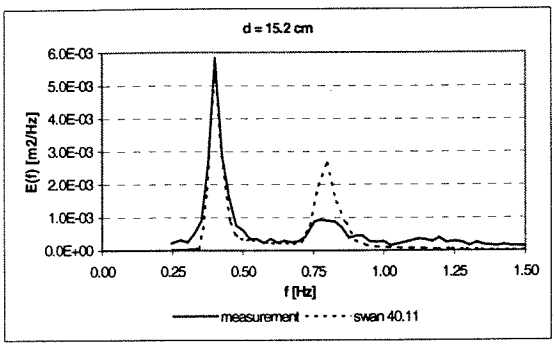
d = 15.2 cm
E(f) [m2/Hz]
6.0E-03
5.0E-03
4.0E-03
3.0E-03
2.0E-03
1.0E-03
0.0E+00
0.00 0.25 0.50 0.75 1.00 1.25 1.50
f [Hz]
measurement
swan 40.11

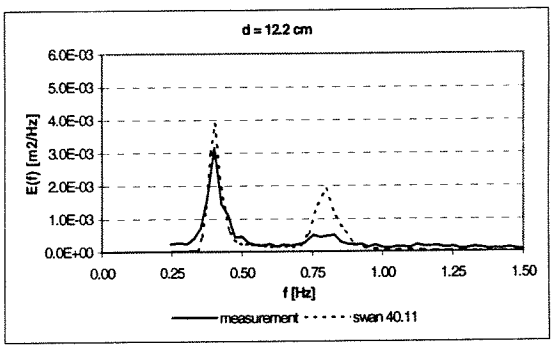
d = 12.2 cm
E(f) [m2/Hz]
6.0E-03
5.0E-03
4.0E-03
3.0E-03
2.0E-03
1.0E-03
0.0E+00
0.00 0.25 0.50 0.75 1.00 1.25 1.50
f [Hz]
measurement
swan 40.11

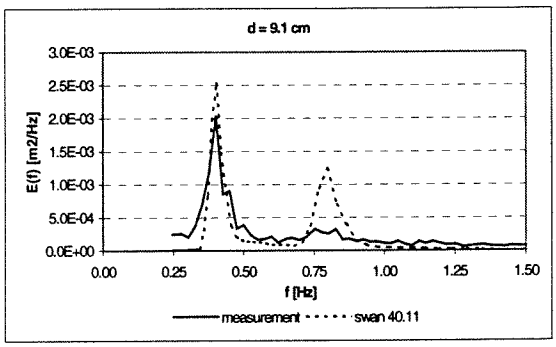
d = 9.1 cm
E(f) [m2/Hz]
3.0E-03
2.5E-03
2.0E-03
1.5E-03
1.0E-03
5.0E-04
0.0E+00
0.00 0.25 0.50 0.75 1.00 1.25 1.50
f [Hz]
measurement
swan 40.11

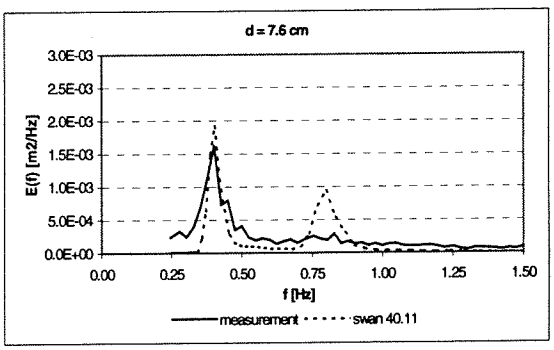
d = 7.6 cm
E(f) [m2/Hz]
3.0E-03
2.5E-03
2.0E-03
1.5E-03
1.0E-03
5.0E-04
0.0E+00
0.00 0.25 0.50 0.75 1.00 1.25 1.50
f [Hz]
measurement
swan 40.11

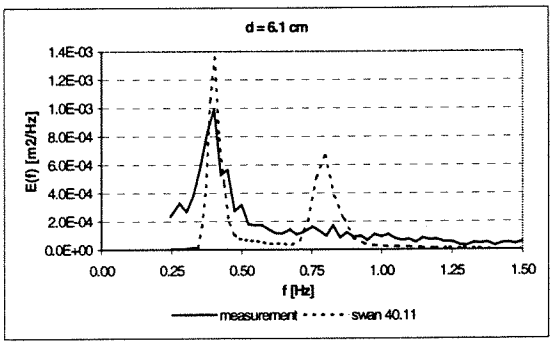
d = 6.1 cm
E(f) [m2/Hz]
1.4E-03
1.2E-03
1.0E-03
8.0E-04
6.0E-04
4.0E-04
2.0E-04
0.0E+00
0.00 0.25 0.50 0.75 1.00 1.25 1.50
f [Hz]
measurement
swan 40.11

SV case 07

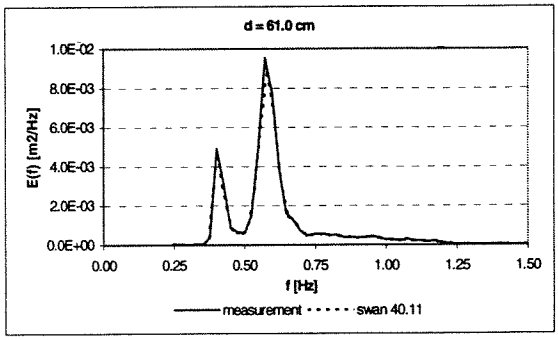
d = 61.0 cm
E(f) [m2/Hz]
1.0E-02
8.0E-03
6.0E-03
4.0E-03
2.0E-03
0.0E+00
0.00 0.25 0.50 0.75 1.00 1.25 1.50
f [Hz]
measurement
swan 40.11

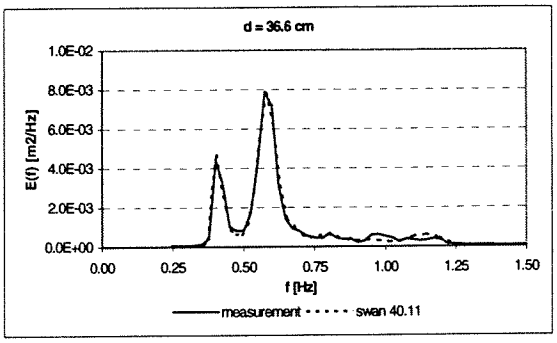
d = 36.6 cm
E(f) [m2/Hz]
1.0E-02
8.0E-03
6.0E-03
4.0E-03
2.0E-03
0.0E+00
0.00 0.25 0.50 0.75 1.00 1.25 1.50
f [Hz]
measurement
swan 40.11

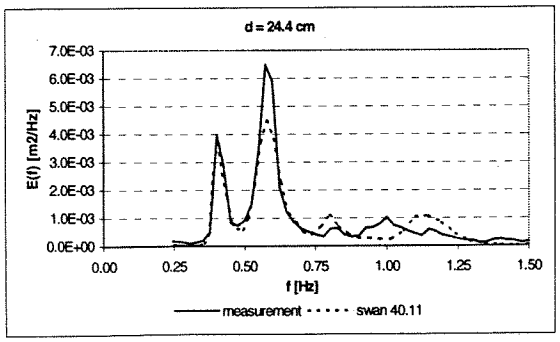
d = 24.4 cm
E(f) [m2/Hz]
7.0E-03
6.0E-03
5.0E-03
4.0E-03
3.0E-03
2.0E-03
1.0E-03
0.0E+00
0.00 0.25 0.50 0.75 1.00 1.25 1.50
f [Hz]
measurement
swan 40.11

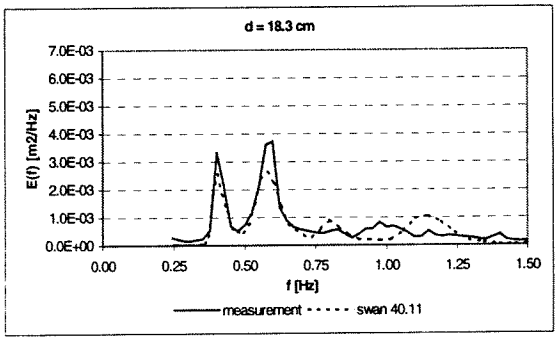
d = 18.3 cm
E(f) [m2/Hz]
7.0E-03
6.0E-03
5.0E-03
4.0E-03
3.0E-03
2.0E-03
1.0E-03
0.0E+00
0.00 0.25 0.50 0.75 1.00 1.25 1.50
f [Hz]
measurement
swan 40.11

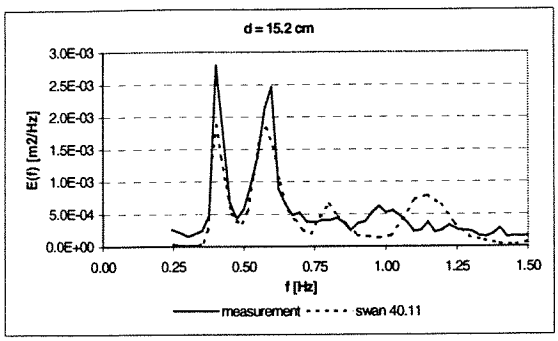
d = 15.2 cm
E(f) [m2/Hz]
3.0E-03
2.5E-03
2.0E-03
1.5E-03
1.0E-03
5.0E-04
0.0E+00
0.00 0.25 0.50 0.75 1.00 1.25 1.50
f [Hz]
measurement
swan 40.11

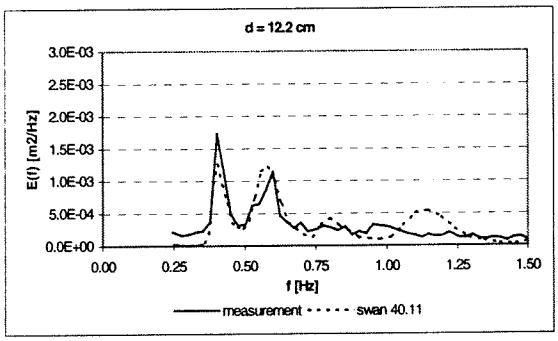
d = 12.2 cm
E(f) [m2/Hz]
3.0E-03
2.5E-03
2.0E-03
1.5E-03
1.0E-03
5.0E-04
0.0E+00
0.00 0.25 0.50 0.75 1.00 1.25 1.50
f [Hz]
measurement
swan 40.11

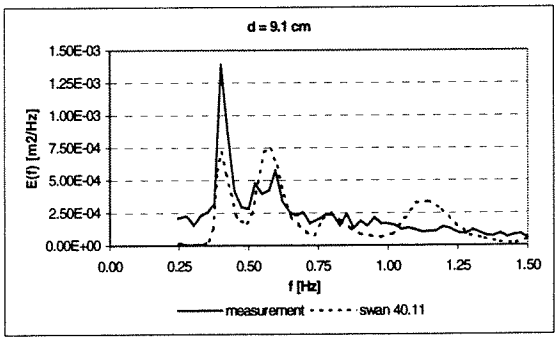
d = 9.1 cm
E(f) [m2/Hz]
1.50E-03
1.25E-03
1.00E-03
7.50E-04
5.00E-04
2.50E-04
0.00E+00
0.00 0.25 0.50 0.75 1.00 1.25 1.50
f [Hz]
measurement
swan 40.11

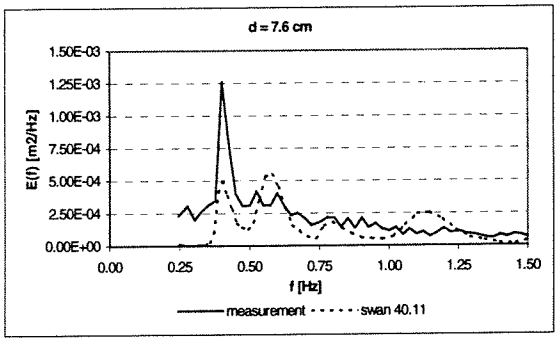
d = 7.6 cm
E(f) [m2/Hz]
1.50E-03
1.25E-03
1.00E-03
7.50E-04
5.00E-04
2.50E-04
0.00E+00
0.00 0.25 0.50 0.75 1.00 1.25 1.50
f [Hz]
measurement
swan 40.11

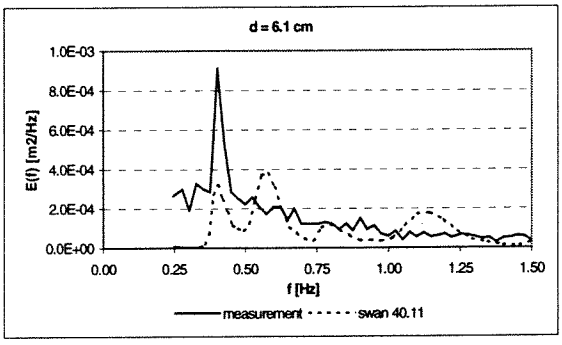
d = 6.1 cm
E(f) [m2/Hz]
1.0E-03
8.0E-04
6.0E-04
4.0E-04
2.0E-04
0.0E+00
0.00 0.25 0.50 0.75 1.00 1.25 1.50
f [Hz]
measurement
swan 40.11

SV case 09

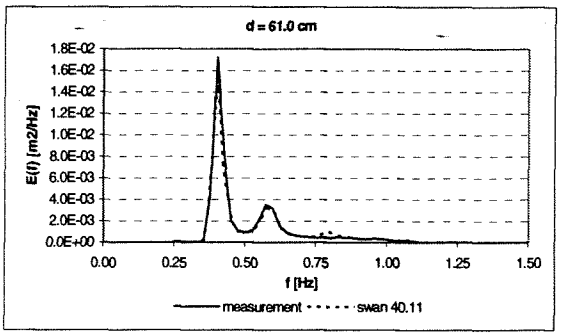
d = 61.0 cm
E(f) [m2/Hz]
f [Hz]
measurement
swan 40.11

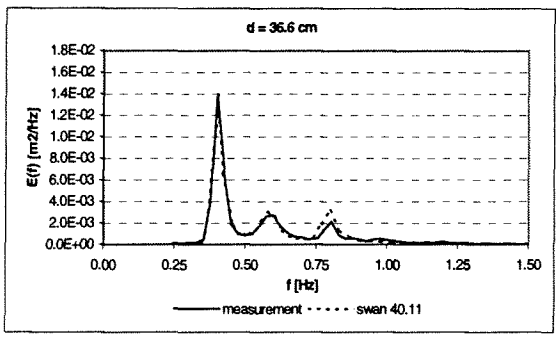
d = 36.6 cm
E(f) [m2/Hz]
f [Hz]
measurement
swan 40.11

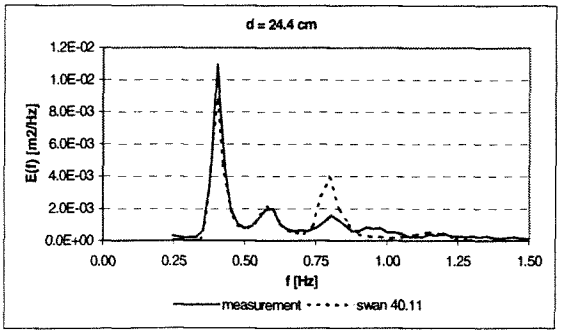
d = 24.4 cm
E(f) [m2/Hz]
f [Hz]
measurement
swan 40.11

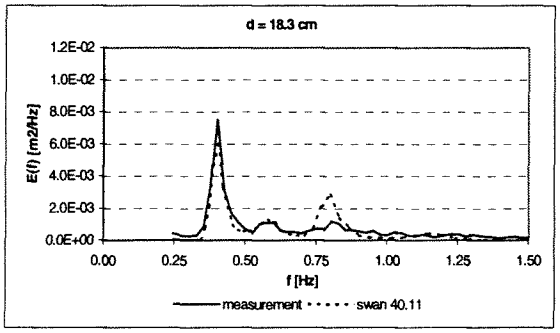
d = 18.3 cm
E(f) [m2/Hz]
f [Hz]
measurement
swan 40.11

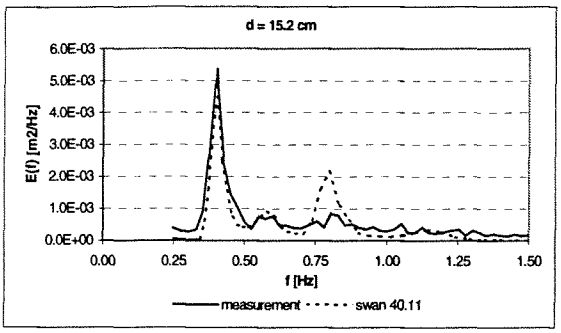
d = 15.2 cm
E(f) [m2/Hz]
f [Hz]
measurement
swan 40.11

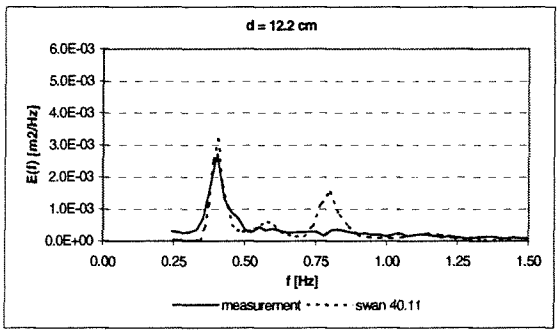
d = 12.2 cm
E(f) [m2/Hz]
f [Hz]
measurement
swan 40.11

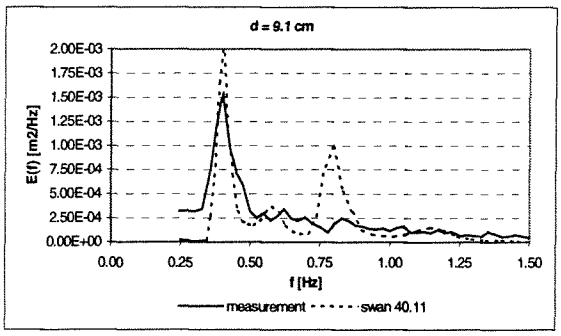
d = 9.1 cm
E(f) [m2/Hz]
f [Hz]
measurement
swan 40.11

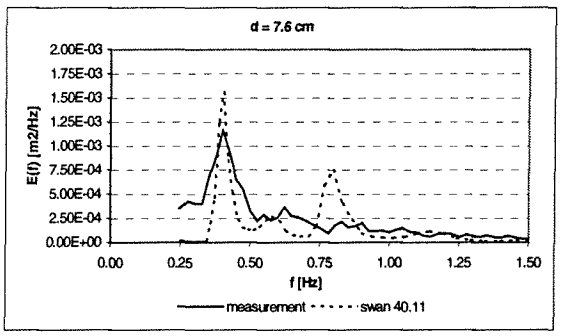
d = 7.6 cm
E(f) [m2/Hz]
f [Hz]
measurement
swan 40.11

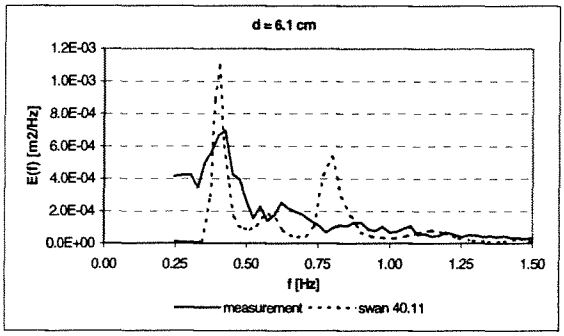
d = 6.1 cm
E(f) [m2/Hz]
f [Hz]
measurement
swan 40.11

4K Comparison of spectra with the equilibrium range in the Petten cases

Petten 1/1/1995 5:00

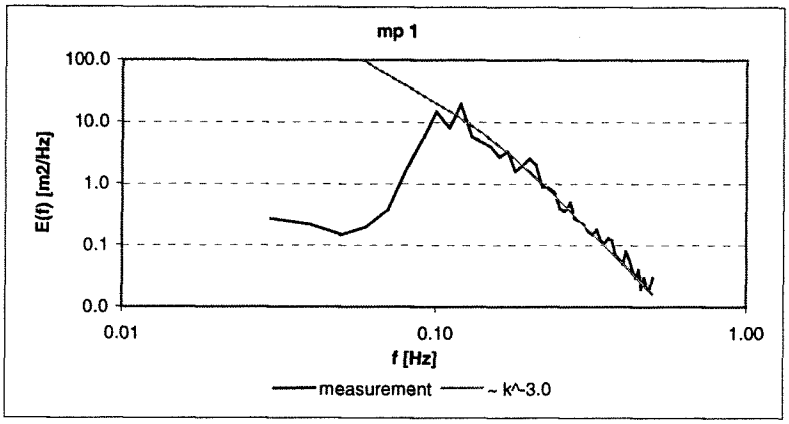

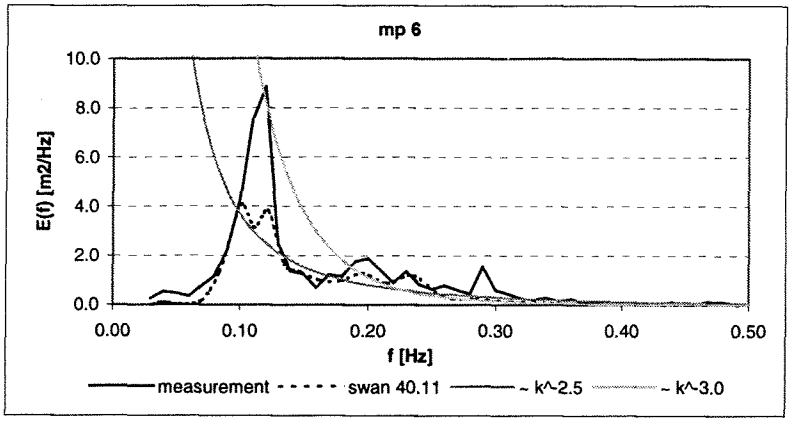

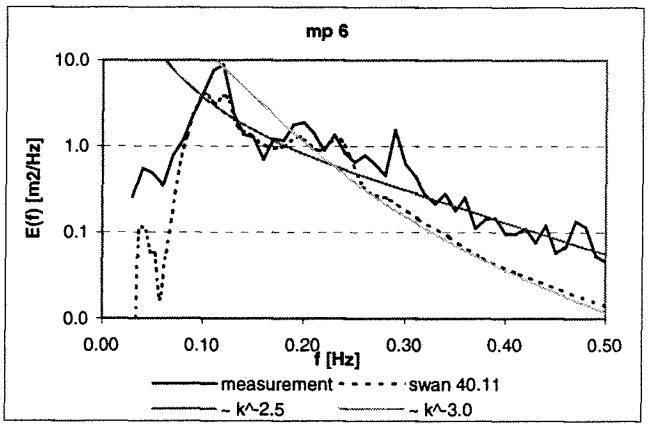

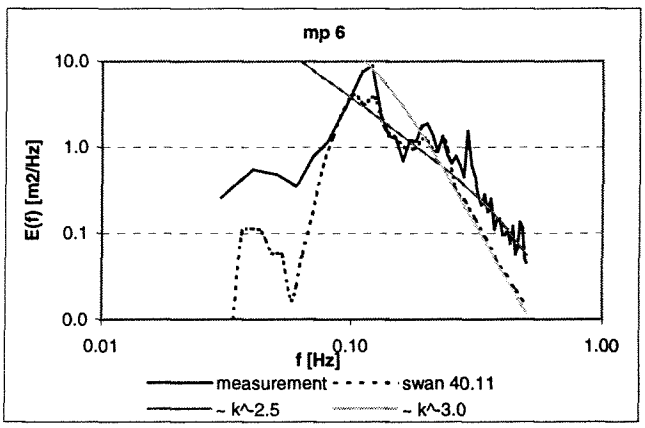

Petten 1/1/1995 18:20

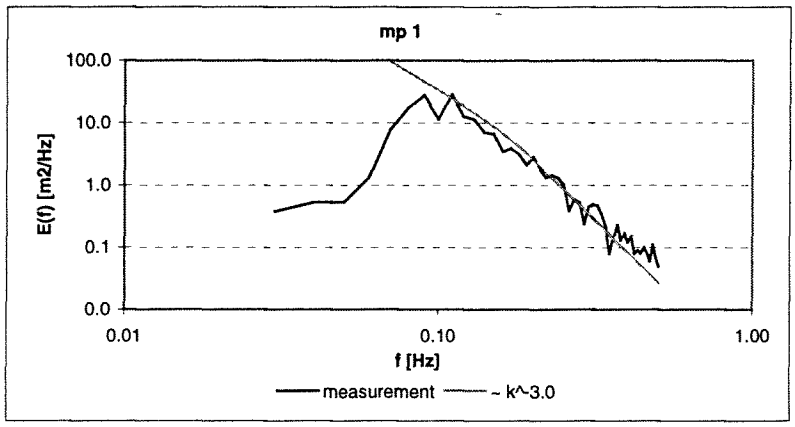

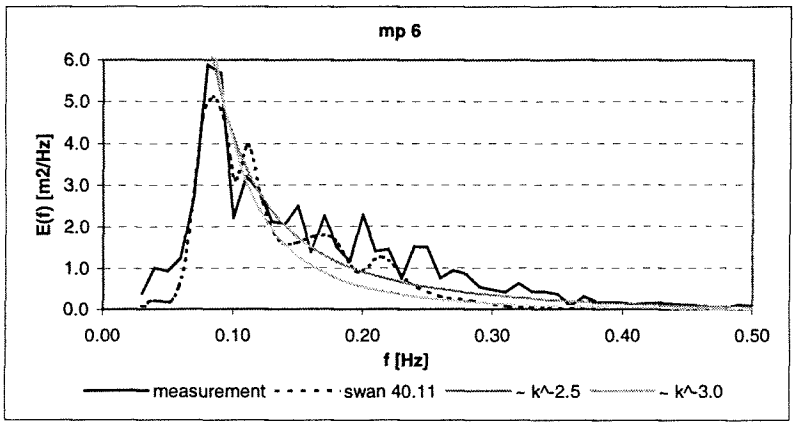

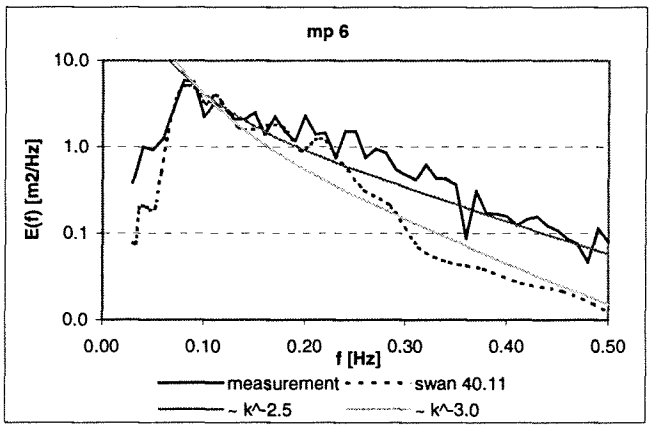

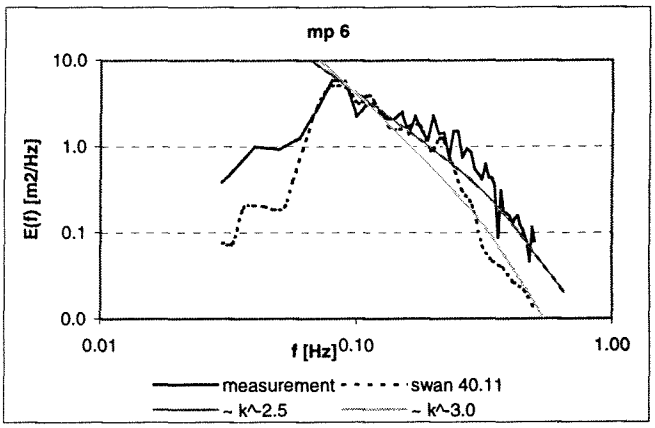

Petten 2/1/1995 6:00

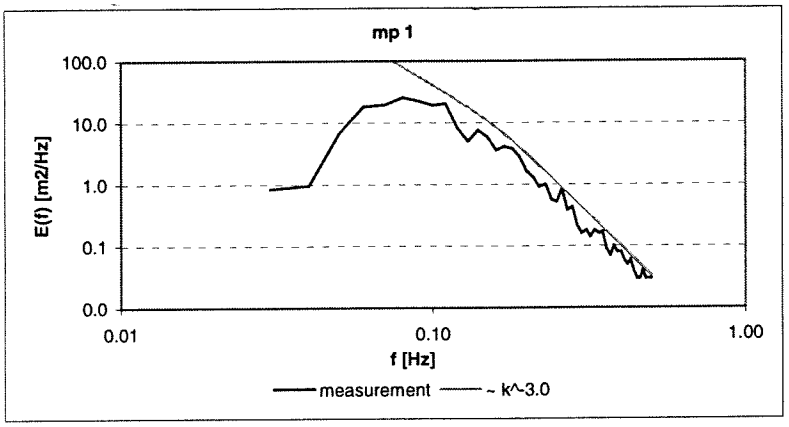

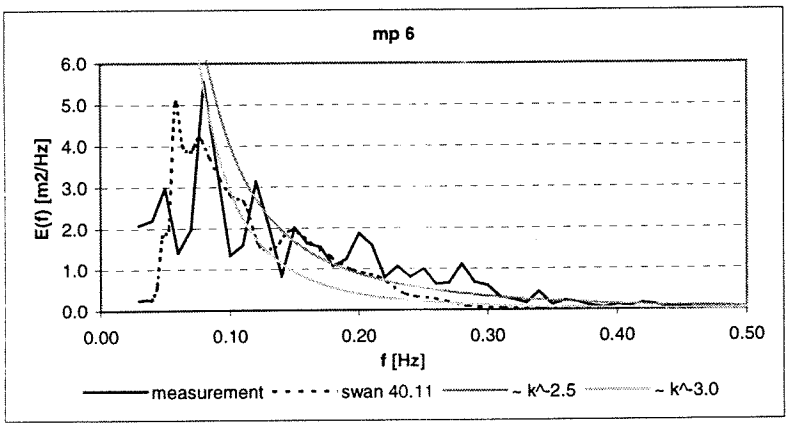

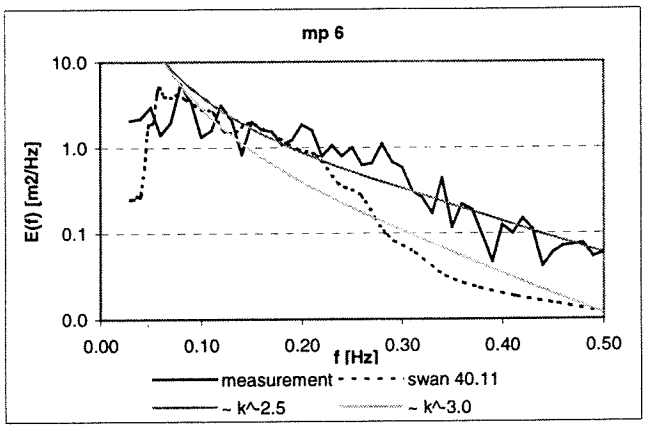

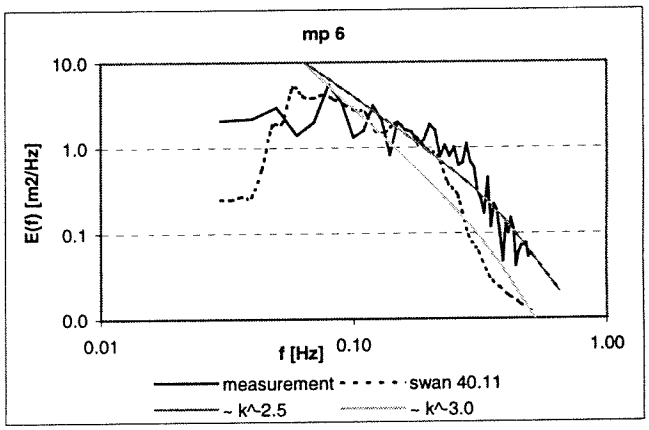

Petten 2/1/1995 17:00

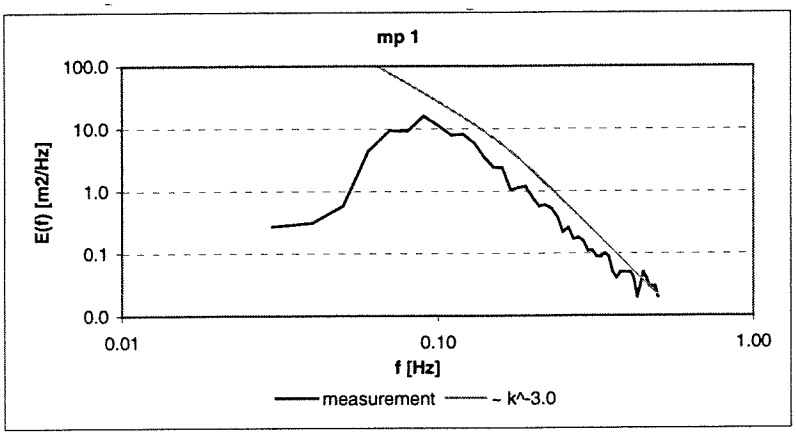

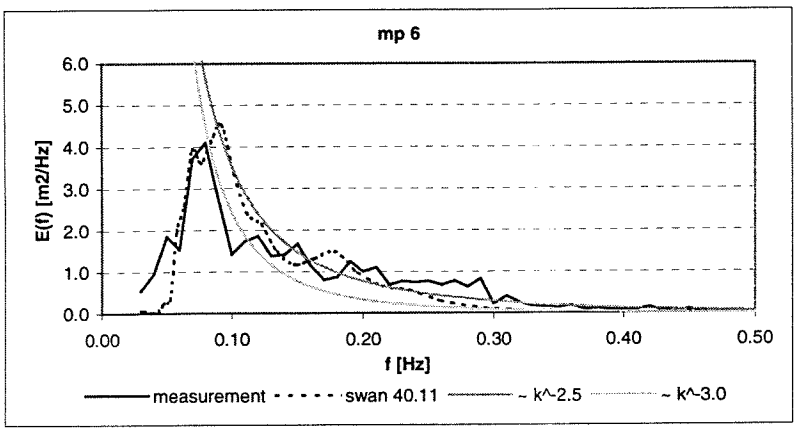

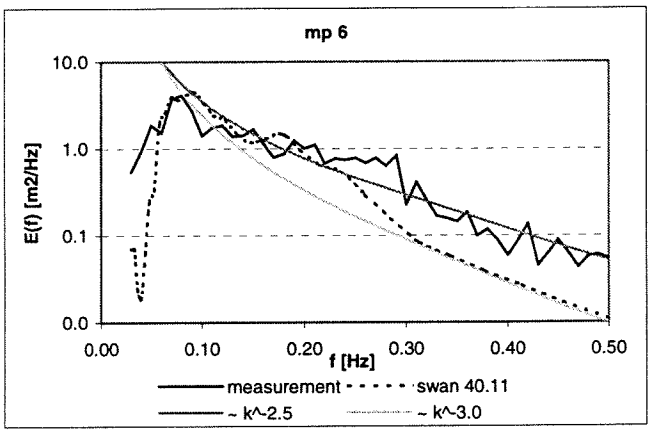

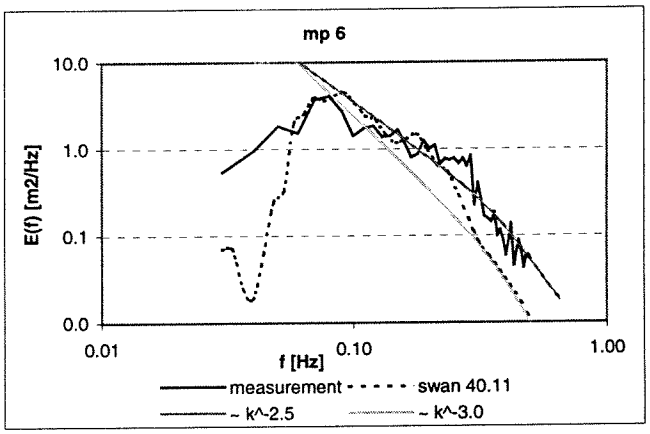

Petten 10/1/1995 11:40

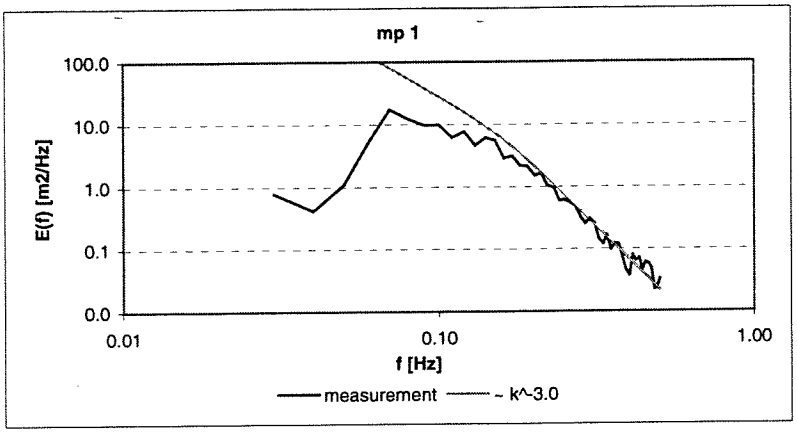

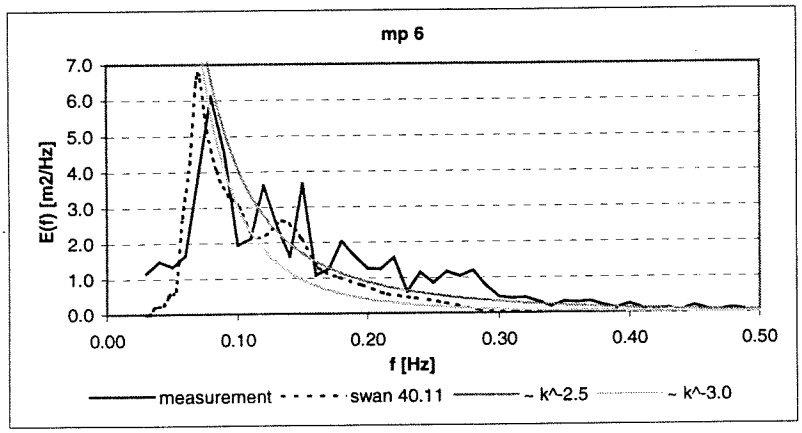

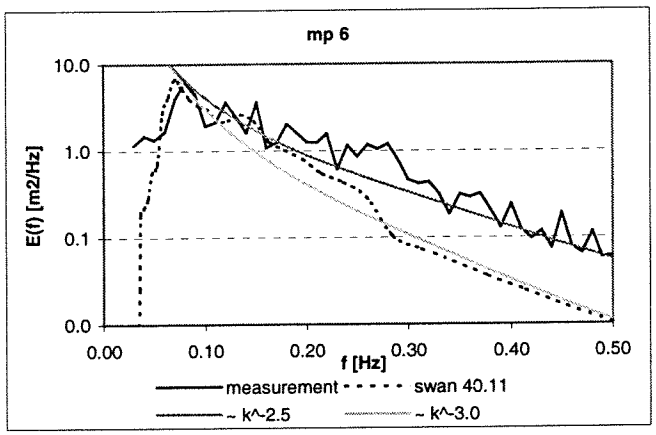

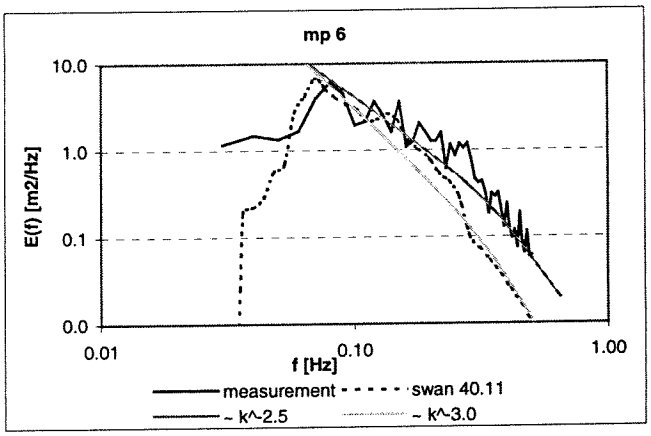

Petten 23-02-99 0:40

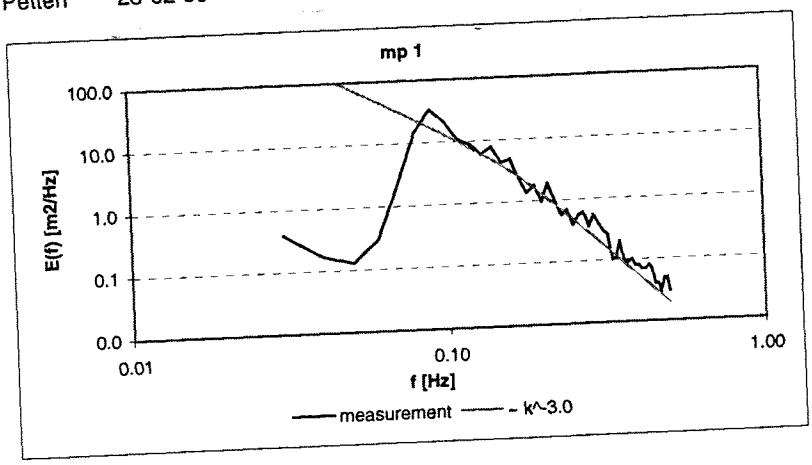

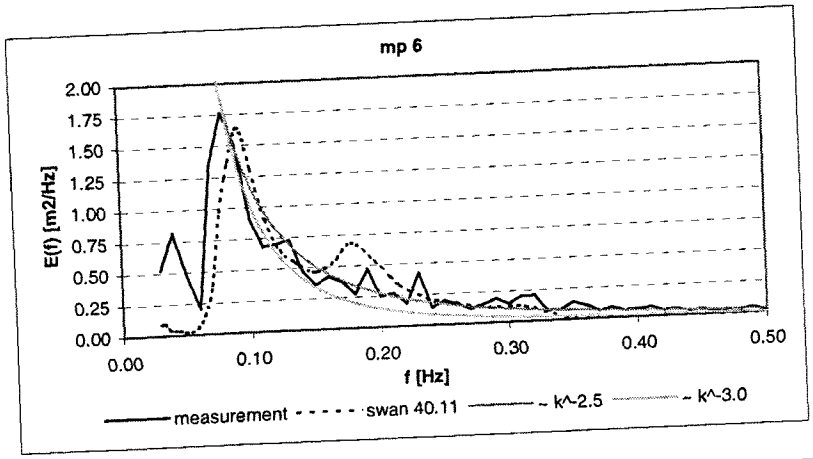

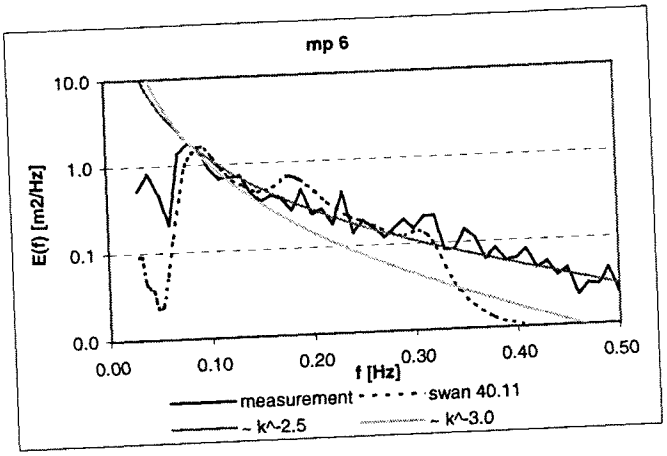

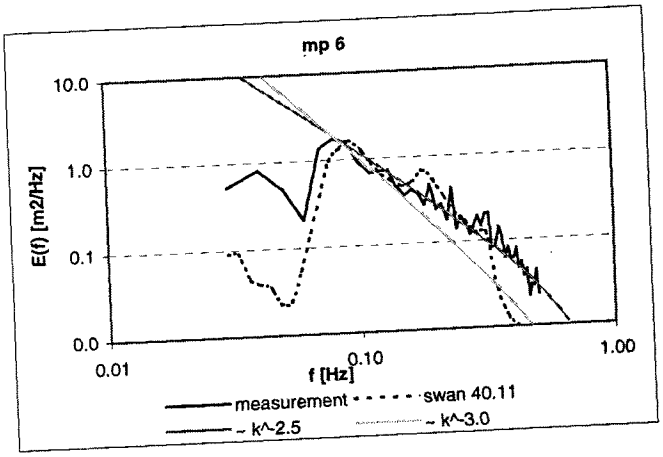

Petten 23-02-99 4:40

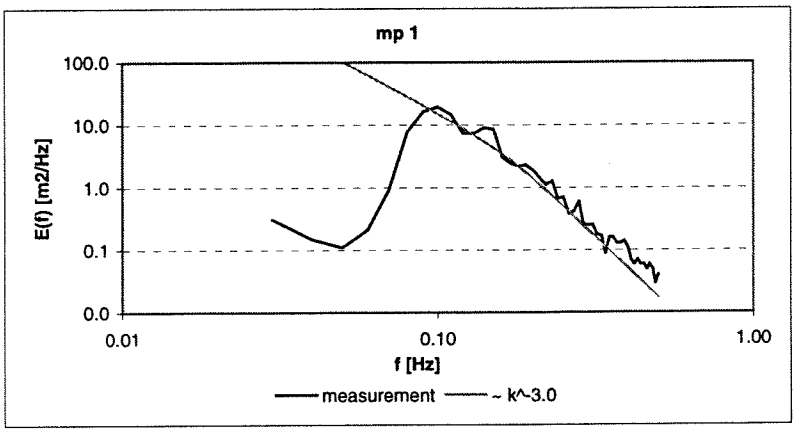

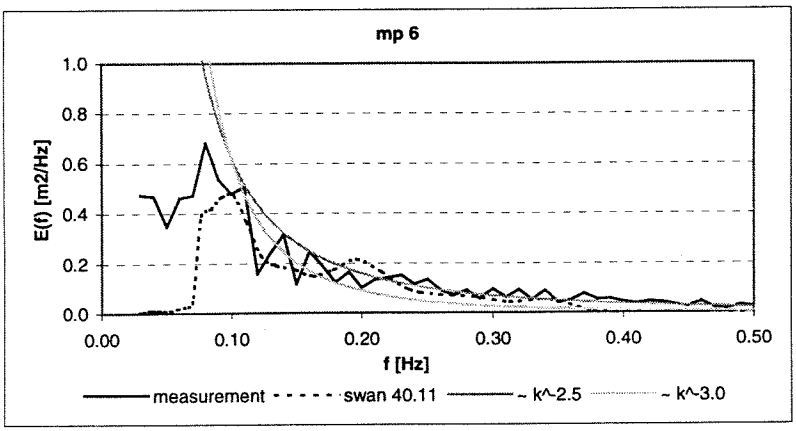

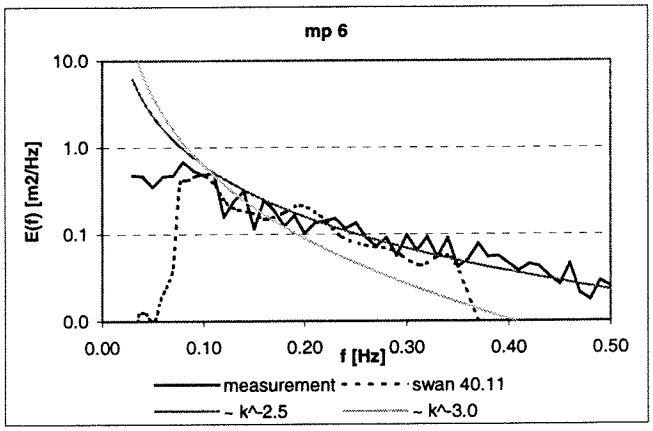

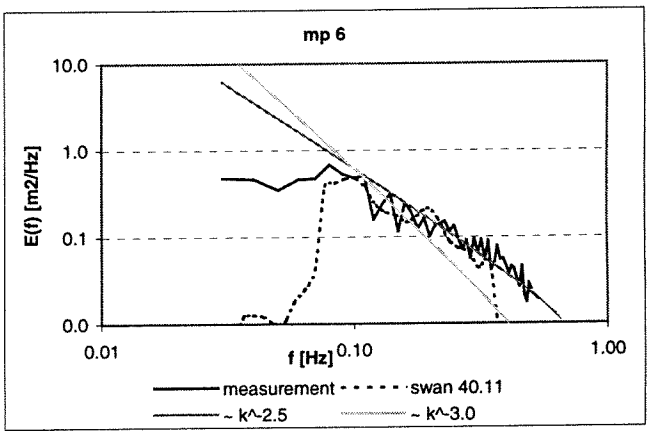

4L Comparison of spectra with the equilibrium range in the Duck '94 cases

Duck 94 case I

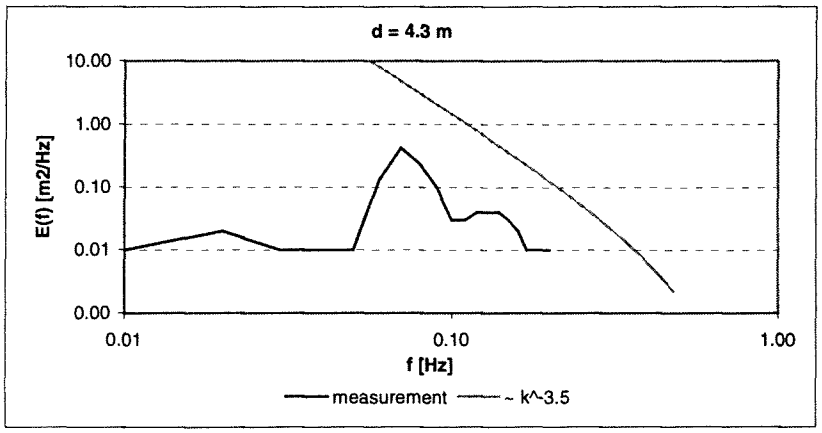

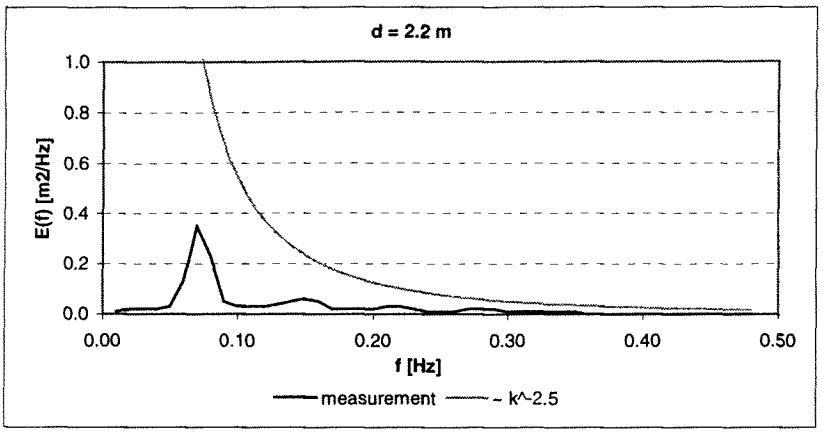

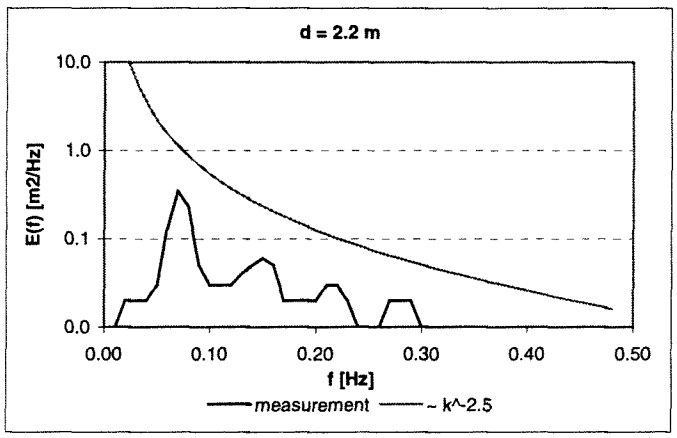

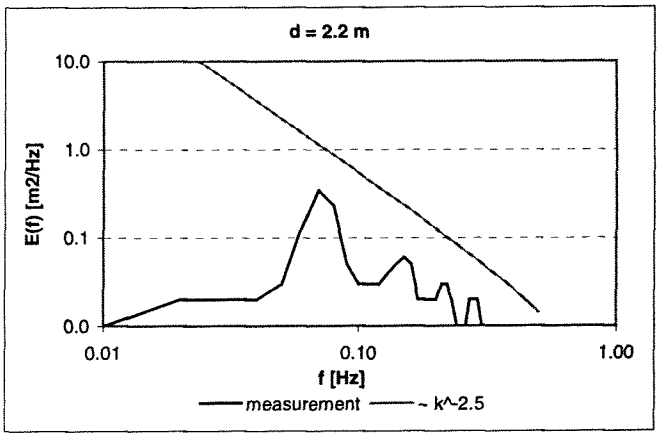

Duck 94 case II

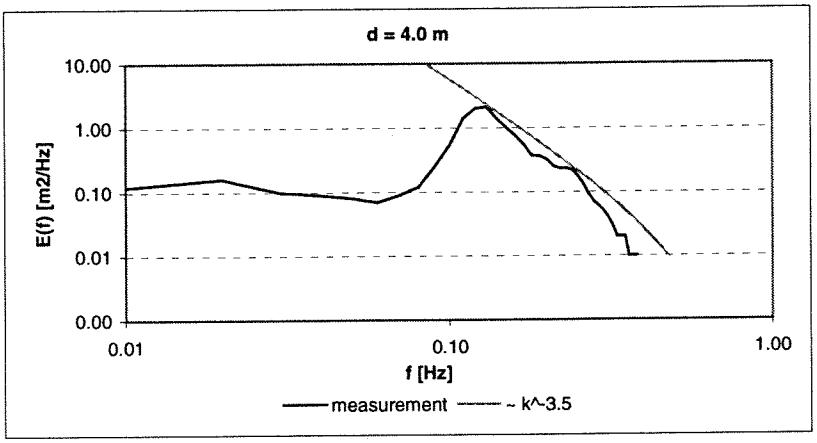

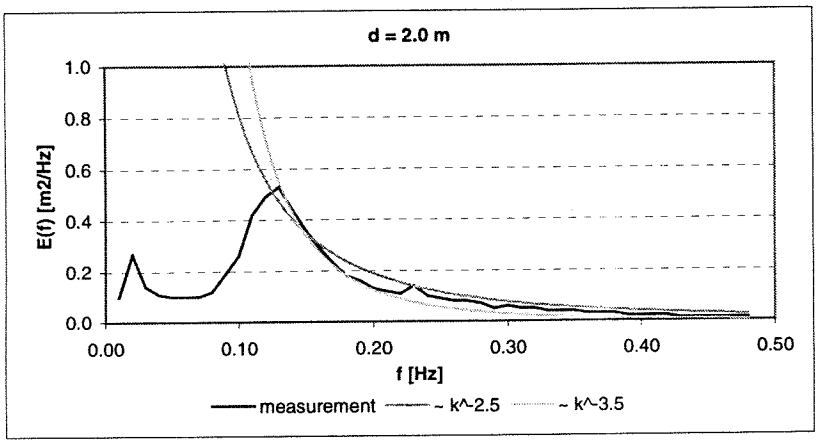

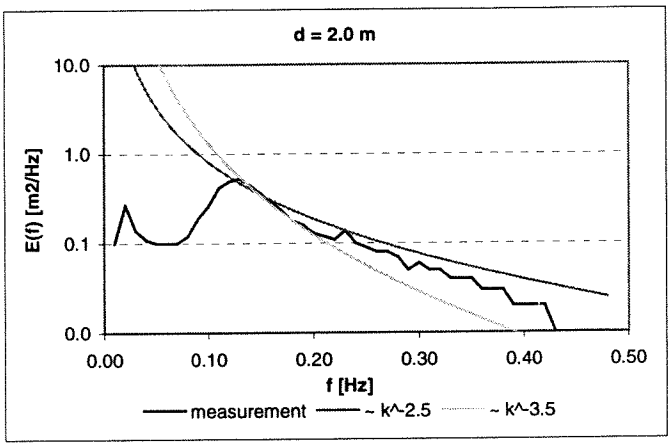

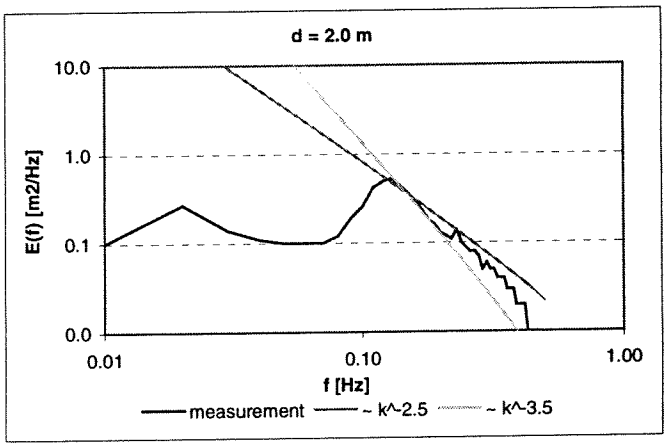

Duck 94 case III

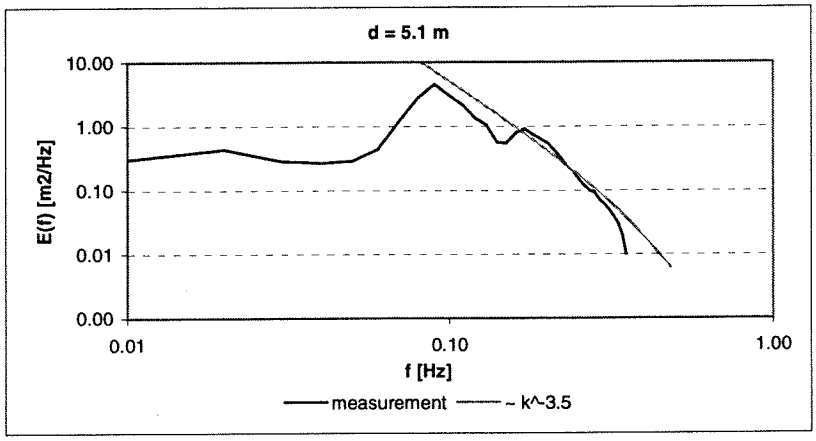

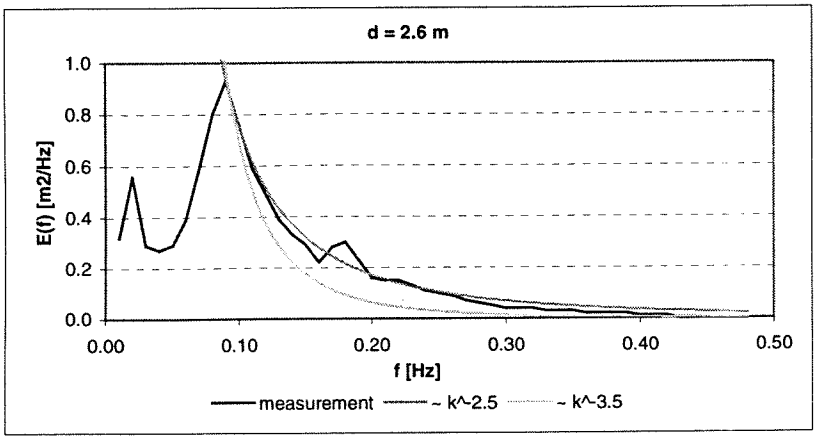

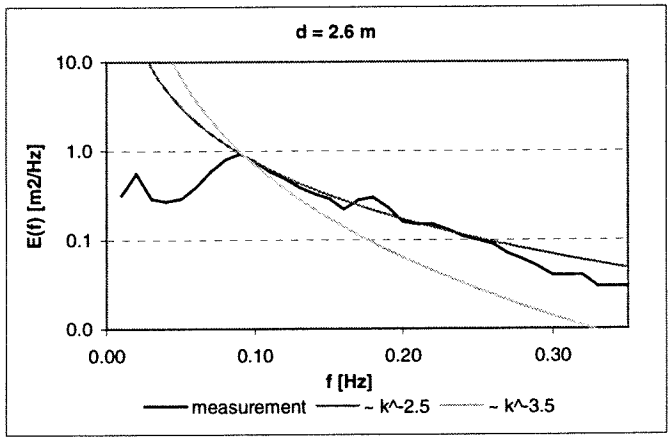

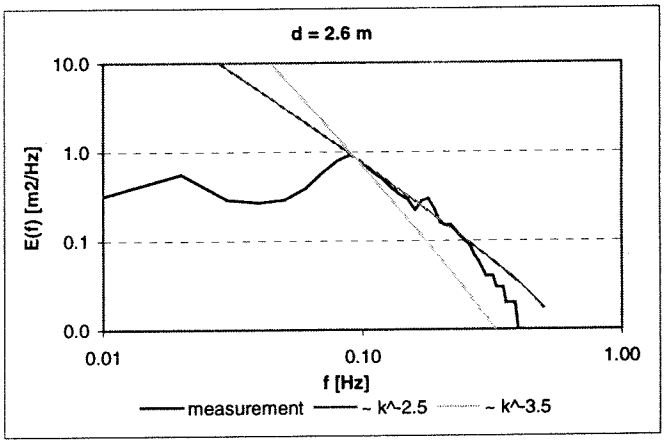

Duck 94 case IV

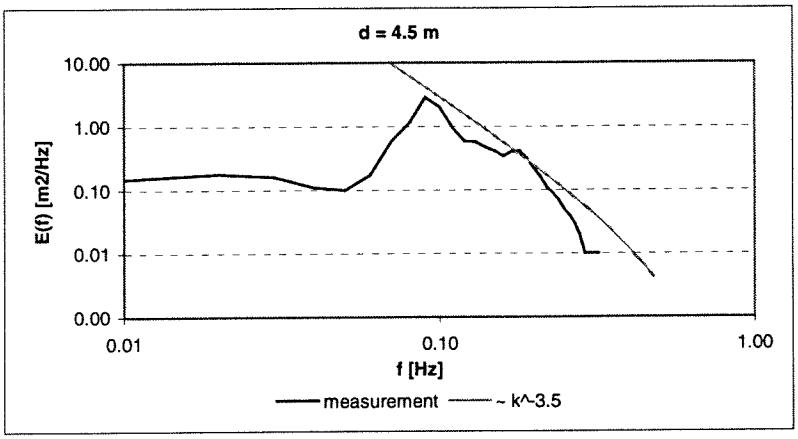

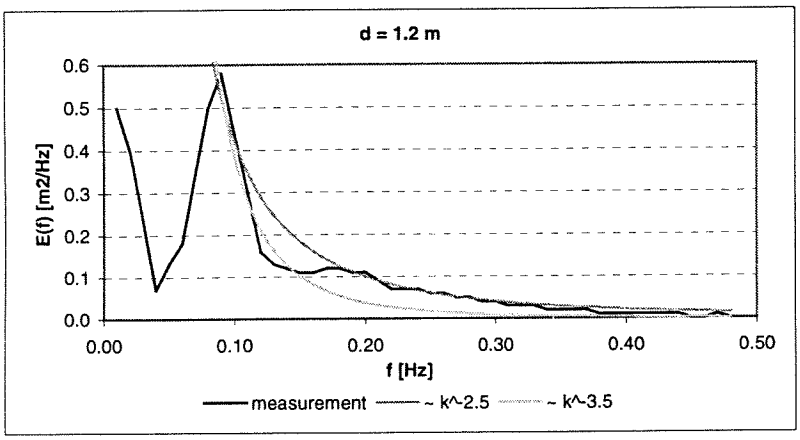

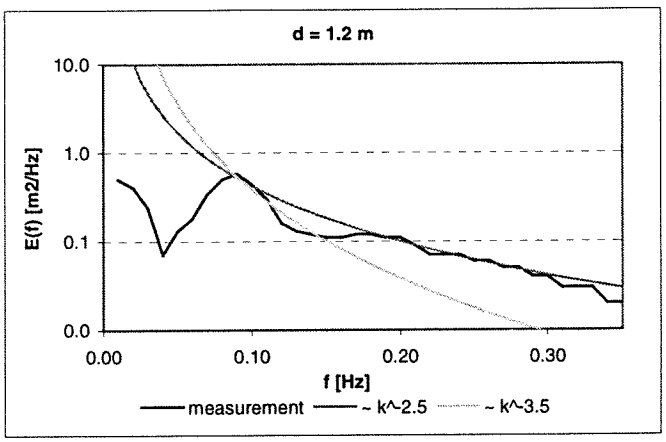

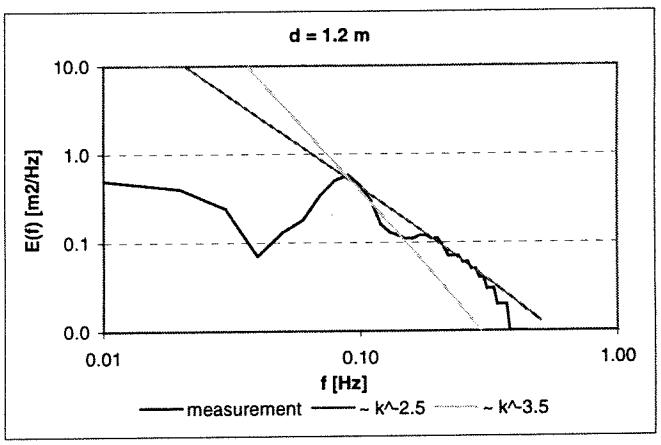

4M _ Wave height distributions in the Petten cases

Petten 1/1/1995 5:00

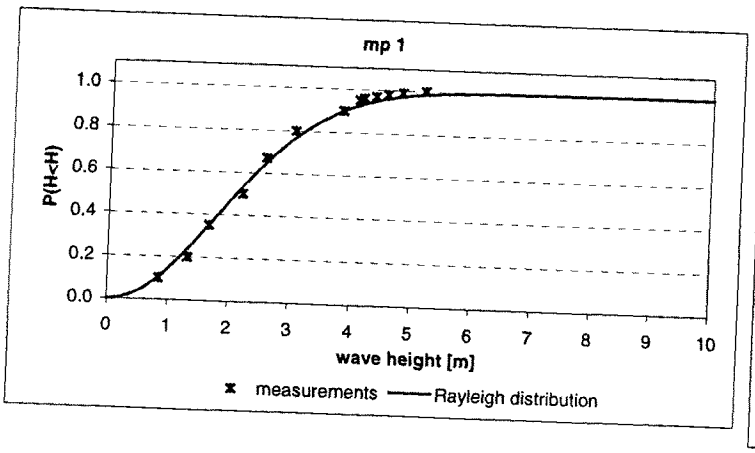

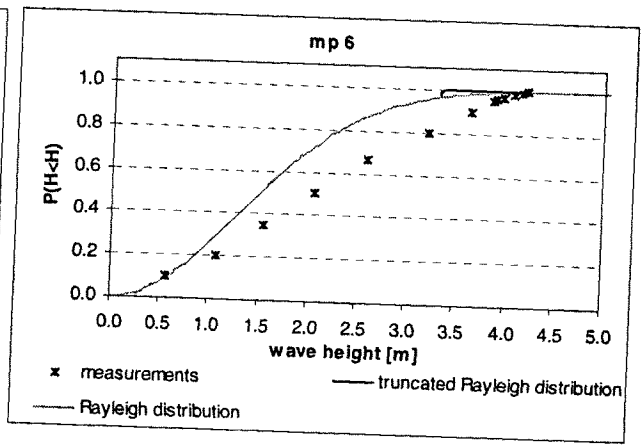

Petten 1/1/1995 18:20

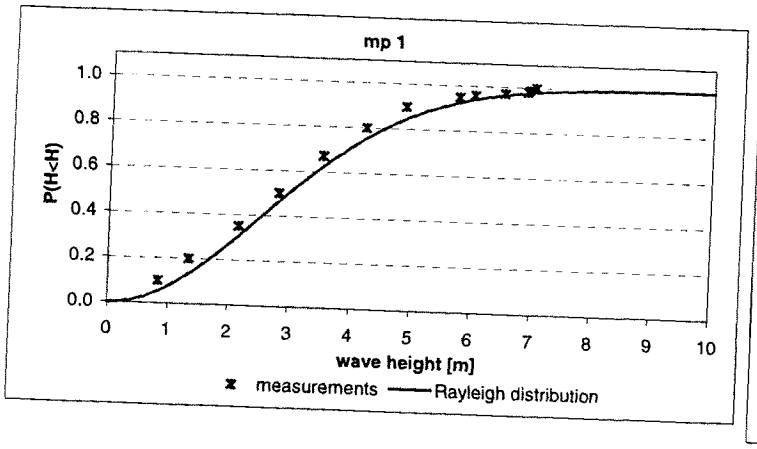

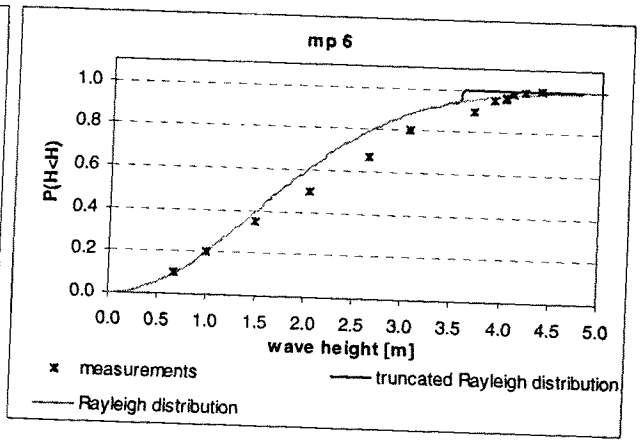

Petten 2/1/1995 6:00

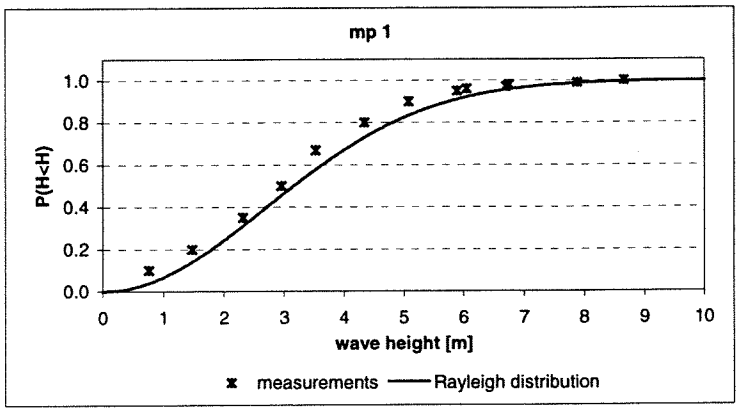

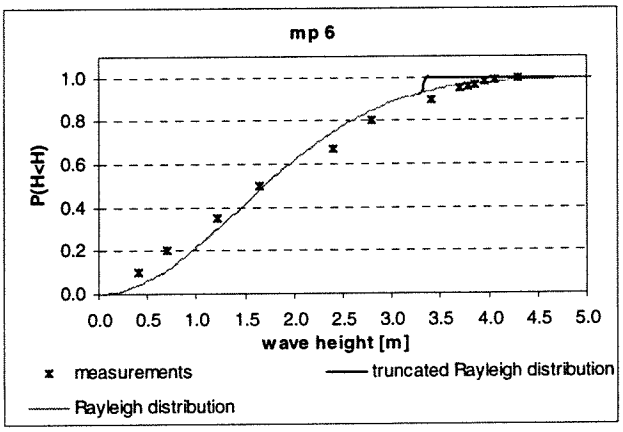

Petten 2/1/1995 17:00

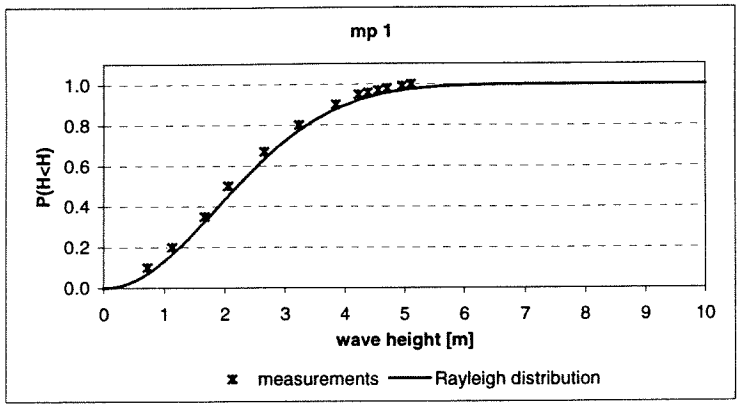

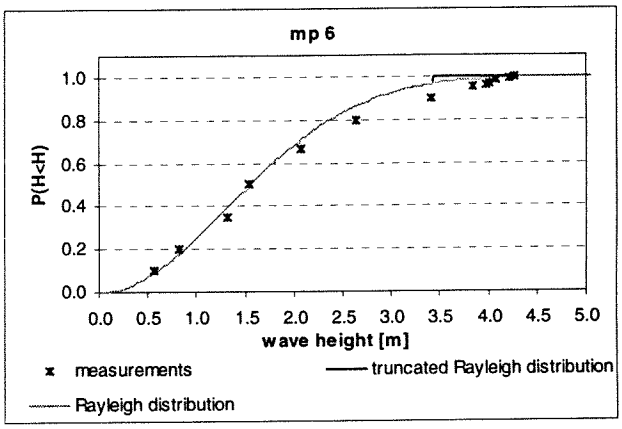

Petten 10/1/1995 11:40

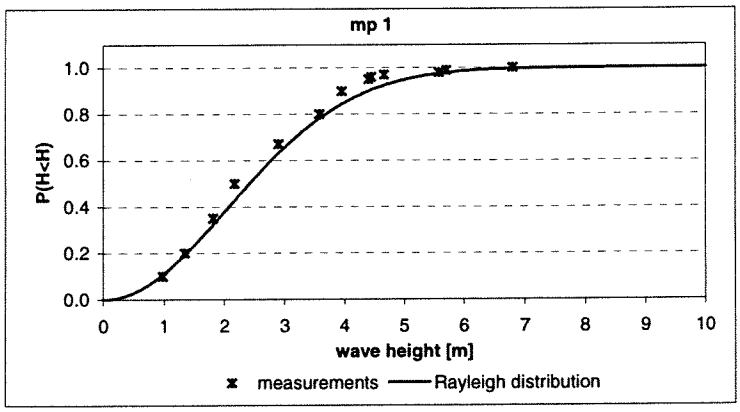

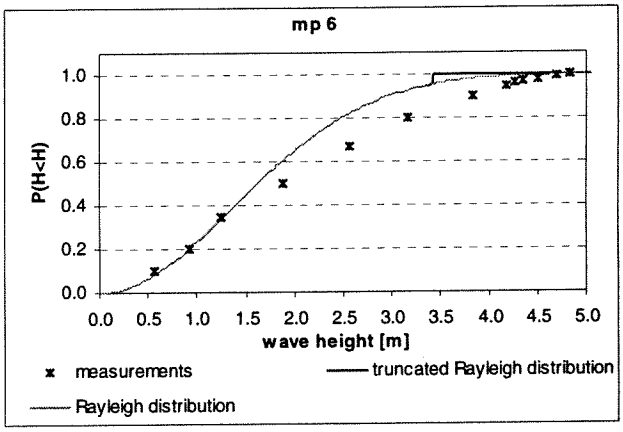

Petten 23/2/1999 0:40

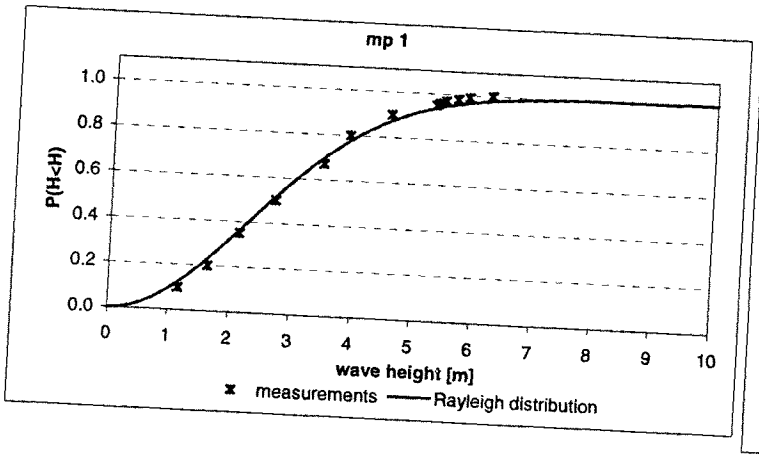

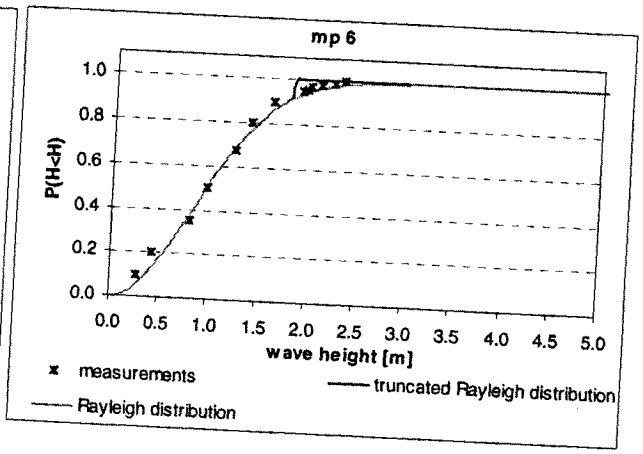

Petten 23/2/1999 4:40

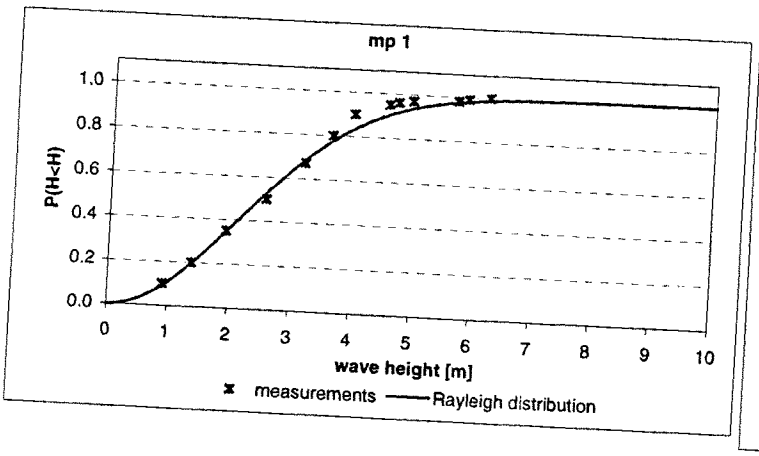

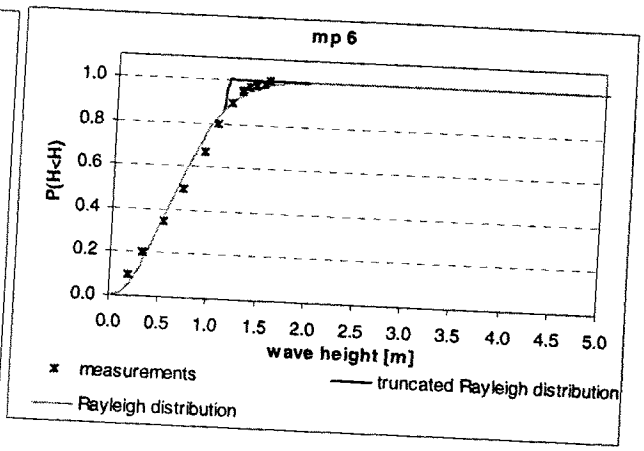

5A Comparison of significant wave heights with SWAN 40.11 and SWAN Baldock in the Petten cases

Petten 1/1/1995 5:00

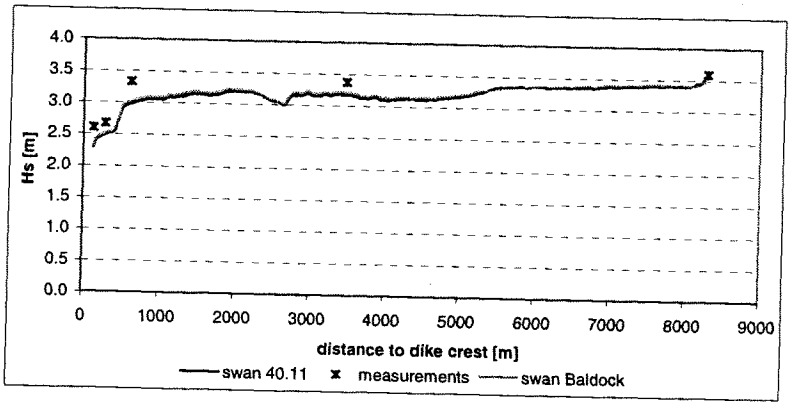

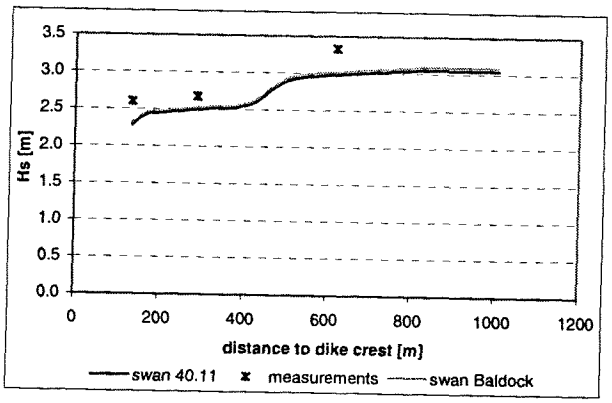

Petten 1/1/1995 18:20

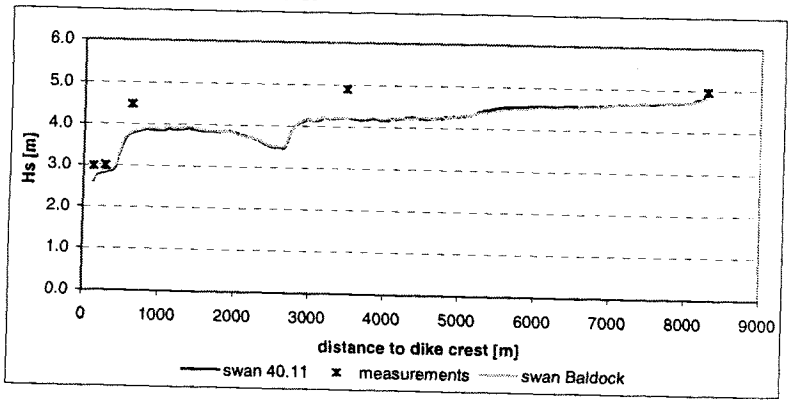

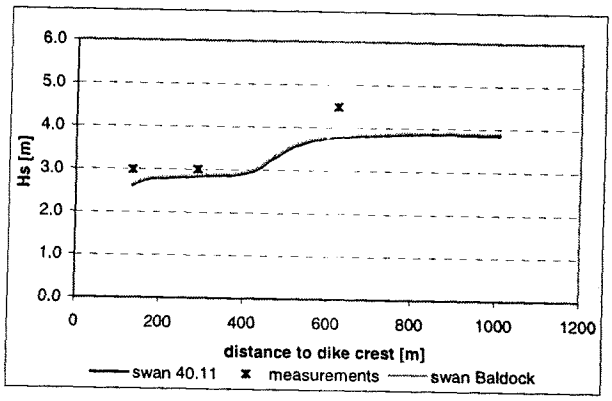

Petten 2/1/1995 6:00

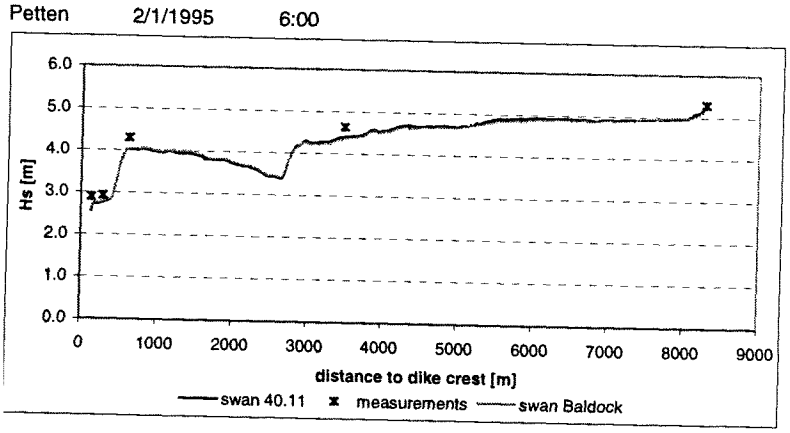

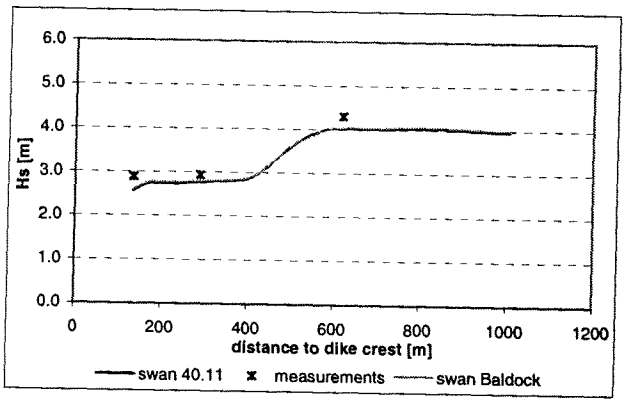

Petten 2/1/1995 17:00

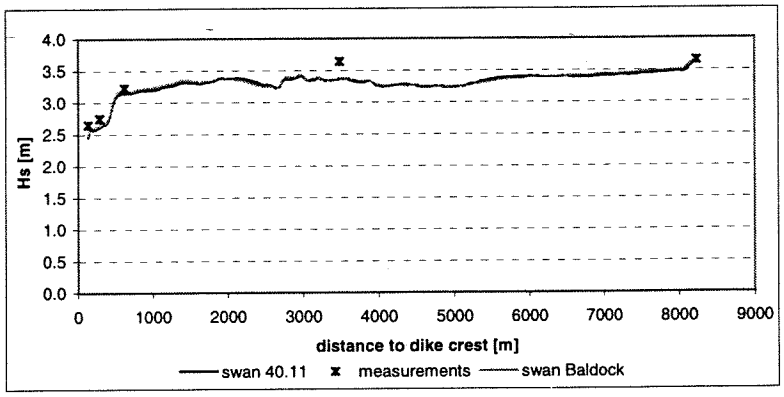

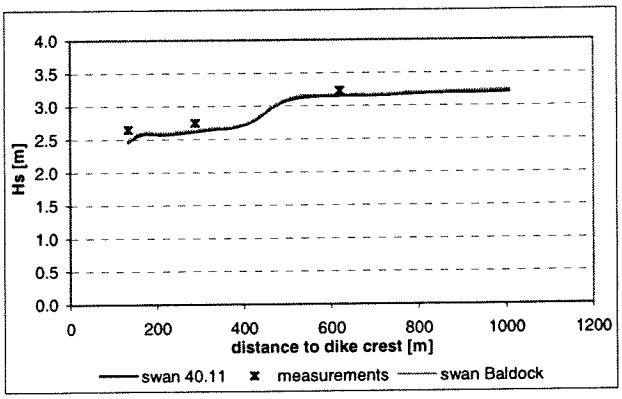

Petten 10/1/1995 11:40

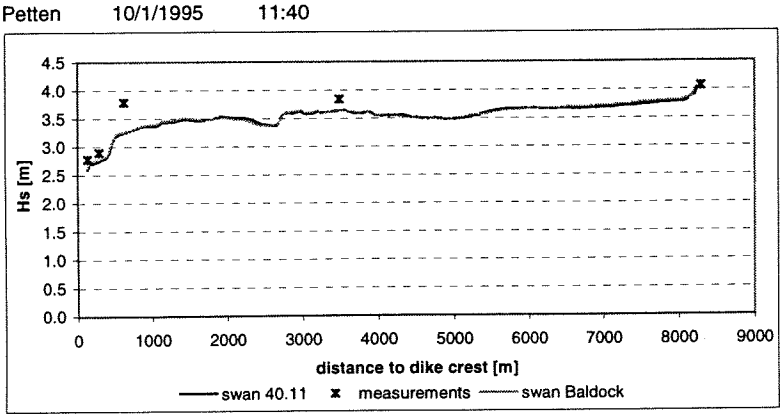

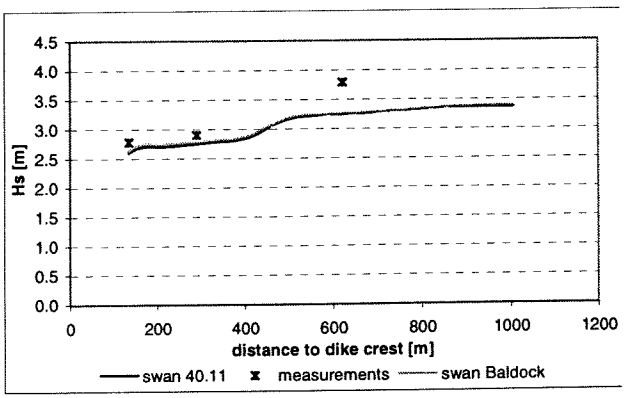

Petten 23-02-99 0:40

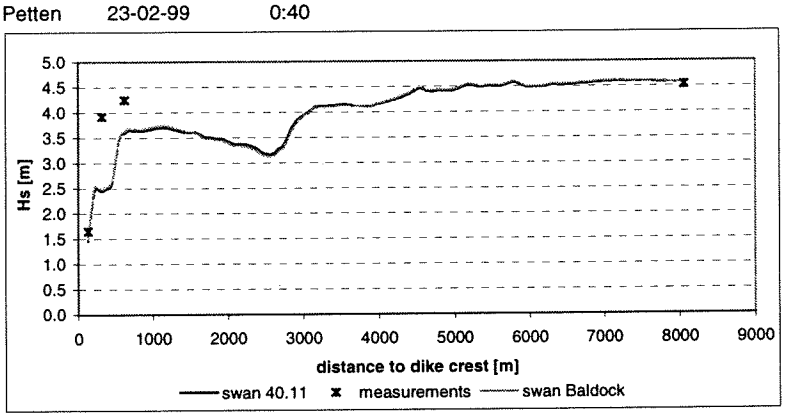

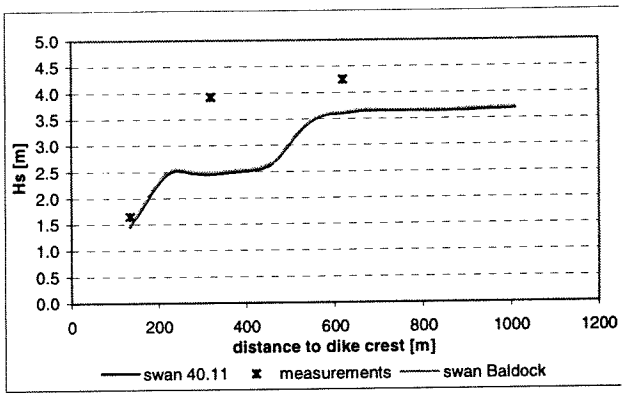

Petten 23-02-99 4:40

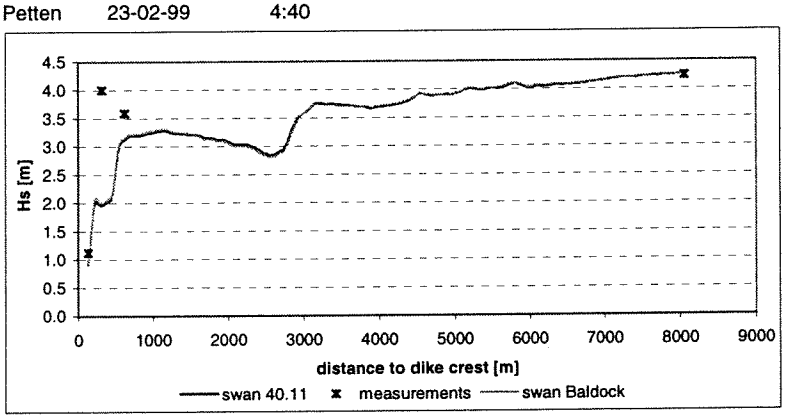

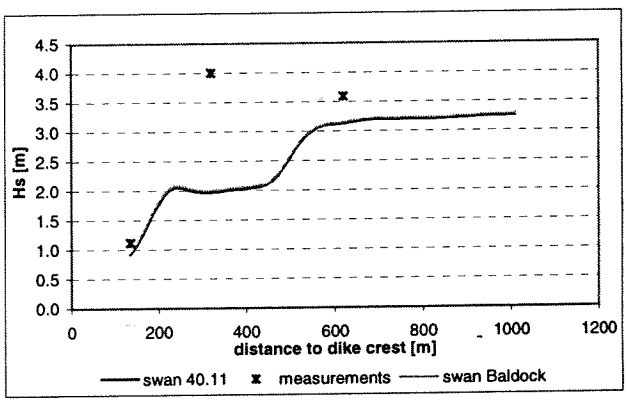

1995

01-01-0500

	measured	swan 40.11		swan Baldock	
	Hs [m]	Hs [m]	difference	Hs [m]	difference
mp 1	3.60	3.60	0%	3.60	0%
mp 2	3.38	3.18	-6%	3.21	-5%
mp 3	3.33	2.98	-11%	3.01	-10%
mp 5	2.67	2.49	-7%	2.52	-6%
mp 6	2.60	2.28	-12%	2.31	-11%

01-01-1820

	measured	swan 40.11		swan Baldock	
	Hs [m]	Hs [m]	difference	Hs [m]	difference
mp 1	4.98	4.96	0%	4.94	-1%
mp 2	4.90	4.21	-14%	4.21	-14%
mp 3	4.48	3.77	-16%	3.80	-15%
mp 5	3.00	2.83	-6%	2.86	-5%
mp 6	2.98	2.60	-13%	2.63	-12%

02-01-0600

	measured	swan 40.11		swan Baldock	
	Hs [m]	Hs [m]	difference	Hs [m]	difference
mp 1	5.39	5.28	-2%	5.30	-2%
mp 2	4.64	4.41	-5%	4.36	-6%
mp 3	4.30	4.02	-7%	4.04	-6%
mp 5	2.93	2.75	-6%	2.79	-5%
mp 6	2.89	2.56	-11%	2.59	-10%

02-01-1700

	measured	swan 40.11		swan Baldock	
	Hs [m]	Hs [m]	difference	Hs [m]	difference
mp 1	3.77	3.77	0%	3.77	0%
mp 2	3.64	3.37	-7%	3.37	-8%
mp 3	3.23	3.15	-2%	3.17	-2%
mp 5	2.75	2.62	-5%	2.64	-4%
mp 6	2.65	2.46	-7%	2.49	-6%

10-01-1140

	measured	swan 40.11		swan Baldock	
	Hs [m]	Hs [m]	difference	Hs [m]	difference
mp 1	4.12	4.10	0%	4.10	0%
mp 2	3.84	3.64	-5%	3.63	-5%
mp 3	3.79	3.25	-14%	3.26	-14%
mp 5	2.90	2.74	-6%	2.79	-4%
mp 6	2.78	2.60	-6%	2.64	-5%

1999

23-02-0040

	measured	swan 40.11		swan Baldock	
	Hs [m]	Hs [m]	difference	Hs [m]	difference
mp 1	4.53	4.54	0%	4.55	0%
mp 3	4.25	3.6	-15%	3.62	-15%
*mp 5**	*3.92*	*2.45*	*-38%*	2.49	-37%
mp 6	1.65	1.46	-12%	1.49	-10%

23-02-0440

	measured	swan 40.11		swan Baldock	
	Hs [m]	Hs [m]	difference	Hs [m]	difference
mp 1	4.23	4.24	0%	4.25	0%
mp 3	3.59	3.13	-13%	3.14	-12%
*mp 5**	*4.00*	*1.97*	*-51%*	*2.00*	*-50%*
mp 6	1.12	0.92	-18%	0.94	-16%

* instrument probably not working

5B Comparison of predicted fractions of breaking waves with SWAN 40.11 and SWAN Baldock in the Petten cases

Petten 1/1/1995 5:00

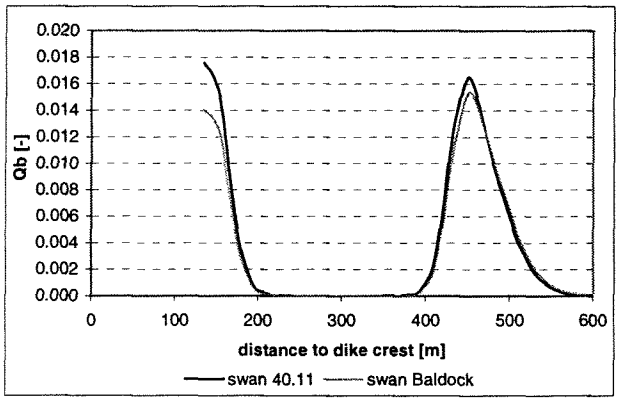

Petten 1/1/1995 18:20

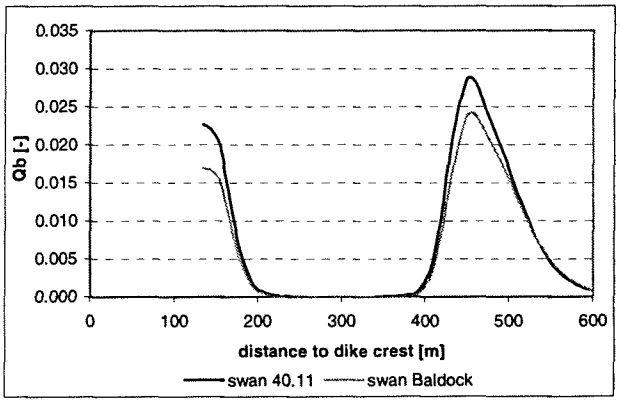

Petten 2/1/1995 6:00

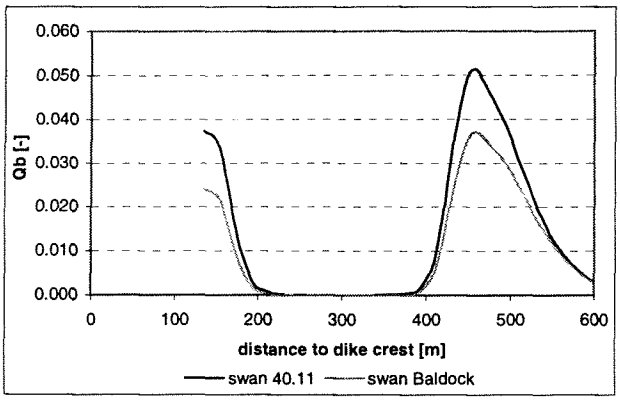

Petten 2/1/1995 17:00

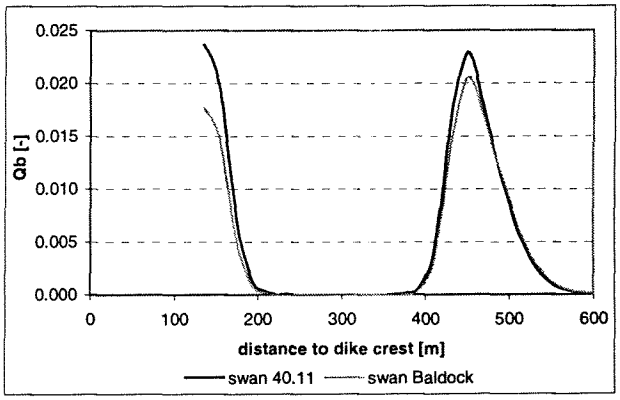

Petten 10/1/1995 11:40

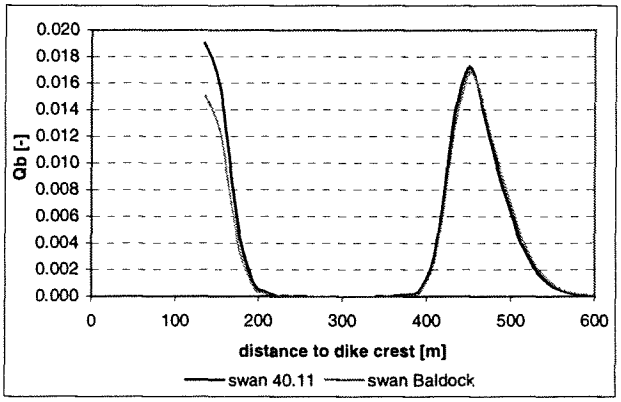

Petten 23-02-99 0:40

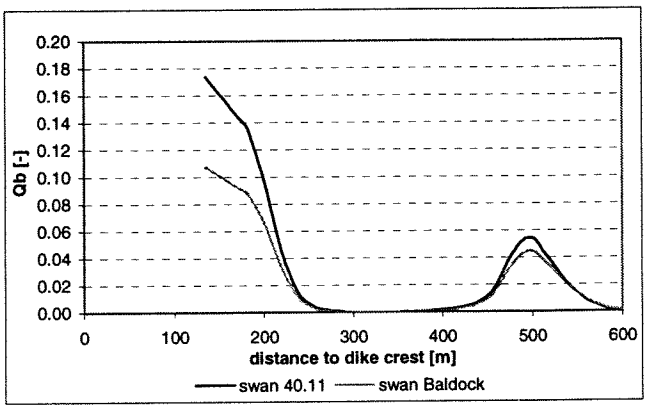

Petten 23/2/1999 4:40

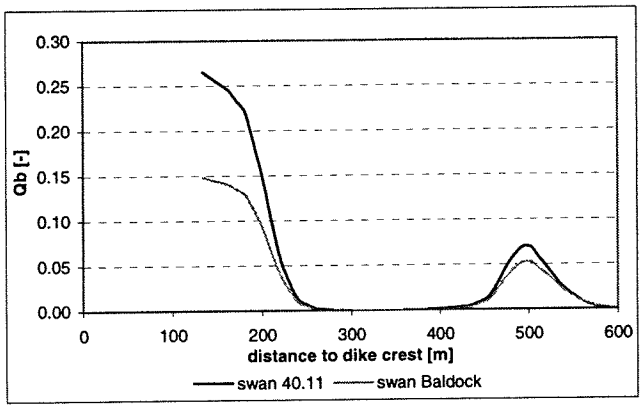

5C Comparison of significant wave heights with SWAN 40.11 and SWAN Baldock in the SV cases

SV case 01

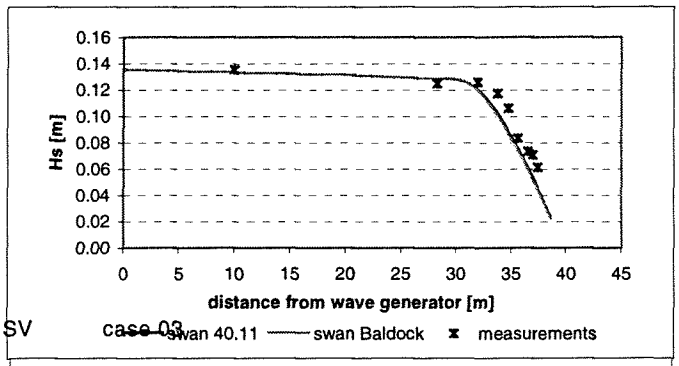

SV case 03

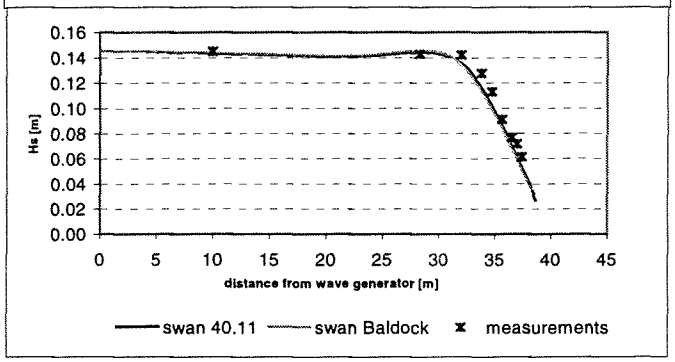

SV case 07

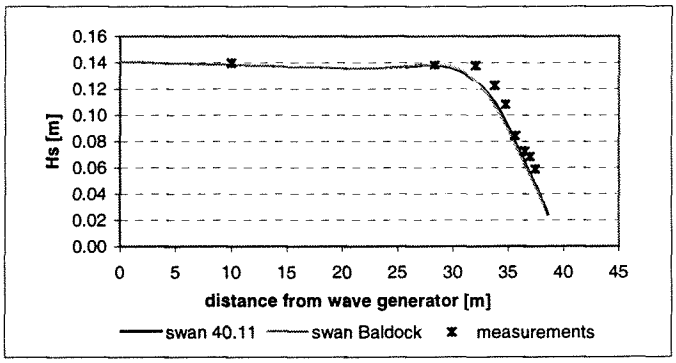

SV case 09

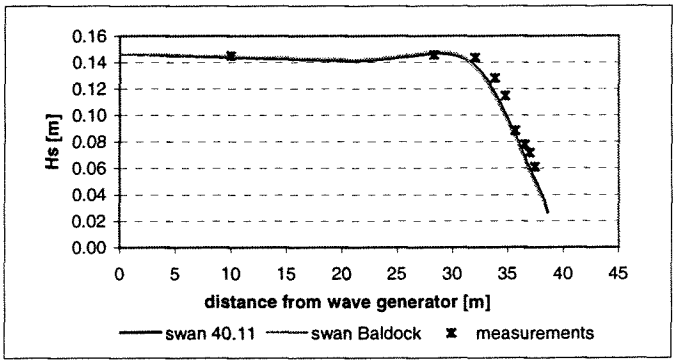

case 1

	measurement	swan 40.11		swan Baldock	
depth [cm]	Hs [m]	Hs [m]	difference	Hs [m]	difference
61	13.5	13.4	-1%	13.4	-1%
36.6	12.5	12.9	3%	12.9	3%
24.4	12.6	12.0	-5%	12.0	-5%
18.3	11.8	10.2	-13%	10.1	-15%
15.2	10.6	8.9	-16%	8.8	-17%
12.2	8.5	7.5	-11%	7.4	-12%
9.7	7.5	6.1	-19%	6.0	-21%
7.6	7.2	5.6	-23%	5.4	-26%
6.1	6.2	4.5	-26%	4.5	-27%

case 3

	measurement	swan 40.11		swan Baldock	
depth [cm]	Hs [m]	Hs [m]	difference	Hs [m]	difference
61	14.5	14.4	-1%	14.4	-1%
36.6	14.3	14.4	1%	14.4	1%
24.4	14.2	13.6	-4%	13.5	-5%
18.3	12.8	11.7	-9%	11.4	-11%
15.2	11.3	10.2	-10%	10.0	-12%
12.2	9.1	8.6	-6%	8.5	-7%
9.7	7.7	7.0	-9%	7.0	-9%
7.6	7.2	6.1	-15%	5.9	-17%
6.1	6.1	5.3	-14%	5.2	-15%

case 7

	measurement	swan 40.11		swan Baldock	
depth [cm]	Hs [m]	Hs [m]	difference	Hs [m]	difference
61	13.98	13.81	-1%	13.81	-1%
36.6	13.81	13.80	0%	13.81	0%
24.4	13.77	12.64	-8%	12.65	-8%
18.3	12.28	10.91	-11%	10.72	-13%
15.2	10.82	9.54	-12%	9.26	-14%
12.2	8.43	8.00	-5%	7.76	-8%
9.7	7.25	6.39	-12%	6.29	-13%
7.6	6.84	5.58	-18%	5.55	-19%
6.1	5.89	4.76	-19%	4.72	-20%

case 9

	measurement	swan 40.11		swan Baldock	
depth [cm]	Hs [m]	Hs [m]	difference	Hs [m]	difference
61	14.51	14.46	0%	14.46	0%
36.6	14.57	14.61	0%	14.73	1%
24.4	14.38	13.74	-4%	13.56	-6%
18.3	12.8	11.69	-9%	11.43	-11%
15.2	11.47	10.14	-12%	9.87	-14%
12.2	8.83	8.50	-4%	8.30	-6%
9.7	7.79	6.83	-12%	6.66	-14%
7.6	7.17	6.00	-16%	5.96	-17%
6.1	6.1	5.07	-17%	5.05	-17%

5D Comparison of predicted dissipation rates and fractions of breaking waves with SWAN 40.11 and SWAN Baldock in the SV cases

SV case 1

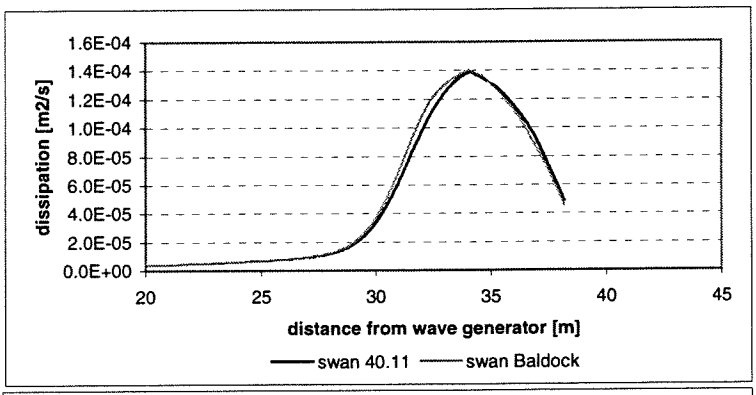

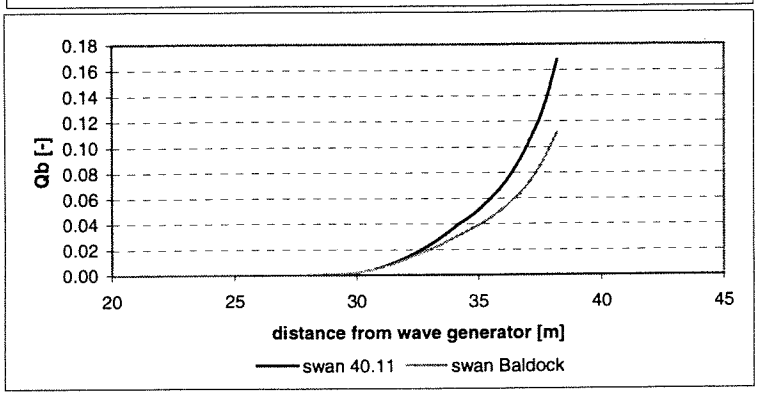

SV case 3

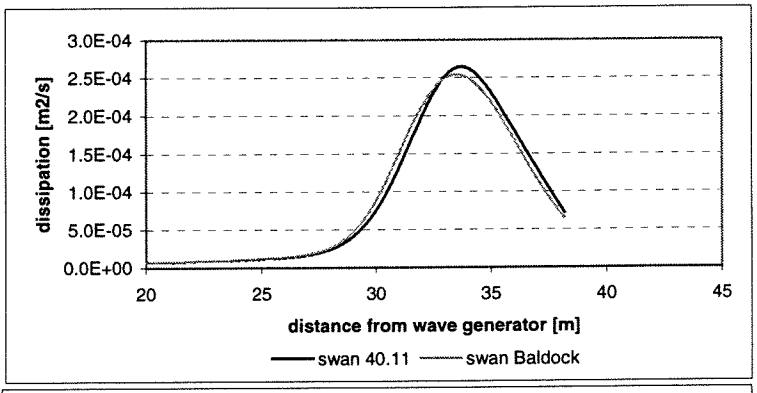

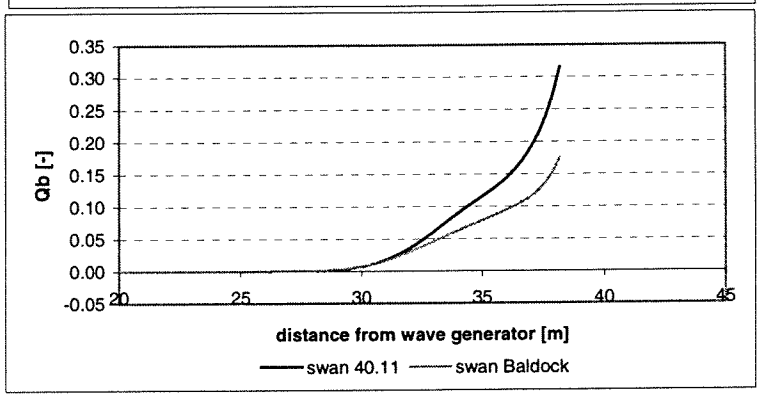

SV case 7

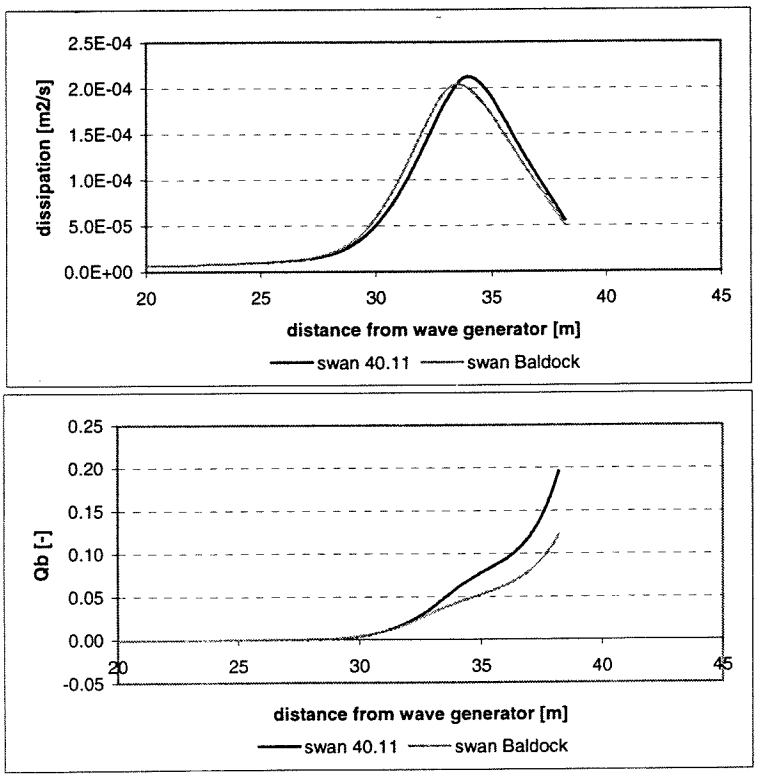

SV case 9

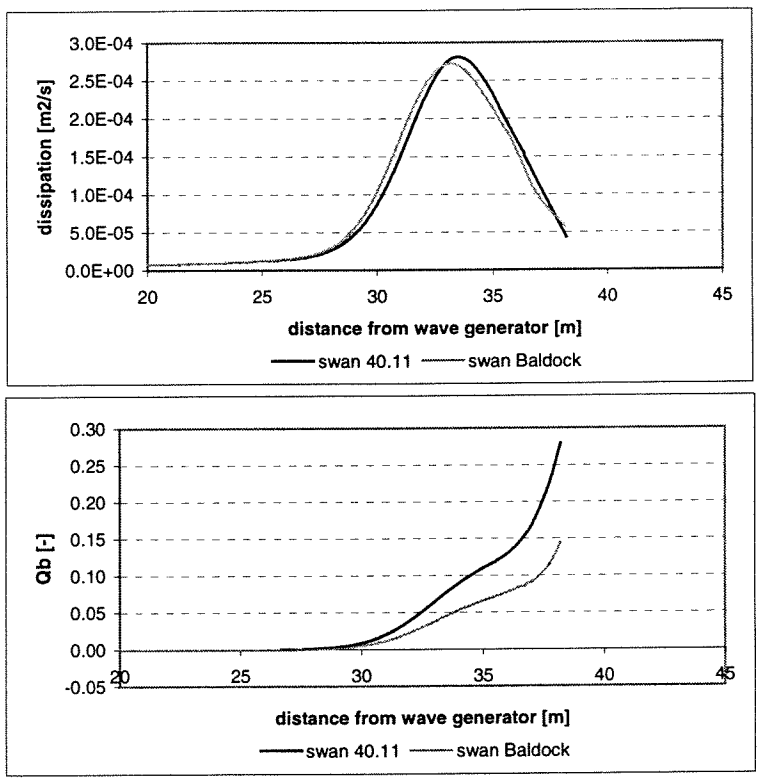

5E Variation of the local wave steepness and the corresponding γ-values in the Petten cases

Petten 1/1/1995 5:00

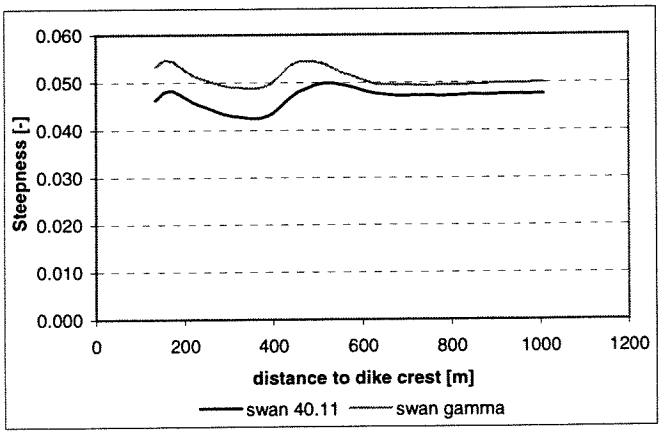

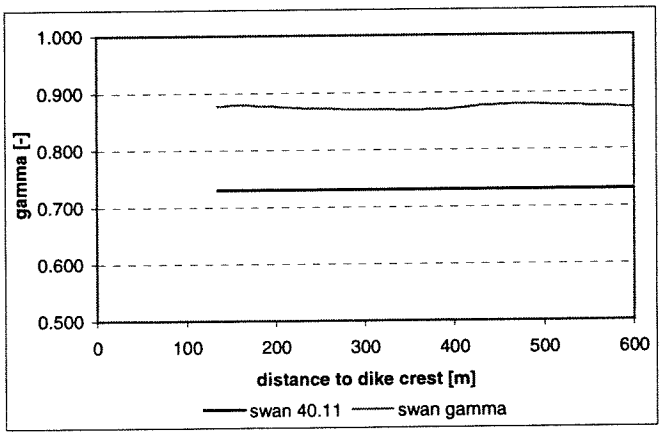

Petten 1/1/1995 18:20

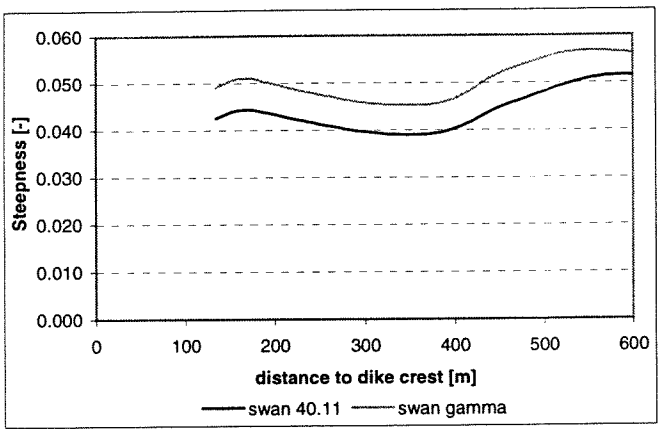

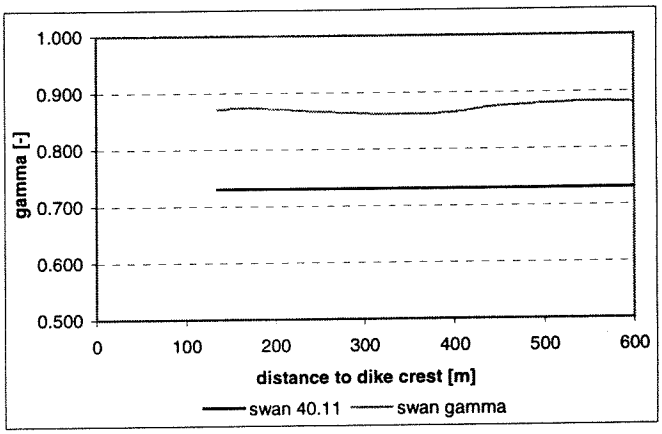

Petten 2/1/1995 6:00

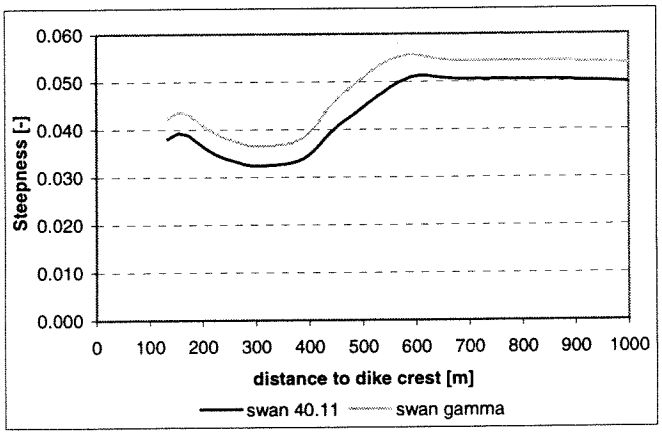

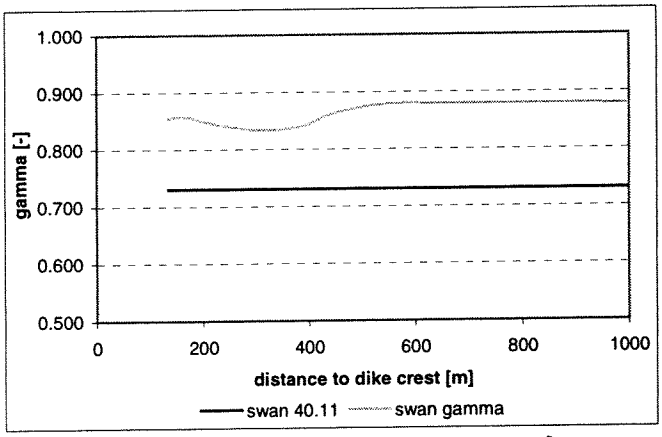

Petten 2/1/1995 17:00

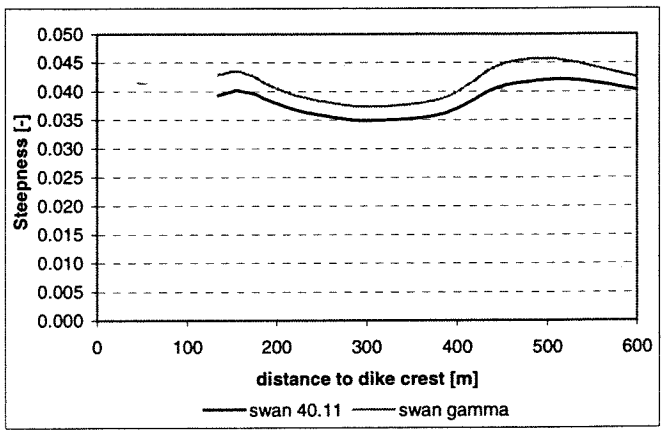

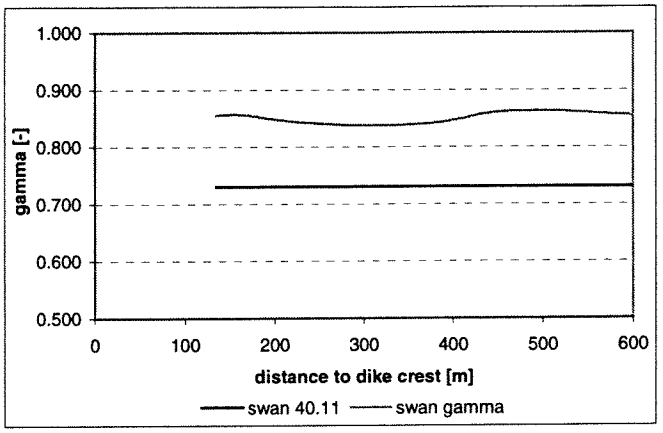

Petten 10/1/1995 11:40

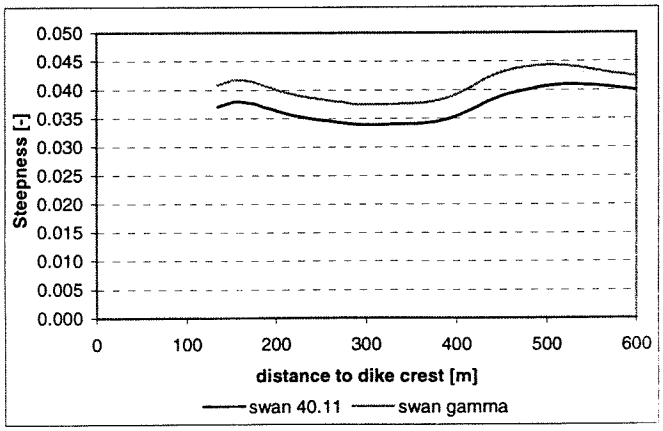

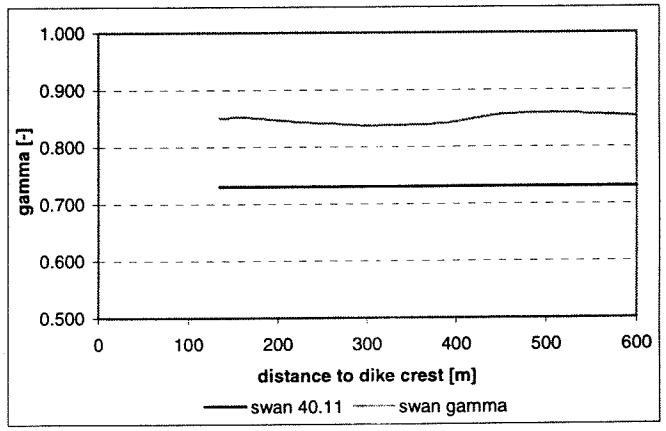

Petten 23/02/99 0:40

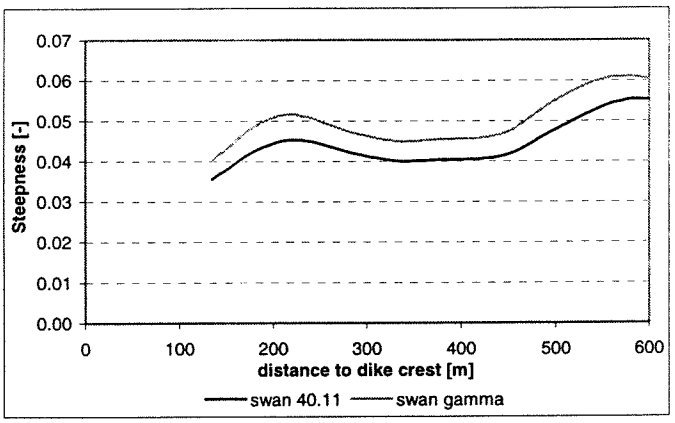

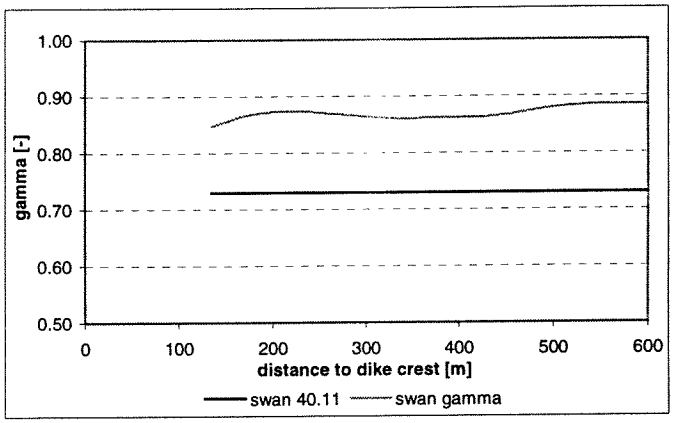

Petten 23/02/99 4:40

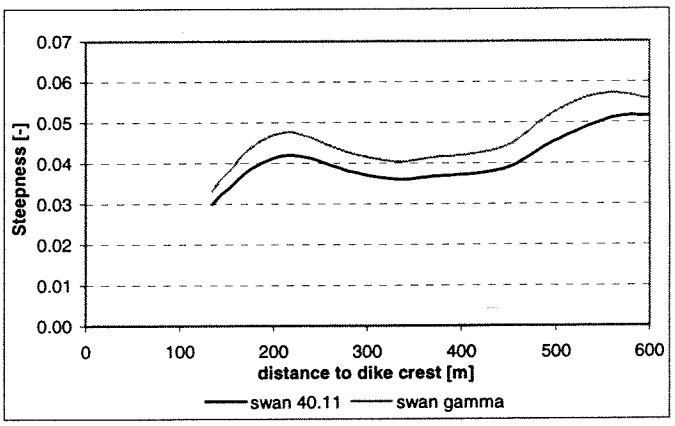

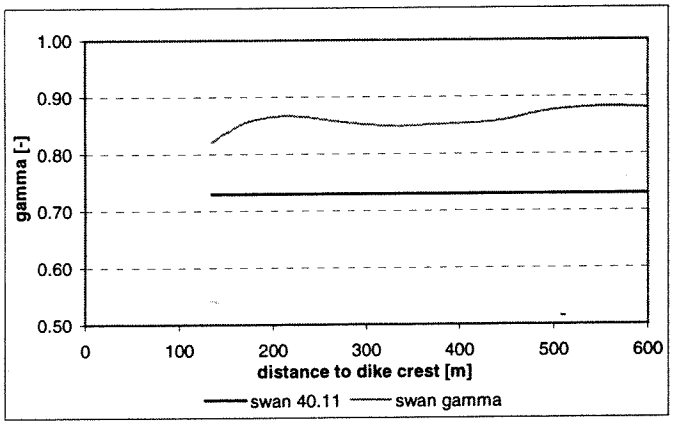

5F Comparison of significant wave heights with SWAN 40.11 and SWAN gamma in the Petten cases

Petten 1/1/1995 5:00

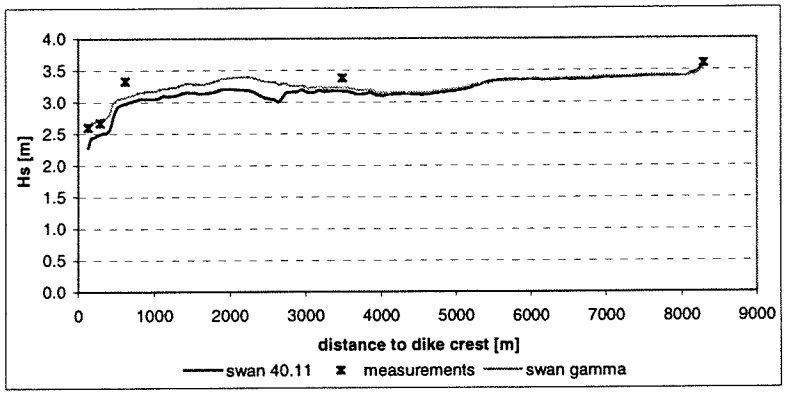

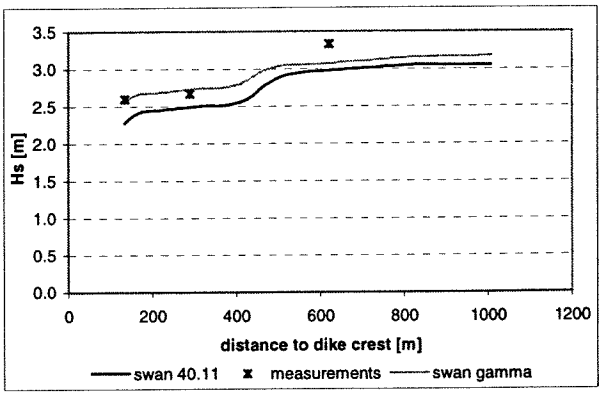

Petten 1/1/1995 18:20

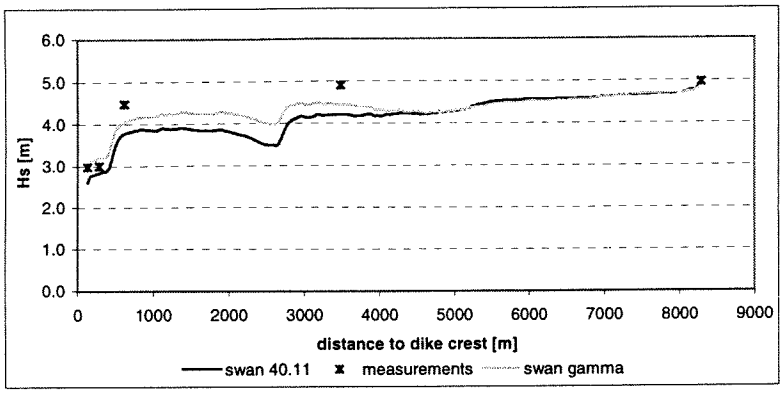

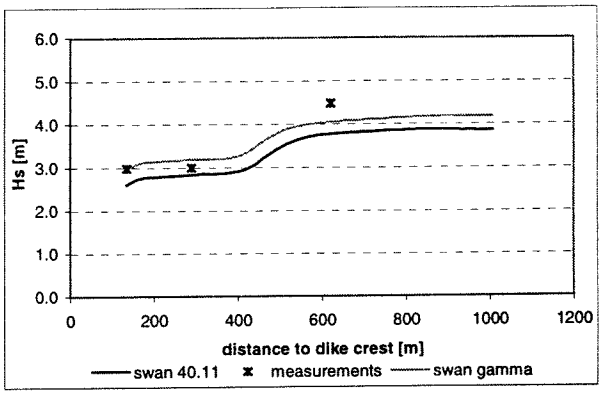

Petten 2/1/1995 6:00

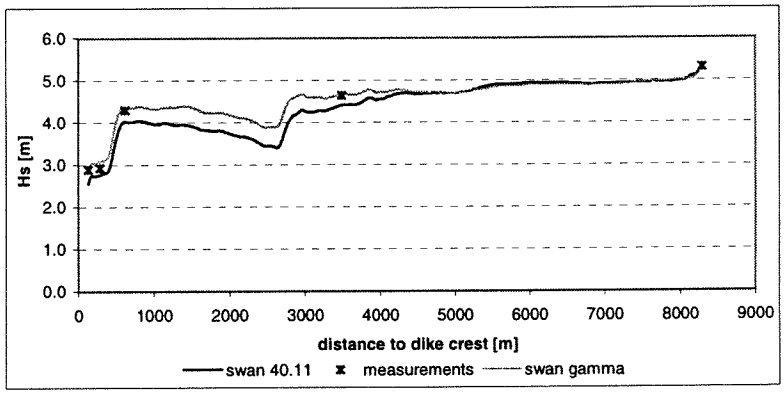

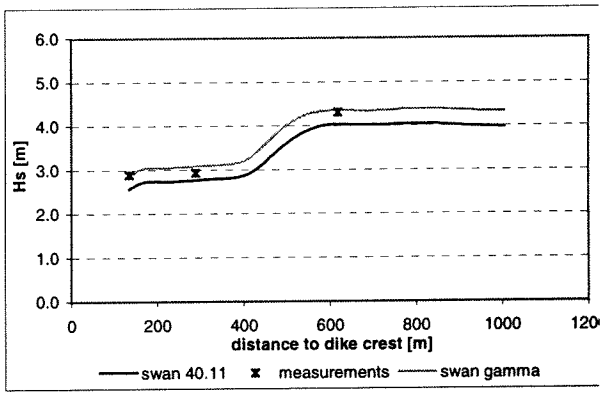

Petten 2/1/1995 17:00

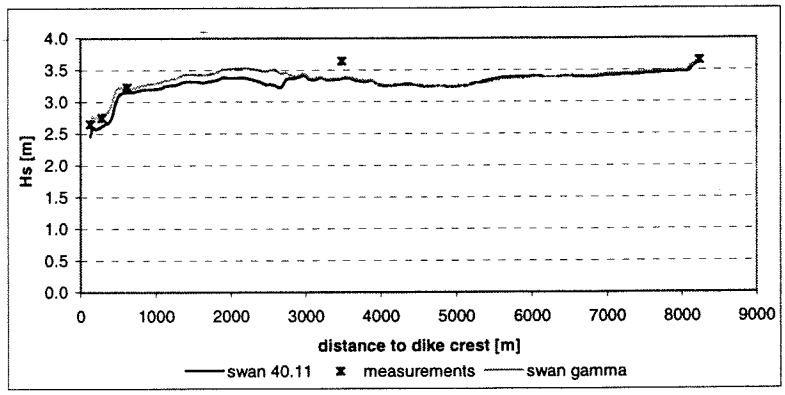

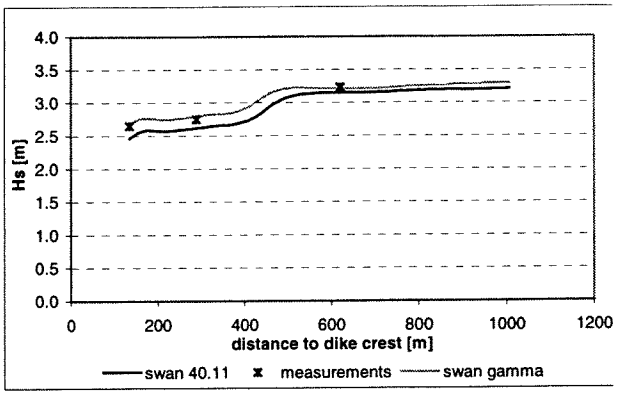

Petten 10/1/1995 11:40

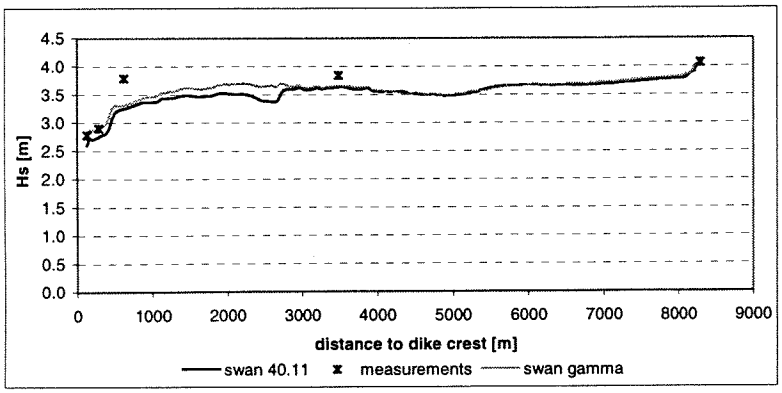

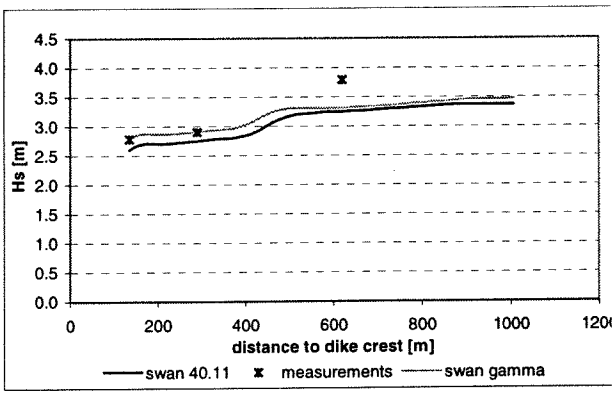

Petten 23-02-99 0:40

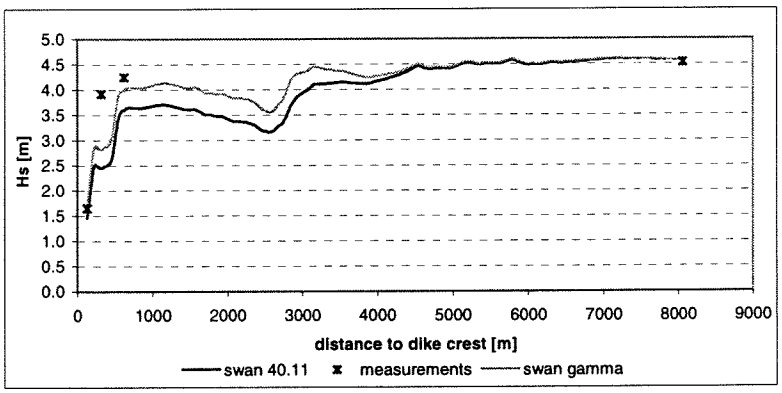

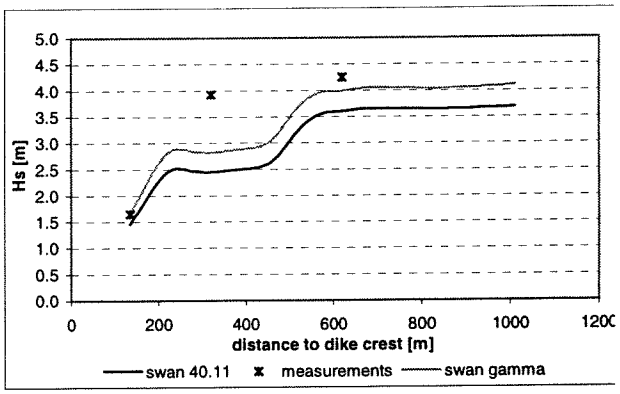

Petten 23-02-99 4:40

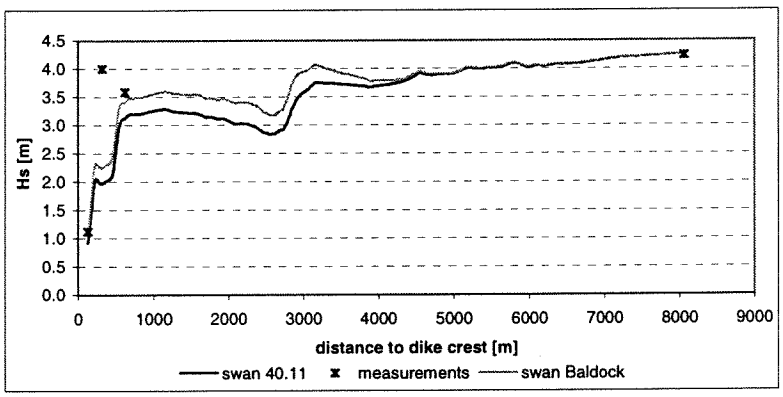

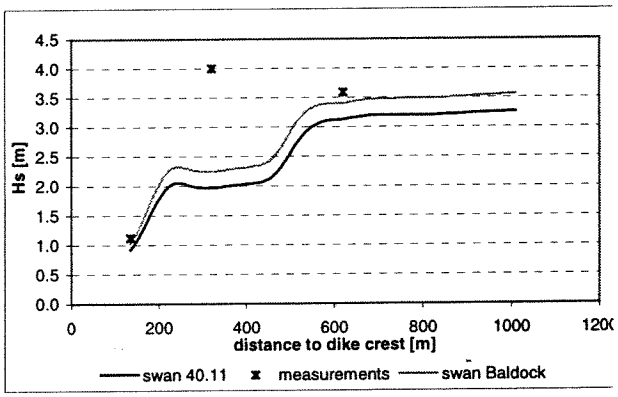

1995

01-01-0500

	measured	swan 40.11		swan gamma	
	Hs [m]	Hs [m]	difference	Hs [m]	difference
mp 1	3.60	3.60	0%	3.60	0%
mp 2	3.38	3.18	-6%	3.22	-5%
mp 3	3.33	2.98	-11%	3.07	-8%
mp 5	2.67	2.49	-7%	2.73	2%
mp 6	2.60	2.28	-12%	2.57	-1%

01-01-1820

	measured	swan 40.11		swan gamma	
	Hs [m]	Hs [m]	difference	Hs [m]	difference
mp 1	4.98	4.96	0%	4.94	-1%
mp 2	4.90	4.21	-14%	4.44	-9%
mp 3	4.48	3.77	-16%	4.05	-10%
mp 5	3.00	2.83	-6%	3.12	4%
mp 6	2.98	2.60	-13%	2.96	-1%

02-01-0600

	measured	swan 40.11		swan gamma	
	Hs [m]	Hs [m]	difference	Hs [m]	difference
mp 1	5.39	5.28	-2%	5.29	-2%
mp 2	4.64	4.41	-5%	4.66	0%
mp 3	4.30	4.02	-7%	4.35	1%
mp 5	2.93	2.75	-6%	3.08	5%
mp 6	2.89	2.56	-11%	2.86	-1%

02-01-1700

	measured	swan 40.11		swan gamma	
	Hs [m]	Hs [m]	difference	Hs [m]	difference
mp 1	3.77	3.77	0%	3.77	0%
mp 2	3.64	3.37	-7%	3.37	-7%
mp 3	3.23	3.15	-2%	3.22	0%
mp 5	2.75	2.62	-5%	2.79	1%
mp 6	2.65	2.46	-7%	2.68	1%

10-01-1140

	measured	swan 40.11		swan gamma	
	Hs [m]	Hs [m]	difference	Hs [m]	difference
mp 1	4.12	4.10	0%	4.10	0%
mp 2	3.84	3.64	-5%	3.66	-5%
mp 3	3.79	3.25	-14%	3.32	-13%
mp 5	2.90	2.74	-6%	2.91	0%
mp 6	2.78	2.60	-6%	2.80	1%

1999

23-02-0040

	measured	swan 40.11		swan gamma	
	Hs [m]	Hs [m]	difference	Hs [m]	difference
mp 1	4.53	4.54	0%	4.54	0%
mp 3	4.25	3.6	-15%	3.99	-6%
*mp 5**	*3.92*	*2.45*	*-38%*	*2.82*	*-28%*
mp 6	1.65	1.46	-12%	1.66	1%

23-02-0440

	measured	swan 40.11		swan gamma	
	Hs [m]	Hs [m]	difference	Hs [m]	difference
mp 1	4.23	4.24	0%	4.25	0%
mp 3	3.59	3.13	-13%	3.40	-5%
*mp 5**	*4.00*	*1.97*	*-51%*	*2.25*	*-44%*
mp 6	1.12	0.92	-18%	1.02	-9%

* instrument probably not working

5G Variation of the local wave steepness and the corresponding γ-values in the SV cases

SV case 1

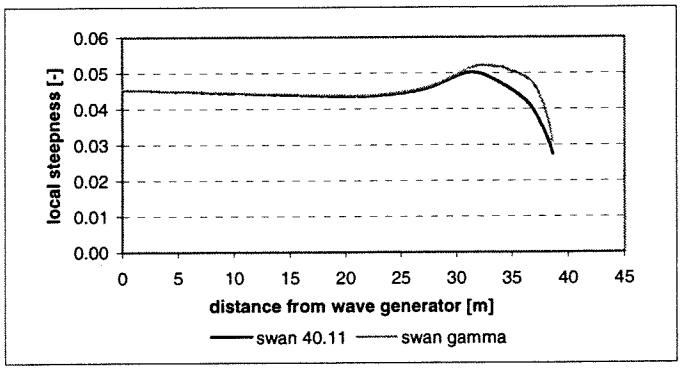

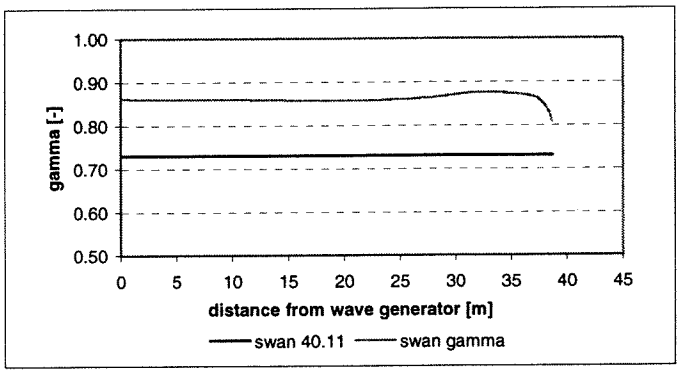

SV case 3

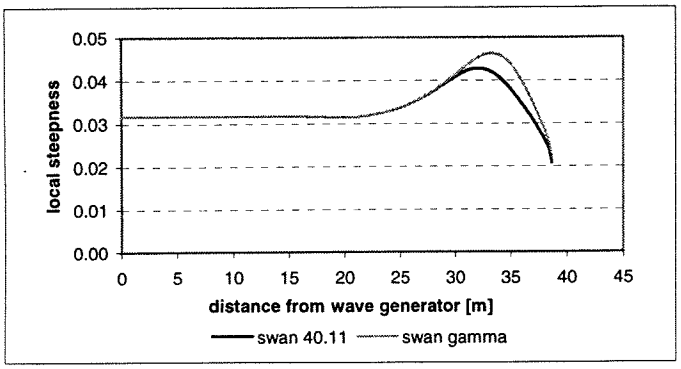

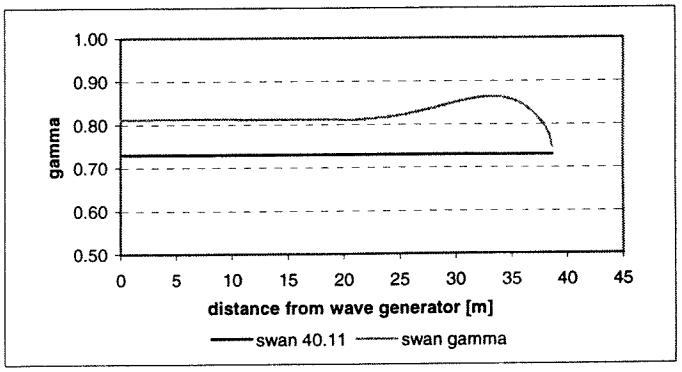

SV case 7

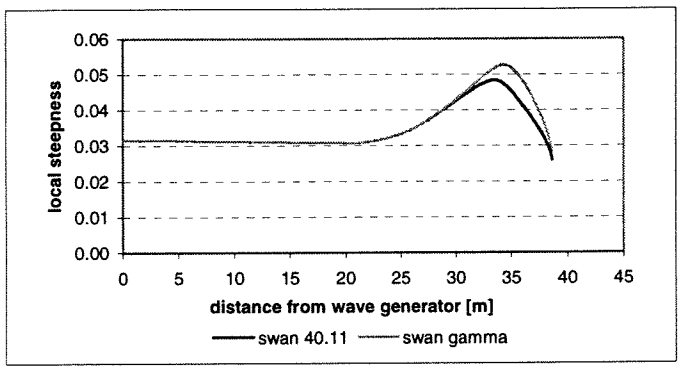

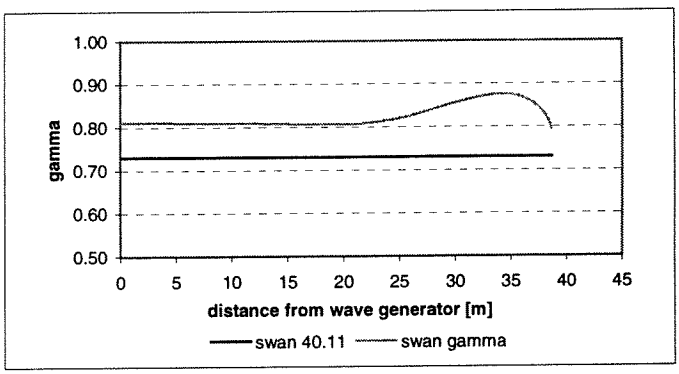

SV case 9

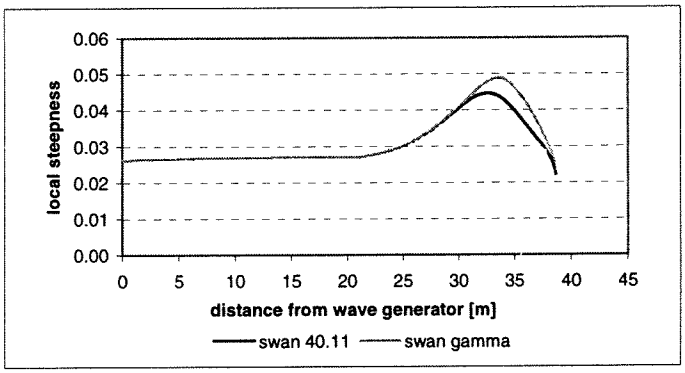

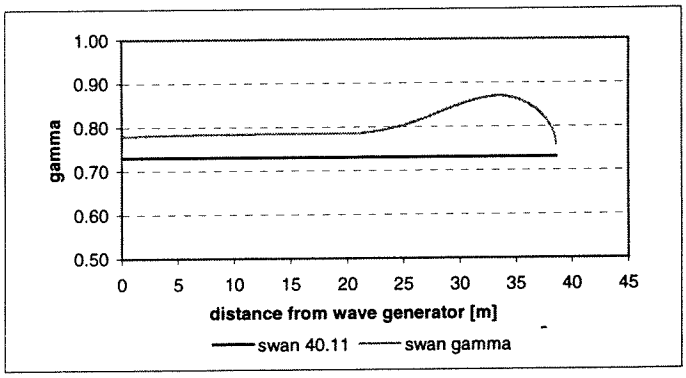

5H Comparison of predicted dissipation rates with SWAN 40.11 and SWAN gamma in the SV cases

SV case 1

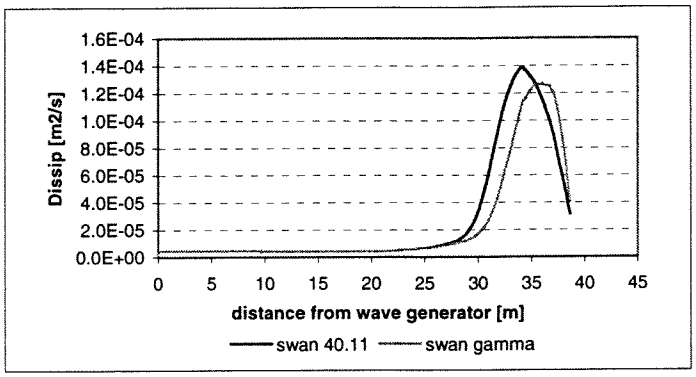

SV case 3

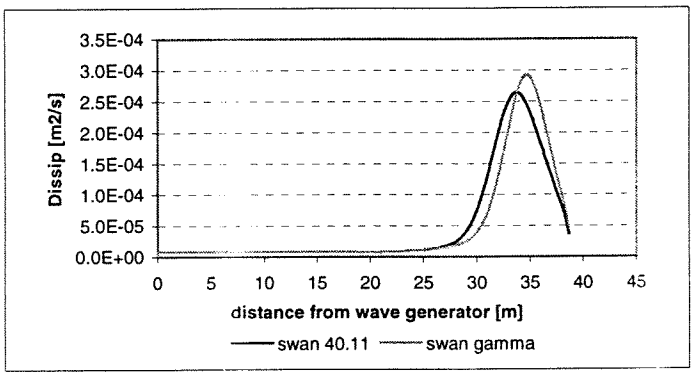

SV case 7

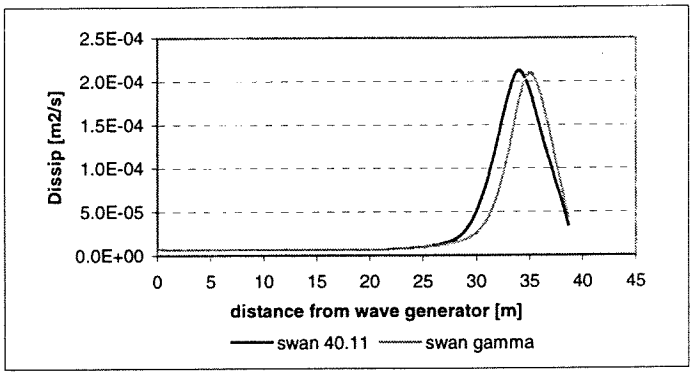

SV case 9

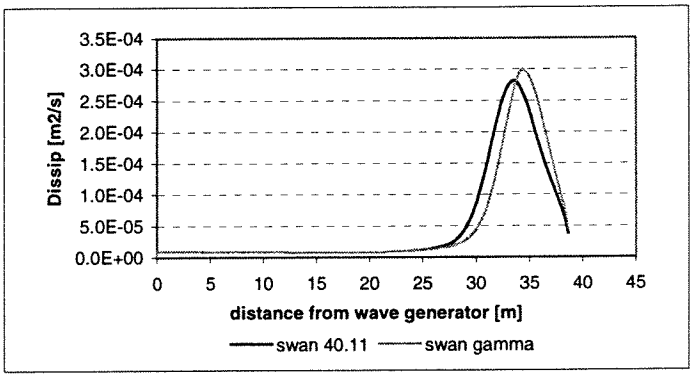

5I Comparison of significant wave heights with SWAN 40.11 and SWAN gamma in the SV cases

SV case 01

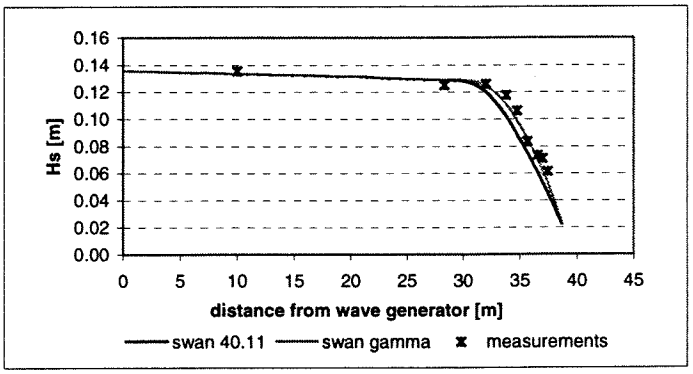

SV case 03

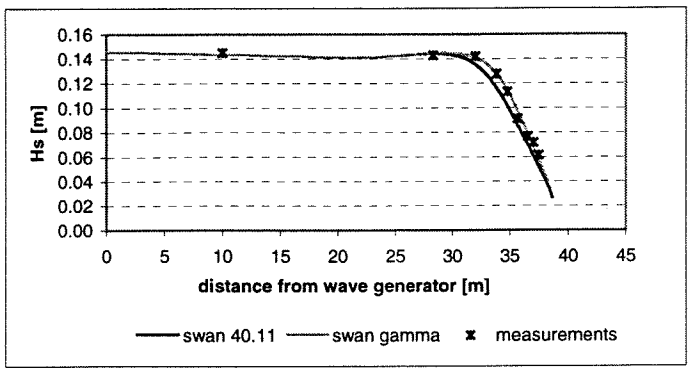

SV case 07

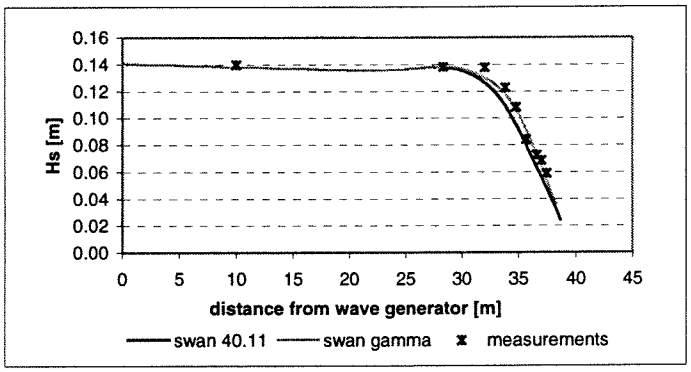

SV case 09

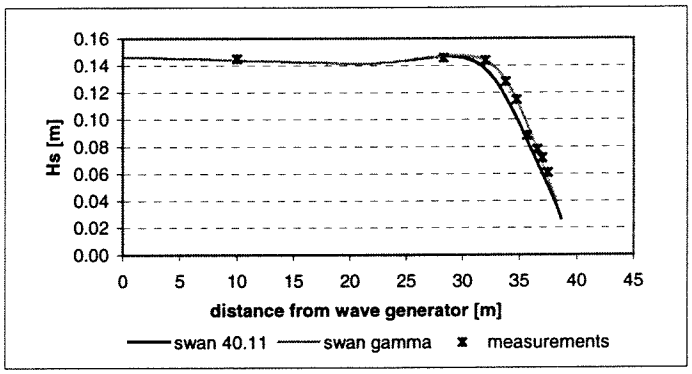

	measurement	swan 40.11		swan gamma	
depth [cm]	Hs [m]	Hs [m]	difference	Hs [m]	difference
61	13.5	13.4	-1%	13.4	-1%
36.6	12.5	12.9	3%	12.9	3%
24.4	12.6	12.0	-5%	12.5	-1%
18.3	11.8	10.2	-13%	11.1	-6%
15.2	10.6	8.9	-16%	9.9	-7%
12.2	8.5	7.5	-11%	8.6	1%
9.7	7.5	6.1	-19%	7.1	-6%
7.6	7.2	5.6	-23%	6.3	-12%
6.1	6.2	4.5	-26%	5.5	-11%

case 3

	measurement	swan 40.11		swan gamma	
depth [cm]	Hs [m]	Hs [m]	difference	Hs [m]	difference
61	14.5	14.4	-1%	14.4	-1%
36.6	14.3	14.4	1%	14.5	1%
24.4	14.2	13.6	-4%	14.1	-1%
18.3	12.8	11.7	-9%	12.8	0%
15.2	11.3	10.2	-10%	11.5	1%
12.2	9.1	8.6	-6%	9.8	7%
9.7	7.7	7.0	-9%	7.9	2%
7.6	7.2	6.1	-15%	6.9	-4%
6.1	6.1	5.3	-14%	5.8	-5%

case 7

	measurement	swan 40.11		swan gamma	
depth [cm]	Hs [m]	Hs [m]	difference	Hs [m]	difference
61	13.98	13.81	-1%	13.81	-1%
36.6	13.81	13.80	0%	13.81	0%
24.4	13.77	12.64	-8%	13.02	-5%
18.3	12.28	10.91	-11%	11.82	-4%
15.2	10.82	9.54	-12%	10.67	-1%
12.2	8.43	8.00	-5%	9.04	7%
9.7	7.25	6.39	-12%	7.34	1%
7.6	6.84	5.58	-18%	6.39	-7%
6.1	5.89	4.76	-19%	5.41	-8%

case 9

	measurement	swan 40.11		swan gamma	
depth [cm]	Hs [m]	Hs [m]	difference	Hs [m]	difference
61	14.51	14.46	0%	14.46	0%
36.6	14.57	14.61	0%	14.70	1%
24.4	14.38	13.74	-4%	14.36	0%
18.3	12.8	11.69	-9%	12.96	1%
15.2	11.47	10.14	-12%	11.48	0%
12.2	8.83	8.50	-4%	9.64	9%
9.7	7.79	6.83	-12%	7.79	0%
7.6	7.17	6.00	-16%	6.79	-5%
6.1	6.1	5.07	-17%	5.79	-5%

5J Comparison of the computed wave spectra with SWAN 40.11 and SWAN gamma in the Petten cases

Petten 1/1/1995 5:00

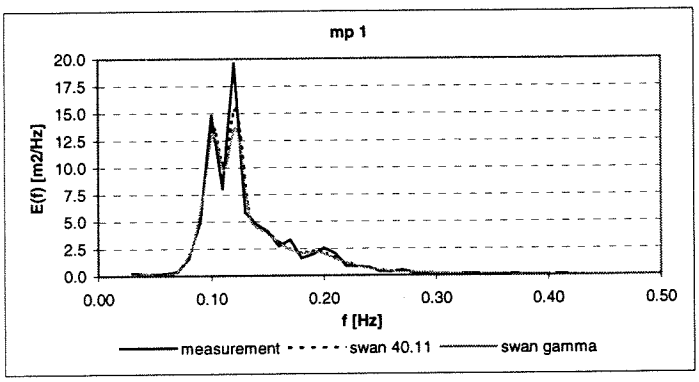

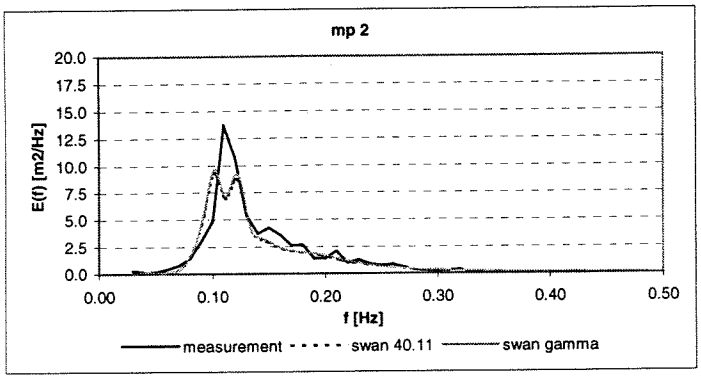

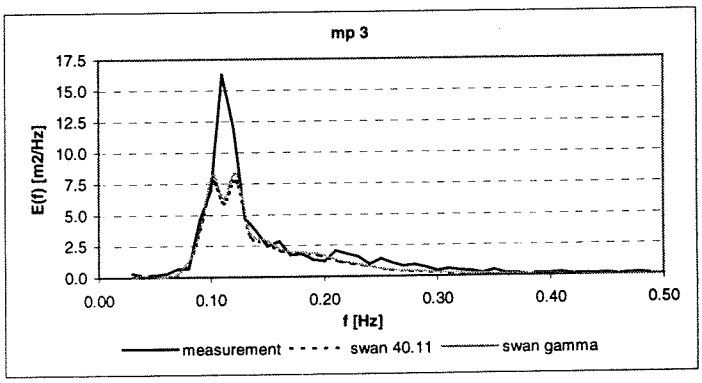

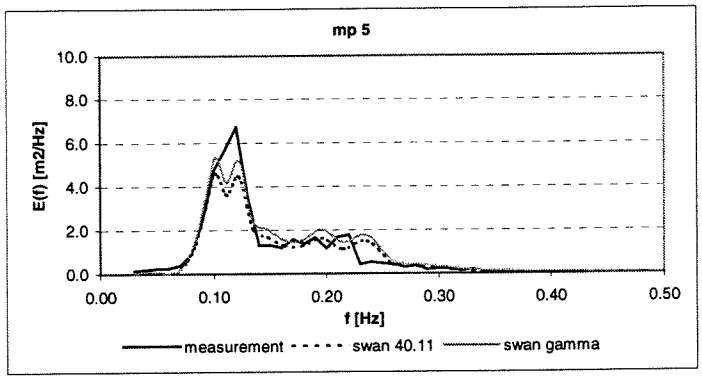

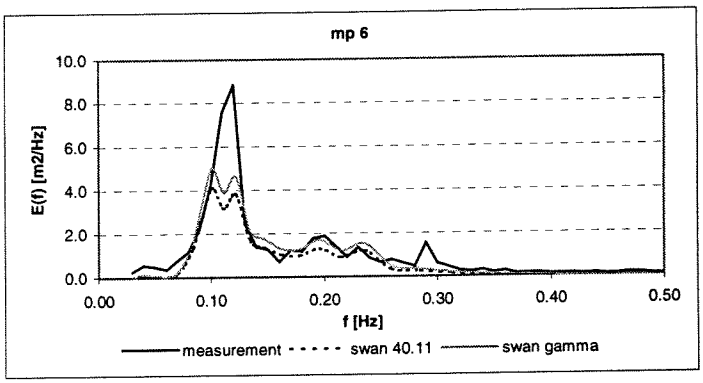

Petten 1/1/1995 18:20

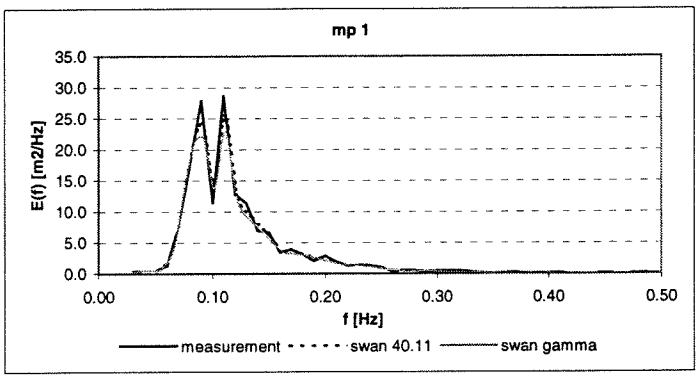

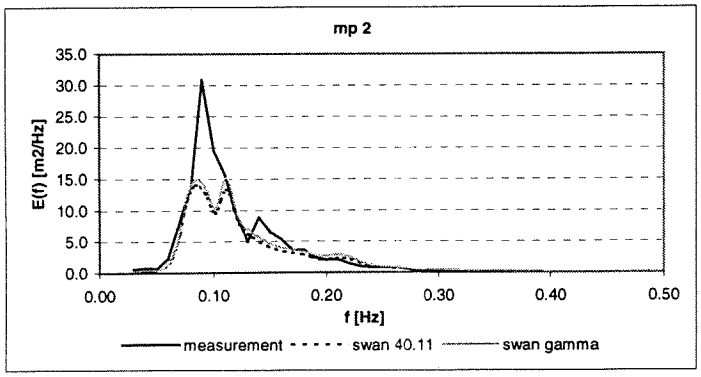

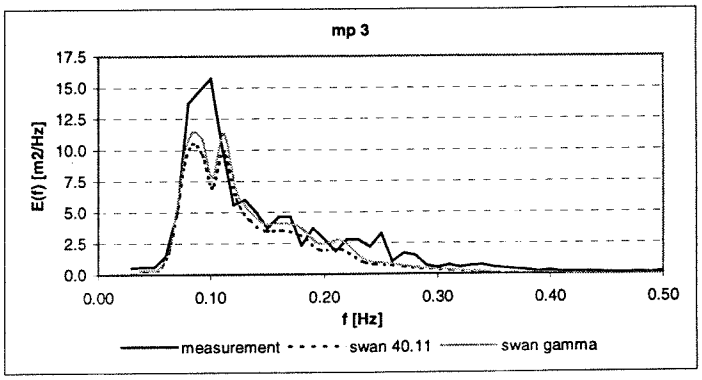

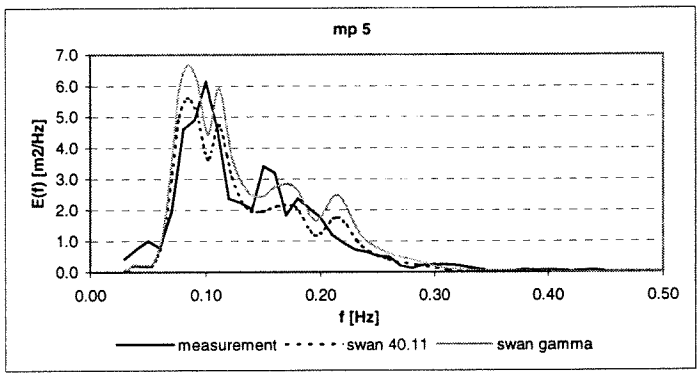

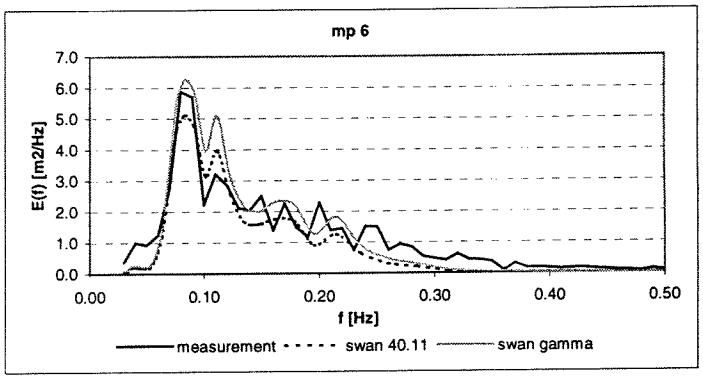

Petten 2/1/1995 6:00

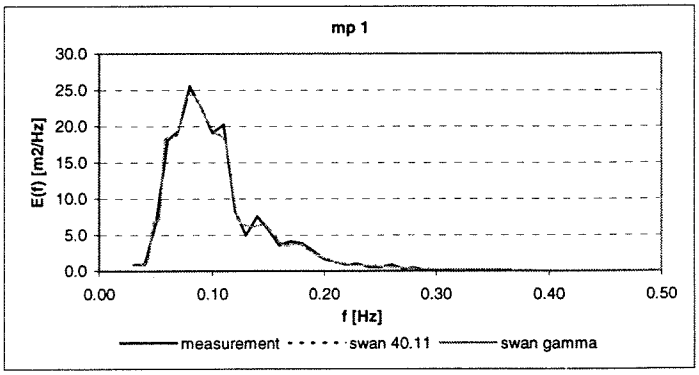

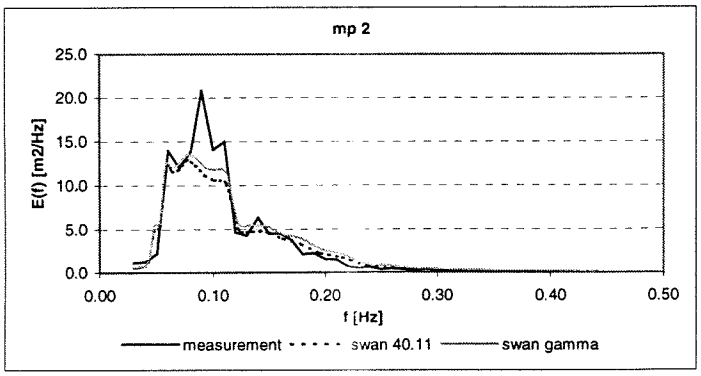

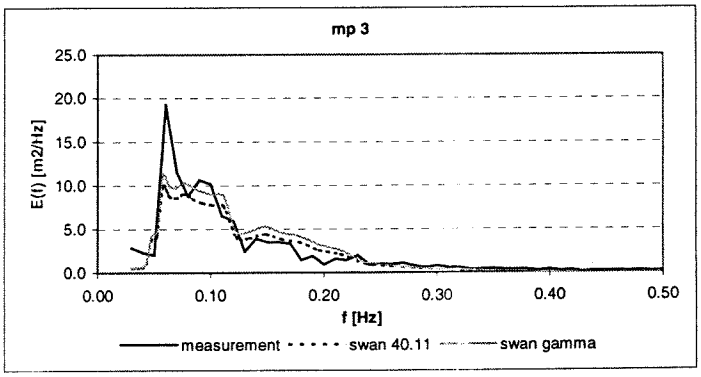

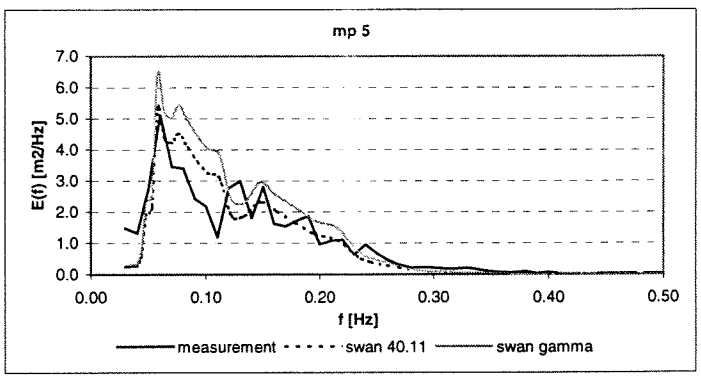

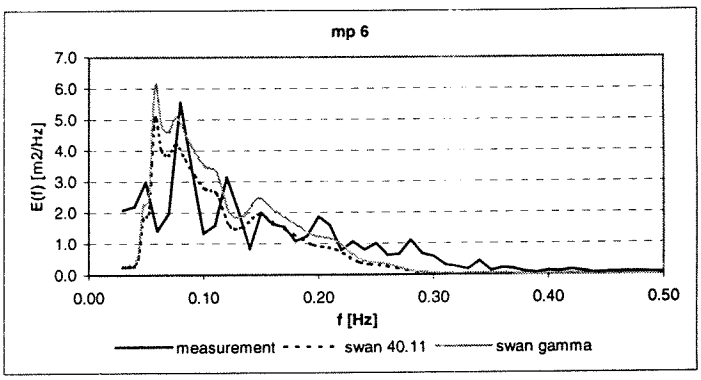

Petten 2/1/1995 17:00

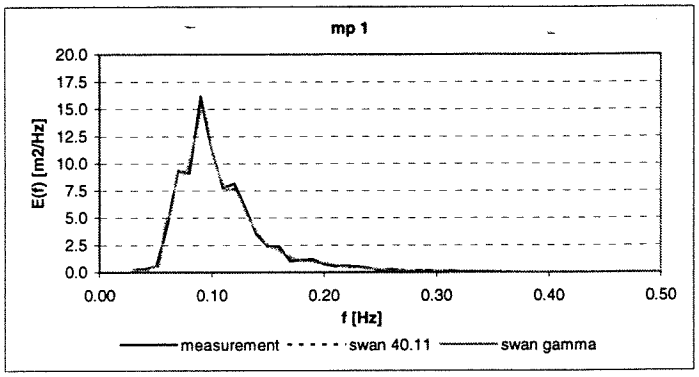

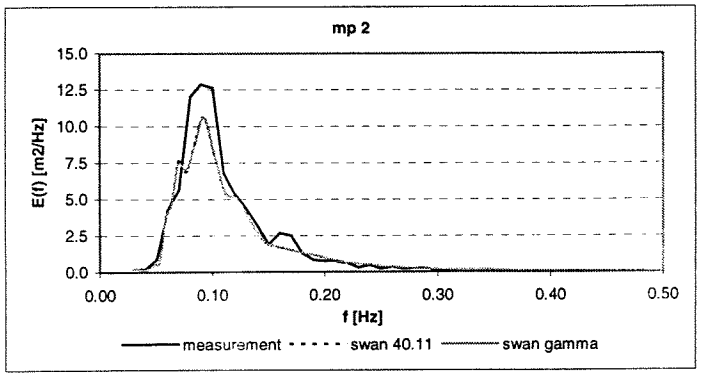

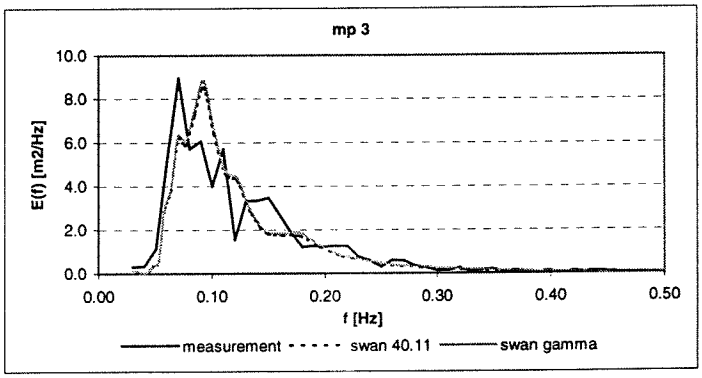

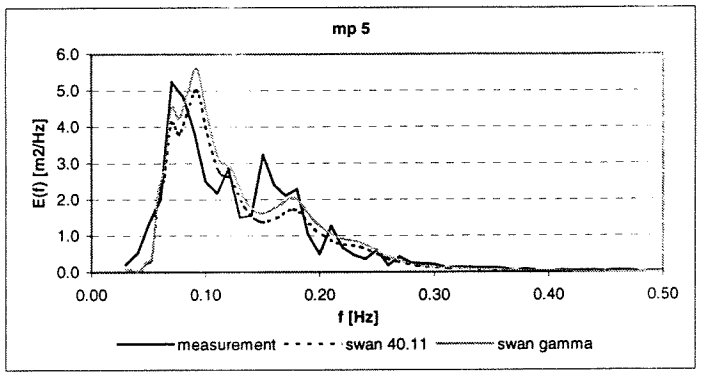

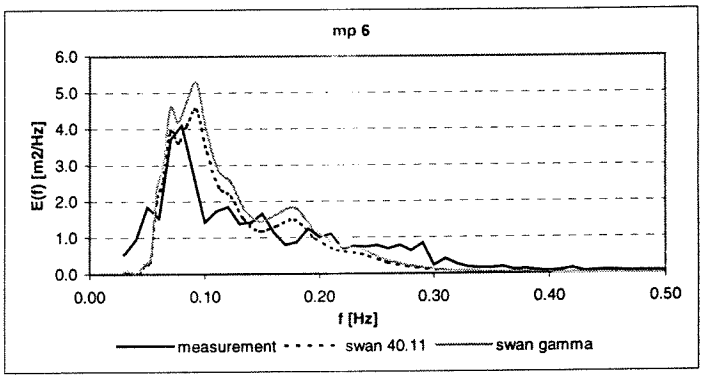

Petten 10/1/1995 11:40

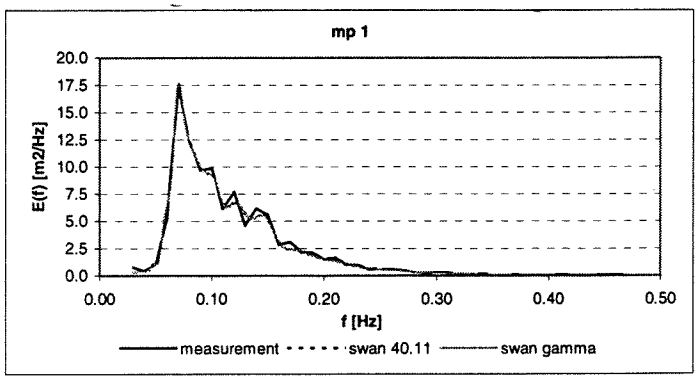

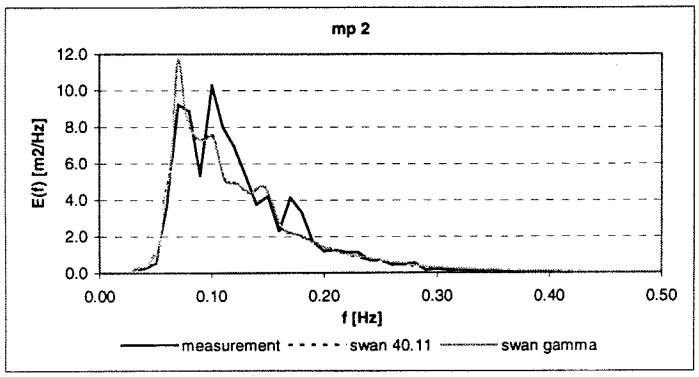

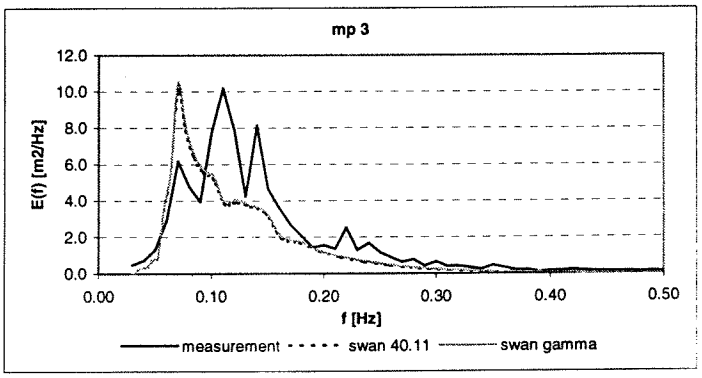

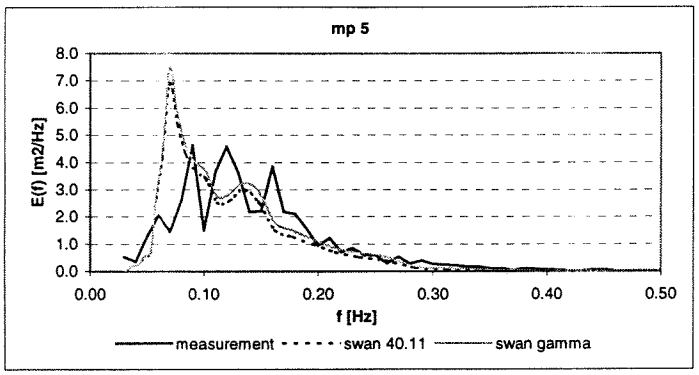

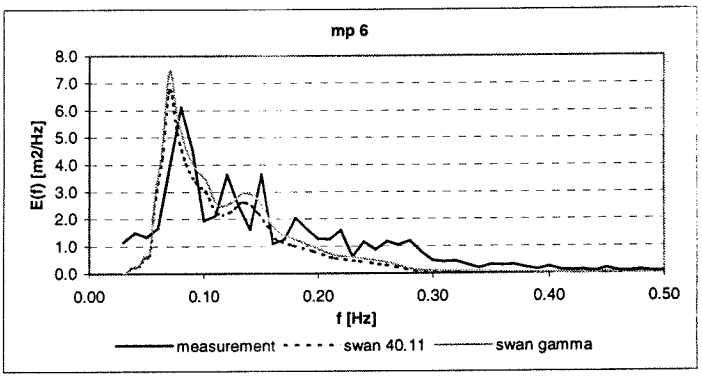

Petten 23-02-99 0:40

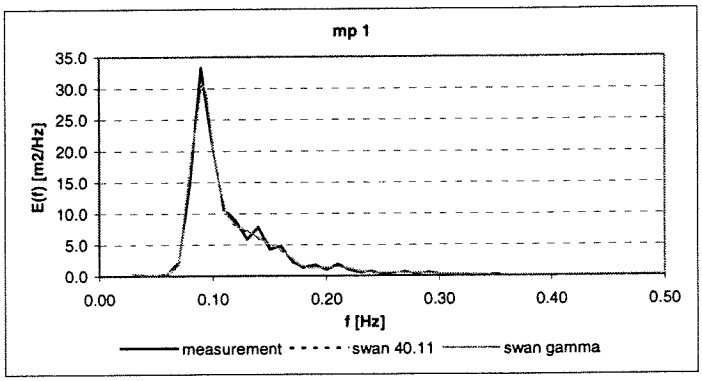

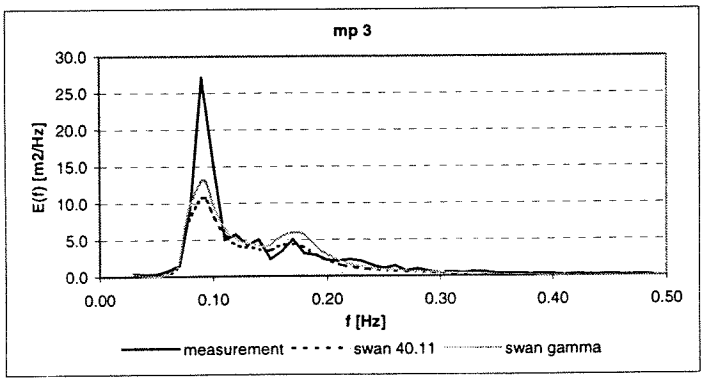

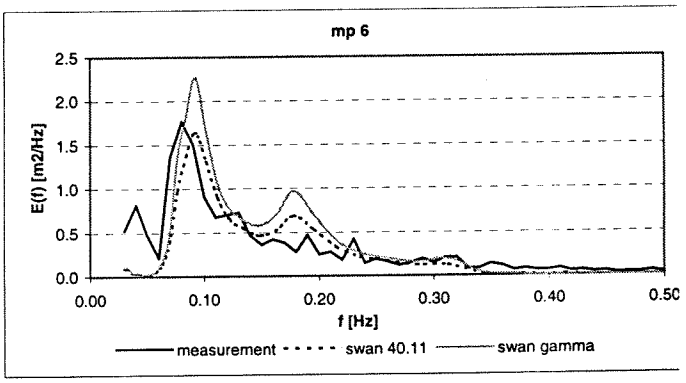

Petten 23-02-99 4:40

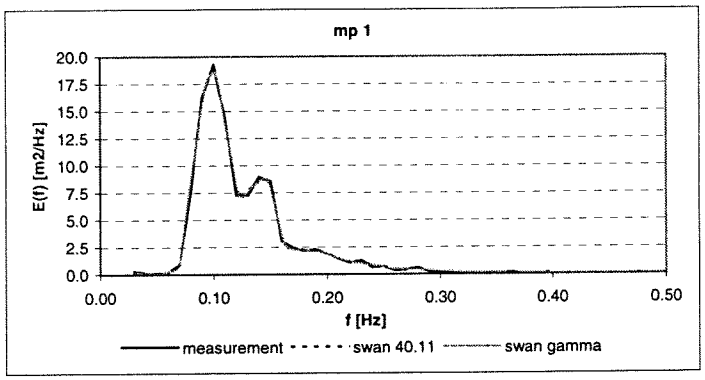

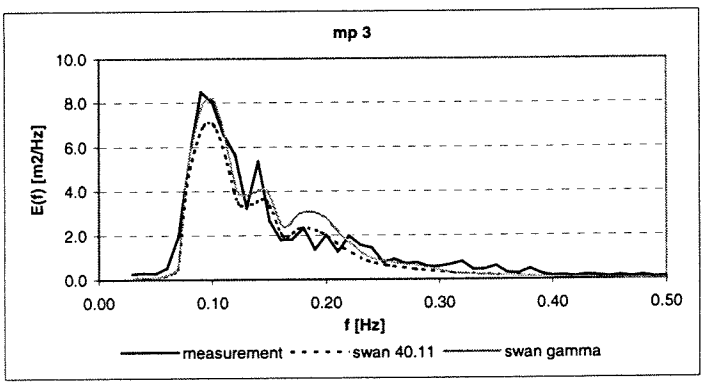

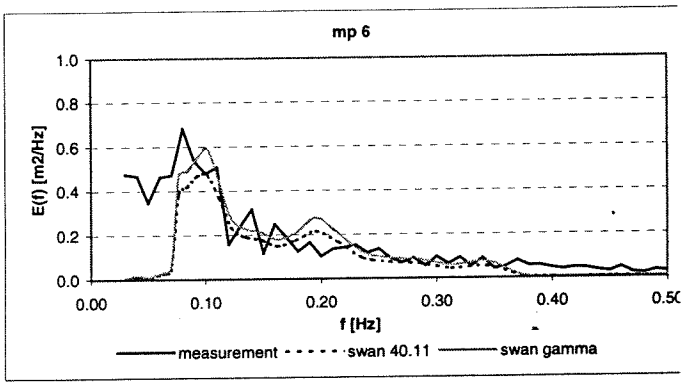

5K Comparison of the computed wave spectra with SWAN 40.11 and SWAN gamma in the SV cases

SV case 01

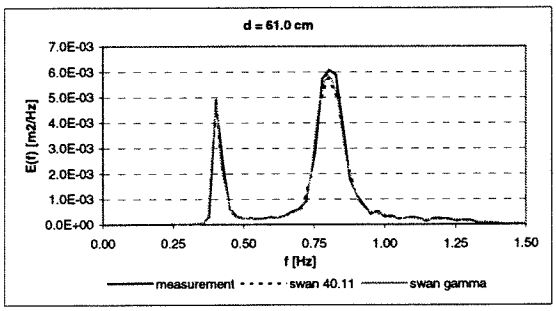

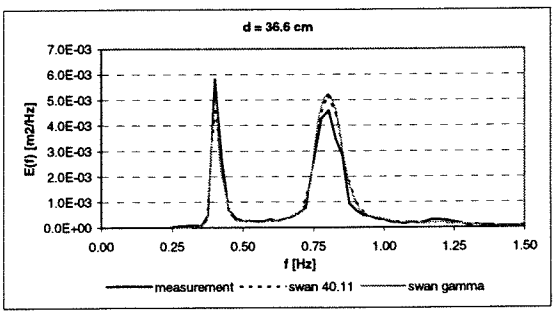

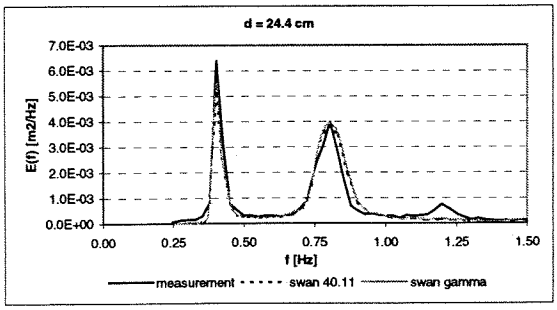

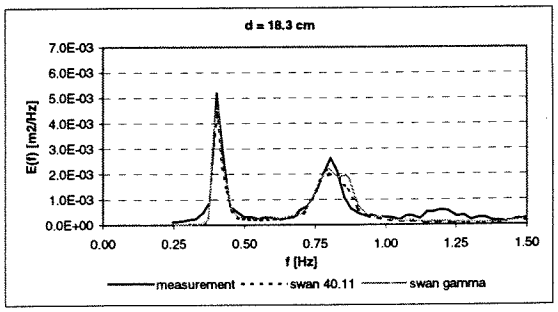

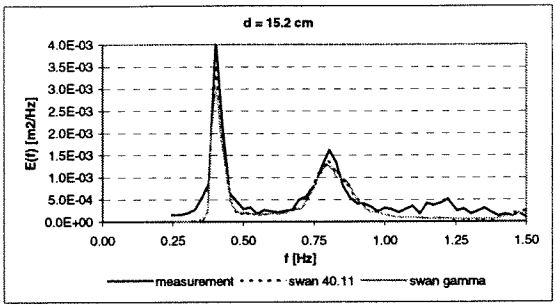

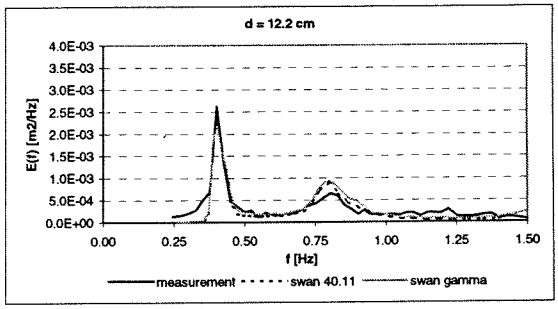

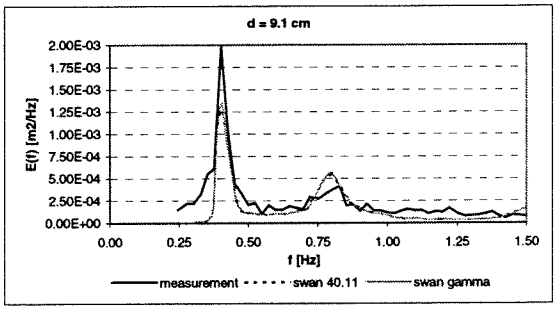

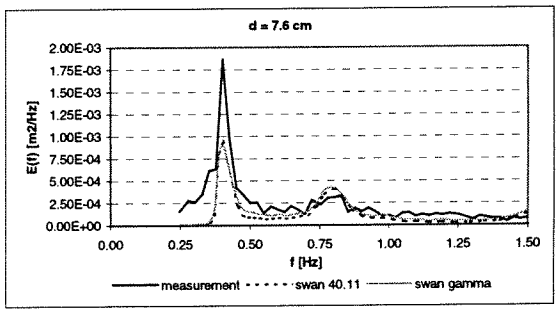

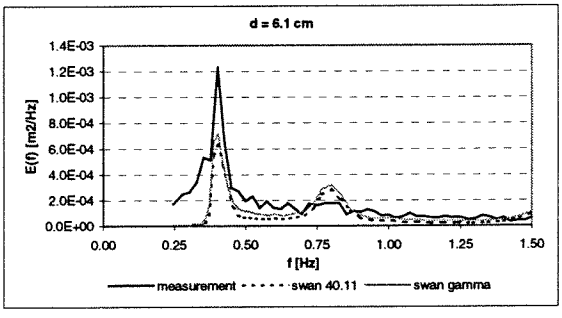

SV case 03

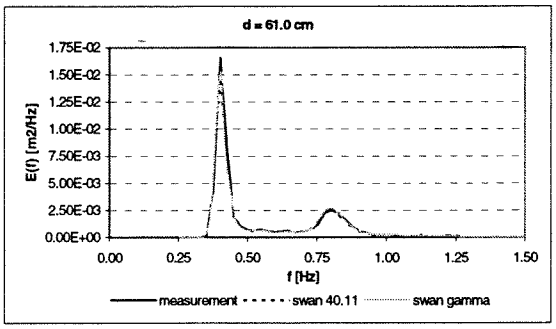
d = 61.0 cm
E(f) [m2/Hz]
f [Hz]
measurement
swan 40.11
swan gamma

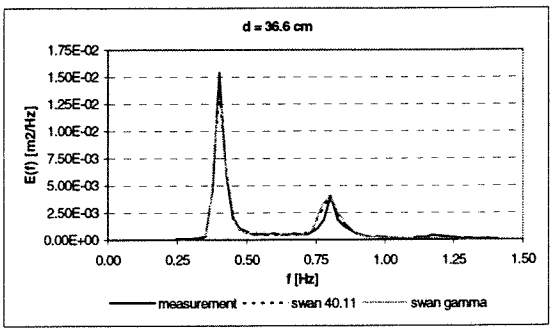
d = 36.6 cm
E(f) [m2/Hz]
f [Hz]
measurement
swan 40.11
swan gamma

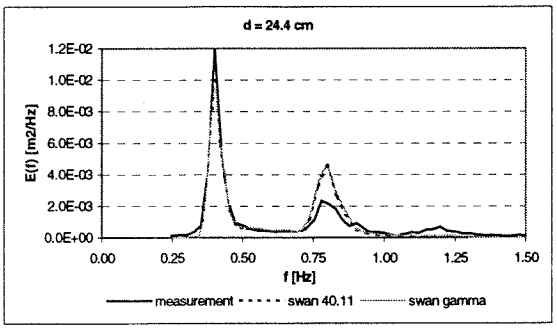
d = 24.4 cm
E(f) [m2/Hz]
f [Hz]
measurement
swan 40.11
swan gamma

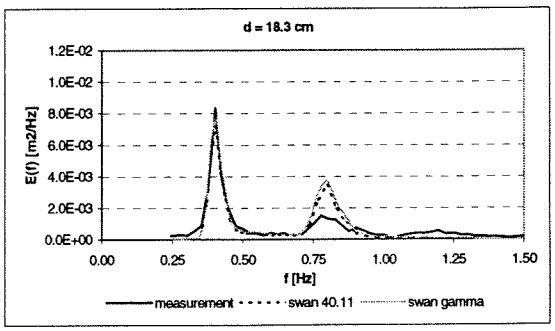
d = 18.3 cm
E(f) [m2/Hz]
f [Hz]
measurement
swan 40.11
swan gamma

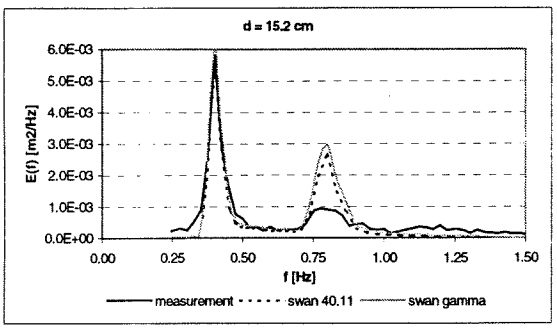
d = 15.2 cm
E(f) [m2/Hz]
f [Hz]
measurement
swan 40.11
swan gamma

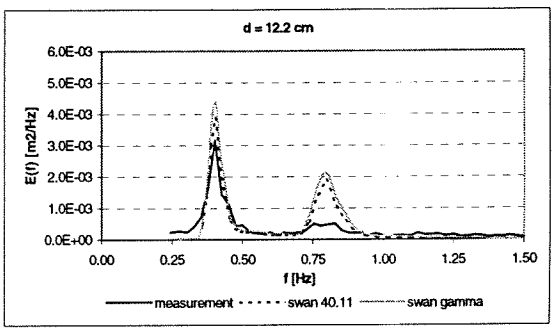
d = 12.2 cm
E(f) [m2/Hz]
f [Hz]
measurement
swan 40.11
swan gamma

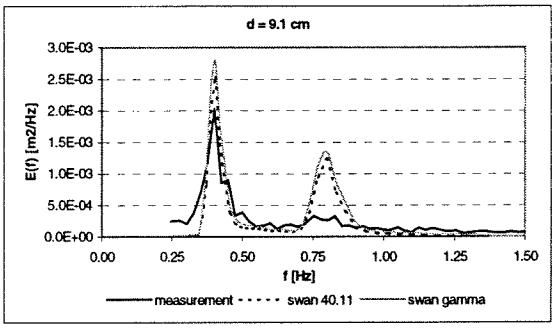
d = 9.1 cm
E(f) [m2/Hz]
f [Hz]
measurement
swan 40.11
swan gamma

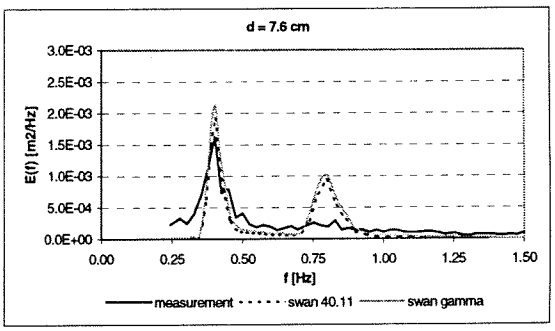
d = 7.6 cm
E(f) [m2/Hz]
f [Hz]
measurement
swan 40.11
swan gamma

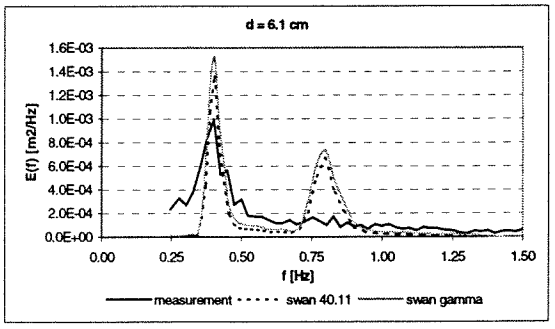
d = 6.1 cm
E(f) [m2/Hz]
f [Hz]
measurement
swan 40.11
swan gamma

SV case 07

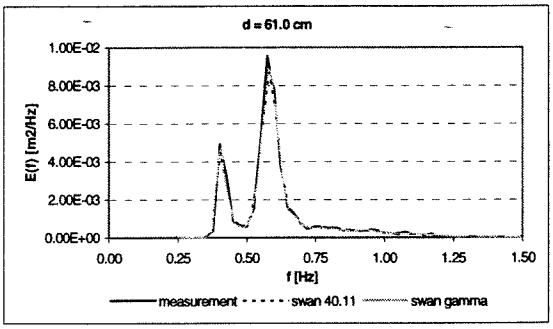
d = 61.0 cm
E(f) [m2/Hz]
f [Hz]
measurement
swan 40.11
swan gamma

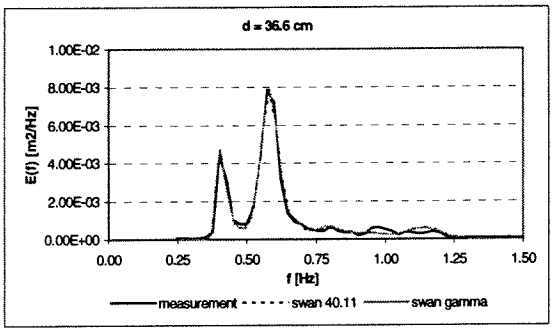
d = 36.6 cm
E(f) [m2/Hz]
f [Hz]
measurement
swan 40.11
swan gamma

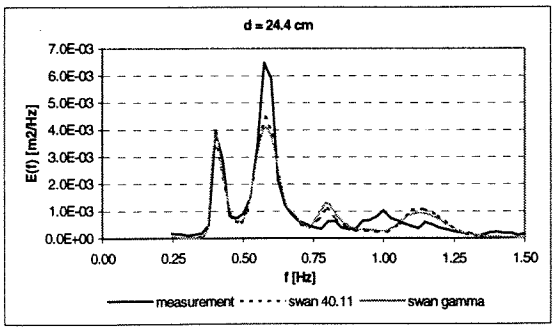
d = 24.4 cm
E(f) [m2/Hz]
f [Hz]
measurement
swan 40.11
swan gamma

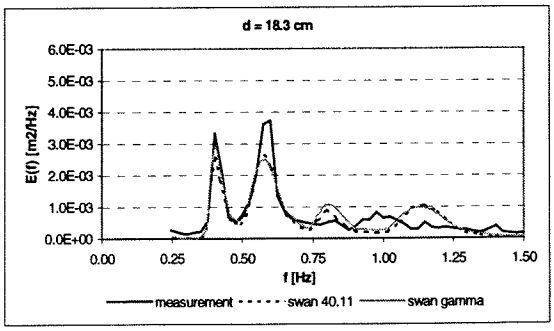
d = 18.3 cm
E(f) [m2/Hz]
f [Hz]
measurement
swan 40.11
swan gamma

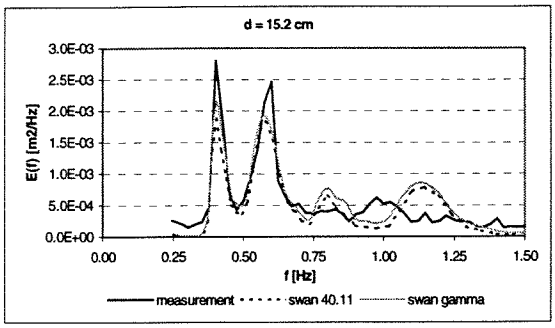
d = 15.2 cm
E(f) [m2/Hz]
f [Hz]
measurement
swan 40.11
swan gamma

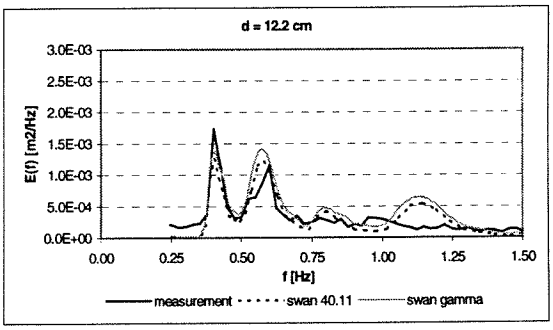
d = 12.2 cm
E(f) [m2/Hz]
f [Hz]
measurement
swan 40.11
swan gamma

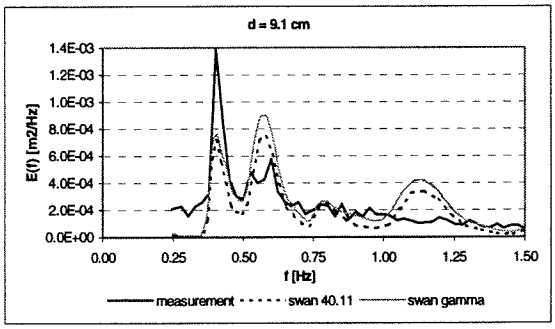
d = 9.1 cm
E(f) [m2/Hz]
f [Hz]
measurement
swan 40.11
swan gamma

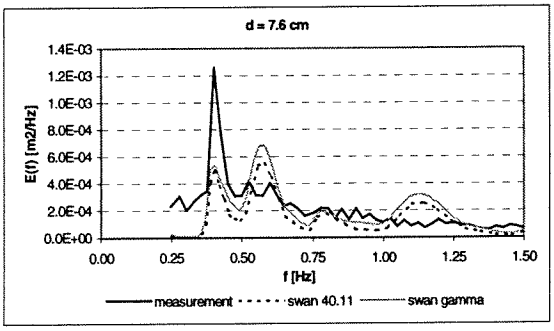
d = 7.6 cm
E(f) [m2/Hz]
f [Hz]
measurement
swan 40.11
swan gamma

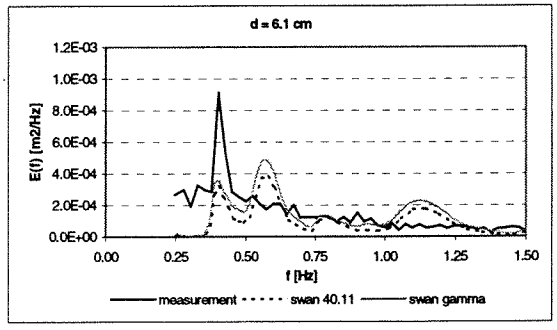
d = 6.1 cm
E(f) [m2/Hz]
f [Hz]
measurement
swan 40.11
swan gamma

SV case 09

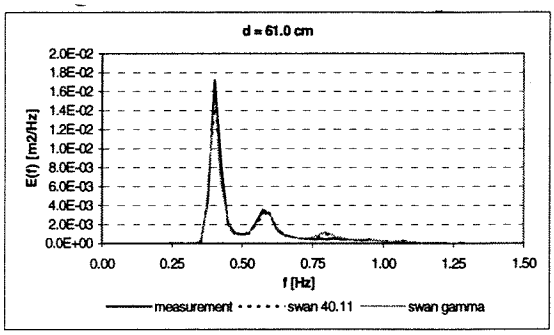
d = 61.0 cm
E(f) [m2/Hz]
f [Hz]
measurement
swan 40.11
swan gamma

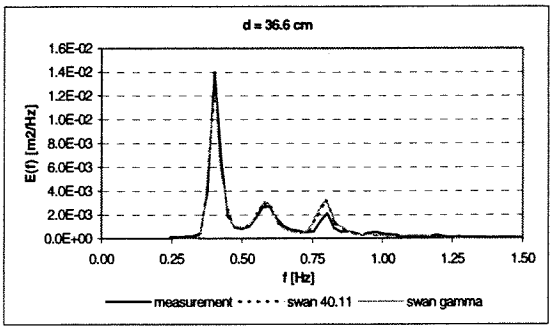
d = 36.6 cm
E(f) [m2/Hz]
f [Hz]
measurement
swan 40.11
swan gamma

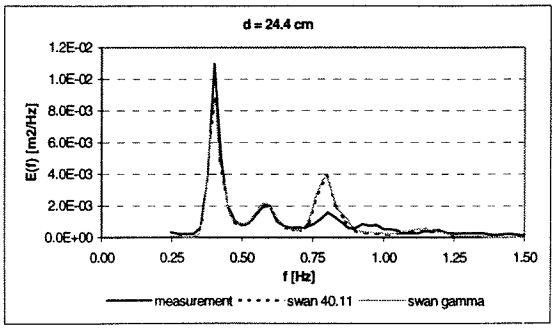
d = 24.4 cm
E(f) [m2/Hz]
f [Hz]
measurement
swan 40.11
swan gamma

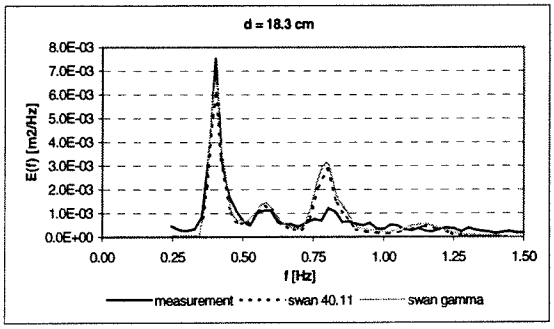
d = 18.3 cm
E(f) [m2/Hz]
f [Hz]
measurement
swan 40.11
swan gamma

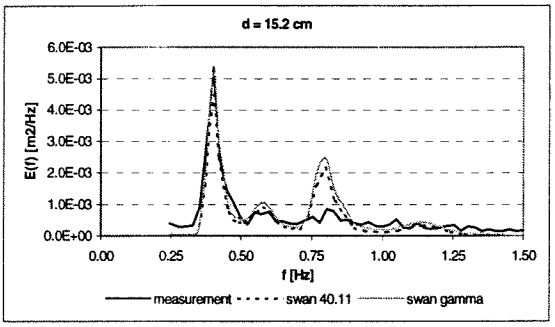
d = 15.2 cm
E(f) [m2/Hz]
f [Hz]
measurement
swan 40.11
swan gamma

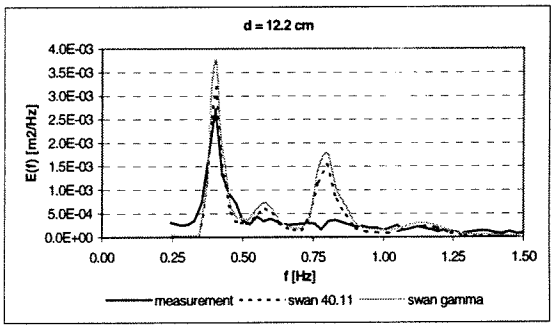
d = 12.2 cm
E(f) [m2/Hz]
f [Hz]
measurement
swan 40.11
swan gamma

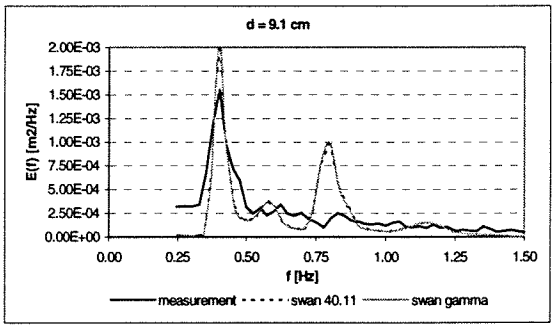
d = 9.1 cm
E(f) [m2/Hz]
f [Hz]
measurement
swan 40.11
swan gamma

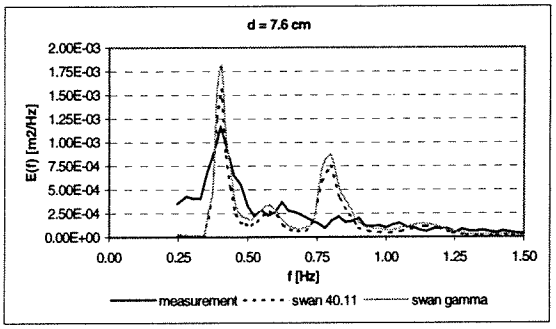
d = 7.6 cm
E(f) [m2/Hz]
f [Hz]
measurement
swan 40.11
swan gamma

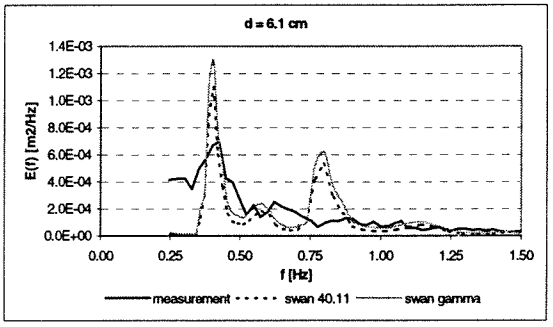
d = 6.1 cm
E(f) [m2/Hz]
f [Hz]
measurement
swan 40.11
swan gamma